

MIT/WHOI 97-27

**Massachusetts Institute of Technology  
Woods Hole Oceanographic Institution**



**Joint Program  
in Oceanography/  
Applied Ocean Science  
and Engineering**



---

**DOCTORAL DISSERTATION**

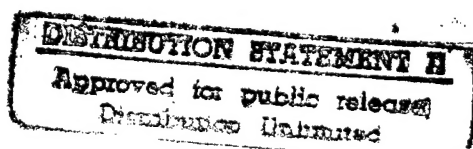
*Temporal Evolution of Tritium-<sup>3</sup>He Age  
in the North Atlantic:  
Implications for Thermocline Ventilation*

by

Paul E. Robbins

September 1997

19971229 237



DTIC QUALITY INSPECTED 6

MIT/WHOI

97-27

Temporal Evolution of Tritium- $^3\text{He}$  Age in the North Atlantic:  
Implications for Thermocline Ventilation

by

Paul E. Robbins

Massachusetts Institute of Technology  
Cambridge, Massachusetts 02139

and

Woods Hole Oceanographic Institution  
Woods Hole, Massachusetts 02543

September 1997

DOCTORAL DISSERTATION

Funding was provided by Office of Naval Research AASERT contract number N00014-95-1-0824.

Reproduction in whole or in part is permitted for any purpose of the United States Government. This thesis should be cited as: Paul E. Robbins, 1997. Temporal Evolution of Tritium- $^3\text{He}$  Age in the North Atlantic: Implications for Thermocline Ventilation. Ph.D. Thesis. MIT/WHOI, 97-27.

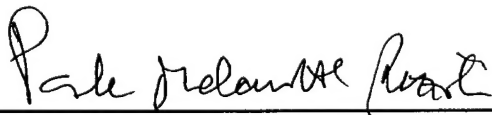
Approved for publication; distribution unlimited.

Approved for Distribution:



Philip L. Richardson, Chair

Department of Physical Oceanography



Paola Malanotte-Rizzoli  
MIT Director of Joint Program



John W. Farrington  
WHOI Dean of Graduate Studies

# Temporal Evolution of Tritium-<sup>3</sup>He Age in the North Atlantic: Implications for Thermocline Ventilation

by

Paul E. Robbins

B.A. Physics, Oberlin College, Oberlin, OH  
(1986)

Submitted in partial fulfillment of the  
requirements for the degree of

Doctor of Philosophy

at the

MASSACHUSETTS INSTITUTE OF TECHNOLOGY

and the

WOODS HOLE OCEANOGRAPHIC INSTITUTION

September 1997

© 1997 Paul E. Robbins

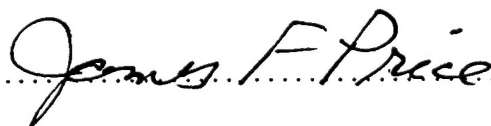
The author hereby grants to MIT and to WHOI permission to reproduce  
and to distribute copies of this thesis document in whole or in part.

Signature of Author .....



Joint Program in Oceanography  
Massachusetts Institute of Technology  
Woods Hole Oceanographic Institution  
September 1997

Certified by .....



James F. Price  
Senior Scientist  
Thesis Supervisor

Certified by .....



W. Brechner Owens  
Senior Scientist  
Thesis Supervisor

Accepted by .....



Paola Rizzoli  
Chair, Joint Committee for Physical Oceanography  
Massachusetts Institute of Technology  
Woods Hole Oceanographic Institution





# Temporal Evolution of Tritium- $^3\text{He}$ Age in the North Atlantic: Implications for Thermocline Ventilation

by  
Paul E. Robbins

Submitted in partial fulfillment of the requirements for the degree of  
Doctor of Philosophy at the Massachusetts Institute of Technology  
and the Woods Hole Oceanographic Institution  
September 1997

## Abstract

This thesis is a study of the physical mechanisms that ventilate the subtropical thermocline of the eastern North Atlantic. The starting point is an analysis of the existent historical database of natural and anthropogenic tracers, with special emphasis on  $^3\text{He}$  and tritium, that can be used to infer rates of ventilation. If the flow is predominantly advective, the temporal evolution of coupled transient tracers can be used to define a tracer age which measures the elapsed time since a water parcel was resident in the surface mixed layer. A principle finding is that the observed tracer age shows a large and systematic change over time. Tritium- $^3\text{He}$  age in the eastern Atlantic thermocline is seen to increase over time; the magnitude of the change is greatest for the deeper, more slowly ventilated layers of the thermocline.

The first hypothesis examined is that the observed shift in the tracer age field is the manifestation of a slackening of the physical ventilation. A time series of the meridional geostrophic velocity shear in the eastern Atlantic shows no indication of a change in the strength of the large-scale circulation. Uncertainty of the geostrophic calculation due to data sparsity and mesoscale eddy contamination prevents conclusive rejection of the hypothesis of a changing circulation. There are other tracers which offer useful clues: comparison of the tritium- $^3\text{He}$  age field with dissolved oxygen reveals a temporal trend in the property-property correlation. The spatial structure of the oxygen field, however, shows no long-term evolution over time. From this line of evidence it is concluded that the physical ventilation of the thermocline has not altered over time and, therefore, the temporal change in the tritium- $^3\text{He}$  age field must be the signal of the tritium invasion itself.

A second hypothesis, which analysis shows is more consistent with the observations, is that the changing tracer age is a consequence of mixing effects in the ventilation of  $^3\text{He}$  and tritium. Numerical simulations of the thermocline ventilation of  $^3\text{H}$  and  $^3\text{He}$  are performed to examine the steadiness of the tracer age field under different advective-diffusive regimes. A one-dimensional model is constructed based on

the assumption that the totality of the fluid in the thermocline derives from subduction out of the surface mixed layer. The temporal behavior of the tracer age field is found to be dependent on the radiotracer Péclet number, which measures the ratio of the diffusive and advective time scales. In a model with steady circulation, the observed temporal behavior of the tracer age field can be reproduced only when the effects of lateral mixing play a significant role in the process of ventilation. The vertical structure and magnitude of the implied lateral diffusivity are, however, inconsistent with other observations. The numerical simulations are next extended to two-dimensions to allow for the presence of a pool of unventilated, re-circulated water within the anti-cyclonic, subtropical gyre. Comparison of the model with the observed transient tracer field in the lower thermocline shows consistency with conventional estimates of lateral mixing rates only when the diffusively ventilated "pool" region extends across the entire zonal domain of the gyre. In contrast, the transient tracer fields in the upper portion of the thermocline are best reproduced when the isopycnal surfaces are ventilated by advection directly from the surface mixed layer. The results obtained here are consistent with numerical simulations which reveal a prominent role for mesoscale eddies in the ventilation of the thermocline.

Thesis Supervisors:

James F. Price

Senior Scientist

Woods Hole Oceanographic Institution

W. Brechner Owens

Senior Scientist

Woods Hole Oceanographic Institution

## Acknowledgments

My protracted duration as a graduate student in the Joint Program has furnished me with the opportunity and pleasure of working with numerous scientists at WHOI and MIT. Firstly, I would like to thank my thesis advisors: Jim Price and Breck Owens. At a time when my prospects to finish graduate school were uncertain, they invited me to start the present project and provided support and encouragement throughout. Jim especially helped to sharpen my focus on the underlying scientific questions of my research and supplied a steady stream of helpful feedback to clarify the presentation of this work and scientific research in general. Breck has been a valuable resource in establishing the framework of this research and specifically for discussing technical issues of models and data assimilation. In addition to my advisors, Bill Jenkins has been exceedingly generous with his time, encouragement and guidance throughout my time as a graduate student. Bill's enthusiasm for science and ability to think creatively are a powerful stimulant; one cannot help but be excited about oceanographic research after a long discussion with him. My interactions with Jim, Breck and Bill have been the foundation for both strengthening the scientific merits of this work as well as contributing to my enjoyment of the research process. I also thank the members of my thesis committee, Mike Spall, Carl Wunsch and Glenn Flierl, for their advice, comments and criticisms, all of which contributed to the improvement of this work.

I suffered a few fits and starts in my march toward the present thesis project. Joe Pedlosky was my first advisor in graduate school. His joy in science and care in researching the dynamics of the ocean and atmosphere continue to inspire me. My initial steps towards independent research were conducted under the guidance of my second advisor, Harry Bryden. I greatly enjoyed working with Harry and continue to listen to his counsel ("Read a paper a day"). He encouraged me to set my sights high and motivate my selection of research topics by thinking about the larger scientific issues and questions. Throughout my graduate career, John Toole has been a ready source for thoughtfully answered questions on a breadth of oceanographic problems. John also hired me at a critical time when I took a leave from graduate school and I am grateful to him for providing a timely boost by guiding me onto an interesting and fruitful research project.

In addition to those mentioned above, I have enjoyed and benefited from courses and discussions with numerous faculty at both WHOI and elsewhere. Bruce Warren is always a good foil for testing my latest (often exceedingly mistaken) ideas about the “real” ocean circulation as well as an enthusiastic compatriot on zestful lexicological quests. Terry Joyce aided me as an interim advisor after Harry Bryden left the institution. A summer course at Friday Harbor Laboratories of the University of Washington organized by Peter Rhines and Jorge Sarmiento provided early inspiration and motivation to approach oceanography as an interdisciplinary science.

The analysis in this thesis was aided by several people. Many years of dedicated collection and measurement by the Helium Isotope Laboratory at Woods Hole have produced a high quality database of  $^3\text{He}$  and tritium measurements, the analysis of which is a central part of this thesis. Mary Landsteiner assembled and painstakingly insured quality control on hydrographic data appended to the climatological atlas of the North Atlantic. Audrey Rogerson aided me in the solution of the analytic model in Appendix C. Karl Helfrich provided helpful suggestions for the implicit numerical integration used in Chapter 4.

My fellow students have contributed much to my advancement and enjoyment during graduate school. My classmates, Keith Alverson, Ed Dever, Pascal Le Grand, Ari Epstein, and Sarah Gille were a source of many stimulating discussions, controversies and explorations during the first few years of course work. Their help and good nature lifted me along through the worst pressures and stresses of classes and exams. Chris Edwards has been an invaluable close friend, colleague and counsel for many years. Susan Wijffels helped guide me through my first years of grappling with hydrographic data sets at WHOI.

While at Oberlin College, two of my professors, Robert Hilborn and Michael Zimmerman, were instrumental in fostering an early interest in science and research. After college I worked for the Physics and Astronomy Department at Haverford College where I benefited from the opportunity to work and teach with all the faculty.

This research was supported by Office of Naval Research AASERT contract number N00014-95-1-0824.

# Contents

<b>Abstract</b>	<b>3</b>
<b>Acknowledgments</b>	<b>5</b>
<b>Table of Contents</b>	<b>7</b>
<b>List of Figures</b>	<b>13</b>
<b>List of Tables</b>	<b>19</b>
<b>1 Introduction</b>	<b>23</b>
1.1 Subduction and Oceanic Ventilation . . . . .	23
1.1.1 Transient Tracers . . . . .	25
1.2 Overview of Thesis . . . . .	27
1.2.1 Goals and Scope . . . . .	27
1.2.2 Key Results of Research . . . . .	28
1.3 Review: Laying the Groundwork . . . . .	29

1.3.1	Tritium and $^3\text{He}$ Geochemistry . . . . .	29
1.3.2	Prior Estimates of Ocean Ventilation Determined from Observed Tritium Inventories . . . . .	31
1.3.3	Tracer Age and Mixing . . . . .	32
1.3.4	Circulation of the Eastern North Atlantic Ocean . . . . .	38
1.4	Organization of Thesis . . . . .	49
1.4.1	Structure of the Thesis . . . . .	49
1.4.2	Comments on Methodology . . . . .	50
<b>2</b>	<b>Temporal Evolution of Tritium and <math>^3\text{He}</math> Fields in the Eastern North Atlantic</b>	<b>55</b>
2.1	Treatment of Data . . . . .	55
2.1.1	Data Distribution . . . . .	55
2.1.2	Large-scale Structure of the Tracer Fields . . . . .	62
2.1.3	Interpolation onto Isopycnal Surfaces . . . . .	67
2.2	Statistical Test of Steadiness . . . . .	72
2.2.1	Polynomial Regressions with Only Spatial Regressors . . . . .	76
2.2.2	Polynomial Regressions with Spatial and Temporal Regressors	81
2.3	Comparison with Previous Estimates of Steadiness . . . . .	90
2.4	Evolution of Tracer fields at Bermuda . . . . .	92
2.5	Temporal Changes in Tritium Inventory . . . . .	95
2.6	Summary . . . . .	99

<b>3</b>	<b>Changes in the Physical Circulation as an Explanation of the Observed Evolution of the Tracer Age Field</b>	<b>101</b>
3.1	Circulation Implied by Tritium- <sup>3</sup> He age Field . . . . .	101
3.2	Large-scale Changes in Advection of Subtropics Diagnosed from Hydrography . . . . .	107
3.3	Changes in tritium- <sup>3</sup> He age Relative to the Distribution of Oxygen . .	111
3.3.1	Steadiness of Oxygen field . . . . .	111
3.3.2	Tritium- <sup>3</sup> He Age Regressions Against AOU . . . . .	115
3.4	Summary . . . . .	119
<b>4</b>	<b>Evolution of Tritium-<sup>3</sup>He Age in a One-Dimensional Model of Thermocline Ventilation</b>	<b>123</b>
4.1	The Effects of Mixing on the Tracer Age Balance . . . . .	123
4.2	A Numerical Model . . . . .	128
4.2.1	Model Description . . . . .	128
4.2.2	General Character of Model Results . . . . .	129
4.3	Comparison of Observed Age Tendencies and Numerical Model Simulations . . . . .	134
4.3.1	Contrast with Local Balance Estimates of Diffusivity . . . . .	142
4.4	Tritium Concentrations and Inventory . . . . .	145
4.4.1	The Tritium Concentration – Tracer Age Relation . . . . .	145
4.4.2	Tritium Inventory Calculations . . . . .	148
4.5	Sensitivity to Surface Boundary Condition . . . . .	153
4.5.1	History of Surface Tritium Concentration . . . . .	153

4.5.2	An Idealized Boundary Condition . . . . .	156
4.5.3	Sensitivity of Model Diagnostics to Boundary Condition Uncertainty . . . . .	157
4.6	Summary . . . . .	164
<b>5</b>	<b>Tritium-<sup>3</sup>He Age Evolution in a Two-Dimensional Model of Thermocline Ventilation</b>	<b>169</b>
5.1	Motivation for Extending Model to Two Dimensions . . . . .	169
5.2	Results of Previous Numerical Studies . . . . .	175
5.3	A Two-dimensional Numerical Model . . . . .	180
5.3.1	Description of Model . . . . .	180
5.3.2	General Character of Simulated Tracer Fields . . . . .	185
5.3.3	Comparison with Tracer Observations on $\sigma_\theta = 27.0$ . . . . .	190
5.4	Application of Two-dimensional Model to Other Isopycnals . . . . .	199
5.5	Summary . . . . .	202
<b>6</b>	<b>Discussion</b>	<b>205</b>
6.1	Summary of Thesis Research . . . . .	205
6.2	Comparison of Results with Other Direct Observations of Thermocline Ventilation . . . . .	212
6.2.1	Advective Ventilation of the Lower Thermocline . . . . .	212
6.2.2	Renewal of Thermocline Waters . . . . .	214
6.3	Comparison with Models of Thermocline Ventilation . . . . .	217
6.3.1	Thermocline Theory . . . . .	217



6.3.2	Simulations of Transient Tracers in General Circulation Models	224
6.3.3	Comments on Fickian Parameterization of Mixing . . . . .	226
6.4	Remarks on Information Content of Tracer Age Observations . . . . .	228
6.5	Directions of Future Work . . . . .	232
<b>A</b>	<b>Climatological Hydrographic Atlas</b>	<b>235</b>
<b>B</b>	<b>Scale Analysis and an Analytic Model of Tracer Age Equation</b>	<b>237</b>
B.1	Scale Analysis . . . . .	237
B.1.1	Case I: Steady State . . . . .	240
B.1.2	Case II: Rapidly Changing Tritium Boundary Condition . . . . .	242
B.2	A Simple Analytic Model . . . . .	246
B.2.1	An Example . . . . .	251
<b>C</b>	<b>Diapycnal Mixing Effects</b>	<b>259</b>
C.1	Scale Analysis of Diffusive Ventilation . . . . .	260
C.2	A Numerical Model . . . . .	261
C.2.1	Model Description . . . . .	261
C.2.2	Examples of Model Solutions . . . . .	262
C.2.3	Diapycnal Diffusive Effects on the Evolution of Tritium- <sup>3</sup> He age in the Lower Ventilated Thermocline . . . . .	263
C.3	Conclusions . . . . .	267
	<b>References</b>	<b>269</b>



# List of Figures

1.1	Time history of tritium delivery to North Atlantic ocean . . . . .	30
1.2	Box model of thermocline ventilation based on observed tritium inventory	31
1.3	The effect of mixing on tracer age when tracer concentrations of water samples are different . . . . .	35
1.4	The effect of mixing on tracer age when tracer concentrations of water samples are same . . . . .	36
1.5	Mean curl of wind stress over North Atlantic Ocean . . . . .	39
1.6	Annual average streamfunction of Sverdrup transport . . . . .	40
1.7	Index map marking major surface currents in eastern North Atlantic .	41
1.8	Streamlines of mean geostrophic transport in the upper 200m of the eastern North Atlantic . . . . .	42
1.9	Schematic diagram of path of Azores Current . . . . .	43
1.10	Map of sea surface density in late winter . . . . .	44
1.11	Estimate of subduction rate of North Atlantic . . . . .	46
1.12	Estimate of Eddy Kinetic Energy along 30°W . . . . .	48
2.1	Location of hydrographic stations . . . . .	56
2.2	Upper thermocline distribution of samples as function of time and density	60

2.3	Lower thermocline distribution of samples as function of time and density	61
2.4	Vertical sections of properties along 25°W . . . . .	63
2.5	Vertical sections of transient tracer fields along 25°W . . . . .	65
2.6	Analytic uncertainty of tritium measurements . . . . .	68
2.7	Example of interpolation error for $^3\text{He}$ profile . . . . .	70
2.8	Number and standard error of age estimates on isopycnal surfaces . .	71
2.9	Example of uncertainty of age estimate following a parcel of water . .	72
2.10	Summary of results of steady multiple regression model . . . . .	77
2.11	Uncertainty in age estimate on an isopycnal due to granularity introduced by mesoscale variability . . . . .	78
2.12	Summary of results of steady multiple regression model accounting for mesoscale variability . . . . .	80
2.13	Normalized residuals on $\sigma_\theta = 27.0$ from linear polynomial regression with only spatial regressors . . . . .	82
2.14	Summary of results of time-dependent multiple regression model . . .	83
2.15	Normalized residuals on $\sigma_\theta = 26.5$ from first order time-dependent polynomial regression . . . . .	84
2.16	Summary of regression model results for tritium- $^3\text{He}$ age on isopycnal surfaces in eastern North Atlantic . . . . .	87
2.17	Age and age tendency on isopycnal surfaces determined from time-dependent multiple regression model . . . . .	88
2.18	Tracer age field on $\sigma_\theta = 27.0$ in 1981 and 1992 predicted from multiple regression model . . . . .	89
2.19	Direct observations of tracer age field on $\sigma_\theta = 27.0$ in 1981 and 1992.	90

2.20	Comparison of two profiles of tritium- <sup>3</sup> He age separated in time by 3.5 years . . . . .	91
2.21	Time series of tritium and tritium- <sup>3</sup> He age at Bermuda . . . . .	93
2.22	Tracer age and age tendency estimated at Bermuda for 1986 . . . . .	94
2.23	Summary of regression model of tritium concentration on isopycnal surfaces in eastern North Atlantic . . . . .	96
2.24	Tritium concentration and temporal tendency of tritium estimated at Bermuda for 1986 . . . . .	98
3.1	Tritium- <sup>3</sup> He age on isopycnal surfaces in lower eastern Atlantic thermocline . . . . .	103
3.2	Velocity field diagnosed from tritium- <sup>3</sup> He age distribution in figure 3.1	103
3.3	Comparison of meridional velocity profile calculated from geostrophic shear and tracer age gradients . . . . .	104
3.4	Time evolution of isopycnal velocity profile deduced from tritium- <sup>3</sup> He age field . . . . .	106
3.5	Velocity difference between $\sigma_\theta = 26.8$ and $27.1$ implied by time-dependent regression to tracer age field . . . . .	107
3.6	Position of hydrographic stations used to calculate gradient of dynamic height in eastern subtropical North Atlantic . . . . .	108
3.7	Time series of dynamic height at 250 dbar referenced to 500 dbar . .	109
3.8	Meridional geostrophic velocity shear between 250 and 500 dbar . . .	110
3.9	Summary of regression model applied to dissolved oxygen concentration on isopycnal surfaces in eastern North Atlantic . . . . .	112
3.10	Distribution of Apparent Oxygen Utilization on $\sigma_\theta = 26.7$ . . . . .	114
3.11	Tritium- <sup>3</sup> He age vs Apparent Oxygen Utilization (AOU) on $\sigma_\theta = 27.0$	115

3.12	Regression coefficients of time-dependent regression of tracer age against AOU . . . . .	117
3.13	Comparison of tendency of tritium- <sup>3</sup> He age field on isopycnal surfaces derived from two independent methods . . . . .	118
4.1	Schematic diagram of one-dimensional model of thermocline ventilation	126
4.2	Time history of surface concentration of <sup>3</sup> H for subtropical North Atlantic	129
4.3	Time-Space diagrams of tracer evolution in one-dimensional model for radiotracer Péclet number = 56 . . . . .	130
4.4	Time-Space diagrams of tracer evolution in one-dimensional model for radiotracer Péclet number = 5 . . . . .	131
4.5	Temporal evolution of tracer age and balance of terms for Péclet number 56 . . . . .	133
4.6	Temporal evolution of tracer age and balance of terms for Péclet number 5 . . . . .	134
4.7	Age tendency vs. mean tracer age in 1986 determined from observations	136
4.8	Age tendency vs. tracer age in 1986 determined from one-dimensional model . . . . .	137
4.9	Lateral diffusivity implied by diagnosed Péclet number and geostrophic velocity scale . . . . .	141
4.10	Implicit length scale for lateral diffusivity estimate . . . . .	142
4.11	Primary balance of terms in the tracer age equation evaluated at 1986.	143
4.12	Tritium concentration vs. mean tracer age in 1986 determined from observations . . . . .	146
4.13	Tritium concentration vs. tracer age in 1986 determined from one-dimensional model . . . . .	147

4.14	Tritium inventory in model domain in 1972 as function of advective and diffusive strengths . . . . .	150
4.15	Tritium inventory in model domain in 1986 as function of advective and diffusive strengths . . . . .	152
4.16	Surface tritium concentration in decay normalized Units . . . . .	154
4.17	Idealized history of the surface tritium concentration . . . . .	157
4.18	Idealized tritium boundary condition and examples of assigned uncertainty . . . . .	158
4.19	Sensitivity of temporal tendency of tracer age to uncertainty in surface tritium history . . . . .	161
4.20	Sensitivity of tritium concentration to uncertainty in surface tritium history . . . . .	163
5.1	Diagram of the potential density of late winter deep convective mixed layers . . . . .	170
5.2	Distribution of Apparent Oxygen Utilization on $\sigma_\theta = 27.0$ . . . . .	172
5.3	Pressure anomaly Montgomery streamfunction on $\sigma_\theta = 27.0$ . . . . .	173
5.4	Schematic of two-dimensional gyre model . . . . .	175
5.5	Schematic diagram of Flow in Directly Ventilated Region . . . . .	177
5.6	Schematic diagram of Flow in Diffusively Ventilated Region . . . . .	178
5.7	Streamfunction for modified Stommel Gyre . . . . .	182
5.8	Fraction of gyre directly ventilated as function of outcrop position and sharpness of eastward jet . . . . .	183
5.9	Simulated tracer fields for Péclet number = 15 and surface outcrop position north of Azores Current . . . . .	187

5.10	Simulated tracer fields for Péclet number = 3 and surface outcrop position north of Azores Current . . . . .	188
5.11	Sensitivity of tracer fields to sharpness of Azores Current . . . . .	192
5.12	Sensitivity of tracer fields to direct versus diffusive ventilation . . . . .	193
5.13	Sensitivity of tracer fields to position of surface outcrop . . . . .	195
5.14	Sensitivity of tracer fields to diffusive time scale of stagnant region . . . . .	197
5.15	Schematic of implied ventilation on $\sigma_\theta = 27.0$ . . . . .	198
5.16	Tritium inventory and age tendency as function of diffusive time-scale for isopycnals spanning thermocline . . . . .	200
6.1	Simulated tracer fields of gyre model superposed on streamlines of flow	213
6.2	Mass source determined from integral air/sea buoyancy flux for North Atlantic Ocean . . . . .	215
6.3	Ventilation rate of isopycnals estimated from tritium inventory of North Atlantic subtropical thermocline. . . . .	216
6.4	Flow patterns on $\sigma_\theta = 26.8$ and $27.1$ from idealized thermocline model of North Atlantic. . . . .	218
6.5	Potential vorticity and tracer age in a numerical model of the ventilated thermocline . . . . .	223
6.6	Relation between tritium and $^3\text{He}$ in the North Atlantic . . . . .	231
6.7	Temporal evolution of $^3\text{He}$ -tritium relation in subtropical thermocline	232
B.1	$^3\text{H}$ and $^3\text{He}$ distribution for one-dimensional model with steady surface $^3\text{H}$ boundary concentration . . . . .	241
B.2	$^3\text{H}$ and $^3\text{He}$ distribution for one-dimensional model with rapidly increasing $^3\text{H}$ boundary concentration . . . . .	243



B.3	Schematic of pseudo-advective forcing function . . . . .	247
B.4	Schematic of regions of solution of analytic age equation . . . . .	248
B.5	Solution of analytic age balance . . . . .	252
B.6	Temporal evolution of age at fixed point as a function of pseudo-advective forcing . . . . .	253
B.7	Time evolution of balance of terms in analytic model . . . . .	255
C.1	Schematic diagram of diapycnal ventilation numerical model . . . . .	261
C.2	Simulated tracer fields of diapycnal model in 1986 . . . . .	264
C.3	Space time diagram of tracer fields in diapycnal model . . . . .	265
C.4	Space time diagram of tracer age on $\sigma_\theta = 27.0$ for different values of diapycnal diffusivity . . . . .	267

# List of Tables

2.1	Summary of cruises measuring $^3\text{H}$ and $^3\text{He}$ . . . . .	58
2.2	Summary of isopycnal surfaces used in analysis . . . . .	59
2.3	F-test results for polynomial model with only spatial regressors . . . .	81
2.4	F-test results for polynomial model with temporal and spatial regressors	85
2.5	F-test results for significance of curvature in a polynomial model with temporal and spatial regressor . . . . .	86
4.1	Radiotracer Péclet numbers estimated from data and one-dimensional ventilation model . . . . .	138
4.2	Ventilation Péclet numbers estimated from radiotracer Péclet number and observed ventilation time . . . . .	140
4.3	Idealized history of surface tritium concentration . . . . .	159
4.4	Previous estimates of lateral diffusivity in the eastern North Atlantic .	168
5.1	Parametric range explored with two-dimensional model . . . . .	185
6.1	Péclet number estimates at different levels of of Atlantic isopycnic nu- merical model . . . . .	225
A.1	Summary of data added to climatological hydrographic atlas . . . . .	236

C.1 Comparison of diffusive time scale point in the main thermocline of the eastern North Atlantic . . . . .	260
---	-----



# Chapter 1

## Introduction

### 1.1 Subduction and Oceanic Ventilation

Communication between the atmosphere/ocean interface and the oceanic interior is a key concern for gauging the oceanic role in global climate as well as for developing theories of the forced circulation of the oceans. Properties imposed on the surface boundary of the ocean spread into the interior through a combination of advection and mixing which, lumped together, ventilate the ocean. Subduction refers to the actual fluid transfer from the surface mixed layer into the stratified thermocline. This thesis explores the ventilation of the permanent thermocline of a subtropical gyre. The ventilation and renewal of waters within the permanent thermocline occurs on time-scales of decades: short compared to the response time of the deep ocean (centuries) but long compared to the surface mixed layer (hours to days) or the seasonal thermocline (months).

It has been long noted that the temperature-salinity relation of the North Atlantic thermocline is similar to the temperature-salinity relation of the surface waters

in winter. *Montgomery* [1938] and *Iselin* [1939] were the first to argue that this was more than coincidence and rather, reflected the process whereby surface properties invaded the oceanic thermocline by lateral advection and mixing primarily along isopycnal surfaces. The basic concept was refined by [*Woods*, 1985] who noted that spatial changes in the winter mixed layer depth lead to the possibility of lateral subduction as well as directly forced Ekman pumping. The notion that ventilating flow follows isopycnal surfaces has served as a foundation for both analytic [*Luyten, Pedlosky and Stommel*, 1983] and numeric [*Bleck et al.*, 1992; *New et al.*, 1995] models of ocean circulation. Measurements of anthropogenically produced tracers in the ocean [*Rooth and Östlund*, 1972; *Jenkins*, 1980; *Fine, Reid and Östlund*, 1981; *Sarmiento, Rooth and Roether*, 1982; *Fine, Peterson and Östlund*, 1987] support the notion that introduction of the surface properties into the interior thermocline is largely confined to transport along isopycnal surfaces and that diapycnal effects are small.

Ventilation and renewal of waters within the ocean is a critical process in the oceanic response to changes in global climate. Atmospheric carbon dioxide levels are currently rising in response to the combustion of fossil-fuels. The increased concentration of atmospheric CO<sub>2</sub> alters the radiative balance of the earth which may lead to warmer global temperatures. Given the large inventory of carbon in the ocean compared to the atmosphere, the ultimate fate of the bulk of this anthropogenic carbon dioxide will be dissolution within the ocean [*Broecker et al.*, 1979]. The rate at which the oceans take up and therefore partly mitigate the increased atmospheric carbon signal depends on the rate of ventilation. Simple models of thermocline ventilation demonstrate that the oceanic uptake of anthropogenic carbon-dioxide is limited by the ventilation of the shielded layers of the ocean rather than the rate of air/sea gas exchange [*Peng and Broecker*, 1985]. Estimates of the present response of the oceanic carbon inventory to the changing carbon cycle are controversial [*Tans, Fung and Takahashi*, 1990; *Sarmiento and Sundquist*, 1992; *Quay, Tilbrook and Wong*, 1992; *Keeling*

and Shertz, 1992]. An improved understanding of the physical processes of ventilation and subduction are crucial for quantifying the present rate of oceanic carbon uptake as well as predicting how this rate may change in the future as part of a changing climate.

Ventilation of the ocean also provides a framework for our dynamical understanding of the upper-ocean circulation. Theories attempting to explain the dynamics of the oceanic thermocline foundered for many years as investigators attempted to solve the complex, nonlinear density and pressure equations with similarity solutions [Pedlosky, 1987]. Simplification of the problem through the use of layer models [Rhines and Young, 1982a; Luyten, Pedlosky and Stommel, 1983] eventually led to significant advancement and a proliferation of analytically tractable models of the baroclinic structure of the upper-ocean circulation. The key component for the solution of these models is the specification of the potential vorticity field. In the model constructions of Luyten, Pedlosky and Stommel [1983], ventilation plays a primary role for determining the potential vorticity structure of the upper ocean. The potential vorticity is determined by its value along the surface outcrop of the isopycnal: after subduction, potential vorticity of the fluid is preserved along the streamlines of the flow. A necessary component of these models is the assumption of weak dissipation (both isopycnal and diapycnal) within the thermocline. Although the layered models of the thermocline have provided an important context for the interpretation of ocean circulation, the key assumption that advection alone determines the structure of property fields is poorly tested.

### 1.1.1 Transient Tracers

Transient tracers offer an appealing tool for studying the ventilation of the ocean. Transient tracers are, by definition, tracers whose concentrations in the environment

change over time. These tracers are deposited into the surface ocean and observations of their subsequent entry into the subsurface interior have been interpreted as markers of the major pathways of oceanic ventilation [*Jenkins and Rhines*, 1980; *Bullister and Weiss*, 1983; *Weiss et al.*, 1985; *Fine, Peterson and Östlund*, 1987; *Fine and Molinari*, 1988; *Östlund and Rooth*, 1990; *Fine et al.*, 1994]. The presence of these transient tracers in the atmosphere and oceans is an unintentional byproduct of anthropogenic activity: nuclear weapons testing ( $^{14}\text{C}$ , tritium,  $^{90}\text{Sr}$ ) or industrial chemical manufacturing (carbon tetrachloride, chloroflourocarbons). To be useful for physical oceanographic study, a transient tracer must meet three criteria:

- Anthropogenic production rates must exceed (at least temporarily) any natural (e.g. cosmogenic, terrigenous or biogenic) production.
- The chemical or isotopic tracers must be analytically detectable at low concentrations after dilution within the ocean.
- The history of input to the ocean must be reasonably well known.

Anthropogenic tracers enter the ocean through a combination of atmospheric deposition/exchange and river runoff. Once deposited into the surface ocean, the process of oceanic ventilation carries the signature of the transient tracers into the interior.

The same feature that provides the utility of transient tracers, their changing concentrations with time, also complicates their use for quantitative interpretation of oceanic ventilation. The kinetic energy of the ocean is spread across a wide range of spatial and temporal scales [*Wunsch and Stammer*, 1995]. Direct observations of oceanic fields are limited and most fields are severely undersampled. Frequently, oceanic data are interpreted under an assumption of steadiness so that observations gathered at different points in time may be combined. The difficulties of interpreting an undersampled data set are amplified for transient tracers since an assump-



tion of steadiness is clearly invalid. On the other hand, transient tracers function as Lagrangian integrators over the time-scale of their ventilation so that the large-scale tracer distributions reflect an average over higher-frequency and non-dissipative motions [Jenkins, 1987]. Additionally, transformation of the tracer concentrations into an “age” estimate yields a directly measurable quantity which may, under some circumstances, be steady over time, offering the opportunity to minimize at least the severest problems of undersampling. The concept of tracer age will be further developed below (§1.3.3) and the interpretation of tracer age is a theme of this thesis.

## 1.2 Overview of Thesis

### 1.2.1 Goals and Scope

This thesis addresses two related questions:

- Is an advectively dominated model of thermocline ventilation valid? What processes are responsible for the communication of surface conditions into the subsurface ocean interior? Are the roles of mixing and dissipation really of secondary importance to advection for renewal of subsurface properties?
- What do transient tracers tell us about ventilation? Do observations of transient tracers yield any information about ocean circulation that is not contained in more “traditional” oceanic measurements: e.g. oxygen, salinity and temperature? What is the impact of diffusion on the observed fields of transient tracers? What types of sampling strategies will best utilize the information contained in the ventilation of transient tracers?

## 1.2.2 Key Results of Research

This thesis presents an analysis of two, coupled transient tracers,  $^3\text{He}$  and tritium, in the subtropical thermocline of the eastern North Atlantic. The observed temporal evolution of  $^3\text{H}$  and  $^3\text{He}$  in the lower thermocline are inconsistent with a model of ventilation which only includes advection by a mean flow. Lateral mixing is determined to be a crucial component in the renewal and evolution of properties in the lower thermocline ( $\sigma_\theta \geq 26.8$ ). Although lateral mixing effects are also apparent in the upper thermocline ( $\sigma_\theta \leq 26.7$ ), they have less impact than advection.

This thesis also highlights a new approach for utilizing transient tracer data. Previous analysis has emphasized the use of transient tracer inventories to estimate the net ventilation rate. Other analysis has demonstrated how the coupled tritium- $^3\text{He}$  system forms a tracer age, or “clock”, which can then be used to estimate circulation speeds and the rates of large-scale biological processes. This thesis examines a measure of bulk mixing rates based on the difference between the observed tritium- $^3\text{He}$  ratio and that expected for a purely advective flow. Tritium- $^3\text{He}$  age forms a convenient diagnostic for examining the coupling between  $^3\text{He}$  and tritium. Unlike a tracer inventory calculation which determines the sum of advective and diffusive ventilation, a diagnostic based on the ratio of coupled transient tracers (e.g. tritium- $^3\text{He}$  age ) yields an estimate of the relative contributions of advective and diffusive effects on the renewal of subsurface properties. The effects of mixing on the instantaneous spatial fields of  $^3\text{H}$  and  $^3\text{He}$  are somewhat subtle and difficult to assess accurately. The present analysis emphasizes the temporal evolution of the tracer fields for which the impact of mixing becomes more apparent. Tritium- $^3\text{He}$  age is found to be a useful diagnostic for observing the effects of mixing in the ventilation of the ocean.

## 1.3 Review: Laying the Groundwork

This section reviews previous relevant work. First, the geochemistry of tritium and  $^3\text{He}$  will be discussed with an emphasis on input rates to the North Atlantic Ocean. Second, estimates of thermocline ventilation based on simple models of the observed tritium inventory are discussed. Next, the concept of tracer age dating is developed as an alternative approach to studying oceanic ventilation with transient tracer data. The impact of mixing on tracer age is a key focus of the present analysis and a pair of simple examples is presented to illustrate the bias that mixing can introduce to a tracer age field. Finally, the circulation of the study region, the eastern North Atlantic, is reviewed concentrating on ventilation and the mean circulation.

### 1.3.1 Tritium and $^3\text{He}$ Geochemistry

Though tritium is naturally produced by incident cosmic rays in the upper atmosphere, tritium produced by the detonation on thermonuclear fusion bombs dominates the modern global inventory [Roether, 1989a]. Tritium is present in the ocean and global hydrological cycle as tritiated water molecules:  $^3\text{H-H-O}$ . Typical tritium concentrations in the upper ocean are 1  $^3\text{H}$  atom per  $10^{17}$ - $10^{18}$  hydrogen atoms. Three principle paths delivered bomb-produced  $^3\text{H}$  into the surface ocean: precipitation, river run-off and water vapor exchange. Deposition into the ocean was greatest at the higher latitudes of the northern hemisphere. An estimate of the history of the tritium input for the North Atlantic Ocean [Doney, Jenkins and Östlund, 1993] is shown in figure 1.1. The input peaked in the early 1960's and decreased rapidly after the signing of the atmospheric test ban treaty in 1963. The uncertainty of the early portion of the tritium budget is difficult to assess; the reconstruction of the tritium history depends on details of the global hydrological cycle and the isotopic fractionation of tritium in water vapor and precipitation. Detailed discussions of the calculation and associated

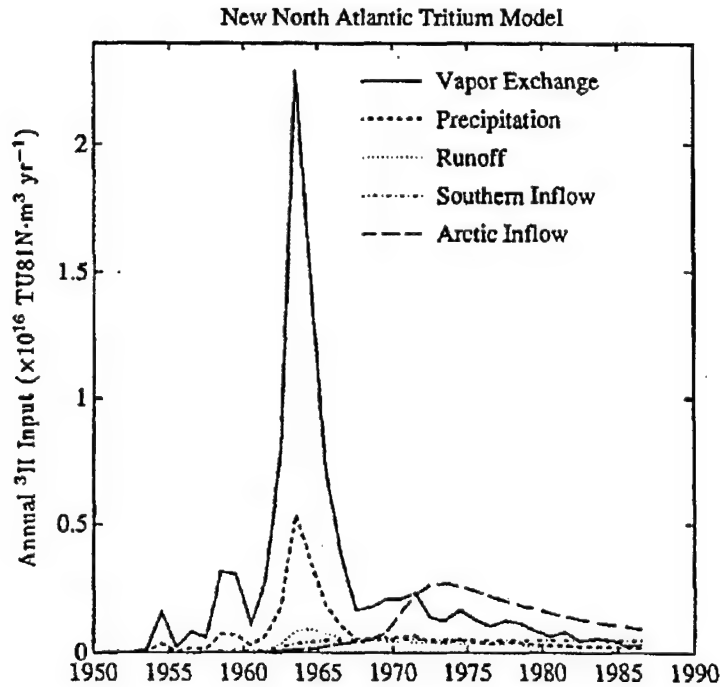


Figure 1.1: Time history of tritium delivery to North Atlantic ocean, 15°–64°N (reproduced from *Doney, Jenkins and Östlund* [1993]). The different line types represent different pathways as labeled on the figure.

uncertainties of the terms represented figure 1.1 can be found in *Doney, Jenkins and Östlund* [1993], *Weiss and Roether* [1980] and *Koster et al.* [1989]. *Doney, Jenkins and Östlund* [1993] assess the uncertainty in the cumulative tritium input through 1981 to be approximately 18%.

Tritium decays radioactively with a half-life of 12.43 yr to  $^3\text{He}$ , a stable, inert isotope of helium. Seawater exposed to the atmosphere equilibrates its gaseous  $^3\text{He}$  burden with atmospheric values on time scales of a few weeks [*Doney and Jenkins*, 1988]. Due to its low molecular weight, atmospheric concentrations of helium are quite small and the equilibrium value of  $^3\text{He}$  in seawater can be accurately calculated as a function of temperature and salinity [*Jenkins*, 1988a; *Roether*, 1989b]. In subsurface waters,  $^3\text{He}$  concentrations above the equilibrium value, often referred to as “excess”  $^3\text{He}$ , originate from two sources: 1) radioactive decay of tritium and 2) injection of terrigenic primordial  $^3\text{He}$  at the sea floor. In the deep ocean, especially the deep

Pacific Ocean, the primordial component of  $^3\text{He}$  dominates the observed distribution. In the upper ocean, especially the North Atlantic, the primordial component of  $^3\text{He}$  is small [Doney, Jenkins and Bullister, 1997] and the observed  $^3\text{He}$  distribution can be interpreted as the result of tritium-decay in subducted waters.

### 1.3.2 Prior Estimates of Ocean Ventilation Determined from Observed Tritium Inventories

The observed tritium field has served as the basis for diagnostic estimates of the bulk ventilation rates of the North Atlantic thermocline. Sarmiento [1983] formed a simple layered box model, oriented along isopycnal surfaces (figure 1.2). He used the

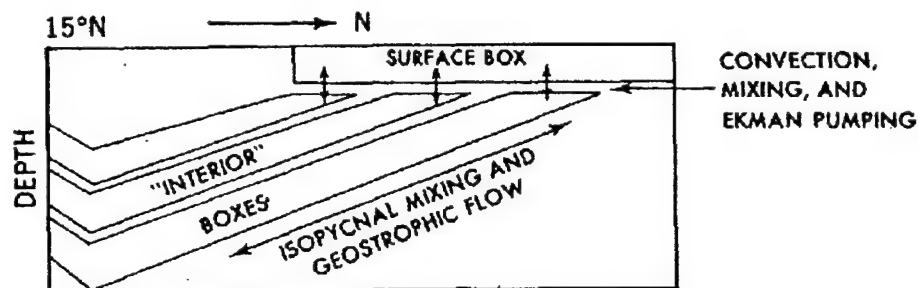


Figure 1.2: Box model of thermocline ventilation based on observed tritium inventory (reproduced from Sarmiento [1983])

observed inventory of  $^3\text{H}$  from the 1972 GEOSECS survey, conducted approximately 7 years after the peak tritium input, in conjunction with an estimate of the history of surface tritium input to determine the bulk exchange rate between the surface mixed layer and the thermocline interior. Estimated exchange rates of the middle and lower thermocline ( $\sigma_\theta \geq 26.4$ ) greatly exceeded the rate of downward Ekman pumping for these density classes, suggesting the need for significant lateral subduction at these levels.

Subsequent investigation by Wunsch [1988a] and Mèmerly and Wunsch [1990] demonstrated that the ventilation exchange rates implied by the observed tritium distribution in the North Atlantic were consistent with those determined from geostrophic transports calculated from the observed density field. The uncertainty in the history of tritium input, especially at open boundary conditions of the model domain, was large enough that the addition of tritium data did not refine their circulation models based on geostrophy and steady-state tracer distributions.

A measure of tracer inventory, e.g. mean tritium concentration, provides an estimate of the bulk ventilation of the thermocline, however it cannot distinguish whether the ventilation is the result of advective subduction or lateral mixing. Both the box models of Sarmiento [1983] and Wunsch [1988a] employ a bulk transport term to model the exchange of properties between finite, boxed regions of the model. Sarmiento defines the bulk transport term to represent the net effects of advection and diffusion. Wunsch [1988a] invokes a similar term to represent the combined effects of advection and diffusion, however, he employs the same bulk transport terms to form a linear vorticity constraint on the model, implicitly casting the exchange terms as advective geostrophic transports. The ability of advective models [Wunsch, 1988a; Mèmerly and Wunsch, 1990] to reproduce the observed tritium concentrations without explicit inclusion of mixing processes suggests that the lateral diffusive transport of tritium cannot be resolved by calculations based on the observed inventory of a single transient tracer

### 1.3.3 Tracer Age and Mixing

Measurements of multiple tracers can be combined to form diagnostics which both minimize the uncertainties of the surface boundary condition and may be steady over time [Thiele and Sarmiento, 1990]. One such derived quantity is tracer “age” which

has the added appeal of being an approximation of the elapsed time since a measured water parcel was resident in the surface mixed layer. Tritium and  $^3\text{He}$  measurements may be combined with the known e-folding time-scale of the radioactive decay,  $\lambda$  to yield the tritium- $^3\text{He}$  age,  $\tau$  [Jenkins and Clarke, 1976]:

$$\tau = \frac{1}{\lambda} \log_e \left( 1 + \frac{^3\text{He}}{^3\text{H}} \right). \quad (1.3.1)$$

Tracer ages may also be computed from observed chloroflourocarbon (CFC) concentrations using either the known evolution of atmospheric ratios or the apparent partial pressure.

Tritium- $^3\text{He}$  age serves as an unbiased diagnostic of the true ventilation age only if two conditions are met. First, the initial, surface concentration of  $^3\text{He}$  must be observed or calculable. Second, after subduction, the  $^3\text{H}$  and  $^3\text{He}$  constituents of a water parcel must evolve solely due to the radioactive mutation of tritium into  $^3\text{He}$ : changes in concentration due to mixing with surrounding water may lead to significant biases in the tracer age as this analysis will show. If both of these conditions are satisfied, however, interpretation of a tracer age diagnostic offers some significant advantages over the individual tracer fields. For a steady circulation, the tracer age field will be steady, even though the separate  $^3\text{He}$  and  $^3\text{H}$  fields evolve, and data collected at different times may be combined to form a single realization of the age field. Additionally, the tracer age is independent of the initial  $^3\text{H}$  content of the water parcel (it only depends on the ratio of  $^3\text{He}$  and tritium) and thus uncertainties in the tritium boundary condition are avoided.

The first of these conditions is reasonably well satisfied. The  $^3\text{He}$  content of surface water equilibrates with the known atmospheric concentration in a few weeks. The effect of finite equilibration time is expected to be greatest in the deepest winter mixed layers and Doney and Jenkins [1988] discuss the impact this may have on observed tritium- $^3\text{He}$  age fields. The impact of finite  $^3\text{He}$  equilibration time should be minimal in the North Atlantic subtropical thermocline.

The second condition, no change in concentration through mixing with surrounding water parcels, is almost certainly not satisfied, however. The importance of lateral mixing in the thermocline has been known since the early work of *Iselin* [1939]. Additionally, the meaning of "age" in the presence of mixing is ambiguous since any given water parcel will be composed of water with a myriad of ages. In such a situation, "age" might best be defined as the volume-weighted mean of the elements composing the water parcel rather than a true advective age. Tracer age, being a function of the ratio of two concentrations, does not mix linearly when fluids of differing age values are combined and thus the resultant tracer age does not equal the true mean age. Figures 1.3 and 1.4 illustrates this for the simple case when two parcels of different ages are combined and thoroughly mixed. The resulting age of the mixed parcel is a weighted average of the individual parcels where the relative weights are a function of the net tracer concentration of each parcel. The example in figure 1.3 illustrates a case where the younger water parcel has a greater concentration of tracer. This situation is analogous to the entry of bomb-tritium into the thermocline since the large increase in bomb-produced tritium inventory will first elevate the tracer burden of the "youngest" water. In this example, the tritium- $^3\text{He}$  age of the mixed water parcel is biased young compared to the true mean age of the two initial water samples.

Figure 1.4 displays a situation where the two water parcels have the same initial age as figure 1.3 but in this case the net tracer concentrations of each initial sample are also the same. This situation is analogous to a steady-state boundary condition for tritium since the net concentration of tracer,  $^3\text{He}$  plus tritium, is independent of the age of the parcel. In this case the resultant tracer age is still not equal to the mean age of the initial parcels, however, the magnitude of the bias is much less than that in figure 1.3. The nonlinearity of the radioactive decay introduces a slight bias under mixing even when the total concentrations of the initial parcels are equal.



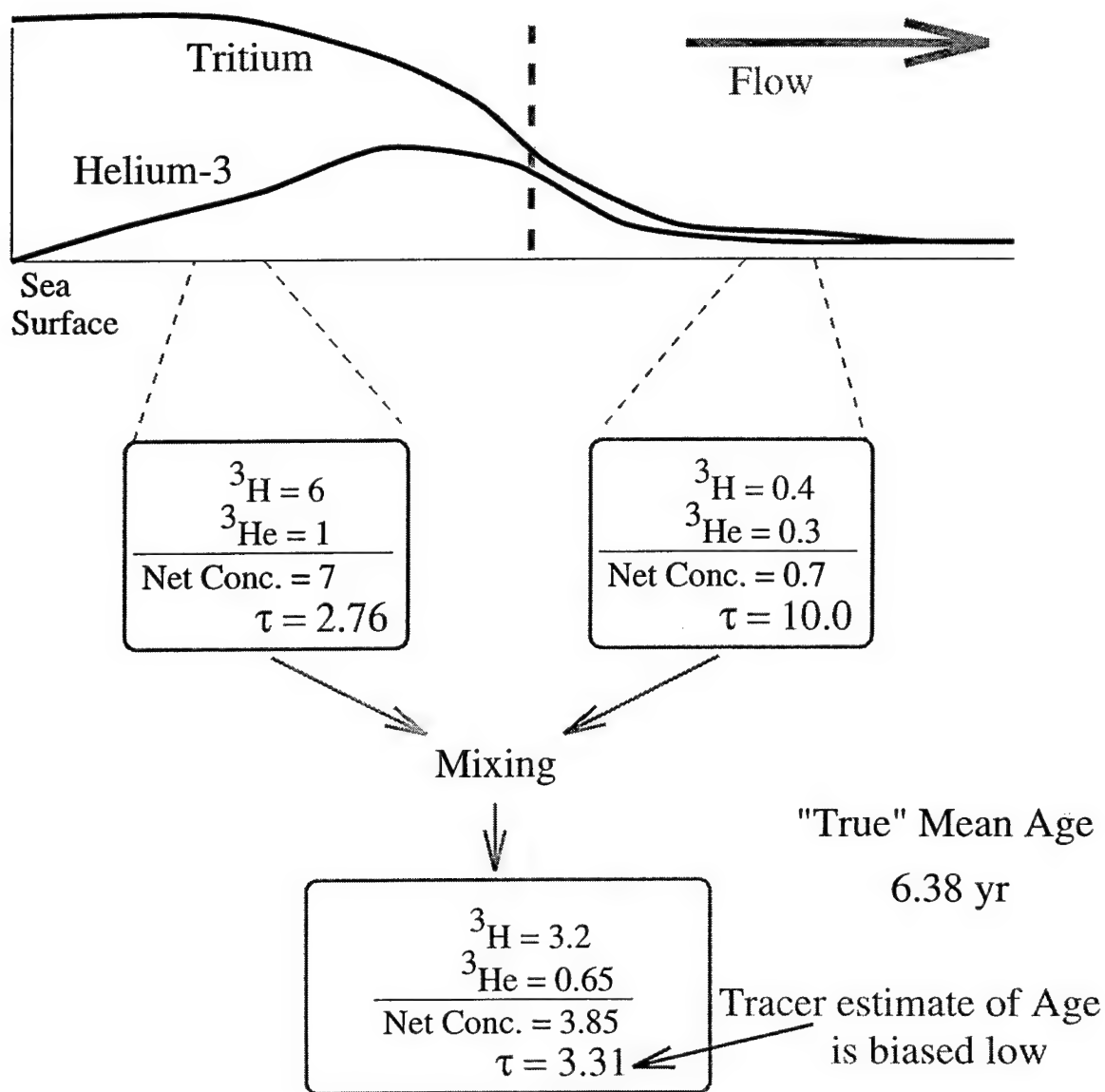


Figure 1.3: The effect of mixing on tracer age when tracer concentrations of the water samples are different. Schematic shows the resulting tracer concentration (TU) and age (yrs) when two water parcels of equal volume shown in upper row are combined and mixed. The volume-weighted age of the initial samples is 6.38 yr. Inventory is defined as the sum of the  ${}^3\text{He}$  and  ${}^3\text{H}$  concentrations. When the initial concentrations are markedly different, the resulting tracer age is biased towards the sample with greater tracer inventory.

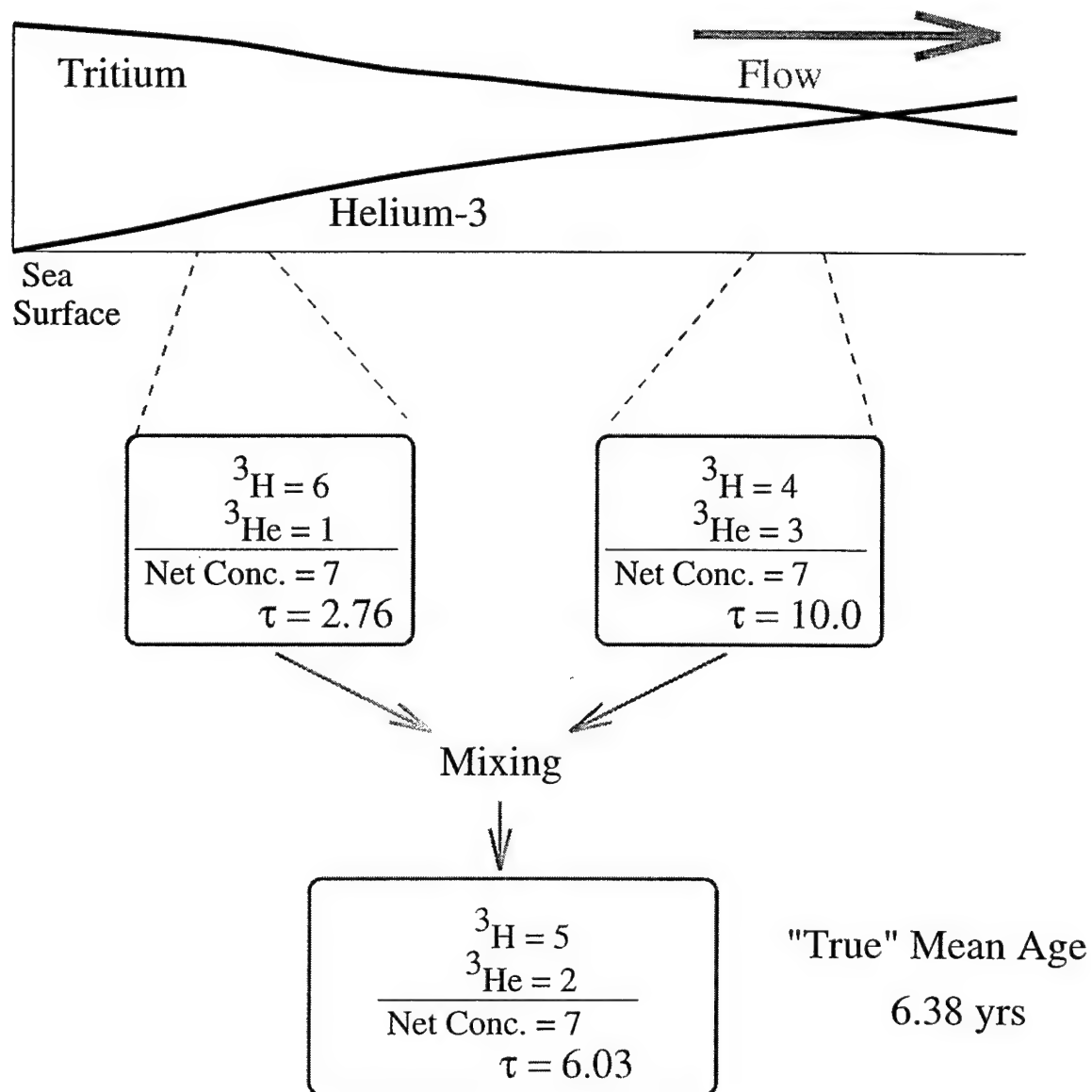


Figure 1.4: The effect of mixing on tracer age when tracer concentrations of the initial water samples are the same. Schematic shows the resulting tracer concentration (TU) and age (yrs) when two water parcels shown in upper row are combined and mixed. The true mean age of the initial samples is 6.38 yr. Inventory is defined as the sum of the  $^3\text{He}$  and  $^3\text{H}$  concentrations. Even in the case when the initial tracer inventories are identical, the resulting tracer age is slightly biased due to the nonlinear radioactive decay.

In the ocean, mixing is continuous and not well represented by these simple scenarios which thoroughly blend two initially separate water parcels. Nonetheless, the illustrations above represent an extreme example of the distortion that mixing can introduce to a tracer age field. Because of these effects of mixing, one expects the diagnostic determined by tritium- $^3\text{He}$  age to be a slightly imperfect measure of the "true" age of a water parcel. Given an independent estimate of the mean age of a water parcel, the discrepancy of the measured tritium- $^3\text{He}$  age from this value could serve as an indicator of the degree of mixing. An independent estimate of a parcel's age requires very precise estimates of the global circulation field. For example, if the mean absolute circulation were well known (determined for instance from geostrophy and direct current measurements), one could estimate the true advective age of a parcel and compare this with the observed tracer age. A discrepancy in the spatial gradient of the advective age with that of the tracer would signal a distortion of the age field introduced by mixing. In practice, however, the small difference between the spatial gradients of the true advective age and the observed tracer age is not easily resolved given the observational uncertainty in determining these fields.

An analysis based on the temporal evolution of tracer age offers an alternative approach for diagnosing the distortion of the tracer age field created by mixing effects. The penetration of the bomb-produced tritium into the ocean will initially increase the net tracer concentrations of the youngest waters. Older waters will have subducted prior to the peak input and thus have lower tritium and  $^3\text{He}$  inventories. Therefore, any effects of mixing, early in the oceanic adjustment to the bomb-tritium, will be analogous to the example in figure 1.3: young waters with high tracer load mixing with old waters with lower inventory. The result of mixing in this scenario, as shown in the simple cartoon, is to bias the tracer age young compared to the actual mean advective age. Over time, however, as the elevated bomb-tritium concentrations wash deeper into the thermocline, one expects the spatial structure of the tracer concentration to

tend towards homogenization.<sup>a</sup> Therefore, at a later date, the example where all water parcels have comparable inventories of tracer (illustrated in figure 1.4) more accurately represents the effects of mixing within the ocean. The degree of bias mixing introduced to the tracer age field will be reduced in comparison to the earlier time period and temporal observations of the age field will show a trend towards older ages. The temporary bias towards younger ages and subsequent recovery in the tracer age field will only occur if mixing effects are significant. If mixing is a minor component of the advective-diffusive balance of  $^3\text{He}$  and tritium, the tracer age will be steady, assuming a steady circulation, regardless of the sudden increase in tritium concentrations resulting from the atmospheric bomb tests. This suggests that monitoring the temporal changes in the apparent tracer may provide an accurate diagnostic of the bulk mixing effects during the ventilation of the transient tracers. The distortion that the tracer age field suffers in response to the large step input of bomb-tritium will be more thoroughly analyzed in a formal scale analysis of the advective-diffusive age equation in §B.1.

### 1.3.4 Circulation of the Eastern North Atlantic Ocean

The transient tracer data analyzed in this thesis come from hydrographic surveys in the eastern subtropical North Atlantic (centered at approximately  $25^\circ\text{N}$ ,  $30^\circ\text{W}$ ). This section discusses the general circulation in the eastern North Atlantic with an emphasis on subduction and the origin of waters which flow into this region.

---

<sup>a</sup>Observations of the temporal development of the isopycnic distribution of tritium [Sarmiento, Rooth and Roether, 1982; Jenkins, 1988a] show a clear tendency towards reduced spatial gradients and homogenization with time.

## Wind Forcing

The surface forcing of the subtropical North Atlantic is characterized by negative wind-stress curl and convergence in the surface Ekman layer. This must result in downward pumping of surface waters which, assuming a linear vorticity balance of the ocean interior, requires southward meridional flow. Figure 1.5 illustrates an estimate

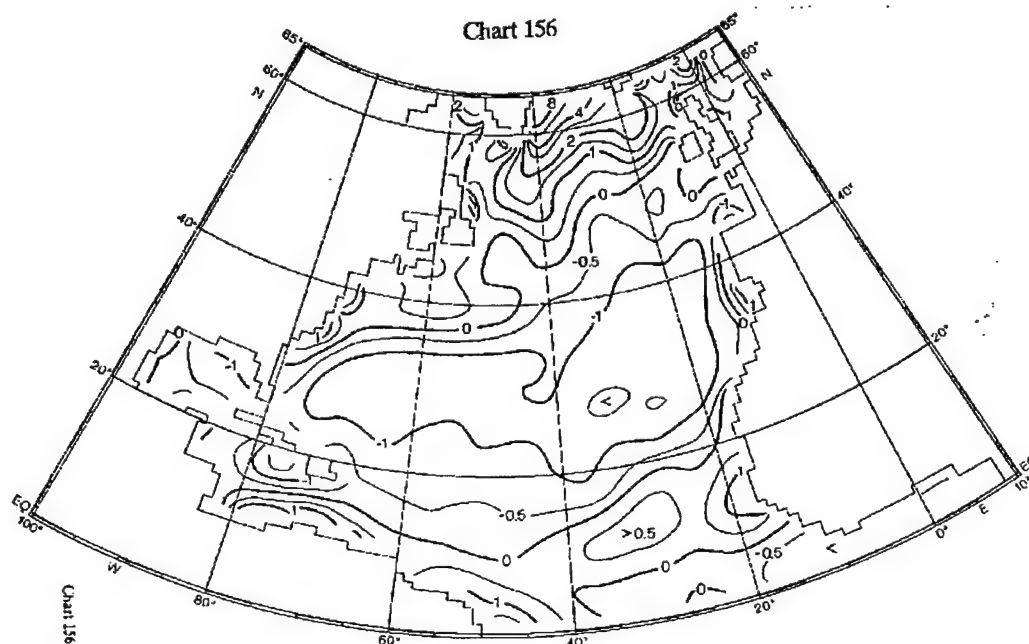


Figure 1.5: Mean curl of wind stress ( $10^{-7} \text{ N m}^{-3}$ ) over North Atlantic Ocean (re-produced from *Isemer and Hasse* [1987]).

of the annual average curl of the wind stress. Negative curl is observed throughout the eastern Atlantic from approximately  $18^{\circ}\text{N} - 45^{\circ}\text{N}$ ; maximum values are found between  $25^{\circ}$  and  $30^{\circ}\text{N}$ . *Böning, Doscher and Isemer* [1991] compare the *Isemer and Hasse* [1987] wind climatology with that of *Hellerman and Rosenstein* [1983] with specific emphasis on the implied Sverdrup Transport. The *Isemer and Hasse* climatology yields a greater mean meridional transport and seasonal variability, in better agreement with direct observations of the Florida Current.

The total Sverdrup transport derived from an estimate of the mean wind-stress curl is shown in figure 1.6. The anticyclonic gyre implied by the wind-stress curl spans

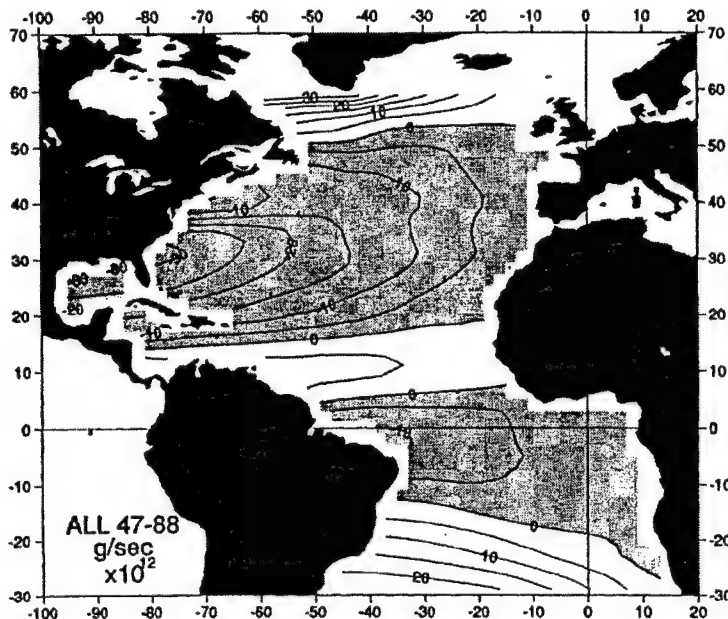


Figure 1.6: Annual average streamfunction of Sverdrup transport ( $\text{g s}^{-1} \times 10^{12}$ ) reproduced from *Mayer and Weisberg [1993]*.

the eastern Atlantic as far north as  $50^\circ\text{N}$ . *Mayer and Weisberg [1993]* recently analyzed 41 years of wind observations in the Atlantic ocean and examined the variability of the implied Sverdrup transport in several frequency bands. The eastern Atlantic shows significant variability in both the annual and interannual (frequencies = .023–.81 cpy) bands. The net transport of the subtropical gyre varies seasonally with maximum values in both summer and winter and minimum values in the fall. At longer time scales, however, analysis of successive pentads shows little variability and are “most notable ... [for] ... their remarkable similarity” [*Mayer and Weisberg, 1993*].

### Mean Circulation of Upper Ocean

Direct observations of the circulation of the eastern North Atlantic confirm the general structure expected from the curl of the wind-stress: broad-scale clockwise flow in the

eastern region of the anti-cyclonic gyre. However, details of the northern limb of the eastern gyre differ from that expected based on a linear-vorticity balance and the observed wind field. Previous analysis of the North Atlantic [Roemmich and Wunsch, 1985b; Bryan, Böning and Holland, 1995] have questioned the validity of the Sverdrup balance for the interior circulation. Figure 1.7 displays an index map marking the key features and currents of the eastern North Atlantic which will be discussed below.

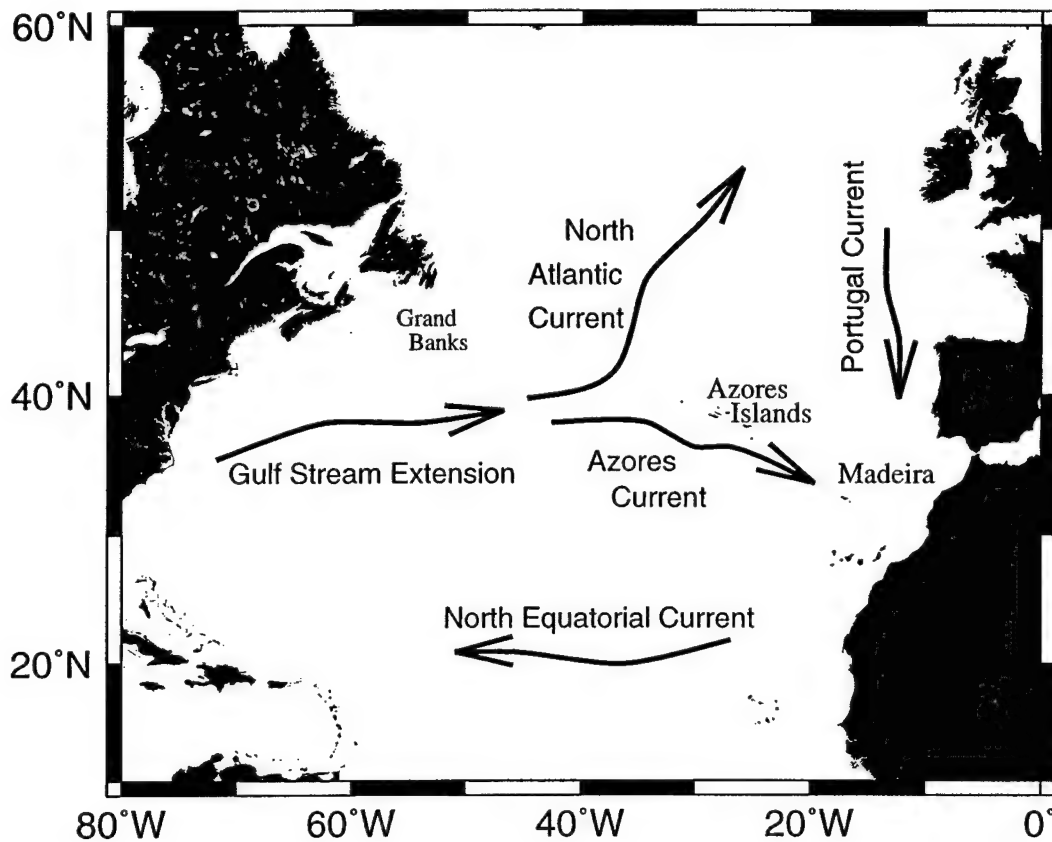


Figure 1.7: Index map marking major surface currents in eastern North Atlantic

Saunders [1982] analyzed the meridional geostrophic transport in the eastern North Atlantic based on the IGY surveys supplemented with two more modern sections. Saunders estimated a net southward flow in the upper 850 m of  $10 \times 10^6 m^3 s^{-1}$  southward across  $32^\circ N$ , however an estimate of the wind-driven Sverdrup transport was used to select the geostrophic reference level so this result cannot be viewed as

an independent confirmation of the accuracy of the Sverdrup transport for the eastern basin. Later estimates by *Stramma* [1984], *Olbers, Wenzel and Willibrand* [1985], *Käse et al.* [1986] and *Sy* [1988] suggest an alternate structure for the circulation between 30° and 50°N in the eastern Atlantic. Stramma estimated the geostrophic transport of the eastern North Atlantic based on a gridded dataset formed from a historical database of hydrographic and CTD measurements. Using a scheme to conserve mass transport within the grid-cells of the domain, he deduced a level-of-no-motion ranging from 1200–1500 m. The resultant transport scheme for the upper ocean (illustrated in figure 1.8) shows the flow in the eastern subtropical gyre originating from the Azores

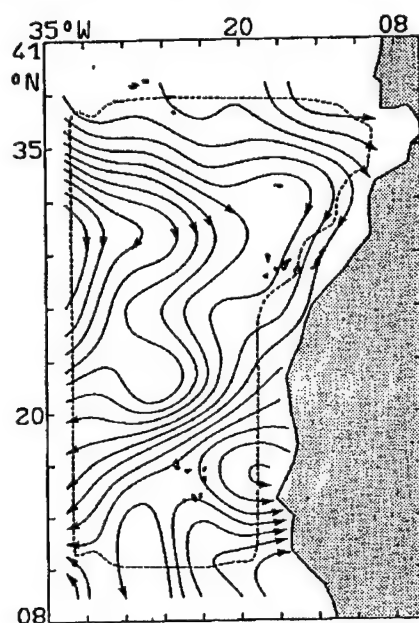


Figure 1.8: Streamlines of mean geostrophic transport in the upper 200m of the eastern North Atlantic (reproduced from *Stramma* [1984]). Contour level is  $0.5 \times 10^6 m^3 s^{-1}$ .

Current rather than southward transport in the region east of the Azores. Similar conclusions can be drawn from analysis of *Levitus* [1982] climatology [*Olbers, Wenzel and Willibrand*, 1985] and the TOPOGULF surveys along the mid-Atlantic ridge [*Sy*, 1988]. Sy determined that the eastward transport across the mid-Atlantic ridge was largely carried in the Azores Current ( $12 \times 10^6 m^3 s^{-1}$ ) and the North Atlantic Current ( $17 \times 10^6 m^3 s^{-1}$ ) (figure 1.7). The North Atlantic synthesis of *Schmitz and McCartney*



[1993], partly based on the above findings, suggests that the majority of the flow into the North Atlantic Current feeds the formation of North Atlantic Deep Water rather than circulating south in the upper ocean between the Azores and Portugal.

In summary, analysis of the circulation of the eastern North Atlantic ocean reveals a general similarity with that expected from the curl of the wind-stress. Between Portugal and the Azores, however, the observed southward flow, sometimes referred to as the Portugal Current, is significantly weaker than expected based on the wind field. Instead, the circulation south of 35°N appears to be fed predominantly by out-flow from the eastward flowing Azores current (figure 1.9). The analyses cited above

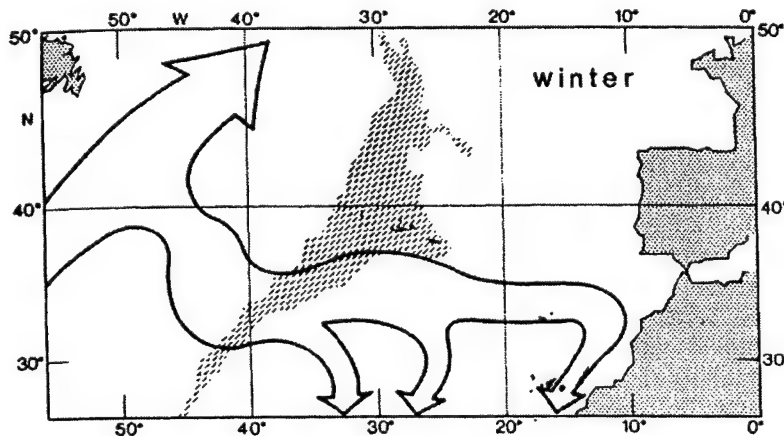


Figure 1.9: Schematic diagram of origin and path of Azores Current reproduced from *Klein and Siedler [1989]*.

have tended to focus on the net transport in the upper (0-500 dbar) of the water column. Analysis of the structure of the mean circulation oriented along isopycnal surfaces will be discussed further in §5.1.

## Subduction and Ventilation

Thermocline waters in the subtropical gyre communicate with the atmosphere along the outcrop where isopycnal surfaces intersect the surface mixed layer. *Stommel [1979]*

pointed out that fluid is predominantly composed of surface water from the late winter when the surface mixed layer reaches its deepest levels. Fluid subducted at other times of year is later entrained back into the surface mixed layer as the mixed layer deepens in the subsequent winter. Figure 1.10 illustrates the surface density of the North Atlantic based on direct hydrographic observations in February and March. In the

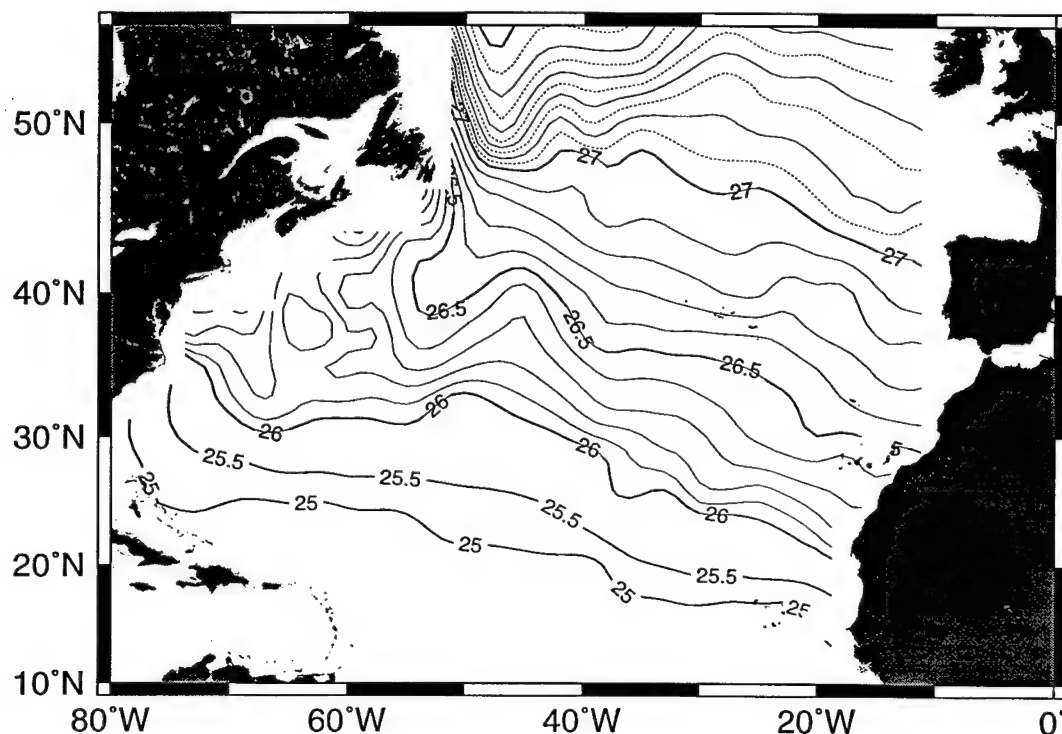


Figure 1.10: Map of sea surface density in late winter. Map is based on hydrographic observations in February and March in the supplemented hydrographic atlas of *Lozier, Owens and Curry* [1995] (Appendix A).

eastern Atlantic, there is a steady progression of increasing density towards the north with a slight NW-to-SE tilt in the isopleths. Fields in the western Atlantic are more complex with the signature of the cold, fresh Labrador current apparent in the lower density waters off the coast of Labrador. In the Gulf Stream, the estimate of the surface density contains smaller scale structure likely to be an artifact of meanders in the Gulf Stream aliased by the sparse data used to construct this map.

*McCartney* [1982] and *McCartney and Talley* [1982] discuss the major mode waters and their circulation throughout the North Atlantic. The dominant mode formed within the subtropical gyre is Eighteen Degree Mode Water [*Worthington*, 1959] with a potential density of approximately  $\sigma_\theta = 26.5$ . Eighteen Degree Mode Water forms from large heat loss to the atmosphere south of the Gulf Stream [*Talley and Raymer*, 1982], apparent in figure 1.10 as the large patch of water with  $26.5 \leq \sigma_\theta \leq 26.6$  south of the Grand Banks. Formation of smaller amounts of mode water of this same class have been documented in the eastern Atlantic near Madeira [*Siedler, Kuhl and Zenk*, 1987]. The rate of Madeira mode water production is estimated to be 10–20% of the total production of mode water at density  $\sigma_\theta \approx 26.5$ .

Isopycnal surfaces less than  $\sigma_\theta \approx 27.1$  outcrop south of the zero line of the wind-stress curl (compare figure 1.10 with figures 1.5 and 1.6) and thus intersect the surface mixed layer within the domain of the anti-cyclonic subtropical gyre implied by the surface wind-stress. Examination of property distributions on the isopycnals  $26.6 \leq \sigma_\theta \leq 27.1$  indicates ventilation and renewal of properties originating from the outcrops in the northeastern Atlantic. Review of prior analyses of the ventilation of these lower layers of the subtropical thermocline will be further discussed in §5.1.

*Marshall, Nurser and Williams* [1993] have examined the rate of subduction over the North Atlantic based on an analysis of climatological hydrography [*Levitus*, 1982] and an estimate of annual average Ekman pumping [*Isemer and Hasse*, 1987]. The estimate of the subduction of water into the main thermocline depends on Ekman pumping but modified to account for two additional processes: 1) meridional transport in the mixed layer and 2) lateral subduction through the base of the mixed layer. Estimates of the various components comprising the net subduction rate are shown in figure 1.11. The Ekman pumping rate shows similarity to figure 1.5 since it is determined from the *Isemer and Hasse* [1987] wind field. The mean lateral circulation in the mixed layer leads to an enhancement in the vertical velocity at the

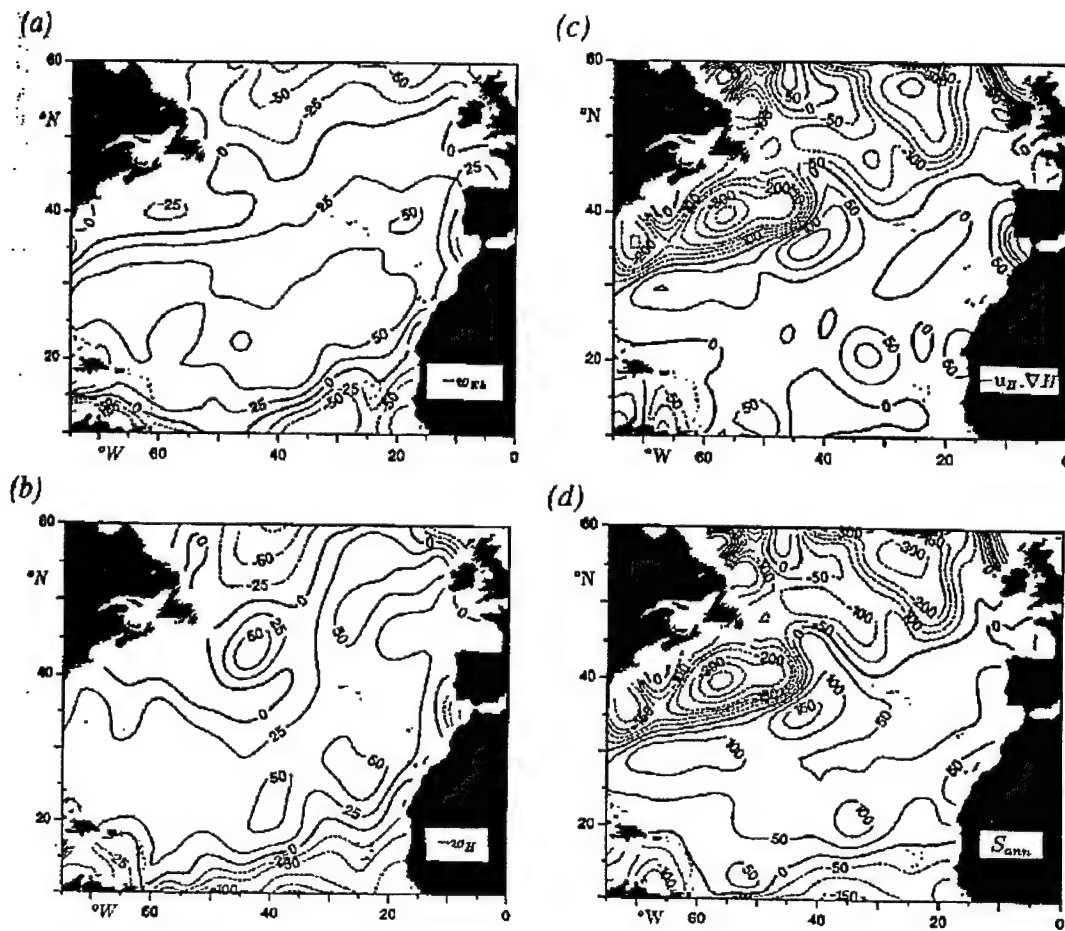


Figure 1.11: Estimate of subduction rate ( $\text{m yr}^{-1}$ ) of North Atlantic reproduced from *Marshall, Nurser and Williams* [1993]. Illustrated fields are (a) annual mean Ekman pumping, (b) annual vertical velocity at base of mixed layer, (c) annual lateral subduction through base of mixed layer, and (d) Net subduction into main thermocline.

base of the mixed layer in the eastern North Atlantic. Lateral subduction through the spatially-varying base of the mixed layer (figure 1.11c) shows large positive values in the mid-ocean associated with a trough of deep winter mixed layers and negative values (obduction) north of the Gulf Stream and throughout most of the ocean north of  $40^\circ\text{N}$ . The resulting estimate of the net subduction (figure 1.11d) shows a field quite different than that implied by Ekman pumping alone. Subduction is still positive across most of the subtropical gyre, however, the line separating positive and negative subduction in the eastern North Atlantic has shifted southward by 10–15 degrees. One

must question the representativeness of the fields illustrated in figure 1.11 since the lateral circulation is calculated from a smoothed, annual mean climatology. Nonetheless, the analysis of *Marshall, Nurser and Williams* [1993] illustrates the important distinctions between the rate of subduction into the permanent thermocline and that implied by the wind-stress at the surface of the ocean (these distinctions had also been discussed previously by *Huang* [1989]). The ventilation of isopycnal surfaces is likely quite different from that expected based on the position of the surface outcrops (figure 1.10) and the Sverdrup transport (figure 1.6).

## Variability

Since the early analysis of *Dantzler* [1977], the subtropical eastern North Atlantic has been identified as a region of relatively low kinetic energy. Though quiescent compared to energetic regions such as the Gulf Stream, any variability can have a large influence on the property fields in the eastern Atlantic due to the weak mean circulation. Estimates of variability based on hydrographic observations and float trajectories have been recently supplemented by the advent of high-precision satellite altimetry. Figure 1.12 shows the eddy kinetic energy (EKE) along 30°W estimated from both drifter observations and satellite altimetry. The center of the subtropical gyre (25°–30°N) is characterized by a minimum in EKE. Values increase to the north with a local maximum at 35°N, likely due to the meandering of the Azores Current. Observations of float trajectories in the eastern Atlantic [*Sundermeyer and Price*, 1997] show dispersion due to the mesoscale eddy field, but analysis of the full two-year records clearly reveals the mean circulation of the anticyclonic gyre above the level of mesoscale variability. *Joyce and Jenkins* [1993] examine the spatial variability of property fields in recently subducted water south of the Azores Current. The amplitude of the mesoscale variability in property fields is largest in the most recently subducted water and rapidly decreases to incoherent levels after 1 year.

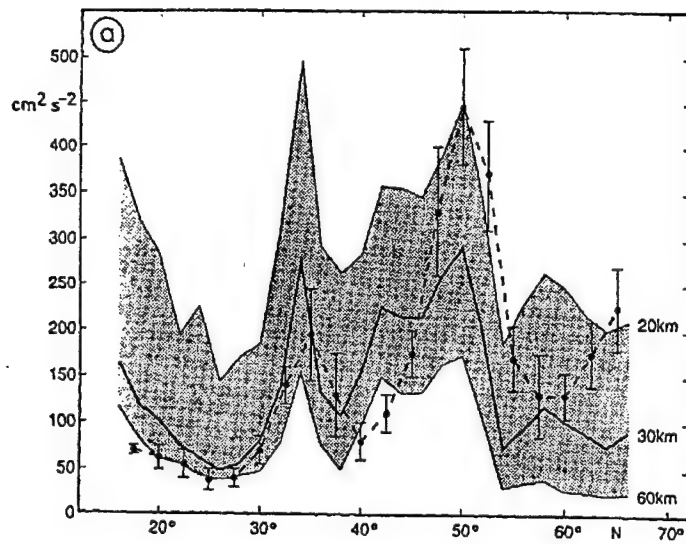


Figure 1.12: Estimate of Eddy Kinetic Energy along 30°W (reproduced from *Stammer and Böning* [1996]). Analysis of TOPEX/POSEIDON data is shown as shaded region defined by smoothing scales of 20, 30 and 60 km. Estimates based on drifter trajectories are shown as dashed line.

Seasonal changes in the large-scale structure of the eastern North Atlantic are also well documented [*Armi and Stommel*, 1983; *Stramma and Siedler*, 1988; *Klein and Siedler*, 1989]. Seasonal variability is expected based on the changes in the wind stress curl [*Mayer and Weisberg*, 1993]. The estimate of wind-forcing also suggests the likelihood of some interannual variability. This thesis examines changes in the transient tracer age fields over time scales of a decade. Analysis of possible changes in the large-scale circulation on these time-scales will be further addressed in Chapter 3.

## Summary

The eastern limb of the anticyclonic wind-driven gyre occupies the eastern subtropical North Atlantic. Isopycnals composing the main thermocline outcrop into the winter mixed layer with successively denser waters outcropping further north. Isopycnal subduction rate based on annual average wind-stress fields and the position of the winter outcrop should be interpreted with caution. Identification of the northern edge of the

subtropical gyre is ambiguous: observations of the mean currents differ significantly from those implied by wind forcing, especially in the eastern basin north of  $35^{\circ}\text{N}$ . In addition, *Marshall, Nurser and Williams* [1993] emphasize the important distinction between surface Ekman pumping and the net subduction into the thermocline. Although the magnitude of eddy kinetic energy in the eastern basin is low compared to high energy regions such as the Gulf Stream, temporal variability at all scales may still be significant owing to the weak mean flow.

## 1.4 Organization of Thesis

### 1.4.1 Structure of the Thesis

The structure of the thesis is as follows. Chapter 2 discusses the spatial and temporal distribution of  $^3\text{He}$  and  $^3\text{H}$  measurements in the eastern North Atlantic. Multivariate linear regressions are then used to show that the observed tritium- $^3\text{He}$  age field is not steady with time. The hypothesis that the observed large-scale changes in the tracer age field reflect a change in the underlying flow field is examined in Chapter 3. The time-history of the mean meridional geostrophic shear shows no evidence for changes over the time period of the measurements. Additionally, comparison of the tracer age to the dissolved oxygen field also indicates no alteration in the large-scale circulation. Lacking evidence that a temporal change in the flow field created the observed shifts in the observed tracer age, Chapter 4 examines the hypothesis that the trend in tracer age is created by the penetration and ventilation of bomb-produced tritium. Scale analysis of the advective-diffusive balance for tritium- $^3\text{He}$  age leads to a simplified partial differential equation governing the temporal evolution of the age field. Analytic solutions of the differential equation reveal how the magnitude of the temporal changes in the age field increase as the Péclet number of the flow decreases. Comparison

between of observations and numerical simulations in a one-dimensional model lead to unexpectedly large estimates of large-scale lateral diffusivity of subducting flow along isopycnals. Chapter 5 extends the basic interpretation developed using the simplified one-dimensional models using two-dimensional models of the subtropical gyre. Two dimensional models allow for the possibility of both direct advective ventilation from the surface outcrop as well as indirect ventilation whereby the interior ocean only feels the surface atmospheric forcing via lateral diffusivity. The observed temporal changes in the tritium- $^3\text{He}$  age field can be reconciled with conventional estimates of the magnitude of lateral diffusivity only if the lower thermocline is predominantly ventilated by diffusion rather than advection. Chapter 6 summarizes the results of the thesis and discusses this work in the context of previous investigations of transient tracers and ventilation of the oceanic thermocline.

### 1.4.2 Comments on Methodology

This thesis presents and analyzes a previously unexplored feature of the tritium- $^3\text{He}$  age field in the North Atlantic thermocline: the secular trend in tracer age values. Chapter 3 demonstrates that the observed trend cannot be accounted for by advective models of thermocline ventilation. To gain an understanding of processes which may contribute to the temporal evolution of tritium- $^3\text{He}$  age, a hierarchy of simple models is explored: a simple partial-differential equation, a numerical model in one-dimension and a two-dimensional gyre model of the subtropical circulation. Comparison of the model simulations with the observed properties of the transient tracer fields is used as a guide to explore the sensitivity of the observed features of the tracer signal to the physical oceanic processes which ventilate the upper ocean.

An alternative approach to the analysis of transient tracer data, not used in this thesis, is to directly incorporate the observations of transient tracers as constraints



on an ocean circulation model. The simplest example of such a calculation is to use the observed tracer inventories and time-history of the boundary condition to cast the issue as a problem in control theory [Wunsch, 1987; Wunsch, 1988b; Wunsch, 1988a; Mémery and Wunsch, 1990]. For the specific case of transient tracer data, such problems pose the question: is the known circulation (or some *a priori* guess) consistent with the tracer observations and history of the input function given the uncertainties of both? Or put another way, can the circulation reproduce the observed tracer concentrations by adjusting the boundary conditions within the range of acceptable values? Transient tracers are deemed to have additional information only if the answers to the above questions are “no”. In this event, additional algorithms are available [Wunsch, 1988b; Wunsch, 1996] to seek modifications to the flow field to find a consistent circulation. Such problems then become examples of parameter estimation in nonlinear models.

The control theory models discussed above are well suited for the incorporation of data which measures the concentration, or inventory, of a conserved transient tracer: essentially the algorithms seek to adjust the internal flows to optimally connect the observed interior concentrations with values along the boundaries. The entry of tritium into the ocean is an example of such a scenario and Wunsch [1988a] and Mémery and Wunsch [1990] analyzed the tritium inventory data in terms of a terminal constraint problem (§1.3.2). They concluded that tritium inventory is, at best, a weak constraint on their circulation models.

The simultaneous measurement of  $^3\text{H}$  and  $^3\text{He}$  allows for the construction of a conserved, or “stable” tritium since tritium decays into  $^3\text{He}$ . Observations of both components of the coupled tritium- $^3\text{He}$  system, however, offers a measure of another diagnostic quantity in addition to tracer inventory. The measure of total inventory discards the information that the  $^3\text{H}$  mutates to  $^3\text{He}$  at a constant, known rate. Analysis of the relative magnitudes of  $^3\text{H}$  and  $^3\text{He}$  is one means of capturing the information of

the known radioactive decay process. Thus the ratio of  $^3\text{H}$  and  $^3\text{He}$  contains information different than that contained in the inventory measurement. Tritium- $^3\text{He}$  age is simply a more convenient expression of this ratio which uses the known decay rate to transform the measured ratio to a quantity with units of time. Additionally, tritium- $^3\text{He}$  age “normalizes” the effects of tracer concentration because it is a diagnostic of the ratio of observed  $^3\text{He}$  and tritium.

Unfortunately, the diagnostic tritium- $^3\text{He}$  age is not easily adapted to the formal methodology developed for incorporating transient tracer data into ocean models. The difficulty arises because ratios, such as tritium- $^3\text{He}$  age, do not obey a linear advective-diffusive equation (equation 4.1.1): the ratios of quantities are not preserved under mixing (e.g. see §1.3.3). As will be shown in this thesis, the observed temporal trends in tritium- $^3\text{He}$  age result from the effects of mixing on the ratio of the two tracers as the high concentrations of bomb-produced tritium invade the thermocline.

Although tritium- $^3\text{He}$  age may be viewed as an impractical construct due to this nonlinearity, there are important conceptual advantages. The “true” or “ideal” age of a water parcel (defined as the elapsed time since the water was resident in the mixed layer) is a property of the flow field which independent of the details of tracer concentration and boundary conditions. Tritium- $^3\text{He}$  age provides a diagnostic estimate of the “true” age of a water parcel. To the extent that tritium- $^3\text{He}$  age is a good approximation of the “true” age, it provides many of the diagnostic advantages of the latter. First, the construction of a tracer age value transforms the measurements to a value which has a known, constant surface boundary condition, zero. Second, gradients of tritium- $^3\text{He}$  age provide direct independent estimates of rates of oceanic processes. Finally, there is the expectation that, under certain conditions, the tracer age field will be steady with time. It is precisely this expectation of steadiness and the discrepancy with observations in the eastern North Atlantic, which highlights both the

failure of advective models of ventilation as well as the unique information contained in the ratio of  $^3\text{He}$  to tritium.

This thesis does not attempt to construct a formal nonlinear parameter estimation model which could incorporate the nonlinear advective-diffusive equation of tritium- $^3\text{He}$  age. If there is information about the ocean to be gained from tritium- $^3\text{He}$  age, that same information must be contained in the constituent fields,  $^3\text{He}$  and tritium, which, owing to their linearity, can be more easily incorporated into inverse models. The method of this thesis is to use the conceptual advantages of the tritium- $^3\text{He}$  age formulation, to explore what, if anything, the known coupling of tritium and  $^3\text{He}$  can tell us about the ocean. The conclusion is that, provided one has reasonable estimates of the advective field, the ratio of  $^3\text{H}$  and  $^3\text{He}$  records information of bulk mixing within the ocean.



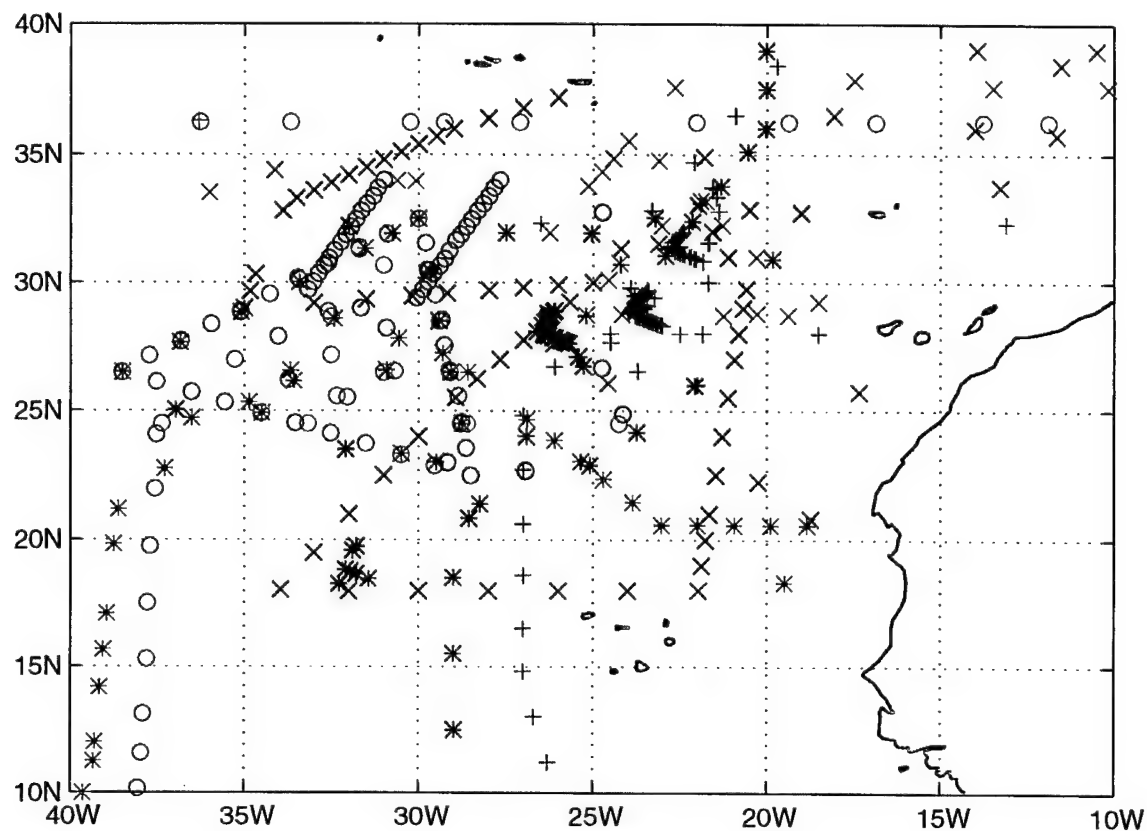
## Chapter 2

# Temporal Evolution of Tritium and $^3\text{He}$ Fields in the Eastern North Atlantic

## 2.1 Treatment of Data

### 2.1.1 Data Distribution

In terms of tritium and  $^3\text{He}$  measurements, the eastern North Atlantic is the most thoroughly sampled region of the world's oceans. Locations of the stations with both tritium and  $^3\text{He}$  measurements are displayed in figure 2.1 and tabulated information about the station data is contained in table 2.1. The first cruise in this region sampling for both tritium and  $^3\text{He}$  was conducted in 1978 on the *R/V Oceanus*; however the sampling strategy on this cruise was oriented towards the depths of the Mediterranean outflow. The earliest samples concentrated within the thermocline were collected in 1979 as part of the  $\beta$ -Triangle experiment [Armi and Stommel, 1983]. Samples were



X Oceanus-52 1978	X TTO 1981	X Meteor-69 1984	X Subduction Seasoar 1992
O Atlantis II-107 1979	O Atlantis II-109 1981	O Endeavor-143 1986	O Subduction Largescale 1992
* Oceanus-79 1980	* TAS 1983	* Oceanus-202 1988	* Subduction Mesoscale 1993
+ Meteor-56 1981	+ Meteor-64 1983	+ Subduction Mesoscale 1991	

Figure 2.1: Location of hydrographic stations in eastern North Atlantic with  $^3\text{H}$  and  $^3\text{He}$  measurements.

collected on the edges of the triangle (nominally 22°N to 33°N) as well as along a meridional section extending southward to 9°N. Additional samples were collected the following year when the  $\beta$ -Triangle hydrographic survey was repeated. Three large-scale surveys passed through the region in 1981 providing the most extensive single year of tritium and  $^3\text{He}$  measurement activity prior to the Subduction Experiment. Two transatlantic zonal sections conducted by *R/V Atlantis II* along 24°N and 36°N [Roemmich and Wunsch, 1985a] also included a diversion for measurements again in the  $\beta$ -Triangle region. Also in 1981, the *F/S Meteor* surveyed a meridional hydrographic section along nominally 25°W [Thiele *et al.*, 1986] and the *Transient-Tracers in the Ocean* (TTO) program included sampling in the northern portion of the eastern subtropical gyre. The *Tropical Atlantic Survey* (TAS), a companion program to TTO, entailed a hydrographic survey through the southern portion of the region in 1983. Two German cruises (*F/S Meteor-64* and *F/S Meteor-69*) [Fuchs, 1987] provide a few additional stations during the period 1983-1984. In 1986, the pilot subduction cruise [Joyce and Jenkins, 1993] carried out extensive sampling in the neighborhood of the Azores Current at 30°W. This survey included two nearly meridional sections and two mesoscale grided surveys. Another meridional transect extending from 3°S to 63°N nominally along 20°W was surveyed in 1988 by the *R/V Oceanus* [Tsuchiya, Talley and McCartney, 1992]. Chlorofluorocarbons were measured in addition to the tritium and  $^3\text{He}$  measurements and the comparison of the tracer ages is discussed in Doney, Jenkins and Bullister [1997]

The field program portion of the Subduction Experiment was conducted from 1991 through 1993. The program included both large and meso-scale hydrographic surveys. Tritium and  $^3\text{He}$  samples were collected on "L-shaped" surveys in 1991 and 1993 designed to characterize the meso-scale property distributions of recently subducted waters. A few samples were also collected during a 1992 Seasoar cruise [Pallant *et al.*, 1995]. A large-scale survey to characterize the general hydrography of the region

Cruise/Ship	Year	Stations	Tritium Samples	<sup>3</sup> He Samples
<i>R/V Oceanus-52</i>	1978	13	184	107
<i>R/V Atlantis II-107</i>	1979	44	420	380
<i>R/V Oceanus-79</i>	1980	18	72	72
<i>F/S Meteor-56</i>	1981	15	306	119
TTO	1981	54	524	448
<i>R/V Atlantis II-109</i>	1981	37	306	261
TAS	1983	29	311	139
<i>F/S Meteor-64</i>	1983	7	18	69
<i>F/S Meteor-69</i>	1984	8	41	71
<i>R/V Endeavor-143</i>	1986	60	446	421
<i>R/V Oceanus-202</i>	1988	13	189	180
Subduction Mesoscale	1991	69	230	283
Subduction Seasoar	1992	5	82	61
Subduction Large-scale	1992	57	564	619
Subduction Mesoscale	1993	67	383	365

Table 2.1: Summary of cruises measuring <sup>3</sup>H and <sup>3</sup>He displayed in figure 2.1. Only data for samples within the domain of the eastern Atlantic are included.

was conducted in 1992. Although the survey pattern of the 1992 Subduction cruise was somewhat constrained by concurrent mooring operations, this survey provides the best single realization of the large scale transient tracer fields in the eastern North Atlantic.

The combination of tritium and <sup>3</sup>He measurements from all the individual survey programs provides a unique set of transient tracer observations. The 15 hydrographic surveys span 15 years and include 496 stations with both tritium and <sup>3</sup>He measurements. A total of 4076 samples were processed for tritium analysis and 3595 for <sup>3</sup>He with the greatest number of samples collected in the early 1980's and early 1990's. Owing to differing cruise objectives, the spatial coverage, both geographically and with depth, is far from uniform over the 15 years of coverage. While some cruises surveyed the large scale structure of the subtropical gyre (the  $\beta$ -Triangle surveys, long-line transects and the large-scale 1992 Subduction Experiment cruise), others



sampled only small regions, albeit with fine-resolution (the pilot subduction cruise and the Subduction Experiment meso-scale surveys).

$\sigma_\theta(kgm^{-3})$	pressure (dbar)	$\Theta$ ( $^{\circ}C$ )	Salinity (psu)
26.4	93	18.0	36.5
26.5	131	17.4	36.4
26.6	178	16.6	36.2
26.7	226	15.7	36.1
26.8	287	14.8	36.0
26.9	360	13.8	35.8
27.0	444	12.8	35.7
27.1	540	11.8	35.6
27.2	640	10.9	35.5
27.3	732	10.2	35.4

Table 2.2: Summary of isopycnal surfaces used in analysis. Pressure and potential temperature of each density surface at  $30^{\circ}W$ ,  $30^{\circ}N$  are evaluated from the climatological atlas of *Lozier, Owens and Curry* [1995].

Likewise, the vertical resolution of the hydrographic sampling varied depending on the intent of the survey. Figure 2.2 shows the total number of samples collected in each year for individual isopycnal layers for the upper portion of the thermocline (properties of all the isopycnals used in this study are summarized in table 2.2). The shallower portion of the thermocline ( $\sigma_\theta < 26.8$ ) was sampled much more intensively during the subduction experiment than at anytime prior to 1990. In the lower part of the thermocline (figure 2.3), however, the data coverage is more uniform in time. As mentioned before, the first survey in the eastern Atlantic in 1978 was focused on the outflow of the Mediterranean water so almost all the samples in this year were taken below the thermocline. The TTO, TAS and long-line transects (1981,1983) were conducted as exploratory cruises for a wide suite of geochemical tracers and provided balanced coverage throughout the water column. The mesoscale surveys performed in conjunction with the Subduction Experiment (1991, 1993) focused on the most recently subducted water in the upper thermocline and so the bulk of the measurements

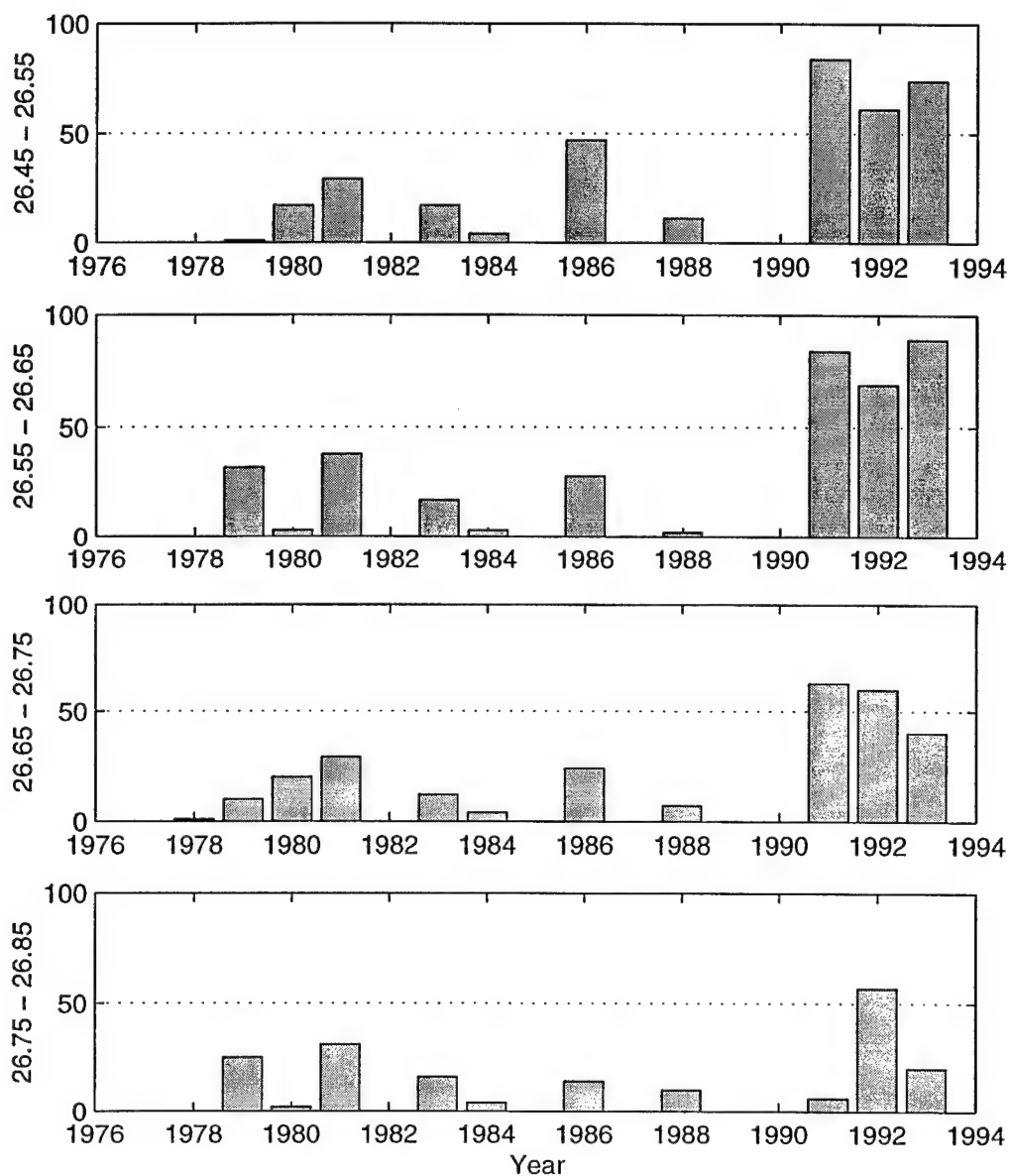


Figure 2.2: Upper thermocline distribution of  $^3\text{H}$  and  $^3\text{He}$  sample measurements as function of isopycnal.

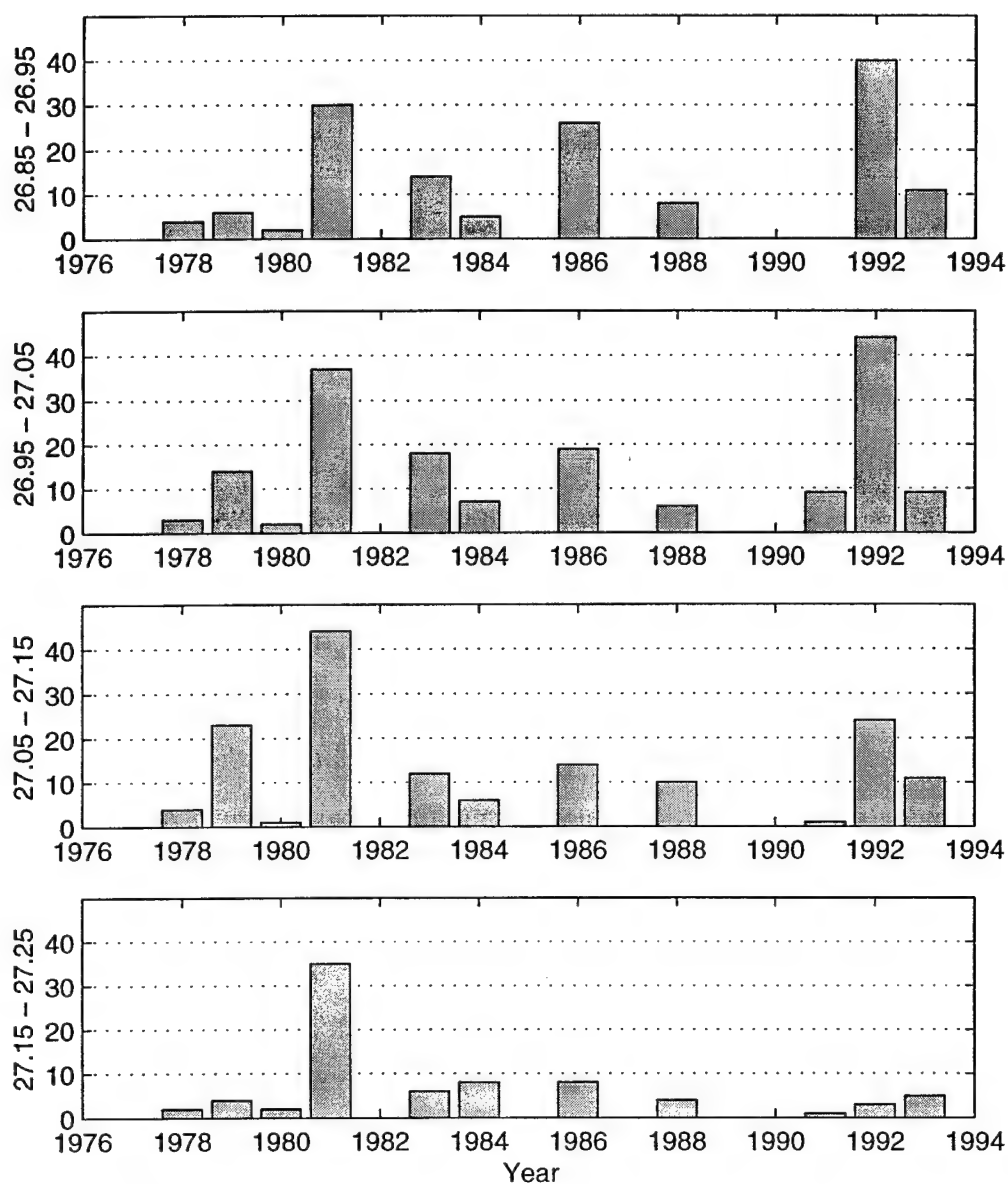


Figure 2.3: Lower thermocline distribution of  $^3\text{H}$  and  $^3\text{He}$  sample measurements as function of isopycnal.

are above  $\sigma_\theta = 26.7$ . The large-scale survey of the Subduction Experiment (1992), however, sampled a wider range within the thermocline, generally at least as deep as  $\sigma_\theta = 27.1$ . In general the best sampling is through the central thermocline (between  $\sigma_\theta = 26.4$  and  $\sigma_\theta = 27.1$ ) with the periods of greatest coverage in 1981 and 1992. Other cruises with fewer measurements supplement these “data-rich” times so that gaps in the temporal record never exceed 2 years.

### 2.1.2 Large-scale Structure of the Tracer Fields

Since the transient tracer fields are evolving with time, it is not straightforward to combine all the data represented in figure 2.1 to form a composite picture of the structure of the tracer fields in the thermocline. In lieu of this, tracer properties along a single meridional hydrographic section will be presented in order to illustrate the typical meridional structure of the tracer fields across the subtropical gyre. In 1988, a hydrographic survey was conducted aboard the *R/V Oceanus* following a north-south track between 20° and 30°W [Doney, Jenkins and Bullister, 1997; Tsuchiya, Talley and McCartney, 1992]. Sample spacing for  $^3\text{He}$  and  $^3\text{H}$  is not as dense as other surveys in the region but this is the best single survey for providing a picture of the tracer fields across both the northern and southern boundaries of the subtropical gyre.

Figure 2.4 displays contoured sections of the pressure, salinity and dissolved oxygen along a portion of the *R/V Oceanus*-202 survey. The vertical axis in all the plots is potential density referenced to the surface with values of density chosen to span the permanent thermocline. The horizontal extent runs from 12°N to 46°N, crossing both the tropical-subtropical boundary of the Cape Verde Front at approximately 20°N and the Azores front at 35°N. Lower values in all the panels are shaded more darkly.

The pressure of the isopycnal surfaces along the hydrographic section is presented in figure 2.4a. The “bowl” of the subtropical gyre is transformed in density co-

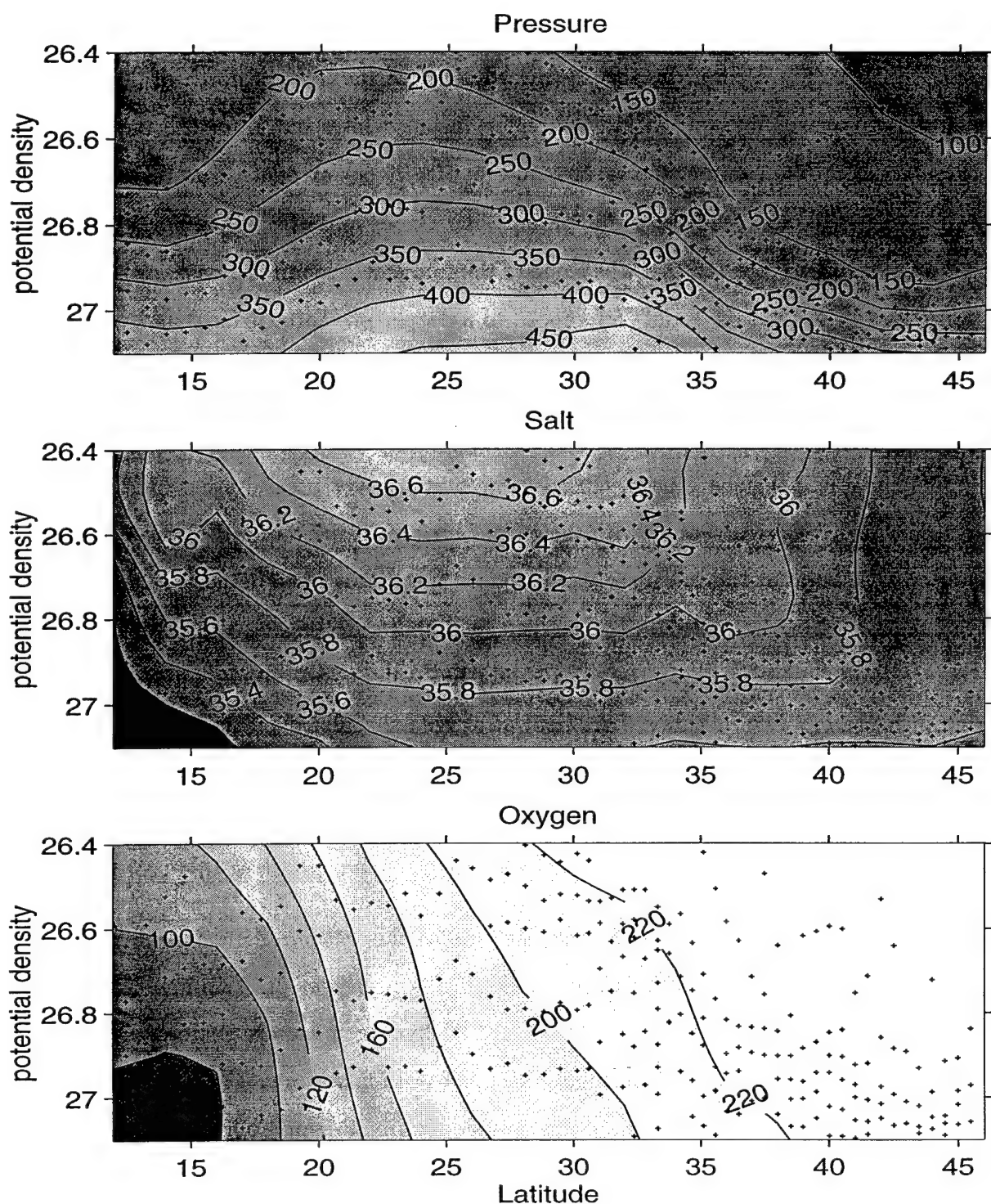


Figure 2.4: Vertical sections of properties along nominal 25°W: a) Pressure (dbar) b) Salinity (psu) and c) Oxygen  $\mu\text{mol} - \text{kg}^{-3}$ . Grided fields were obtained by objectively mapping the measurements with a Gaussian correlation function with characteristics scales of three degrees in the horizontal and  $0.25 \text{ kg} - \text{m}^{-1}$  in the vertical.

ordinates into the upward bowing of the isobars. Northward shoaling of the lighter isopycnals is represented by the downward slope of the isobars north of 30°N. The lighter isopycnals outcrop within the region in late winter but since this survey was conducted in late summer the surface outcropping is not evident. Two regions of increased meridional gradient are apparent: the Cape Verde frontal region (15-20°N) and the Azores Front (35°N). The slope of the isopycnals requires a eastward geostrophic flow in the Azores Front (referenced to a deeper pressure surface) and westward flow in the Cape Verde Front.

The salinity field (figure 2.5b) shows the characteristic salinity maximum of the subtropical surface waters. Excess evaporation over precipitation increases the salinity of subtropical waters with the effect being most pronounced for waters which outcrop at mid-latitudes. Dissolved oxygen (figure 2.5c) has highest values at the northern end of the section. The oxygen field shows decreasing values towards the south due to biological respiration in subducted waters and mixing with low-oxygen tropical water. The meridional gradient of oxygen sharply increases across the Cape Verde front and the lowest oxygen values are seen in the lower tropical thermocline. In contrast to the pronounced oxygen gradient at the tropical-subtropical boundary, the oxygen field shows a much reduced signature at the position of the Azores front.

Figure 2.5 displays contoured sections of the tritium,  $^3\text{He}$ , tritium- $^3\text{He}$  age along the *R/V Oceanus-202* transect. Tritium is presented in Tritium Units (TU) where 1 TU is defined as 1  $^3\text{H}$  atom per  $10^{18}$  hydrogen atoms. Values of  $^3\text{He}$  are reported as excess above atmospheric saturation [Jenkins and Clarke, 1976]. The tritium- $^3\text{He}$  age is calculated according to its definition in equation 1.3.1. The revised value of  $\lambda$ ,  $(17.92 \text{ yr})^{-1}$ , is used throughout all calculations [Taylor and Roether, 1982].

Tritium (figure 2.5a) shows highest values in the surface waters at the north end of the section. Tritium concentrations decrease towards the south but are fairly

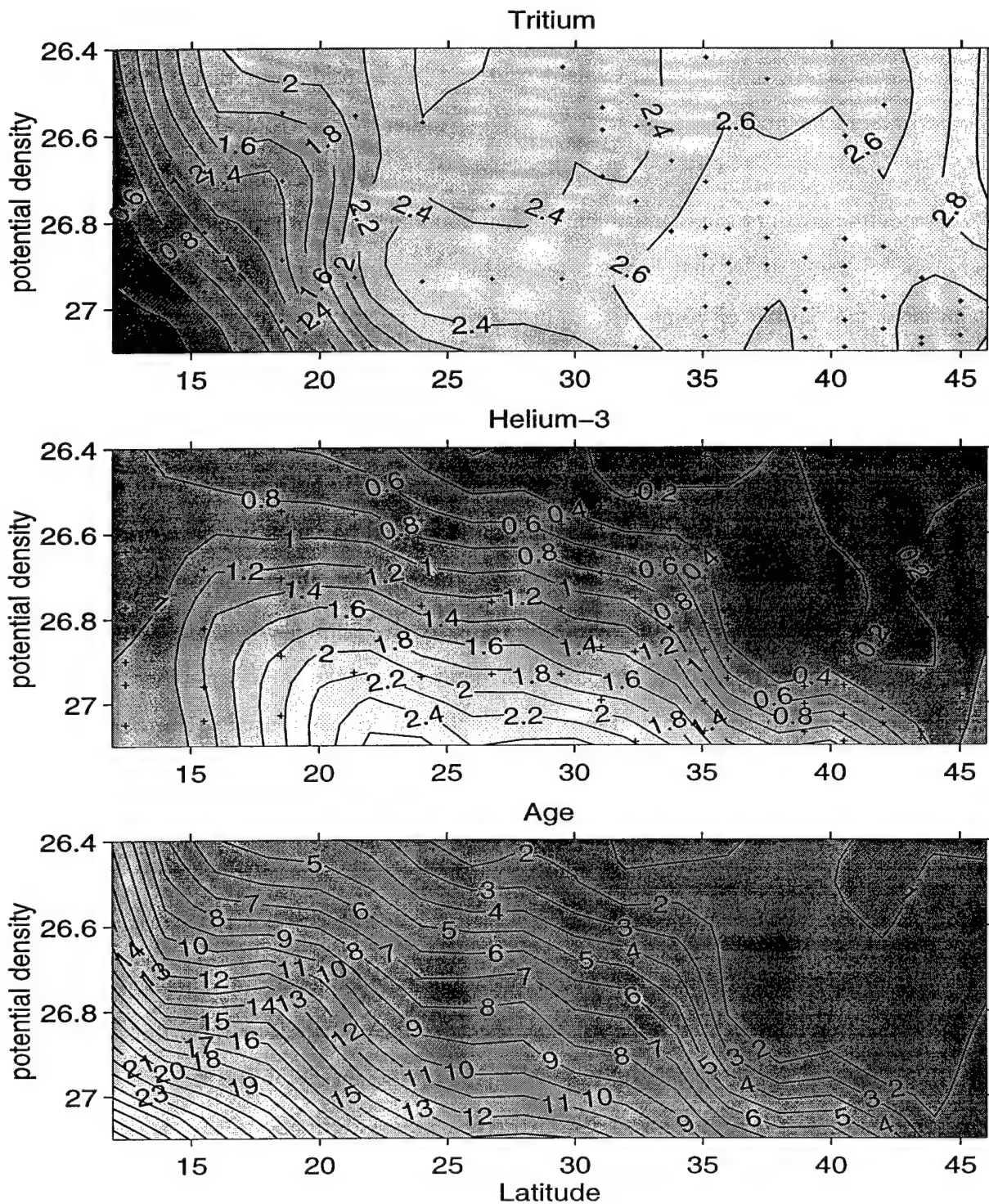


Figure 2.5: Vertical sections of transient tracer fields along 25°W. a) Tritium (T.U.) b) <sup>3</sup>He (T.U.) and c) tritium-<sup>3</sup>He age (years) sections along nominal 25°W. Position of <sup>3</sup>H and <sup>3</sup>He samples are indicated by small crosses. Age is calculated from the grided fields of <sup>3</sup>H and <sup>3</sup>He.



uniform across the bulk of the subtropical gyre north of the Cape Verde front. A slight subsurface maximum is evident centered in the mid-lower thermocline at approximately  $\sigma_\theta = 26.9$ . Low tritium values, indicative of tropical water, are seen at the southern end of the section. The near uniformity of values of tritium in the thermocline north of the tropical-subtropical boundary is a signature of the large-scale homogenization of  $^3\text{H}$  that has occurred in the northern warm-water sphere since the input of the "spike" of bomb-tritium in the mid-1960's.

In contrast to tritium,  $^3\text{He}$  values are lowest in the surface waters to the north, due to depletion of excess  $^3\text{He}$  by gas exchange with the atmosphere. Radioactive decay of  $^3\text{H}$  in subducted waters leads to an increase in  $^3\text{He}$  both to the south and with depth. Between  $35^\circ$  and  $20^\circ\text{N}$ ,  $^3\text{He}$  values on isopycnal horizons increase smoothly to the south. At the southern edge of the gyre, the meridional gradient of  $^3\text{He}$  changes sign and values decrease across the Cape-Verde front. Bomb produced tritium entered the oceans predominantly in the northern hemisphere [Weiss and Roether, 1980] so tropical waters have reduced burdens of both  $^3\text{H}$  and  $^3\text{He}$  compared to northern hemisphere thermocline waters. At  $35^\circ\text{N}$ , a sharp front of  $^3\text{He}$  is observed coinciding with the eastward flowing Azores current. The cross-frontal gradient is evident at all densities but appears sharpest in the upper thermocline ( $\sigma_\theta < 27.0$ ), a feature which is also confirmed by other synoptic sections across the Azores front.

The tritium- $^3\text{He}$  age computed from the independently interpolated tritium and  $^3\text{He}$  fields is presented in figure 2.5c. Because the distribution of tritium is nearly uniform across much of the subtropical gyre, the structure of the age field closely resembles that of the  $^3\text{He}$ . Low tritium- $^3\text{He}$  age values are found in the surface waters in the north. Age increases both towards the south and with increasing density. Strong meridional gradients are evident at both the Azores and Cape Verde frontal regions. The greatest ages are found south of the Cape-Verde front where  $^3\text{He}$  concentrations exceed those of tritium.



### 2.1.3 Interpolation onto Isopycnal Surfaces

Measurements of the tritium and  $^3\text{He}$  concentrations in sea water are performed on discrete water samples in shore-based laboratories. Samples are collected at sea in Niskin bottles which capture water samples from selected depths during hydrographic casts. The analysis of data for this thesis is carried out on surfaces of constant potential density. As such, measurements from different casts and cruises must first be interpolated onto common density values. Tritium and  $^3\text{He}$  are interpolated independently and then the tritium- $^3\text{He}$  age can be calculated from the interpolated values of the individual tracers.

The bottle data is first linearly interpolated in potential density space. The preference of interpolation in density space, rather than in pressure, for instance, reflects a choice of a vertical coordinate scaled by stratification rather than depth. Linear interpolation is chosen for simplicity. In addition to interpolating the tracer value to standard isopycnal surfaces, an error must be assigned to each interpolated value. The error of an estimate of tracer concentration on isopycnal surfaces consists of a component due to uncertainty in the laboratory measurement as well as a component due to the error of the interpolation process.

Measurement error for tritium and  $^3\text{He}$  depend on the analytic precision of the laboratory equipment as well as the tracer concentration itself. Tritium concentrations are determined from individual event counts on samples processed on a mass spectrometer. The error of the measurement is dependent upon the counting statistics, size of sample and length of sample storage before analysis. Each individual tritium measurement is assigned an error estimate based on both the analytic accuracy of the sample preparation and the counting uncertainty. Figure 2.6 illustrates the increase in measurement accuracy of tritium with time for the data used in this analysis. The

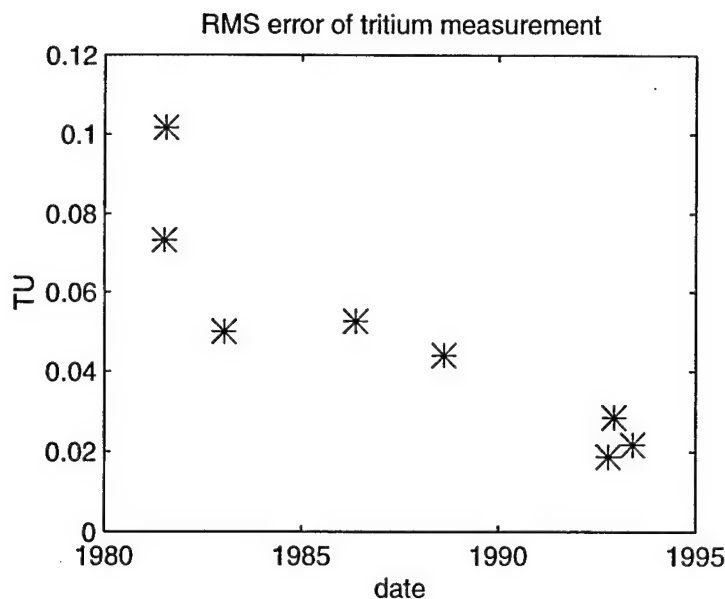


Figure 2.6: Analytic uncertainty (r.m.s.) of tritium measurements performed at the WHOI HIL facility.

uncertainty of the  $^3\text{He}$  measurement is less dependent on individual sample concentrations. Uncertainties for  $^3\text{He}$  measurements made at the WHOI Helium Isotope Lab are taken to be 0.03 TU while data from the German cruises are assigned an error of 0.45 TU for *F/S Meteor-56* and 0.35 TU for *F/S Meteor-64* and *69*.

Error introduced by interpolation is estimated on an *ad hoc* basis and consists of three components added in quadrature:

$$\sigma_{interpolant} = (\sigma_1^2 + \sigma_2^2 + \sigma_3^2)^{1/2} \quad (2.1.1)$$

The first component,  $\sigma_1$  is calculated by linearly interpolating the measurement error of each sample, while the other two components are designed to represent sampling errors. The second component is chosen to reflect the increased uncertainty of the interpolation estimate when the sample interval poorly resolves large gradients in the tracer field. The uncertainty estimate is proportional to the product of the difference in concentrations between successive samples and the distance from the

interpolated point to the nearest sample position:

$$\sigma_2 = 2\alpha \|C_i - C_{i+1}\| \left(1 - \left\| \frac{Z_i + Z_{i+1} - 2Z}{Z_i - Z_{i+1}} \right\| \right) \quad (2.1.2)$$

where  $Z$  is the position of the interpolated value and  $C_i$  represent measurement values at positions  $Z_i$ . This form maximizes the uncertainty at the mid-point between two measurements. The magnitude of the maximum uncertainty is the difference between bracketing measurements scaled by the parameter  $\alpha$ . The uncertainty decreases linearly as  $Z$  approaches the position of each measurement. The value of  $\alpha$  is selected *ad hoc* to be 0.25.

The final component of the interpolation error is proportional to the difference between the value estimated from linear interpolation and that obtained from a spline fit [Akima, 1970] to the data.

$$\sigma_3 = \|C_{spline} - C_{linear}\| \quad (2.1.3)$$

This uncertainty grows when the curvature of the tracer field is large and is chosen to represent the uncertainty arising from the difference between two plausible methods of interpolation. When the two methods agree, the magnitude of  $\sigma_3$  is small.

Figure 2.7 shows an example of the interpolation error for a typical tritium profile from the Subduction 1992 large-scale cruise. Locations of bottle measurements are shown by the '\*'s. The dashed lines illustrate the uncertainty envelope given by the equation 2.1.2. The minimum error occurs at the location of the data points and is equal to the analytic error of the measurements. When the difference in neighboring tritium samples is large, the component  $\sigma_2$  becomes significant and obtains its largest value halfway between the data locations. Where the curvature is large, such as near  $^3\text{He}$  maximum and at  $\sigma_\theta = 27.7$ , the spline and linear interpolation schemes yield different estimates so the component  $\sigma_3$  dominates the uncertainty estimate. Both the  $\sigma_2$  and  $\sigma_3$  components tend to attain their greatest value at the midpoint between successive measurement locations.

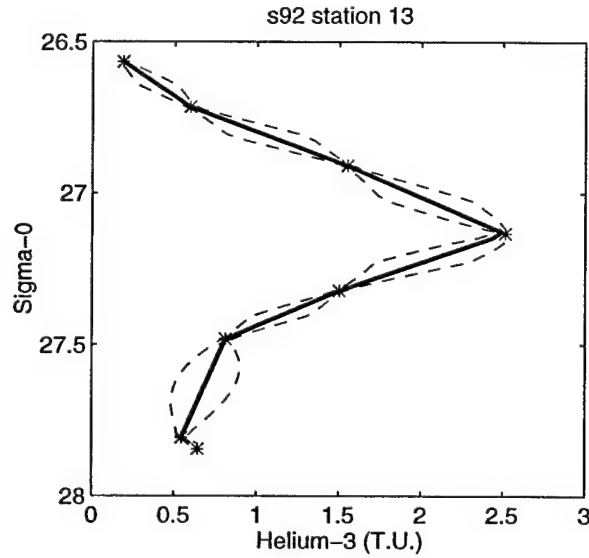


Figure 2.7: Example of interpolation error for  $^3\text{He}$  profile. Asterisks represent the position of measurement samples. The dark solid line is the linearly interpolated values and the uncertainty envelope of this estimate is shown by the dashed line.

Measured tritium and  $^3\text{He}$  values are interpolated onto isopycnal surfaces and then the interpolated values are used to calculate estimates of tritium- $^3\text{He}$  age on the isopycnal. Figure 2.8 shows the total number of interpolated age estimates for each isopycnal surface for the eastern subtropical gyre, chosen here to be defined as the region bounded by 20 to 33°N and 15 to 40°W. The total number of points exceeds 250 for the mid-thermocline and is above 100 for all surfaces above  $\sigma_\theta = 27.1$ . Each individual  $^3\text{He}$  and  $^3\text{H}$  estimate on the isopycnal surface has a unique uncertainty determined from the interpolation uncertainty expressed in equation 2.1.1. In practice, the interpolation error for each estimate is based largely on the proximity of bottle locations in density space for each hydrographic cast. The typical uncertainty for the age calculation for each isopycnal surface can be obtained from:

$$\tilde{\sigma} = (r.m.s(\sigma_{interpolation}^{-1}))^{-1}. \quad (2.1.4)$$

The r.m.s. standard error of age estimates for each isopycnal surface is shown in figure 2.8b. The typical uncertainty of age estimates is less than 0.3 yr for the upper portion of the thermocline. The combination of courser bottle spacing and inherently

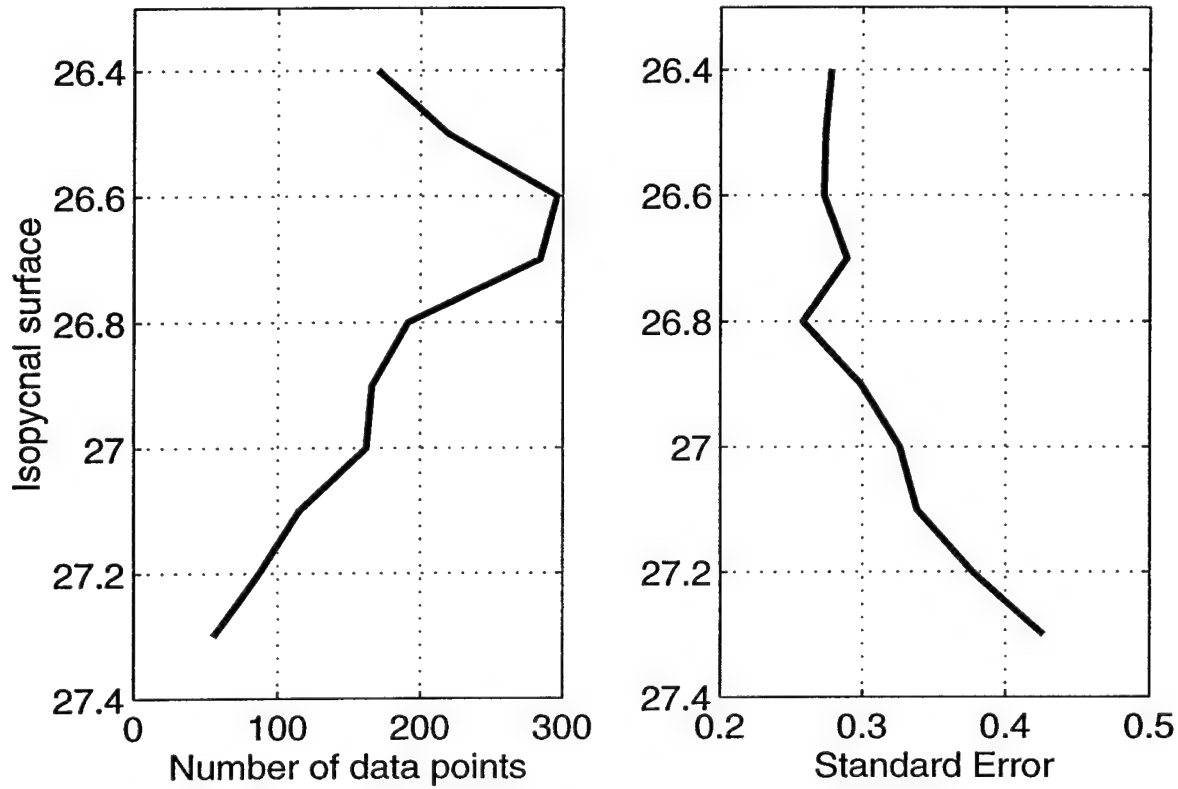


Figure 2.8: a) Number of age estimates for each isopycnal surface b) standard error (years) of interpolated age measurements on each isopycnal surface.

larger uncertainty of age estimates for older ages leads to increased uncertainty with depth.

The uncertainty of a tritium- $^3\text{He}$  age estimate depends on the both the magnitudes and uncertainties of the component tracers according to

$$\sigma_\tau = \frac{1}{\lambda} \left[ \left( \frac{^3\text{He}}{^3\text{H}} \left( \frac{1}{^3\text{He} + ^3\text{H}} \right) \right)^2 \sigma_{(^3\text{H})}^2 + \left( \frac{1}{^3\text{He} + ^3\text{H}} \right)^2 \sigma_{(^3\text{He})}^2 \right]^{0.5}. \quad (2.1.5)$$

Equation 2.1.5 shows that the uncertainty of the age estimate increases as the ratio of  $^3\text{He}$  to  $^3\text{H}$  burden of a water parcel increases. Figure 2.9 shows an example of how the uncertainty of age increases for older water parcels. In this example a hypothetical water parcel with a specified tritium content and no  $^3\text{He}$  is isolated from the atmosphere. The tritium and  $^3\text{He}$  content are allowed to evolve over time as prescribed by radioactive decay. If the analytic uncertainties of the  $^3\text{H}$  and  $^3\text{He}$  measurements are

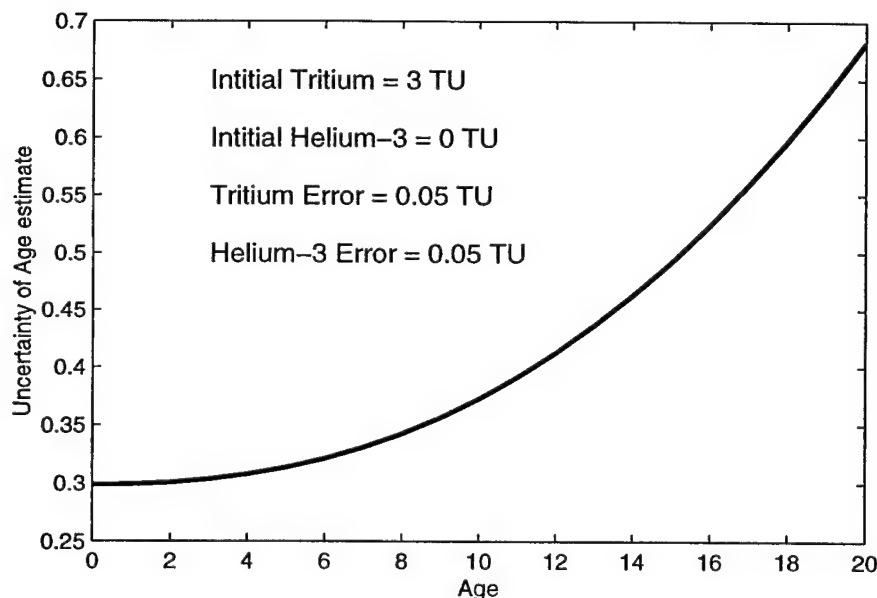


Figure 2.9: Example of uncertainty of age estimate following a parcel of water with initial tritium content of 3 TU. The analytic uncertainty of the measurement is assumed to be constant at 0.05 TU.

fixed, the uncertainty of the derived age increases as tritium mutates to  $^3\text{He}$ . Comparison of figure 2.9 and 2.8b suggests that the observed increase in age uncertainty with depth is primarily caused by inherent increase in uncertainty for waters with larger tritium- $^3\text{He}$  age values.

## 2.2 Statistical Test of Steadiness

Combining transient tracer measurements to form a tracer age has the potential advantage of obtaining a composite diagnostic field which is steady in the ocean provided ventilation and circulation characteristics of the ocean do not change drastically with time. A steady distribution of a diagnostic field, if it exists, aids the interpretation of observations gathered over a period of many years, since measurements from different times may be combined to form a single picture of the tracer age field. The fifteen years of data coverage in figure 2.1 provide a data set with which to test for the

steadiness of the tritium-<sup>3</sup>He age field. The mixed geographic coverage of the different cruises in figure 2.1 preclude a direct estimate of changes in tritium-<sup>3</sup>He age; there is no time series of measurements at any fixed point in the eastern subtropical gyre. One can, however, take advantage of the large-scale structure of the age field to combine and compare data from different locations.

An age tracer increases its value at a constant rate following the flow. For broad-scale flows, such as those characteristic of the oceanic interior, the age field is expected to have a smoothly increasing large-scale structure. A convenient means to extract this large-scale structure is through the use of a polynomial regression where the regressor variables are geographic coordinates. For example, one can attempt to fit the measured tritium-<sup>3</sup>He age values on an isopycnal surface with a multivariate regression model such as

$$\tau_1(x, y) = \mathcal{F}(x, y) = \tau_0 + aX + bY + cX^2 + dY^2 + eXY + \dots \quad (2.2.6)$$

where

$$X = [\textit{longitude} - \textit{longitude}_O],$$

$$Y = [\textit{latitude} - \textit{latitude}_O]$$

and a, b, c, ... are the regression coefficients. The order of the regression in equation 2.2.6 can be chosen to obtain a model statistically consistent with the data.

If it is suspected that the tracer age field is evolving over the course of the measurements, one might seek to fit the data with a functional regression of the form

$$\tau(x, y, t) = \mathcal{H}(x, y, t). \quad (2.2.7)$$

Separating  $\mathcal{H}$  into a time-independent,  $\mathcal{F}$ , and time-dependent,  $\mathcal{G}$ , components and expanding the latter in a Taylor expansion leads to:

$$\tau(x, y, t) = \mathcal{F}(x, y) + \frac{\partial \mathcal{G}(x, y, t)}{\partial t} \partial t + \frac{\partial^2 \mathcal{G}(x, y, t)}{\partial t^2} \partial t^2 + \dots \quad (2.2.8)$$

If one seeks to model that portion of the age field which is slowly changing compared to the length of the observational record, higher order terms in the Taylor expansion may be neglected. Furthermore, if the temporal tendencies of the tracer age field are predominantly broad-scale, then one can model the partial derivative in equation 2.2.8 as

$$\frac{\partial \mathcal{G}(x, y, t)}{\partial t} = \alpha + \beta X + \gamma Y + \dots \quad (2.2.9)$$

where  $X$  and  $Y$  are as above and  $\alpha, \beta, \gamma$  are again regression coefficients. Combining equation 2.2.9 with the previous expression for the time-independent component of the age field (equation 2.2.6) results in a spatially and temporally-dependent polynomial regression for tracer age:

$$\tau_2(x, y, t) = \tau_0 + aX + bY + cX^2 + dY^2 + eXY + T * (\alpha + \beta X + \gamma * Y) + \dots \quad (2.2.10)$$

where

$$T = [time - time_0].$$

The time-dependent term is taken to be simply proportional to time, but the coefficient of proportionality is allowed to vary in space.

Least-squares solutions for all of the above regression models can be obtained by casting the regression models into matrix notation:

$$\mathbf{E} * \mathbf{m} = \tau \quad (2.2.11)$$

where  $\tau$  is the interpolated tracer age,  $\mathbf{E}$  is a matrix of the regressor values and  $\mathbf{m}$  is a vector of the model coefficients. The solution for model coefficients is then:

$$\mathbf{m} = (\mathbf{E}'\mathbf{W}\mathbf{E})^{-1}\mathbf{E}'\mathbf{W}\tau \quad (2.2.12)$$

where primes indicate the transpose operator and the weighting matrix  $\mathbf{W}$  possesses diagonal elements proportional to the inverse of the data uncertainties:

$$\mathbf{W}_{ii} = (\sigma_{interpolation})^{-2}. \quad (2.2.13)$$



The ability of a regression model to explain a set of data can be measured quantitatively by examining the magnitude of the residuals between data and the model predictions. The typical measure is the sum of the squares of the residuals, RSS:

$$RSS = \sum_i (Em - \tau). \quad (2.2.14)$$

For a weighted-least squares solution this value must be normalized by the uncertainty of the data:

$$RSS = \sum_i \frac{(Em - \tau)}{\sigma_\tau}. \quad (2.2.15)$$

In general, adding more regressor variables, in this case increasing the order of the polynomial fit, will always decrease the value of RSS. It is crucial to differentiate between a decrease in RSS created by an improvement in the model structure as opposed to a decrease in RSS due simply to a decrease in the degrees of freedom of the model. To determine if this improvement in the model fit is statistically significant, the RSS of two models can be compared with an F-statistic:

$$F = \frac{\frac{RSS_0 - RSS_1}{p_1 - p_0}}{\frac{RSS_1}{N - p_1}} \quad (2.2.16)$$

where the subscripts represent the two models,  $p$  is the number of regressors for each model and  $N$  is the total number of data points. In this case the value of  $p_1$  is greater than  $p_0$  indicating that model 1 has more regressor coefficients than model 0. The denominator of equation 2.2.16 is a measure of the variance of the model with the greater number of regressor variables. The numerator is the reduction in variance of the more complex model compared to the simpler model. A large F-value indicates that the higher order model leads to a substantial reduction in the variance of the residuals. The critical value for a statistically significant reduction of variance is a function of  $N$ ,  $p_1$ ,  $p_0$  and a desired confidence level. F-tests will be used as a criterion of the ability of differing regression models to fit the observed age measurements.

### 2.2.1 Polynomial Regressions with Only Spatial Regressors

Regressions of the observed isopycnal age distributions were first performed using only the geographic position of the measurements as regressor variables. Selection of data for computing the regression was confined to the interior of the subtropical gyre (18-35°N). Data from the frontal regions along the northern and southern edges of the gyre (figure 2.5) are not included since the spatial gradients in these regions may reflect mixing between differing water types rather than the aging of water following the flow.

The standard deviations of the normalized residuals for a polynomial regressions with orders zero through three are shown in figure 2.10a. The thinnest line is the standard deviation of the residual for the zero-order fit, which is simply the error-weighted average of all the age measurements on the isopycnal within the eastern subtropical gyre. The standard deviation of the residual of the zero-order fit increases with depth from a minimum value of 5 on  $\sigma_\theta = 26.4$  to 9.5 on  $\sigma_\theta = 27.3$ . Increasing the order of the polynomial regression to include linear terms leads to a reduction in the magnitude of the residuals but further increases, to quadratic and cubic polynomials (not illustrated), show only marginal improvements except at the densest isopycnal surfaces. The standard deviation of the residual for the cubic model varies from 2.5 to 5.5. That this magnitude is substantially greater than unity indicates that either the model is insufficient or that the interpolation errors underestimate the true noise of the measurements. The latter of these possibilities will be explored below.

The fraction of the total variance explained by the regression model is shown in figure 2.10b. The linear model explains approximately 50% of the variance across the majority of the isopycnal surfaces. Increasing the order above linear leads to no visible gain in the explanatory power of the model except for the deepest portion of the thermocline. At the lightest and densest extremes, addition of quadratic curvature

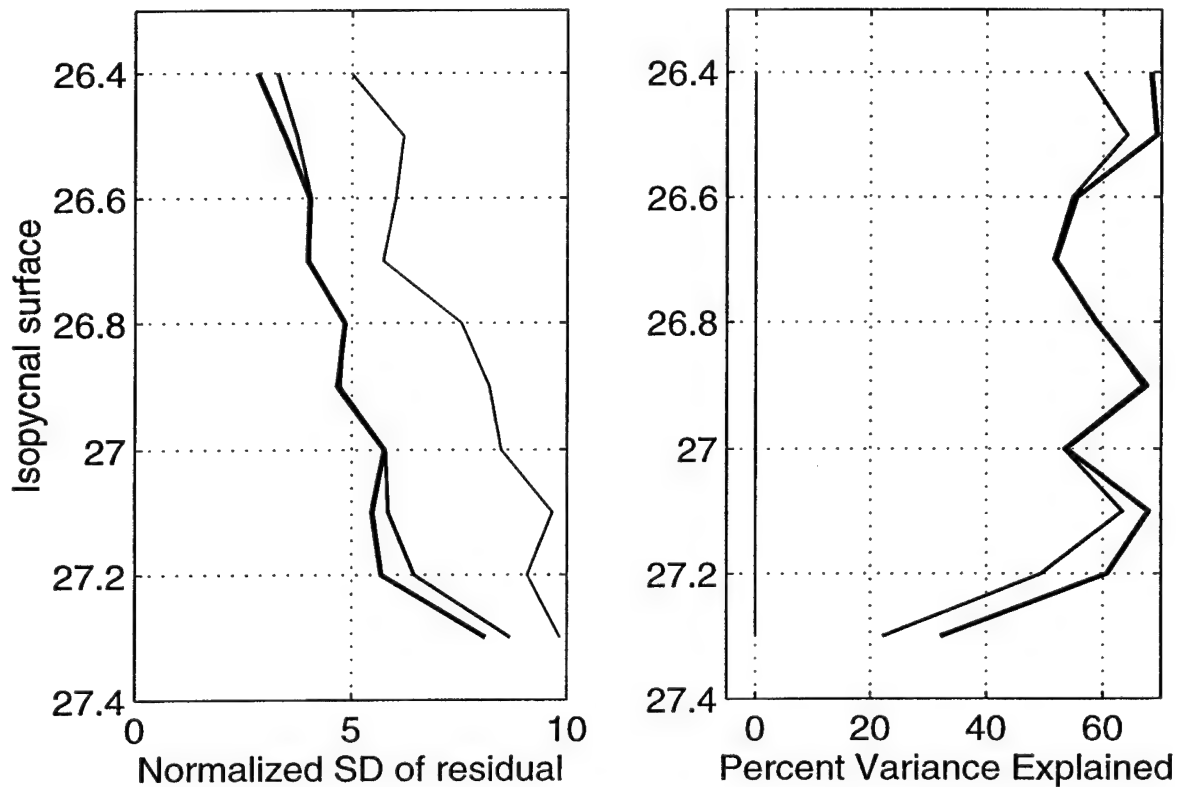


Figure 2.10: a) Normalized standard deviation of residual from polynomial regression with only spatial regressors. Estimated noise of measurements based only on interpolation and measurement errors. b) Percent of total variance explained. The three lines represent polynomial fits of increasing order with the thinnest being a fit of zero-order and progressively thicker lines of higher order up to order 2.

terms does increase slightly the ability of the model to represent the data but the magnitude of the enhancement is small compared to the increases gained by using just a linear model.

Figure 2.10a suggests that the uncertainty of the age estimate based on measurement and interpolation uncertainties is not consistent with the magnitude of the residuals of the model fit. Are there other sources of uncertainty that have been neglected? Stirring due to mesoscale variability can impart a degree of graininess to property distributions if significant property gradients exist. If such granularity is significant, it would introduce additional uncertainty that must be accounted for when attempting to model observed data with large-scale polynomial expansions. The

magnitude of the deviations introduced by mesoscale stirring should scale as a mixing length times the mean gradient [Armi and Stommel, 1983; Jenkins, 1987; Joyce and Jenkins, 1993]:

$$\tau' = l' |\nabla \tau| \quad (2.2.17)$$

where  $l'$  is the mixing length. Adopting a mixing length of 100 km<sup>a</sup> and a large scale gradient based on the minimum and maximum age value observed on each isopycnal, equation 2.2.17 can be used to estimate the uncertainty of an age estimate due to eddy “noise”. Figure 2.11 illustrates the potential effect of the mesoscale stirring on

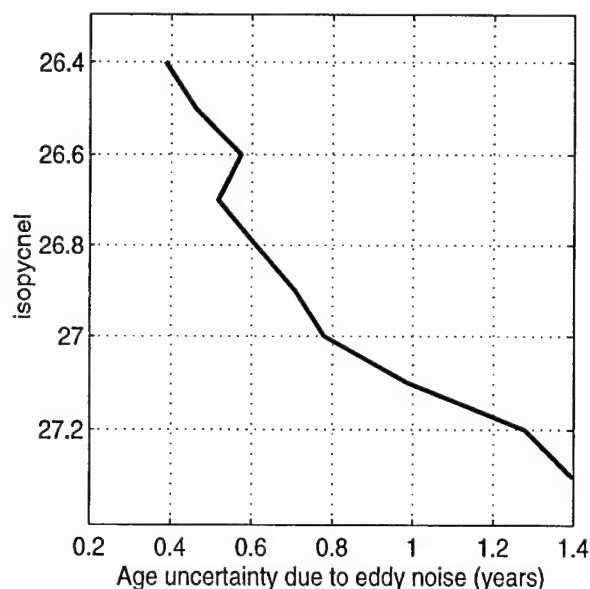


Figure 2.11: Uncertainty in age estimate on an isopycnal due to granularity introduced by mesoscale variability. Magnitude of uncertainty is based on large scale gradient of age field and a mixing length of 100 km.

sampling error of the large scale age field. Comparison of figure 2.11 with figure 2.8b shows that the eddy “noise” is comparable to the typical interpolation error in the

<sup>a</sup>A length-scale of 100 km is at the lower end of the estimates of published values of length scale based on observed mesoscale distribution of tracer fields [Armi and Stommel, 1983; Jenkins, 1987; Joyce and Jenkins, 1993]. The alongtrack auto-correlation function from TOPEX/POSEIDON altimeter data in the eastern Atlantic suggests a comparable length scale [Stammer and Böning, 1996]. Integral length scales determined from float dispersal in this region result in estimates ranging from 20 to 80 km [Böning, 1988].

upper thermocline but increases to a magnitude of roughly three times the value of the interpolation error for the lower thermocline.

Including the additional uncertainty due to mesoscale graininess, we can revise the estimate of the noise variance for the weighting matrix in equation 2.2.13 to

$$\mathbf{W}_{ii} = [(\sigma_{interpolation})^2 + (\sigma_{mesoscale})^2]^{-1} \quad (2.2.18)$$

where  $\sigma_{mesoscale}$  is given in figure 2.11. The revised noise estimate of equation 2.2.18 sets a minimum noise level for each estimation of tracer age regardless of the precision of the analytic measurements or smallness of the interpolation error.

The model results using the revised estimate of the noise variance are summarized in figure 2.12. Comparison with figure 2.10 shows that the normalized variance of the residuals is now reduced, and though not equal to unity, the hypothesized noise variance is more consistent with the residuals of the model fit. The standard deviation of the model fit does still increase with depth but less dramatically since the addition of mesoscale noise has the greatest impact on the deeper surfaces. The fraction of total variance explained by the model is roughly as before except for the isopycnal surface  $\sigma_\theta = 27.3$ , where the the model explains virtually none of the variance of the data. Again, most of the explanatory power of the geographic model derives from the linear coefficients with higher order curvature terms contributing little or no additional information. Table 2.3 shows this quantitatively by displaying the results of an F-test comparison of the explanatory power of successive higher order regression models. As expected from inspection of figure 2.12, the linear model is a statistically significant improvement over a constant fit, excepting  $\sigma_\theta = 27.3$ . Addition of quadratic terms to the model appears to lead to statistical improvement in the model on several of the isopycnal surfaces. The isopycnal  $\sigma_\theta = 27.3$  appears anomalous in both figure 2.12 and table 2.3. There are fewer data points available on this surface which could be part of the explanation. Also, this isopycnal surface outcrops far to

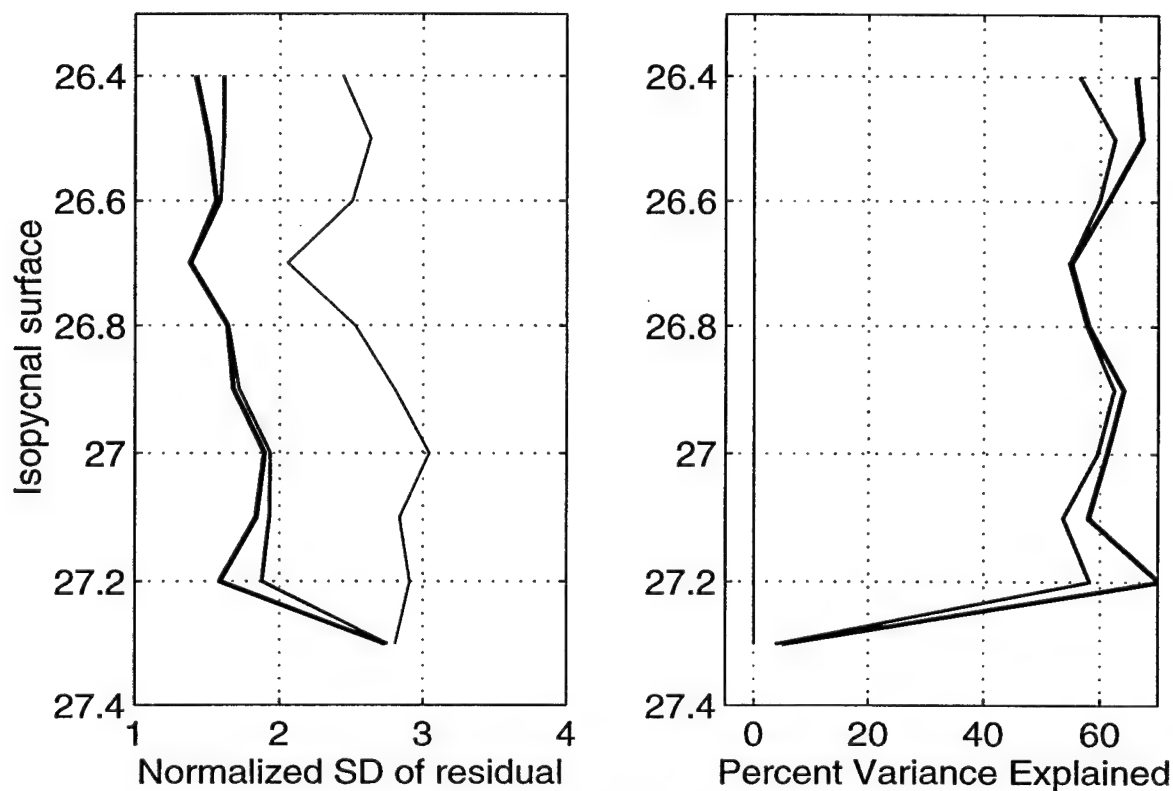


Figure 2.12: a) Normalized standard deviation of residual from polynomial regression with only spatial regressors. Noise estimate of measurements based on uncertainty of both interpolation and mesoscale variability. b) Percent of total variance explained. The three lines represent polynomial fits of increasing order with the thinnest being a fit of zero-order and progressively thicker lines of higher order up to order 2.

the north in the subpolar gyre so the observed differences between this and lighter surfaces could signify differing ventilation processes.

Examination of the structure of the residuals of the polynomial regressions reveals an apparent dependence on the time of sample collection. The magnitude of this temporal effect appears most dramatically on the denser isopycnal surfaces where figure 2.12 indicates larger residual variance of model fits based only on spatial regressors. The residuals from a linear polynomial fit on  $\sigma_\theta = 27.0$  are shown as a function of time of survey in figure 2.13. A clear downward trend exists in the residuals indicating that inclusion of time as an additional regressor should lead to improved explanatory power of the multiple regression.

Isopycnal	1 <sup>st</sup> vs. 0 <sup>th</sup>	2 <sup>nd</sup> vs. 1 <sup>st</sup>
26.4	*	*
26.5	*	*
26.6	*	*
26.7	*	
26.8	*	
26.9	*	*
27.0	*	
27.1	*	*
27.2	*	*
27.3		

Table 2.3: F-test results for polynomial model with only spatial regressors. Asterisks indicate when the higher order model provides a significant reduction in variance of the residuals at a 98% confidence level.

### 2.2.2 Polynomial Regressions with Spatial and Temporal Regressors

The structure of the residuals displayed in figure 2.13 suggests that the tritium-<sup>3</sup>He age field is not steady in the eastern North Atlantic and a polynomial regression model used to explain the tritium-<sup>3</sup>He age observations should contain a component proportional to the time of observation such as proposed in equation 2.2.10. This form of multiple regression assumes that the changes in the observed age field vary linearly with time but that the magnitude of this trend may vary in space.

The previous section, as summarized in the statistical results shown in table 2.3, determined that the time-independent component of the polynomial regression is chiefly explained by a model which is first order of the spatial coordinates. Figure 2.14 compares the explanatory power of a hierarchy of time-dependent polynomial regression models with the first-order time-independent model of the previous section. The thinnest line in figure 2.14 displays the model results of a first order regression model with no time component. The increasingly thicker lines show the performance of a time-dependent model where the temporal coefficient is a) constant, b) first-order in

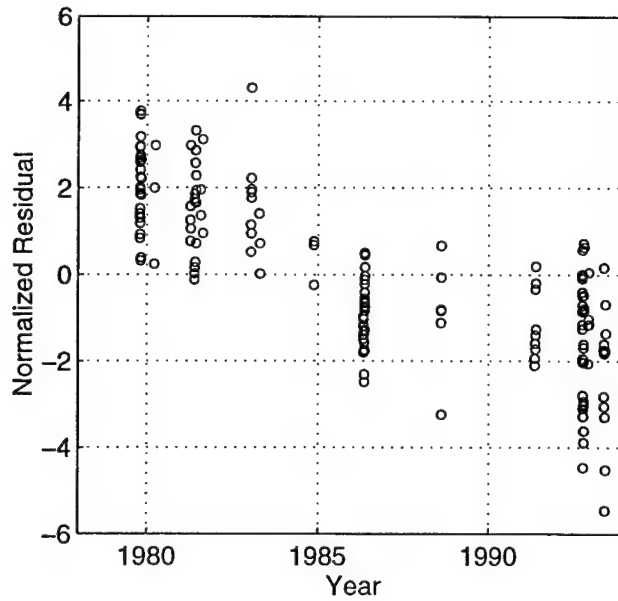


Figure 2.13: Normalized residuals on  $\sigma_\theta = 27.0$  from linear polynomial regression with only spatial regressors.

spatial coordinates, and c) second order in spatial coordinates. Inclusion of a time component in the model substantially decreases the variance of the residual as well as the total variance explained by the model.

The increase in performance of the time-dependent model is most pronounced in the lower portion of the thermocline. Compared to the time-independent model, the normalized variance at  $\sigma_\theta = 27.0$  decreases by a factor of 4 and the fraction of the total variance explained increases by 30%. The vast majority of this improvement appears from the simple addition of a constant (spatially independent) tendency term. On  $\sigma_\theta = 27.3$ , virtually all of the model's explanatory power derives from the temporally dependent components. The magnitude of the normalized standard deviation is order one implying agreement between the model fit and the *a priori* hypothesis of noise. The model does less well in the upper portion of the thermocline,  $\sigma_\theta < 26.7$ , where the addition of the temporal terms only marginally improves the explanatory power of the regression. Some process other than a long-term temporal drift, is required to fully understand the spatial and temporal structure of the tritium- $^3\text{He}$  age observations in



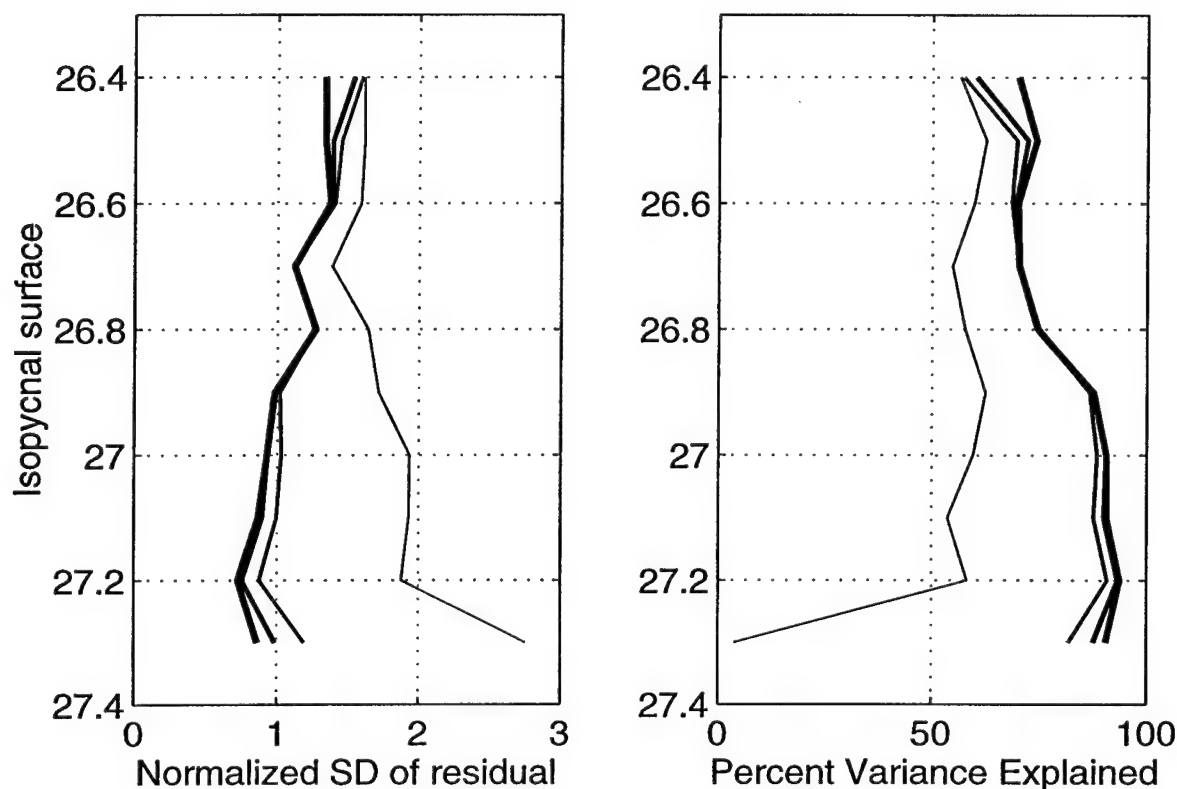


Figure 2.14: a) Normalized standard deviation of residual from polynomial regression with both temporal and spatial regressors. Estimated noise of measurements based on interpolation, measurement and mesoscale noise. b) Percent of total variance explained. The four lines represent polynomial fits of increasing order with the thinnest being for a model with only spatial regressors. The thicker lines represent the results of increasing the order of the temporal component of the model from 0 through 2.

the upper thermocline. Problems from aliasing caused by temporal under-sampling would be expected to have the largest impact at the short time-scales. The interplay of the seasonal effects of late winter subduction and the month of hydrographic sampling could possibly explain a portion of the variance of the lightest surfaces where the tritium- $^3\text{He}$  age is typically only a year or two. Measurements taken in spring near the location of the winter outcrop position will have an age of a few months whereas measurements at the same location but taken in the fall might be expected to have ages of 8-10 months. Examination of the residuals (figure 2.15), however, reveals no obvious unaccounted for seasonal effect. Comparison of the residuals in the upper

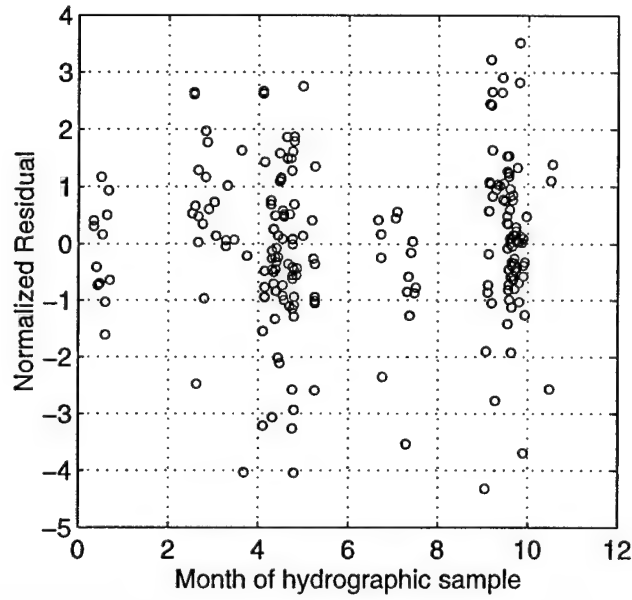


Figure 2.15: Normalized residuals on  $\sigma_\theta = 26.5$  from first order time-dependent polynomial regression.

thermocline with other measured water properties (salinity, oxygen) also failed to expose other possible ways to improve the regression model.

Application of the F-test (table 2.4) shows that a tendency term that varies linearly in space, though explaining only a small fraction of the variance, does provide a statistically significant improvement in fit on most of the isopycnals. In the mid-thermocline ( $\sigma_\theta \approx 26.7$ ), however, a model with a geographically-independent temporal trend performs best.

The results of the time-dependent model show that there is a statistically significant trend to the temporal evolution of the age field in the lower eastern subtropical thermocline. The large explanatory power of the time-dependent model, as portrayed in table 2.4, requires a re-examination of the conclusions drawn from the time-independent model. Table 2.3 implies that the quadratic curvature of the age field determined from the 2<sup>nd</sup> order regression model is statistically significant. To what extent is this finding an artifact of the failure to incorporate the temporal tend-

Isopycnal	0 <sup>th</sup> vs. steady	1 <sup>st</sup> vs. 0 <sup>th</sup>	2 <sup>nd</sup> vs. 1 <sup>st</sup>
26.4		*	*
26.5	*	*	*
26.6	*	*	
26.7	*		
26.8	*		
26.9	*	*	
27.0	*	*	
27.1	*	*	
27.2	*	*	
27.3	*	*	*

Table 2.4: F-test results for polynomial model with temporal and spatial regressors. The steady portion of the model is set to first order. The first column compares a model with a zero-order temporal regressor component with the a model employing only spatial regressors. The subsequent columns examine the statistical effect of increasing the order of the temporally-dependent component of the model. Asterisks indicate when the higher order model provides a significant reduction in variance of the residuals at a 98% confidence level.

ency terms in the design of the regression model? To explore this question, table 2.5 compares the statistical significance of two time-dependent models with differing regression order in the steady component. The temporal tendency term is taken to be first-order in both cases. Table 2.5 shows that when the temporal evolution is properly accounted for, there is no significant curvature of the fields on isopycnal surfaces across the main thermocline between  $\sigma_\theta = 26.5$  and  $\sigma_\theta = 27.1$ .

The results of the statistical comparison of all the regression models in tables 2.5, 2.4, and 2.3 signify that the tritium-<sup>3</sup>He age observations in the bulk of the eastern North Atlantic thermocline can be best explained by a polynomial regression in which both the age and the age tendency are planar functions of latitude and longitude. If there is curvature of the age field in the main thermocline within this region, it cannot be resolved with the present data. Furthermore, comparison of figures 2.11 and 2.8b implies that attempts to map the large-scale age distribution are limited predominantly

Isopycnal	2 <sup>nd</sup> vs 1 <sup>st</sup>
26.4	*
26.5	
26.6	
26.7	
26.8	
26.9	
27.0	
27.1	
27.2	*
27.3	*

Table 2.5: F-test results for significance of curvature in a polynomial model with temporal and spatial regressors. The temporal portion of the model is set to first order. The table compares a model with a first-order time-independent component against a model with quadratic time-independent component. Asterisks indicate when the higher order model provides a significant reduction in variance of the residuals at a 98% confidence level.

by distortions created by mesoscale variability as opposed to the analytic uncertainty of  $^3\text{He}$  and  $^3\text{H}$  measurements.

Anomalous behavior of the regression model is evident in the upper and lower extremes of the thermocline. On the lightest surface examined,  $\sigma_\theta = 26.4$ , higher order models appear appropriate both for the steady (table 2.5) as well as time-dependent components (table 2.4) of the model. This isopycnal surface outcrops within the region of study and the presence of two regimes (both a seasonal and permanent thermocline) likely introduces higher order structure to the mean age fields. The deeper surfaces analyzed,  $\sigma_\theta > 27.2$ , are substantially denser than any water which outcrops within the subtropical gyre. The predominance of the tendency term and the significant curvature of these fields at these levels could be a signal of the action of a different ventilation process, but may also simply arise from the greater sparsity of data at this depth (see figure 2.8a).

A summary of the key parameters of the temporally-dependent regression model is shown in figure 2.16. The magnitude of the tritium- $^3\text{He}$  age tendency term at

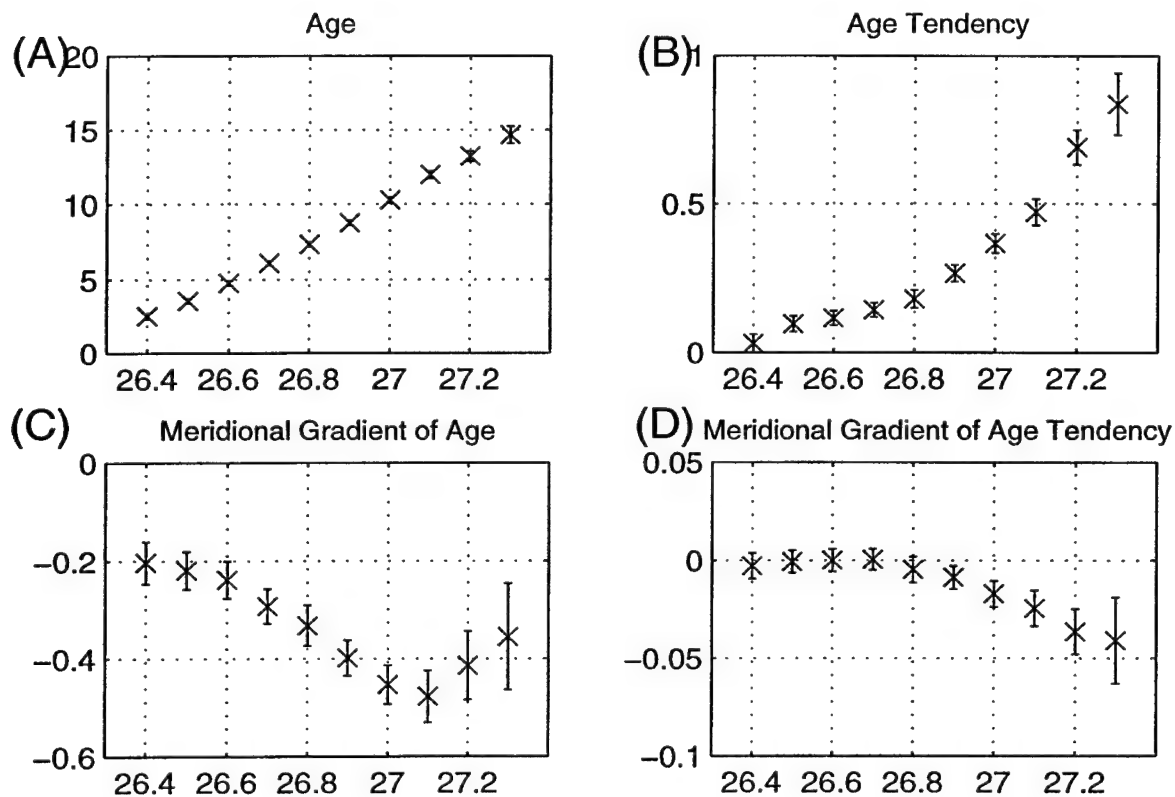


Figure 2.16: Summary of regression model results for tritium-<sup>3</sup>He age on isopycnal surfaces in eastern North Atlantic evaluated for the year 1986: A) mean tritium-<sup>3</sup>He age (yr), B) temporal tendency of tritium-<sup>3</sup>He age, C) mean meridional age gradient of tritium-<sup>3</sup>He age (yr · degrees<sup>-1</sup>), and D) tendency of meridional age gradient (degrees<sup>-1</sup>). Error bars show 95% confidence limits. Age is expressed in years and gradients are in degrees latitude.

the center of the analysis region is shown in figure 2.16B. The mean tendency term is non-zero on all surfaces, consistent with the finding that the addition of time-dependent terms improves the explanatory power of the regression model. The size of the tendency term increases dramatically with increasing density.

Age distributions on select isopycnals determined by the first-order time-dependent regression model are shown in left-hand column of figure 2.17. Since the age distribution is evolving with time, a date within the middle of the observation period, 1986, was selected for displaying the representative large-scale age field. The youngest tritium-<sup>3</sup>He age on each of the isopycnal surfaces are observed in the north-

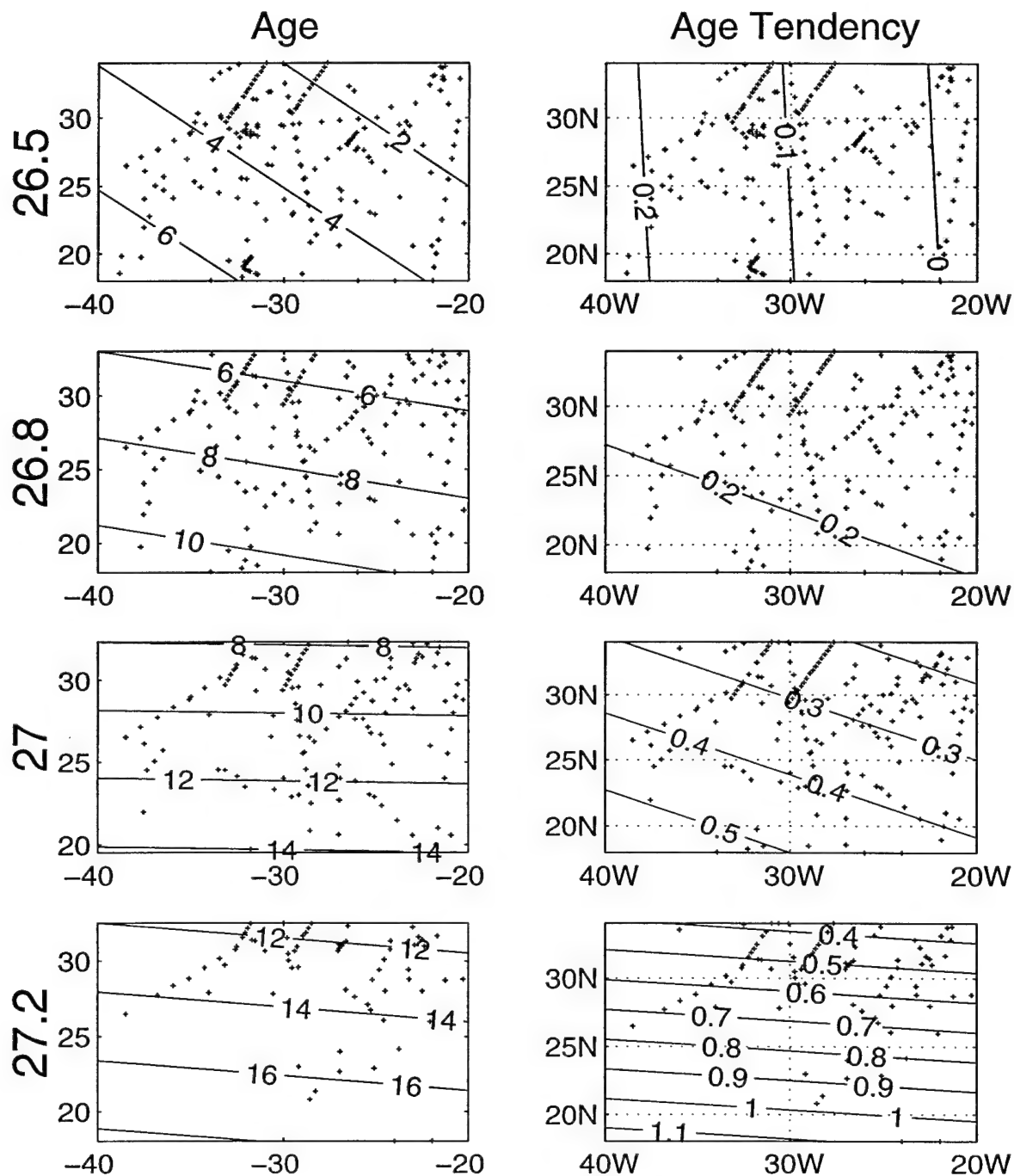


Figure 2.17: Tritium- $^3\text{He}$  age distribution in 1986 and age tendency on isopycnal surfaces determined from a regression model of first order in both steady and time-dependent components. Potential density of each isopycnal surface is shown in left hand column. Contour levels of tritium- $^3\text{He}$  age are 2 years and those for age tendency are 0.1. Positions of tritium- $^3\text{He}$  age data points on each surface are indicated by small crosses.

east corner of the region. Age values increase towards the southwest with the strength of the tritium- $^3\text{He}$  age gradient increasing with depth. Also apparent in figure 2.17 is a counter-clockwise rotation of the age gradient with depth. The right-hand column of figure 2.17 shows the age tendency field determined from the polynomial regressions. Changes in the age field appear to fall into two regimes: in the upper thermocline, where the tendency of the age field has the least explanatory power, the magnitude of the tendency is small and the geographic structure displays a zonal gradient. On  $\sigma_\theta=26.7$  and  $26.8$ , the magnitude of the age tendency is significant (0.2) but there is no significant geographic structure in the tendency term (table 2.4). The lower thermocline, in contrast, shows significantly larger rates of change and the structure of the tendency is similar to that of the tritium- $^3\text{He}$  age field itself: lowest values in the northeast. The similarity of the structure of tritium- $^3\text{He}$  age and tritium- $^3\text{He}$  age tendency in the lower thermocline indicates that the “oldest” age values are the ones that are changing most rapidly.

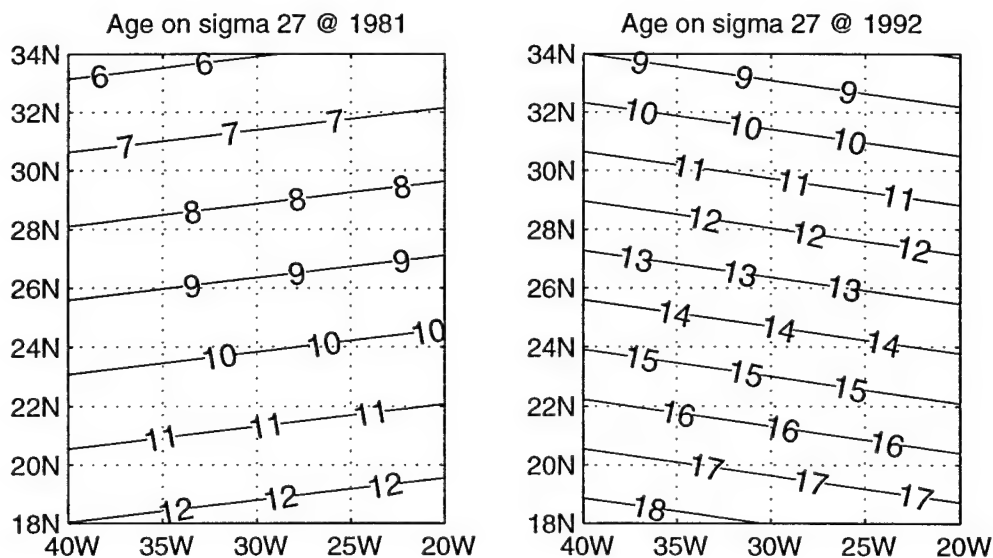


Figure 2.18: Two realizations of the tritium- $^3\text{He}$  age field on  $\sigma_\theta = 27.0$  as determined by the time-dependent regression model. Left-hand figure shows age field in 1981 and right-hand figure shows age in 1992

On the deeper isopycnal surfaces the temporal tendency has large impact on the observed age field over the course of the observations. Figure 2.18 shows the estimate

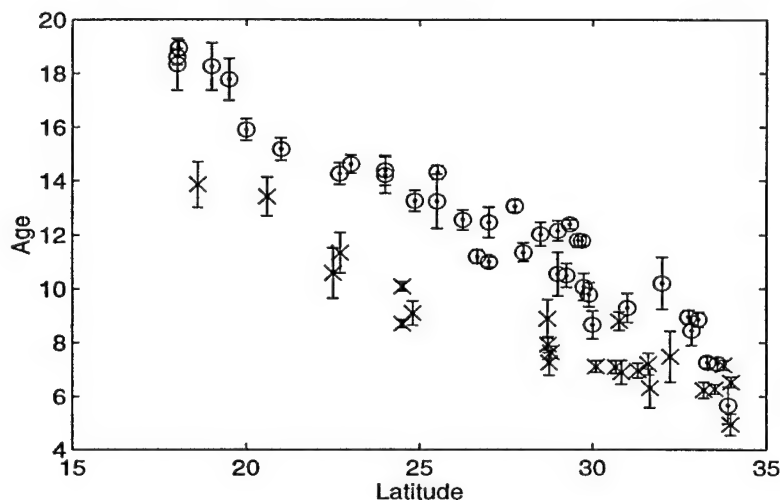


Figure 2.19: Tritium- $^3\text{He}$  age on  $\sigma_\theta = 27.0$  at two different years. Samples collected in 1992 are indicated by a 'o' while those from 1981 are represented with an 'x'. Error bars represent uncertainty to the combined analytic and interpolation errors.

of the age field on  $\sigma_\theta = 27.0$  at the two years with the most observations: 1981 and 1992. Changes in both the mean age as well as the age gradient are evident. Shifts in the age field of this magnitude are also clearly visible in the raw data itself 2.19. The changes seen over the course of the observations are far greater than the data uncertainty.

## 2.3 Comparison with Previous Estimates of Steadiness

Prior estimates of the steadiness of the tritium- $^3\text{He}$  age field in the eastern North Atlantic thermocline have concluded that the magnitude of the age tendency is significantly less than found in this study. Roether [1989b] compared data from two hydrographic casts taken 3.5 years apart at  $28^\circ\text{N}$ ,  $25^\circ\text{W}$  (his graph of the data is



reproduced here as figure 2.20). Observing the close similarity of the profiles, Roether

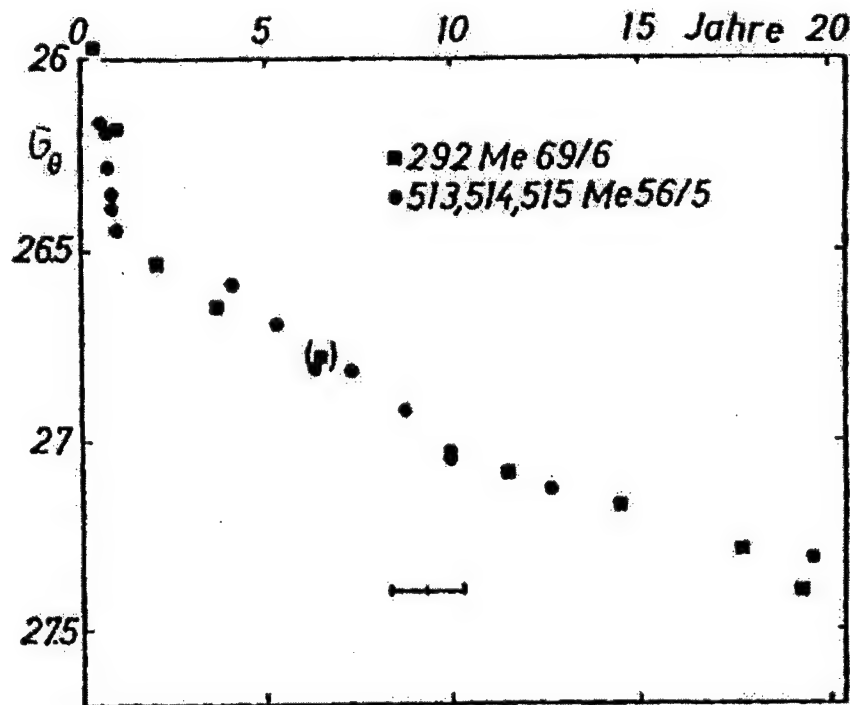


Figure 2.20: Comparison of two profiles of tritium-<sup>3</sup>He age separated in time by 3.5 years reproduced from Roether [1989b]. Both station were occupied near 28°N, 25°W, in April 1981 (F/S Meteor 56/5) and November 1984 (F/S Meteor 69/6).

concluded that the upper limit on the tendency of the age field was about 0.15. Following from the conclusion of the relatively small estimate of age tendency, Roether argued for the application of the equation  $u \cdot \nabla \tau = 1$  as an accurate diagnostic of the velocity field. For comparison, the tritium-<sup>3</sup>He age tendency diagnosed in this study for  $\sigma_\theta = 27.3$  is  $0.8 \pm 0.1$ .

Why is there such a large difference in the estimate of the steadiness of the tracer age field? The present estimate of the tendency is based on regression models applied to isopycnal surfaces using typically 100-200 independent data points while Roether's conclusion was based on the comparison of only two hydrographic casts. However, as shown in this chapter, the expected eddy noise of any individual measurement is large owing to substantial spatial gradients of the age field (figure 2.11). Thus, two

hydrographic casts separated by 3.5 years are probably not sufficient for testing the steadiness of the tracer age field.

## 2.4 Evolution of Tracer fields at Bermuda

The Helium Isotope Laboratory at Woods Hole conducted a time series of  $^3\text{H}$  and  $^3\text{He}$  measurements at a hydrographic station near Bermuda ( $32^\circ 10'\text{N}$ ,  $64^\circ 30'\text{W}$ ) from 1977 through 1988. Portions of this time series have been previously discussed in terms of thermocline ventilation [Jenkins, 1980; Jenkins, 1982a; Jenkins, 1997], air-sea gas exchange [Jenkins, 1988a], isopycnal diffusivity [Jenkins, 1991], and the vertical flux of nitrate [Jenkins, 1988b]. The hydrographic time series at Bermuda is representative of changes throughout the western portion of the subtropical gyre [Joyce and Robbins, 1996] which, unlike the eastern North Atlantic, is characterized by strong recirculation from the western boundary current rather than direct ventilation from the surface mixed layer [Luyten, Pedlosky and Stommel, 1983; Schmitz, Jr. and McCartney, 1993].

Figure 2.21 displays the time series of decay-normalized tritium and tritium- $^3\text{He}$  age as a function of isopycnal. The tritium inventory shows a subsurface maximum associated with the subtropical mode water ( $\sigma_\theta = 26.5$ ) formed south of the Gulf Stream [Worthington, 1959; Talley and Raymer, 1982]. The temporal trend in  $^3\text{H}$  suggests a slight decrease over time but the predominant feature is the temporal steadiness of the tritium inventory once changes due radioactivity decay are accounted for. Section 2.5 discusses the changes in  $^3\text{H}$  concentrations and compares the eastern and western regions of the basin. The distribution of tritium- $^3\text{He}$  age (figure 2.21b) increases uniformly with depth. On all isopycnals, there is a temporal trend of increasing tracer age values over the span of the time series.

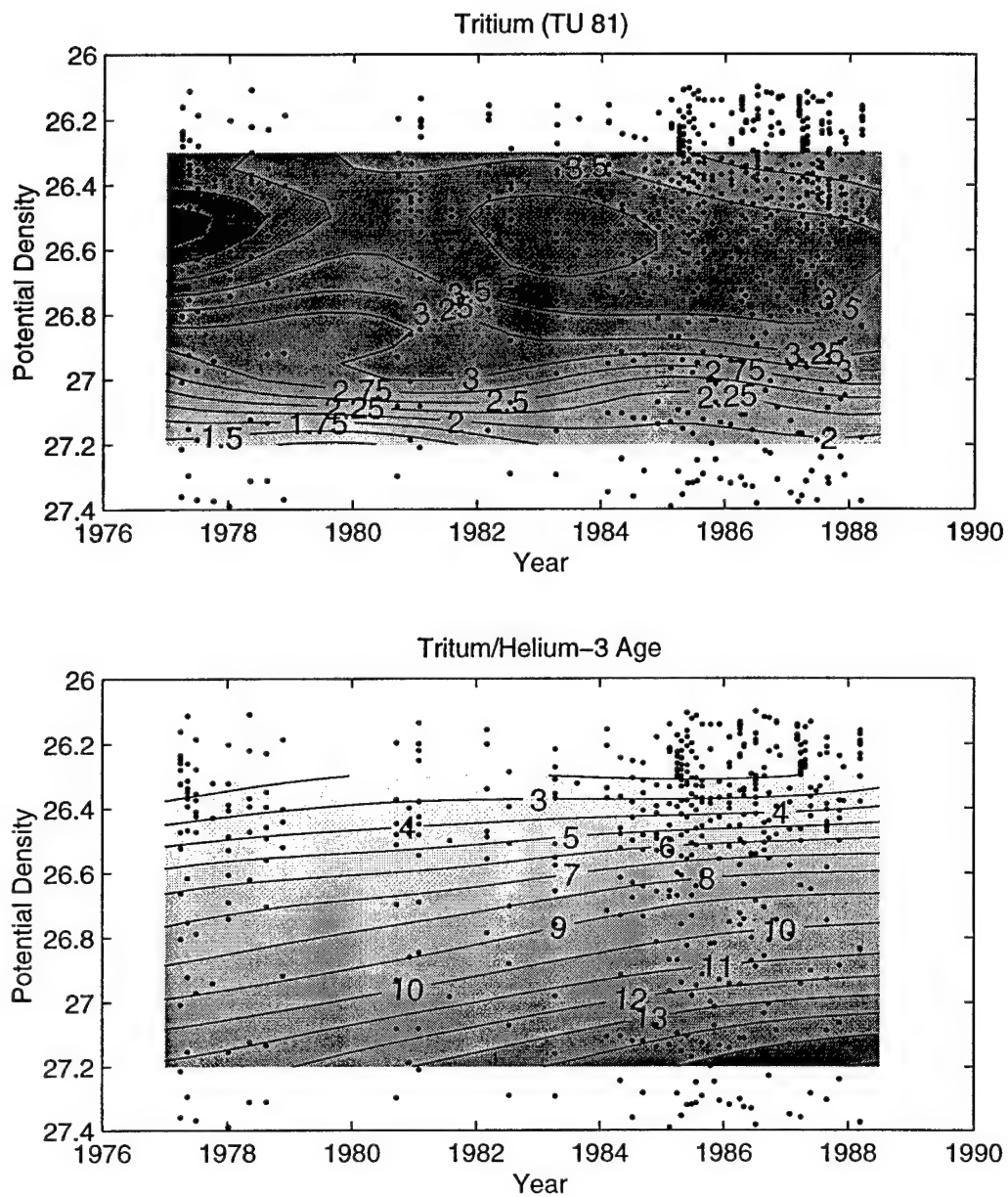


Figure 2.21: Time series of a) decay-normalized tritium (TU81) and b) tritium- $^3\text{He}$  age (years) at Bermuda. Position of data points is indicated by dots. Gridded fields were obtained from an objective-analysis assuming a Gaussian covariance with characteristic scale of 4 years and 0.2 sigma-units. Contour interval is 0.25 TU for tritium and 1 year for tracer age.

To quantify the change in tracer age, a time series of the tritium- $^3\text{He}$  age on isopycnal surfaces is constructed by interpolating data from the hydrographic casts onto density surfaces using the methodology described in §2.1.3. Data on each isopycnal surface is then fit to a function with a linear trend in time:

$$\tau = \tau_0 + \frac{\partial \tau}{\partial t}(t - t_0), \quad (2.4.19)$$

where  $t$  is time and  $\tau_0$  and  $\frac{\partial \tau}{\partial t}$  are unknowns.

The estimates of  $\tau_0$  and  $\frac{\partial \tau}{\partial t}$  at Bermuda for isopycnal surfaces spanning the thermocline are shown in figure 2.22. Included for comparison are the values estimated

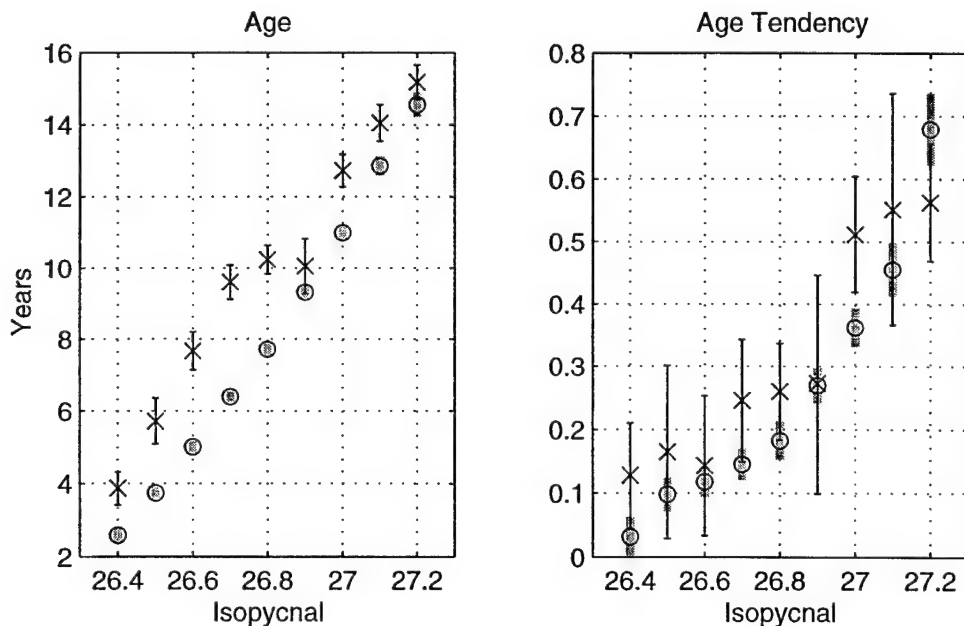


Figure 2.22: A) Tritium- $^3\text{He}$  age and B) age tendency estimated on isopycnal surfaces at Bermuda for the year 1986. Values determined from time-series at Bermuda are indicated by x's. For comparison the estimates of mean age and age tendency in the eastern North Atlantic are indicated by o's. Error bars for both sets of measurements represent the 95% confidence intervals.

in §2.2.2 for the eastern North Atlantic. On each isopycnal the tracer age is a few years older at Bermuda reflecting the greater distance between Bermuda and the surface outcrop. The trend of increasing tritium- $^3\text{He}$  age and age tendency with density

is similar in both the western and eastern regions of the subtropical thermocline. The uncertainties of the estimates at Bermuda are greater due to fewer data points from which the estimate is derived. The general agreement in the two data sets, however, support the conclusion of a systematic trend in tracer age based on the polynomial regressions in the eastern portion of the gyre and further demonstrates that the findings in the eastern Atlantic are representative of a pattern extending throughout the subtropical gyre.

## 2.5 Temporal Changes in Tritium Inventory

The multivariate regression models of §2.2.2 can also be applied to the observed transient tracer inventory in the eastern North Atlantic. I choose to measure inventory based on measured tritium values normalized to a common year, 1981<sup>b</sup> by using the known decay rate:

$${}^3H_{81} = {}^3H e^{\lambda(t-1981)}, \quad (2.5.20)$$

where  $t$  is the date of the tritium observation. Normalized tritium values provide a convenient means of comparison with other recent analysis of tritium in the North Atlantic [*Doney, Jenkins and Östlund*, 1993; *Jenkins*, 1997] which use identical measures of inventory. An alternative measure of inventory, “stable tritium”, composed of the sum of the observed  ${}^3H$  and  ${}^3He$  concentrations,

$$\zeta = {}^3H + {}^3He, \quad (2.5.21)$$

has also been employed in analyses in the North Atlantic [*Jenkins*, 1987; *Jenkins*, 1997; *Wunsch*, 1988a]. The choice is somewhat arbitrary, but for time-series analysis, decay-normalized tritium is preferable because effects of dilution are simpler to diagnose.<sup>c</sup>

---

<sup>b</sup>Designated by the tritium unit: TU81

<sup>c</sup>An isolated parcel of water at the surface will preserve its decay-normalized tritium value if not subject to any dilution with tritium-free water. On the other hand, the “stable tritium” concentration

Figure 2.23 displays the key parameters of multivariate regression models applied to the tritium dataset in the eastern North Atlantic. The standard error of the

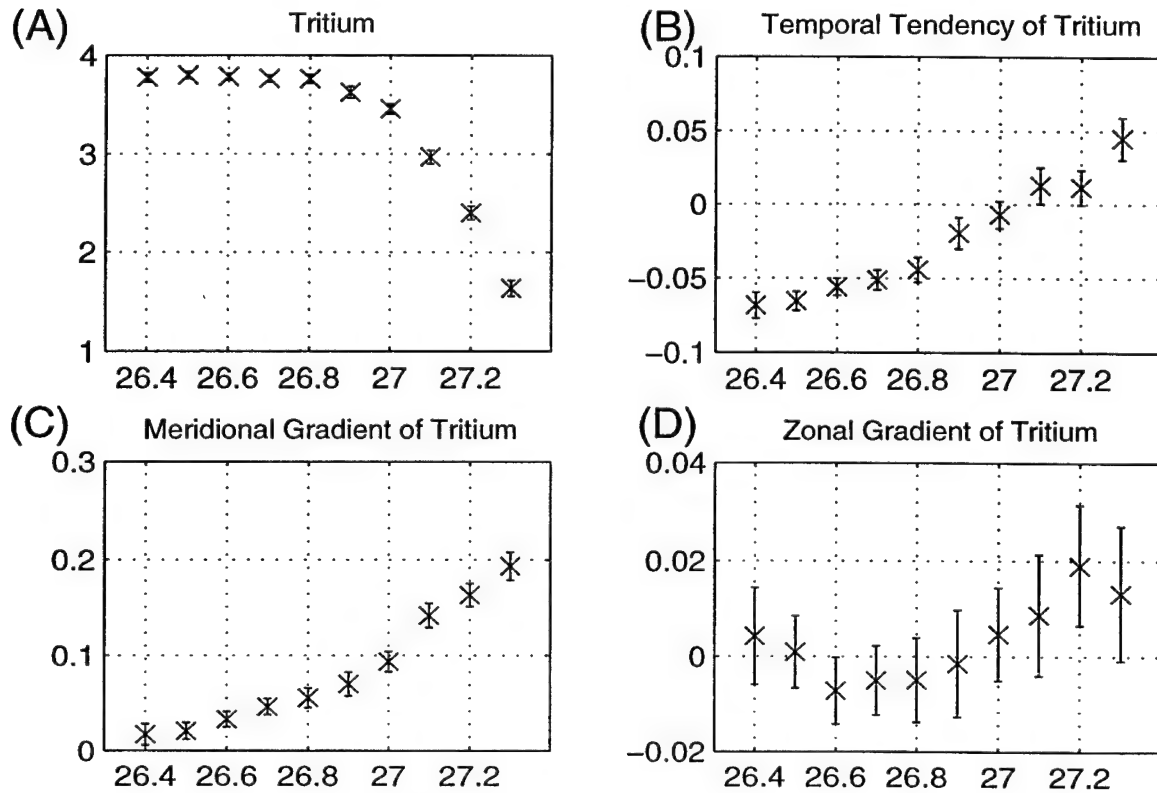


Figure 2.23: Summary of regression model of tritium concentration on isopycnal surfaces in eastern North Atlantic evaluated for the year 1986: A) mean tritium (TU81), B) temporal tendency of tritium (TU81 yr<sup>-1</sup>), C) meridional tritium gradient of (TU81 degrees<sup>-1</sup>), and D) zonal tritium gradient of (TU81 degrees<sup>-1</sup>). Error bars show 95% confidence limits.

fit is approximately 1.5 (TU81) for all density surfaces and the fraction of the total variance explained ranges from 55-80%. Tritium inventories are uniform in the upper thermocline ( $\sigma_\theta \leq 26.8$ ) and decrease rapidly in the lower thermocline. The slow rate of ventilation of the deeper layers below the main thermocline leads to the observed low tritium values at  $\sigma_\theta = 27.3$ .

of the same parcel will decrease over time as tritium mutates into <sup>3</sup>He and vents into the atmosphere. It is therefore more difficult to attribute observed decreases of "stable tritium" in the ocean to dilution as opposed to atmospheric exposure.

The temporal tendency of the tritium inventory shows opposing trends in the upper and lower thermocline. In the upper thermocline, the tritium inventory is decreasing over time (figure 2.23B), indicative of dilution with waters of lower tritium value. Tritium values in surface waters generally increase to the north so the decreasing inventory in the upper thermocline must be due to dilution with cross-equatorial transport of southern hemisphere waters. At  $\sigma_\theta = 27.0$  the tritium inventory is observed to be steady within the uncertainty of the calculation. On deeper isopycnals tritium inventory values increase with time as the bomb-produced tritium signal slowly spreads into the deep North Atlantic.

Examination of the spatial gradients of the fields of tritium inventory (figure 2.23C and D) reveals larger changes meridionally than zonally. The meridional gradient of decay-normalized tritium shows decreasing values towards the south at all levels. The single sign of the meridional gradients at all levels is somewhat surprising since, as discussed above, tritium inventories in the the upper levels are diluting while those on the densest surfaces are increasing. The tritium-free waters diluting the upper thermocline must enter the gyre either through a combination of transport in the northward Ekman flux and the western boundary current, which subsequently feed the southward subducting flow which renews these layers. Zonal gradients of tritium are weak and not distinguishable from zero except at the deepest levels analyzed.

### Comparison with Tritium measurements at Bermuda

Figure 2.24 compares the estimate of the tritium concentration and tendency in the eastern Atlantic with the directly measured time-series at Bermuda. *Jenkins [1997]* presents a time-history of tritium at Bermuda extending back to 1968. As expected based on Bermuda's greater distance from the surface outcrops and slower ventilation, tritium concentrations are slightly lower at Bermuda on all isopycnal surfaces. Also,

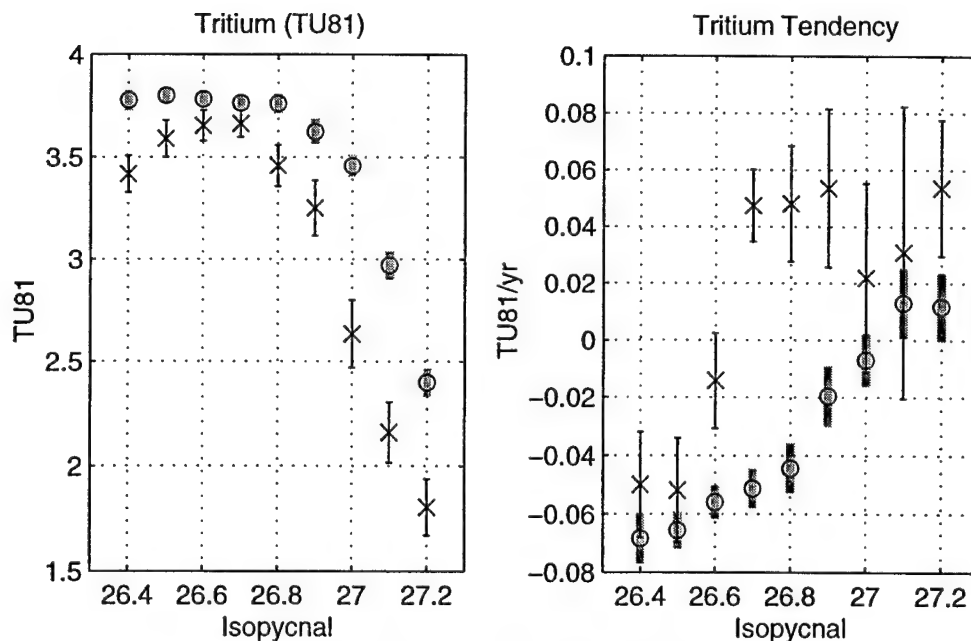


Figure 2.24: A) Tritium (TU81) and B) temporal tendency of tritium (TU81 yr<sup>-1</sup>) estimated on isopycnal surfaces at Bermuda for the year 1986. Values determined from time-series at Bermuda are indicated by x's. For comparison the estimates of mean tritium and tritium tendency in the eastern North Atlantic are indicated by o's. Error bars for both sets of measurements represent the 95% confidence intervals.

as apparent in the contoured space-time diagram of tritium at Bermuda (figure 2.21), a subsurface maximum is observed at Bermuda but not in the eastern North Atlantic.

The estimate of the temporal tendency at Bermuda has much greater uncertainty than that in the eastern Atlantic owing to fewer observation points. Nonetheless, figure 2.24 displays evidence for distinctly different temporal evolution of tritium inventory on either side of the subtropical gyre. While the vertical structure of tendency in the eastern North Atlantic shows a smooth progression from lighter to denser surfaces, the tritium record at Bermuda divides into two distinct modes. At density classes ventilated nearby ( $\sigma_\theta \leq 26.5$ ; Eighteen Degree Water), tritium inventories are decreasing with time indicating a dilution of the tritium inventory. On all deeper isopycnals, the tritium inventory is increasing with time at a rate which roughly appears to be independent of the density class. The lower inventories and positive tendency



of the deeper isopycnals at Bermuda is consistent with the concept of a closed recirculation pool in the western subtropical gyre (e.g. *Rhines and Young* [1982a]). The "pool" region of the gyre is expected to be slowest region to accumulate transient tracer inventory: hence the low, but increasing tritium concentrations.

## 2.6 Summary

The large scale age distribution of  $^3\text{H}$  and  $^3\text{He}$  on isopycnal surfaces in the eastern subtropical thermocline are well described by low-order polynomial regressions in space and time. The portion of the total variance of the observations explained by the time-dependent component of the regression model increases with densities indicating increasing non-steadiness of the age field in the lower thermocline. The magnitude of the age change in the lower thermocline is large and significantly contributes to the balance of terms governing the advective-diffusive balance of tracer age. Furthermore, on the deeper isopycnals, the time dependent portion of the regression model has statistically significant spatial structure such that the "oldest" water is also that with the highest rate of change in tracer age value. In the upper thermocline, where isopycnal surfaces are quickly ventilated, the observed temporal changes in the age fields are small and spatially uniform. Comparison to a directly measured time-series in the western North Atlantic demonstrates that the observed changes in the age field of the eastern portion of the gyre typify a pattern which extends throughout the subtropical thermocline. Decay-normalized tritium shows the greatest concentrations in the upper thermocline and decreasing values with depth. The temporal trend of tritium inventory has opposing signs in the upper and lower thermocline. The upper thermocline is characterized by decreasing tritium values indicating dilution with southern-hemisphere waters. In contrast, decay-normalized tritium values in the lower thermocline are seen to increase as the bomb-produced tritium transient slowly invades these waters.



## Chapter 3

# Changes in the Physical Circulation as an Explanation of the Observed Evolution of the Tracer Age Field

### 3.1 Circulation Implied by Tritium- $^3\text{He}$ age Field

Any trend or secular change in the large-scale circulation of the subtropical gyre has the potential to alter the internal distribution of observed chemical tracer fields. This chapter will examine the hypothesis that the observed temporal evolution of the tritium- $^3\text{He}$  age field is created solely by changes in the circulation of the subtropical gyre. Two aspects of the physical circulation, acting in concert or independently, could lead to trends in the internal tritium- $^3\text{He}$  age distribution: changes in outcrop position or changes in advective speed. Since tritium- $^3\text{He}$  age is an estimate of elapsed time since a water parcel was last at the ocean surface, increasing the distance from a point within the thermocline to the winter outcrop location will serve to increase the tracer age measured at that point. Likewise, if the circulation were to slow, the transit time

from the surface outcrop to a fixed point in the interior would increase, and thus, increase the measured tracer age.

What magnitude of advective changes would be needed to explain the observed trends in tritium-<sup>3</sup>He age? If we assume that the distributions of tracer fields in the ocean are dominated by advective processes, the tritium-<sup>3</sup>He age distribution can be employed as a direct diagnostic of the velocity field [Roether and Fuchs, 1988]:

$$v = \frac{1}{\nabla \tau}. \quad (3.1.1)$$

Equation 3.1.1 measures only that component of the velocity field normal to the gradients of tritium-<sup>3</sup>He age and furthermore assumes that subducted water parcels behave as “closed-systems” meaning that the <sup>3</sup>He burden of the water parcel is exactly that due to radioactive decay of the <sup>3</sup>H content. Roether and Fuchs [1988] employed equation 3.1.1 to estimate velocity directions and speeds in the lower thermocline of the eastern North Atlantic on isopycnal surfaces  $\sigma_\theta = 27.0$  and  $27.3$ . (figure 3.2).

The mean meridional structure and temporal changes in the tritium-<sup>3</sup>He age field in the eastern subtropical thermocline are summarized in figure 2.16. As noted before, both tritium-<sup>3</sup>He age and the temporal tendency of tritium-<sup>3</sup>He age increase with depth (density). The meridional gradient of tritium-<sup>3</sup>He age increases with depth to the isopycnal surface  $\sigma_\theta = 27.1$  and thereafter decreases. Larger gradients of tritium-<sup>3</sup>He age imply slower advective speeds (eq. 3.1.1) so the trend in tracer age shown in figure 2.16B could be a signal of the changing vertical shear of horizontal velocity across the thermocline. The gradients of tritium-<sup>3</sup>He age show no trends with time for isopycnals  $\sigma_\theta < 26.9$ , however the deeper isopycnals have measurable changes in the meridional gradient of tritium-<sup>3</sup>He age. The sense of the changes illustrated in figure 2.16 is such that the oldest ages on an isopycnal, those furthest south (figure 2.17), are the ones experiencing the greatest rates of change in the tritium-<sup>3</sup>He age value.

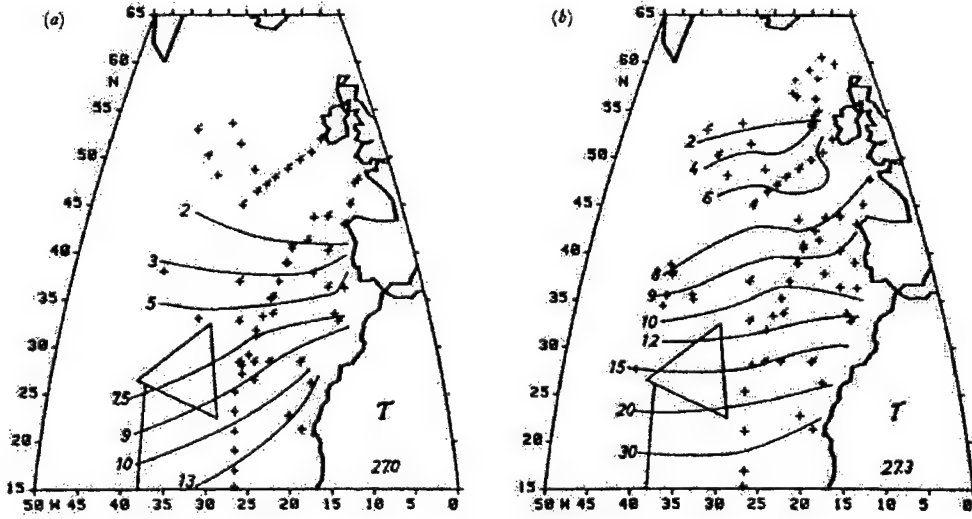


Figure 3.1: Tritium- $^3\text{He}$  age on isopycnal surfaces in lower eastern Atlantic thermocline reproduced from *Roether and Fuchs* [1988]. Tracer Age is contoured (in years) on  $\sigma_\theta = 27.0$  and  $27.3$ . Data positions are indicated as symbols supplemented with data from the  $\beta$ -triangle region in southwest corner of region.

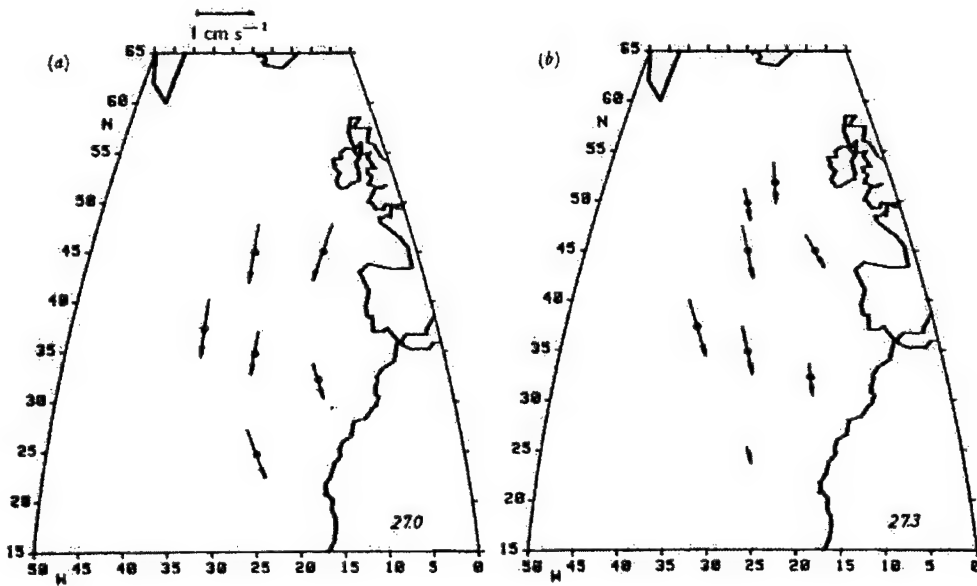


Figure 3.2: Velocity field diagnosed from tritium- $^3\text{He}$  age distribution reproduced from *Roether and Fuchs* [1988]. Velocity magnitude and direction are determined from age fields shown in figure 3.1 assuming  $v = \frac{1}{\nabla \tau}$ .

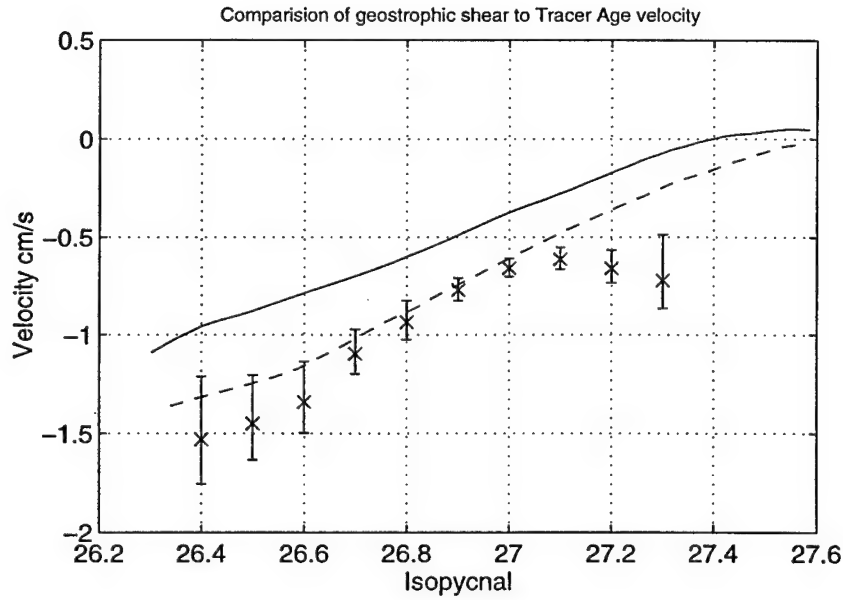


Figure 3.3: Comparison of meridional velocity profile calculated from geostrophic shear and tracer age gradients. Values from tracer calculation (eq. 3.1.1) using a regression model centered on 1986 and gradients centered at  $26^{\circ}\text{N}$ ,  $30^{\circ}\text{W}$  are shown as  $x'$  with 95% confidence limits. Geostrophic profiles are based on gradients of dynamic height referenced to 1300 dbar centered at  $26^{\circ}\text{N}$ ,  $30^{\circ}\text{W}$ . Longitude windows of  $10^{\circ}$  (solid line) and  $20^{\circ}$  (dashed line) were used to calculate the spatial zonal gradient of dynamic height. Dynamic height is calculated from the mean density field of the the supplemented hydrographic atlas of *Lozier, Owens and Curry* [1995] (Appendix A). Raw data was gridded with the Hydrobase software package [Curry, 1996] using a specified grid size of 1 degree and a search radius of 2 degrees.

Comparison of the tracer derived advection speeds with those determined from the the geostrophic shear of the mean hydrography (figure 3.3) shows agreement in the direction and magnitude of the flow, however the estimate of the mean geostrophic velocity shows some sensitivity to the zonal interval over which the gradients are calculated. The tracer age derived advective speed is based on data which spans approximately 20 degrees of longitude. When the geostrophic velocity is calculated over the same scale there is quantitative agreement between the two estimates for densities less than  $\sigma_{\theta} = 27.0$ . If a shorter zonal scale of ten degrees is used, the magnitude of the geostrophic velocity is less than that determined from the tritium- $^3\text{He}$  age field. This suggests that the tracer distribution reflects the smoothed large-

scale circulation of the region. Alternatively, the near constancy of the offset between the tracer-derived age and the geostrophic shear for 10 degrees of separation could arise from the failure of the geostrophic calculation to include the meridional velocity component of the flow at the reference surface. This ambiguity highlights a potential problem which arises when using large scale distributions of tracers to determine reference level velocities for dynamic calculations [Jenkins, 1997]: the scale of the flow field represented by the gradients of the observed tracer age field is not clearly defined.

For isopycnal surfaces denser than  $\sigma_\theta = 27.0$ , there is a disagreement in the sense of the shear determined from the two methods. The tracer-derived advective speeds suggest that the velocity reaches a minimum at  $\sigma_\theta = 27.1$  and then increases with depth. The minimum, however, is not unambiguously resolved within the uncertainty due to the sparsity of data on these deep isopycnal surfaces. The geostrophic profile shows no corresponding evidence of this structure. Possible causes for the discrepancy of meridional velocity estimates in the lower thermocline will be examined further below.

Considering the change in velocity field implied by the changing age field, under the assumption of equation 3.1.1, figure 3.4 shows the isopycnal velocity profile as a function of potential density for the years 1981 and 1991. Changes in the upper thermocline (above  $\sigma_\theta = 26.7$ ) are small, especially when compared to the magnitude of the implied flow. As noted previously, the magnitude of the change increases with depth, and figure 3.4 emphasizes that this change is even greater if considered as a fraction of the mean velocity on each isopycnal. The increase in the magnitude of the age tendency field with depth requires the vertical shear of velocity to change over time. The change in shear is not consistent with a changes in the first baroclinic mode of the ocean. The velocity response to the first baroclinic mode has a maximum at the surface and decreases with depth to the nodal point near the base of the thermocline. A time varying change in shear is expected for a baroclinic variability but the change

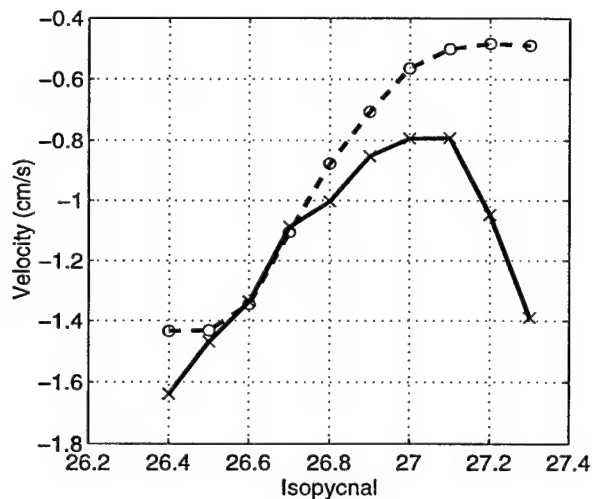


Figure 3.4: Time evolution of isopycnal velocity profile deduced from evolution of tritium- $^3\text{He}$  age field. Solid line: 1981; Dashed line: 1991.

in shear would be characterized by the largest velocity changes in the shallowest water, the opposite to what is observed.

If such changes have occurred in the large-scale velocity field, are they detectable by other methods? In terms of typical oceanic measurements, the changes are not large: the change in velocity on  $\sigma_\theta = 27.0$  is 0.26 cm/s over a decade. Independent measures of changes in absolute velocity to such precision are not readily available. On the other hand, the change in vertical shear of the velocity offers a potentially more robust signal to compare against: the shear between  $\sigma_\theta = 26.8$  and 27.1 changes from 0.14 cm/s to 0.36 cm/s between 1981 and 1991 (figure 3.5). Geostrophic shear can be accurately determined by the structure of the density field of the subtropical gyre. Figure 3.3 demonstrates that the tritium- $^3\text{He}$  age field appears to capture the velocity structure typical of the larger scales of the circulation. A time series of dynamic height at points spanning the region of the eastern subtropical gyre will next be constructed to check for possible changes in the large-scale geostrophic shear over the time span of the  $^3\text{H}$  and  $^3\text{He}$  measurements.



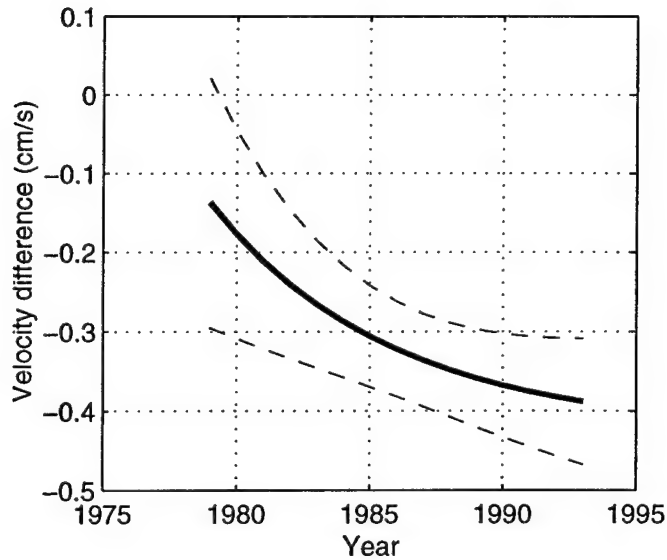


Figure 3.5: Velocity difference between  $\sigma_\theta = 26.8$  and  $27.1$  implied by time-dependent regression to tritium- $^3\text{He}$  age field and equation 3.1.1. Dashed lines indicate envelope of standard error.

## 3.2 Large-scale Changes in Advection of Subtropics Diagnosed from Hydrography

The historical database of hydrographic observations provides the opportunity to test for long term changes in vertical shear of velocity in the eastern North Atlantic. The key assumption of this approach is that the large-scale flow field of the interior subtropical gyre is in geostrophic balance so that the vertical shear can be well determined from observations of the large-scale density structure. The tritium- $^3\text{He}$  age calculation from the previous section provides an estimate for the change in meridional velocity shear centered at  $30^\circ\text{W}$ ,  $26^\circ\text{N}$  assuming a purely advective balance (eq. 3.1.1). To test the validity of this assumption, we can use hydrographic data to obtain an independent estimate of the temporal stability of the velocity shear. The geostrophic distribution of hydrographic data is chosen to estimate the meridional velocity profile over scales comparable to those which determined the structure of the tracer age fields.

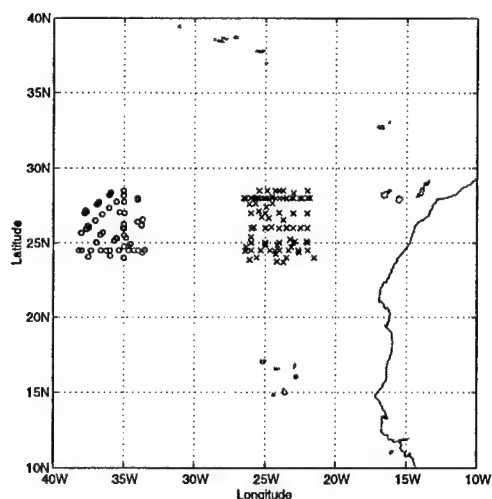


Figure 3.6: Position of hydrographic stations used to calculate gradient of dynamic height in eastern subtropical North Atlantic.

Figure 3.6 shows the distribution of hydrographic stations occupied between 1970 and 1994 in two subregions of the North Atlantic. The data is selected from the NODC archives as reported by *Lozier, Owens and Curry [1995]* and supplemented with more recent observations as summarized in Appendix A. The selected subregions span the central point used in the polynomial regressions of tritium- $^3\text{He}$  age. A time series of dynamic height can be calculated for each subregion and the zonal difference used to estimate the mean geostrophic velocity shear for the interjacent region, centered at  $30^\circ\text{W}$ ,  $26^\circ\text{N}$ .

Each subregion displayed in figure 3.6 is defined by a square box with side lengths of five degrees. The dimension of the boxes were chosen in order to obtain sufficient data to construct a time series. The western box contains 111 hydrographic stations while the eastern box has 108. Dynamic height between 250 and 500 dbar is calculated at each station. The pressure surfaces of 250 and 500 dbar are chosen to represent the lower thermocline where the tracer results of the previous section imply large changes in the velocity shear. The spatial structure of dynamic height within each box is removed using a linear regression in latitude and longitude. Removing

the low-order spatial structure adjusts each observation to form an estimate of the dynamic height at the central point of each box. The magnitude of the correction for the spatial structure within the box is small compared to the size of the differences between boxes: the r.m.s. of the correction is less than 0.05 dyn-m.

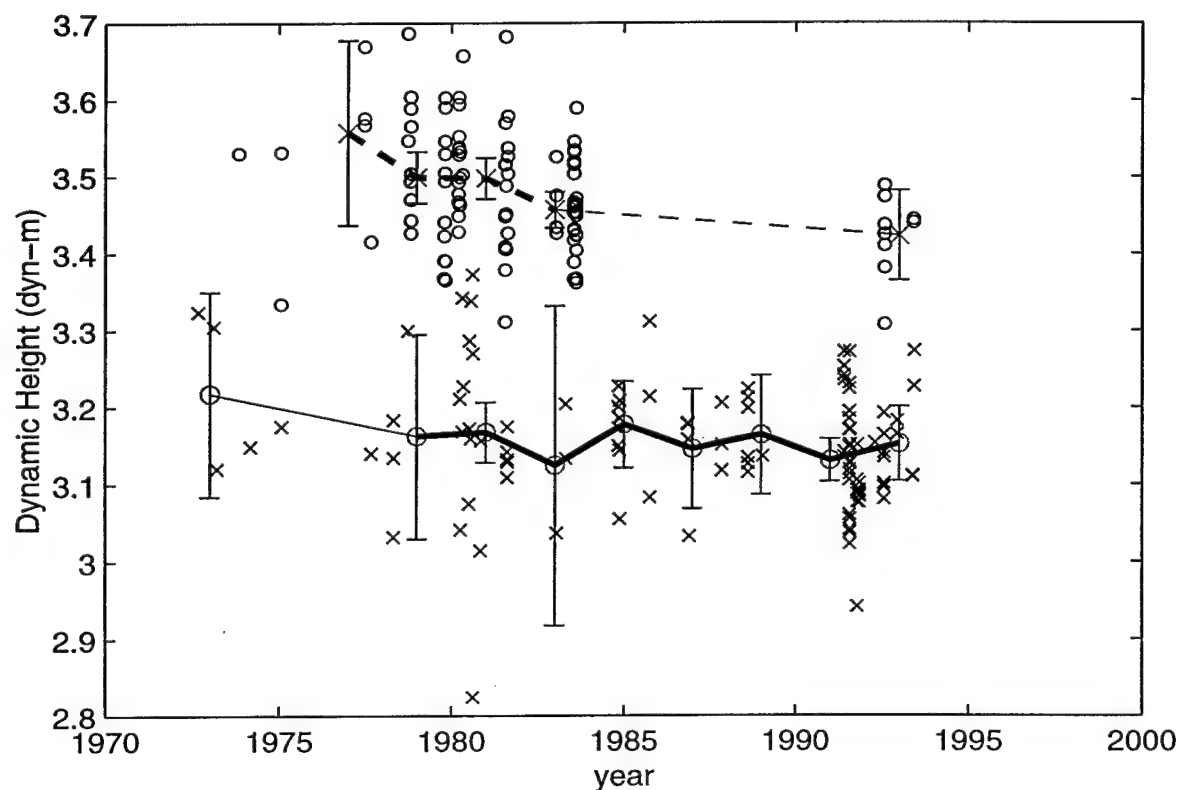


Figure 3.7: Time series of dynamic height at 250 dbar referenced to 500 dbar to two points centered at 26°N, 36°W (o) and 26°N, 24°W (x). Solid and dashed lines display mean values, with 95% confidence intervals, calculated from two year bins of the data time series.

The time series of dynamic height between 250 and 500 dbar is shown in figure 3.7. Dynamic height difference for each of the individual stations in the eastern box are shown as x's while those in the western box are displayed as o's. The western box has fairly consistent coverage over the time period displayed but the eastern box contains no observations between 1984 and 1992. Dynamic height is larger towards the west consistent with the deepening bowl of the subtropical gyre and the greater inventory of lighter waters. The mean difference of dynamic height between the two

regions supports a pressure gradient which balances the southward flow of the eastern limb of the gyre. The geostrophic velocity shear is given by

$$(v_1 - v_2) = \frac{\partial}{\partial x}(\Phi_1 - \Phi_2). \quad (3.2.2)$$

where  $\Phi$  is dynamic height and the subscripts represent two pressure levels.

The dynamic height data in each box is temporally binned using bin widths of 2 years and mean values are calculated for each time bin. A standard error for each bin is calculated from the variance estimate of all the data in each subregion in conjunction with the number of points within each bin. Variability of individual observations around the mean are predominantly due to mesoscale variability within the region and the total variance estimate based on  $O(100)$  points should provide a good estimate of the magnitude of this mesoscale variability. As such, the standard errors in figure 3.7 include the aliasing effects arising from limited samples in a highly variable environment.

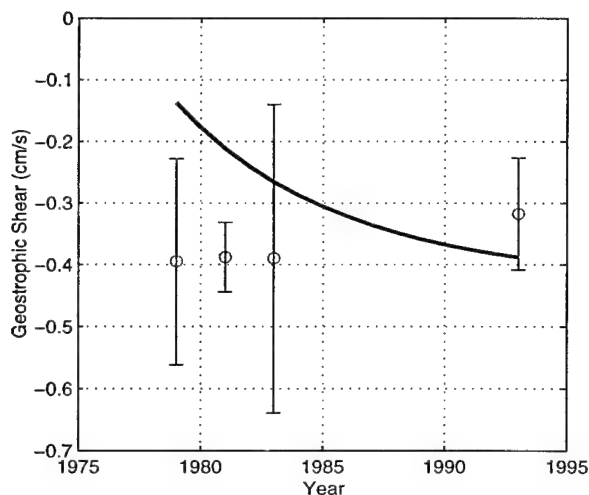


Figure 3.8: Meridional geostrophic velocity shear between 250 and 500 dbar centered at  $26^\circ\text{N}$ ,  $30^\circ\text{W}$ . Error bars represent 95% confidence intervals. For comparison, the solid line shows implied shear from evolution of tracer age signal.

A time series of geostrophic velocity shear, calculated from the difference of the two time series of dynamic height is shown in figure 3.8. The time series of calculated

shear has large gaps for years for which there are not estimates of dynamic height in both the eastern and western subregions. Although the uncertainty of individual estimates is large, there is not a visible trend in the data. Specific comparison of year 1993 to 1981 shows that the increase of shear implied by the application of equation 3.1.1 (figure 3.5) is not consistent with detectable changes in the density structure of the subtropical gyre. Figures 3.8 and 3.5 suggest that the observed temporal changes in the tritium- $^3\text{He}$  age field are not created by any local changes in the strength of the circulation of the subtropical gyre. Undetectable changes in mean circulation on these time scales are consistent with the observed surface wind forcing of the North Atlantic (discussed in § 1.3.4) which shows little change in mean wind-stress curl on time periods greater than 5 years [*Mayer and Weisberg, 1993*]. This conclusion can be further supported by comparing the evolution of the tritium- $^3\text{He}$  age field to the distribution of dissolved oxygen.

### 3.3 Changes in tritium- $^3\text{He}$ age Relative to the Distribution of Oxygen

#### 3.3.1 Steadiness of Oxygen field

Tritium- $^3\text{He}$  age is not the only passive tracer in the ocean sensitive to the physics of ventilation. The distribution of dissolved oxygen also records the evolution of subducted waters as the water leaves the highly oxygenated surface mixed layer and penetrates the oceanic interior where biological respiration slowly depletes the oxygen content of the water. Unlike the  $^3\text{He}$ -tritium system, oxygen distributions are at or near a steady state within the ocean. The surface boundary condition, the oxygen content of the atmosphere, is constant over all but geological time scales. Changes in rates of biological production and respiration could alter the interior oxygen fields

but there is no evidence of this in the observations in the eastern North Atlantic over the time period which  $^3\text{He}$ -tritium measurements were gathered. Time dependent regression models applied to the oxygen field, identical to those applied to the tracer age fields in §2.2.2, yield no statistically significant temporal changes in the oxygen fields within the thermocline (figure 3.9).

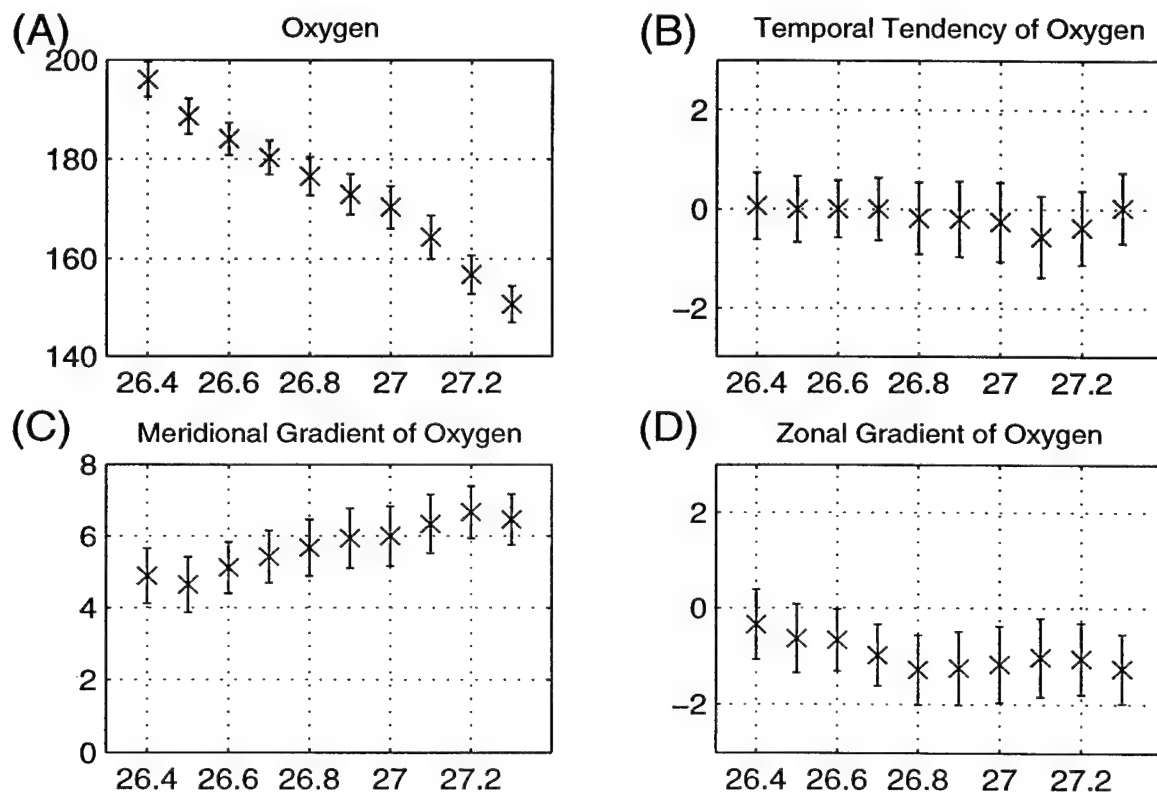


Figure 3.9: Summary of regression model applied to dissolved oxygen concentration on isopycnal surfaces in eastern North Atlantic evaluated for the year 1986: A) mean oxygen ( $\mu\text{mol kg}^{-1}$ ), B) temporal tendency of oxygen ( $\mu\text{mol kg}^{-1} \text{ yr}^{-1}$ ), C) meridional oxygen gradient of ( $\mu\text{mol kg}^{-1} \text{ degrees}^{-1}$ ), and D) zonal oxygen gradient of ( $\mu\text{mol kg}^{-1} \text{ degrees}^{-1}$ ). Error bars show 95% confidence limits. Standard error of regression model varies from 2.0–2.3  $\mu\text{mol kg}^{-1}$ .

Measured oxygen values can be transformed to a more convenient variable for ventilation studies by accounting for the maximum saturation oxygen content for a given parcel of water. Seawater in the surface mixed layer equilibrates its oxygen burden to a saturation value dependent on the temperature and salinity of the water.

The difference between the measured oxygen content of a water parcel and the oxygen saturation value for a parcel with the measured temperature and salinity is termed the Apparent Oxygen Utilization (AOU):

$$AOU = O_2(saturation) - O_2(measured). \quad (3.3.3)$$

A water parcel exiting the surface mixed layer will have an AOU value near zero: supersaturation of oxygen created by biological effects can lead to small negative values of AOU in the surface mixing layer. After subduction, the parcel's AOU will increase with time as biological consumption removes dissolved oxygen from the water. Figure 3.10 displays an example of AOU along the isopycnal  $\sigma_\theta = 26.7$ . Low values are observed in the northeast in the region of the surface outcrop with progressively higher values towards the south and west.

If biological consumption is uniform in space and time, AOU will uniformly increase and function as a linear “age” tracer. Indeed, the structure of the AOU field in figure 3.10 is quite similar to that for tritium- $^3\text{He}$  age in the North Atlantic [Jenkins, 1988a], however, the greater sparsity of the  $^3\text{H}$  and  $^3\text{He}$  data requires much greater smoothing when constructing basin-wide maps. Typically, independent estimates of biological consumption of oxygen, termed the Oxygen Utilization Rate (OUR), are not well known so that in practice, AOU cannot be employed directly as an age tracer. Nonetheless, the general distribution of the AOU field in the ocean does behave like an “uncalibrated” age tracer and any changes in the physical circulation which alter the tritium- $^3\text{He}$  age field should be apparent in the AOU field as well. Lack of any statistical changes in the large scale oxygen field (figure 3.9B) is compelling evidence that the magnitude and structure of the large-scale circulation have not significantly changed over the course of the tritium- $^3\text{He}$  measurements and that the previously diagnosed changes in the tritium- $^3\text{He}$  age field must have their root in some other process.

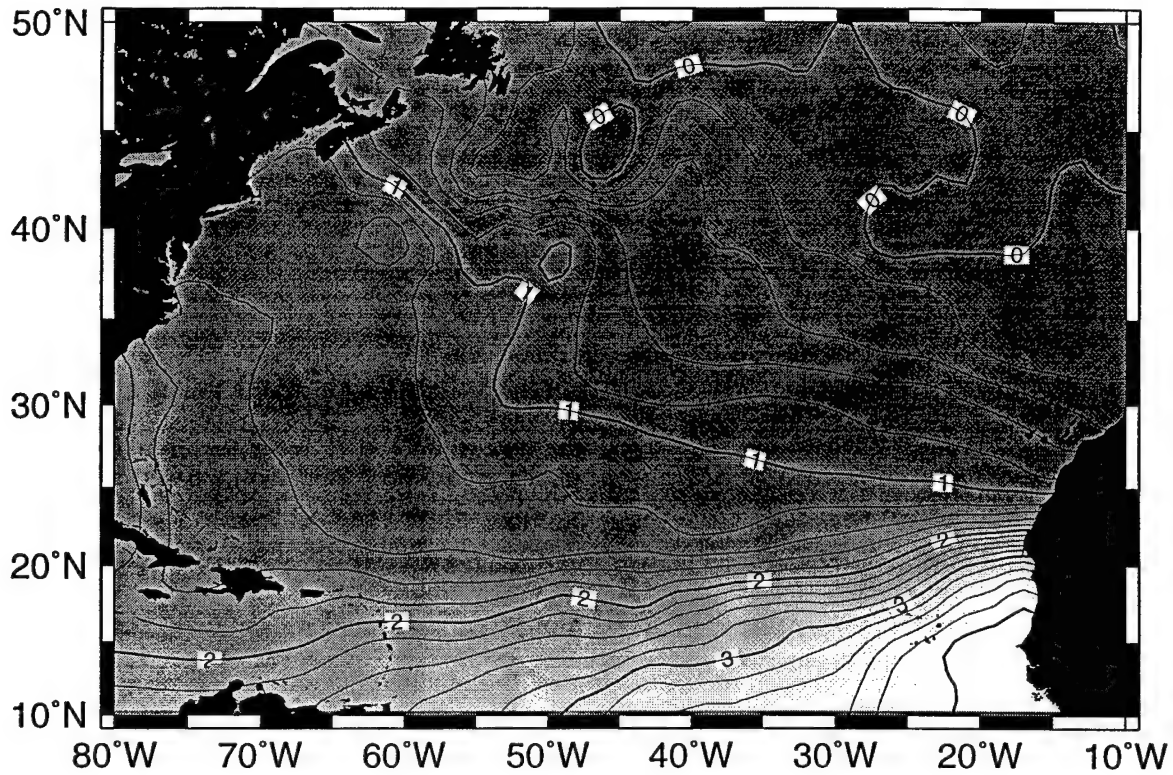


Figure 3.10: Distribution of Apparent Oxygen Utilization on  $\sigma_\theta = 26.7$ . Gridded field is produced from data in the supplemented hydrographic atlas of *Lozier, Owens and Curry* [1995] (Appendix A) mapped onto isopycnal surfaces using the Hydrobase software package [Curry, 1996].

Directly comparing AOU and tritium- $^3\text{He}$  age measurements on a density surface shows the property-property correlation between the two tracers is evolving over time. Figure 3.11 displays the correlations on  $\sigma_\theta = 27.0$  and exemplifies the changing property relations over time. For low values of apparent oxygen utilization (AOU  $< 80 \mu\text{mol kg}^{-1}$ ), tritium- $^3\text{He}$  age and AOU appear roughly correlated however the slope of this relation is increasing with time. Assuming that tritium- $^3\text{He}$  age is an accurate measure of the true ventilation age, the inverse slope of the age-AOU relation is a measure of the large scale OUR [Jenkins, 1982b]. Higher values of AOU (AOU  $> 80 \mu\text{mol kg}^{-1}$ ), represent samples taken in the southern limb of the subtropical gyre where the influence of the low oxygen, high age tropical waters alters the apparent slope of the correlation. A constant ratio of tracer age and AOU is only expected if



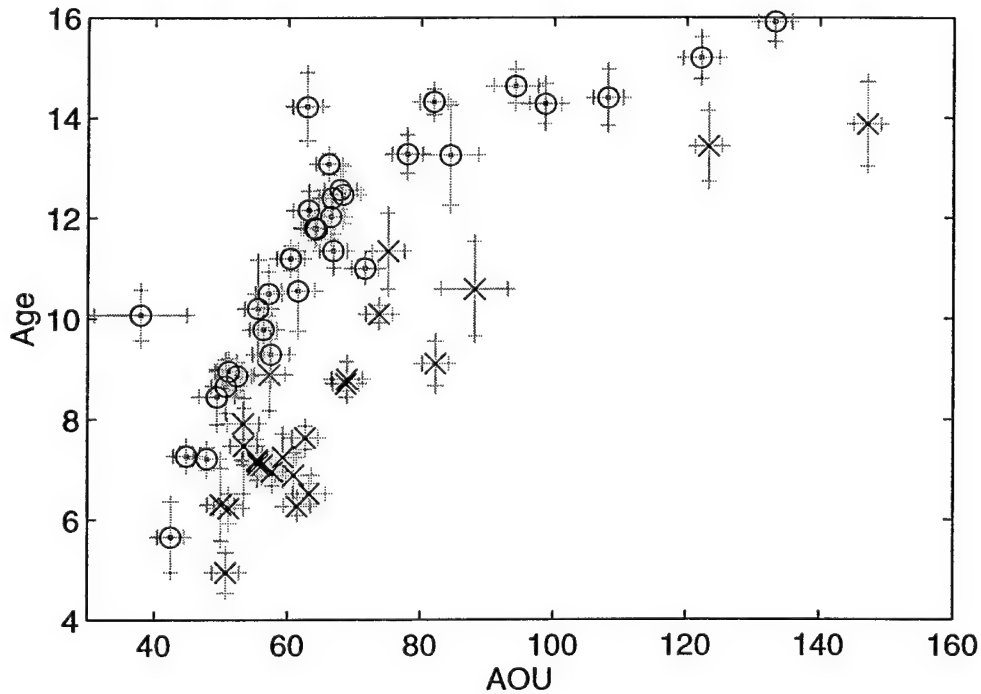


Figure 3.11: Tritium-<sup>3</sup>He age vs Apparent Oxygen Utilization (AOU) on  $\sigma_\theta = 27.0$  for two years: 1981 (x's) and 1992 (o's). Age is expressed in years and AOU in  $\mu\text{mol kg}^{-1}$

oxygen consumption is spatially uniform and the tracers evolve simply as a function of flow along streamlines. Mixing with tropical waters across the Cape Verde Front breaks the latter assumption by laterally exchanging waters with differing end-member characteristics.

### 3.3.2 Tritium-<sup>3</sup>He Age Regressions Against AOU

Given the apparent large-scale steadiness of the oxygen fields, the evolution of the property-property relation, as shown in figure 3.11 offers an independent means to quantitatively estimate the temporal changes in the tritium-<sup>3</sup>He age field. A multiple regression model can be used to explain the tritium-<sup>3</sup>He age field as a function of observed AOU and time:

$$\tau = \mathcal{F}(\text{AOU}, \text{time}) = a + b * \text{AOU} + T * (c + d * \text{AOU}); \quad (3.3.4)$$

where  $a, b, c, d$  are regression coefficients and  $T$  is time relative to 1986. Constructing a regression model based on the property-property relation removes all spatial information from the calculation. The model assumes that both oxygen and tracer age are evolving with time as they are carried along by the flow but places no requirement or constraint on the details of the topology of the flow paths. In this sense the model based on the changing property-property relation is more general than the spatial regression model which necessarily assumed a large scale structure to the flow field and introduced additional noise to account for the mesoscale eddy perturbations on top of the large-scale field. Regressions are performed on each isopycnal in the thermocline in the manner outlined in chapter 2. On each isopycnal, only data below a specified cut-off value of AOU are used to limit the regression to waters that are clearly north of the influence of the Cape Verde front.

Figure 3.12 shows the values of each of the regression coefficients of equation 3.3.4 for isopycnal surfaces spanning the thermocline. As previously determined from the multiple regressions of tritium- $^3\text{He}$  age against geographic regressors, both the magnitude of the mean age (fig. 3.12A) and the age tendency (fig. 3.12C) increase with depth in the thermocline. The magnitude of the non-steadiness of the age field is comparable to that determined in chapter 2 and a quantitative comparison will be shown below. The slope of the correlation between age and AOU (fig. 3.12B) shows small values at the surface and a maximum in the lower thermocline near  $\sigma_\theta = 26.9$ . Oxygen utilization rates are estimated from the inverse of this slope and vary from near  $20 \mu\text{mol kg}^{-1} \text{yr}^{-1}$  at  $\sigma_\theta = 26.4$  to  $6 \mu\text{mol kg}^{-1} \text{yr}^{-1}$  in the lower thermocline. The apparent increase in OUR below  $\sigma_\theta = 26.9$  likely arises from the failure of the mean tritium- $^3\text{He}$  age gradient to accurately reflect the true ventilation rate on these isopycnals. As shown in figure 3.3, the advective speeds implied by the tracer gradient on these isopycnals greatly exceeds the estimated velocity determined by geostrophy. The correlation between age and AOU is not constant over time as suggested in fig-

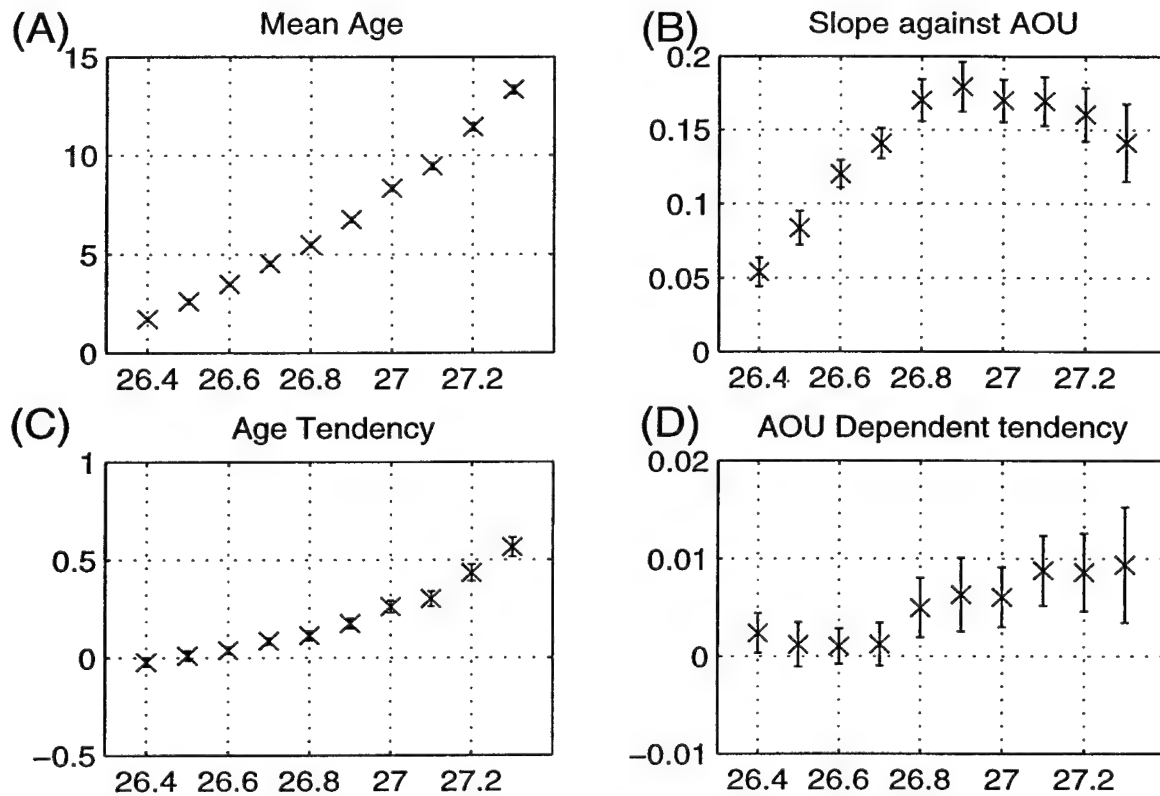


Figure 3.12: Regression coefficients of equation 3.3.4 determined along isopycnal surfaces in the eastern subtropical gyre evaluated around year 1986: A) mean tritium- $^3\text{He}$  age (yr), B) mean regression dependence on AOU ( $\text{yr } \mu\text{mol}^{-1} \text{ kg}$ ), C) temporal tendency of tracer age and D) time-dependent regression on AOU ( $\mu\text{mol}^{-1} \text{ kg}$ ). Error bars indicate 95% confidence intervals.

ure 3.11 and shown quantitatively in figure 3.12D. The positive values of the AOU dependent tendency along the deeper isopycnals imply that the temporal tendency of the age field is not uniform but, rather, is greater for waters with larger AOU values. Again this is consistent with the results of the geographic regression (figure 2.16) where it was found that the older waters further to the south showed the largest observed changes with age.

Figure 3.13 displays a direct comparison of the age tendency determined from the tracer age regression against AOU to the results of the geographic regression. The two methods show consistent results for all isopycnal surface below  $\sigma_\theta = 26.7$ . This strongly supports the conclusion that the observed changes in the tritium- $^3\text{He}$  age

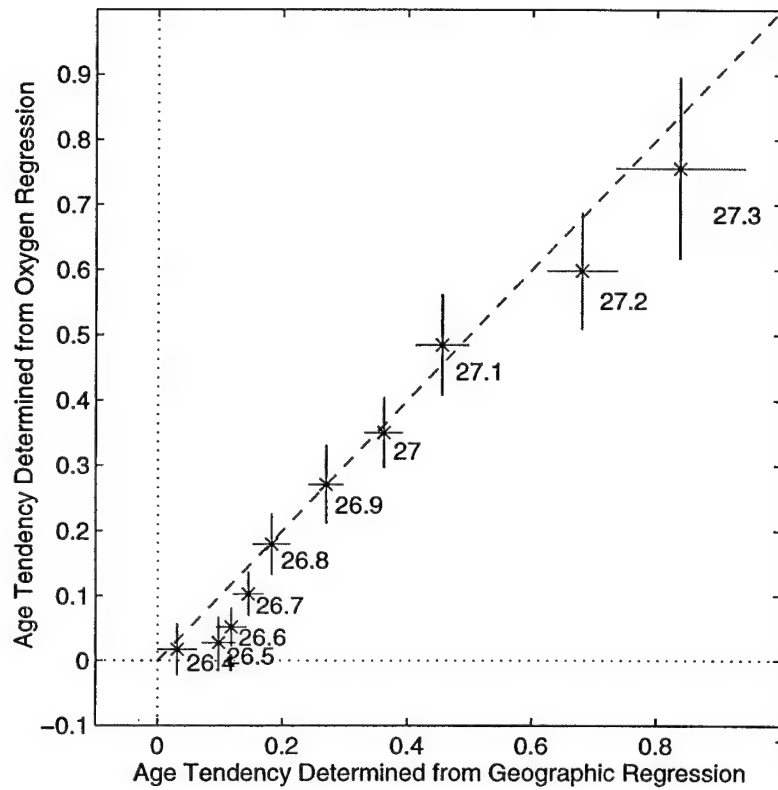


Figure 3.13: Comparison of tendency of tritium- $^3\text{He}$  age field on isopycnal surfaces derived from two independent methods: regression against geographic coordinates (abscissa) and regression against Apparent Oxygen Utilization (ordinate). Dashed line shows a 1:1 correspondence and the error bars indicate 95% confidence intervals.

field are not the results of changes in the physical circulation such as decreased gyre transport or changes in ventilation rates. Any change in the physical circulation would be expected to impact both the age and AOU fields in a comparable manner. In such a case, changes in the age and oxygen fields would be correlated and the tritium- $^3\text{He}$  age field would show no trend with respect to the measured AOU. The quantitative congruence of the changes in age field to both a geographic coordinate system and in relation to the oxygen field demonstrate that it is the tracer age field that is evolving over time and that this change is not a manifestation of significant changes in the mean physical circulation. Furthermore, the numeric agreement between the two differing regression models lends credence to the methodology of the spatial regression model by illustrating that the former results do not arise from aliasing due to the sparse sampling

in space and time. The consistency of the two results provides strong evidence that the temporal and spatial sampling is sufficient to accurately determine the tendency of the tracer age field.

In the upper thermocline, however, the tendency estimated from the correlation to the oxygen field yields lower values than the estimate from the geographic model. For instance, at the level of subtropical mode water ( $\sigma_\theta = 26.5$ ), the oxygen regression yields a tendency indistinguishable from zero while the geographic regression results in a tendency estimate of about 0.1. Advective ages are smaller here indicating relative quick ventilation times. Although there is some evidence of a tendency in the mean age, neither regression method yields results which would support a temporal change in the along-isopycnal velocities: figures 2.16D and 3.12D show coefficients indistinguishable from zero above  $\sigma_\theta = 26.8$ . A northward trend in location of winter outcrop for the isopycnals of the upper thermocline could lead to the small observed shifts in tritium- $^3\text{He}$  age with respect to geographic coordinates without simultaneously showing any manifestation in either the age gradients or the age-oxygen correlations. This hypothesis that the temporal shifts in the tracer age field in the upper thermocline have recorded a secular change in the physical ventilation requires further study.

### 3.4 Summary

Multiple regressions applied to 15 years of  $^3\text{H}$  and  $^3\text{He}$  measurements have revealed changes in the large-scale structure of the tritium- $^3\text{He}$  age field along isopycnal surface in the eastern subtropical North Atlantic. Interpreting the spatial gradients of the age field as solely a projection of the advective velocity field, the observed temporal changes in age require a corresponding change in the large scale velocity field. This chapter has used two unrelated methods to explore the hypothesis that the evolution

of the age field is indeed an indicator of the evolution in the underlying physical circulation.

The first method involved constructing a time series of the geostrophic shear across the lower portion of the southward flowing eastern limb of the subtropical gyre. Hydrographic stations spanning 20 years were used to construct a time series of relative dynamic height at two points which was then used to calculate the spatially averaged geostrophic shear between the two locations. Sparsity of data leads to a time series with large gaps (figure 3.8), however the constructed record of the vertical shear is consistent with a gyre transport that does not display significant change on the decadal time-scale. The time-series of vertical shear recorded in the large-scale density field is not consistent with the changes in the tritium- $^3\text{He}$  age field required by a purely advective tracer age model (figure 3.5). Comparing the implied changes in the vertical shear of the velocity avoids the signal-to-noise difficulties which would arise in any comparison of the temporal evolution of the absolute velocity field.

The second method contrasts the ventilation of tritium- $^3\text{He}$  age with oxygen. Transforming oxygen measurements to an Apparent Oxygen Utilization yields a tracer that behaves as an uncalibrated "age" tracer. The unknown rate of increase of the AOU "age" tracer, dependent on biological processes which are not well quantified and may be highly variable in space and time, limits the direct quantitative interpretation of the fields of AOU. Nonetheless, oxygen ventilates the thermocline on time scales similar to tritium- $^3\text{He}$  age so any changes in the tritium- $^3\text{He}$  age field created by alterations in the physical circulation should also be apparent as temporal changes in the fields of AOU on isopycnals. Employing time-dependent multiple regression models to explain the observed AOU measurements yields no statistically significant temporal change in the oxygen field further supporting the conclusion that the circulation of the subtropical gyre has not changed in a way that has altered the large-scale ventilation of the thermocline. Additionally, regression models based on the time-evolving property

correlation between tracer age and AOU yield estimates of the temporal tendency of the age field that are quantitatively consistent with those obtained in the previous chapter using regression models based on geographic coordinates.

The results presented so far have summarized the observational evidence for large-scale, long-term changes in the structure of the tritium- $^3\text{He}$  age field in the eastern North Atlantic thermocline. The hypothesis that the bulk of these changes are the result of interdecadal trends in the underlying physical circulation has been examined and dismissed. The implications of a changing circulation based on a purely advective balance of the  $^3\text{H}$  -  $^3\text{He}$  fields (eq. 3.1.1) are not supported by other independent methods. The conclusion must be that the purely advective tracer age balance is inconsistent with the observations, and we must seek ways in which the penetration and evolution of  $^3\text{H}$  and  $^3\text{He}$  in a steady ocean circulation could produce the observed changes in the structure of tritium- $^3\text{He}$  age .





## Chapter 4

# Evolution of Tritium- $^3\text{He}$ Age in a One-Dimensional Model of Thermocline Ventilation

### 4.1 The Effects of Mixing on the Tracer Age Balance

The analysis of observations of the tritium- $^3\text{He}$  age field in the eastern North Atlantic thermocline has demonstrated:

- I. Statistically significant changes in the structure and magnitude of the field over the time period 1979-1993.
- II. The extent of the temporal changes on an isopycnal varies inversely with the rate at which the isopycnal surface is ventilated.
- III. Analysis of the mean density field and oxygen distribution found no evidence for significant changes in the underlying physical circulation over this time period.

- IV. The observed changes in the age field cannot be interpreted as a straightforward reflection of changes in the large-scale advective ventilation rate

This chapter will examine the hypothesis that the observed temporal changes in the age field arise solely from the evolution of the transient tracers in a steady flow field. The simplified surface boundary condition ( $\tau_{surface} = 0$ ) and the presumed steadiness of the age field for steady flows offer a potential advantage in the calculated tracer age field rather than the raw tracer concentrations. The diagnostic age calculated from the ratio of the observed chemical concentrations, however, does not behave strictly as a “true” advective age: the advective-diffusive balance equation for tritium-<sup>3</sup>He age,

$$\frac{\partial \tau}{\partial t} = \nabla (\kappa \nabla \tau) - \vec{u} \cdot \nabla \tau + 1 + \kappa \left( \frac{\nabla [^3H]}{[^3H]} + \frac{\nabla [^3H + ^3He]}{[^3H + ^3He]} \right) \cdot \nabla \tau \quad (4.1.1)$$

contains a nonlinear mixing term dependent on the gradients of the component tracers <sup>3</sup>He and tritium. For contrast, the primary balance for a “true” age is given by:

$$0 = \vec{u} \cdot \nabla \tau + 1.$$

The failure of the diagnosed tritium-<sup>3</sup>He age to behave according to the ideal approximation (equation 4.1) suggests that interpretation of the observed tritium-<sup>3</sup>He age field necessitates a consideration of the full advective-diffusive balance given in equation 4.1.1. The nonlinear mixing term, the rightmost term of equation 4.1.1 can act as either an apparent source or sink of age. Time dependence in the nonlinear mixing term will alter the relative balances of the entire equation and potentially lead to large temporal changes in the spatial structure of the age field.

Tritium-<sup>3</sup>He age will serve as a “true” advective age” only if the nonlinear term in equation 4.1.1 is small in comparison to the overall balance. Numerous previous studies have attempted to gauge the overall accuracy of tritium-<sup>3</sup>He age observations by analyzing the dominant balance of the advective-diffusive equation. Prior diagnostic analyses of the nonlinear mixing term [*Jenkins, 1987; Roether, 1989b; Doney,*

*Jenkins and Bullister*, 1997; *Jenkins*, 1997] have employed a combination of *ad hoc* assumptions and the observed spatial gradients of the tracer fields to estimate the relative magnitude of the nonlinear term. *Jenkins* [1987], assuming an isopycnal mixing coefficient of  $500 \text{ m}^2\text{s}^{-1}$ , found the relative magnitude of this term to be  $O(0.01-0.1)$  for the eastern North Atlantic thermocline above  $\sigma_\theta = 27.15$ . *Roether* [1989b] used a combination of scale analysis and observations to examine the balance of terms in the eastern North Atlantic. Led by the small observed temporal change between two stations a few years apart (see figure 2.20) and using a lateral diffusivity of  $400 \text{ m}^2\text{s}^{-1}$ , he concluded that the impact of the nonlinear mixing term's was  $< 0.2$  for tracer ages less than 15 years. Comparing tritium- $^3\text{He}$  age with CFC-based age estimates, *Doney, Jenkins and Bullister* [1997] found the magnitude of the nonlinear mixing term to be significant in the tropical/subtropical frontal region but negligible in the subtropical thermocline above the  $^3\text{He}$  maximum ( $\sigma_\theta < 27.2$ ). Analysis of the data collected during the Subduction Experiment [*Jenkins*, 1987], using a diagnosed isopycnal diffusivity of  $O(1000 \text{ m}^2\text{s}^{-1})$  found maximum values of the nonlinear mixing term of 0.1 on  $\sigma_\theta = 27.1$  with lower values higher in the thermocline. These results suggest the amplitude of the nonlinear mixing term is less than 10% of the first order terms of the advective-diffusive balance of tritium- $^3\text{He}$  age within the eastern thermocline. Below the thermocline and in regions of strong fronts, such as the tropical-subtropical boundary, the relative magnitude of the term increases. A key point of the previous results, however, is that they are all derived from observations conducted after 1980 and therefore apply only to that time period. As will be shown below, the magnitude of the nonlinear term is likely to have been much more significant earlier in the oceanic response to the large input of bomb-tritium in the 1960's. Although the direct effects of the nonlinear mixing are apparently no longer first order in the 1980's, the adjustment to the cumulative distortion of the age distribution may still be evident.

Examination of the temporal evolution of the tracer age balance is most conveniently posed using a one-dimensional model of thermocline ventilation. Previous investigations [Jenkins, 1988a; Doney and Jenkins, 1988; Roether and Fuchs, 1988; Roether, 1989b; Sarmiento *et al.*, 1990; Musgrave, 1990] have used one-dimensional models to interpret observations and explore the sensitivity of the structure of the age field to basic parameters of the flow field. For the most part, prior research has focused on the spatial structure of the tracer field in an effort to compare model simulations with observations obtained during a hydrographic survey. There has been comparatively little effort made to understand the temporal evolution of the age field.

Conceptually, the one-dimensional interpretation developed here will be oriented along isopycnals within the subtropical thermocline as shown in figure 4.1. This

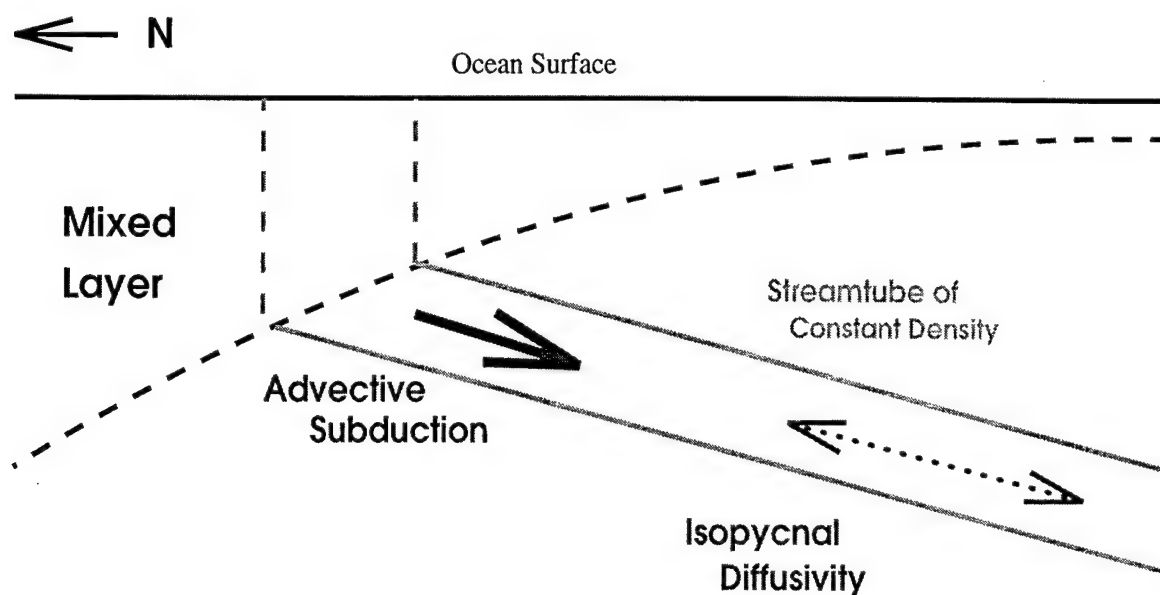


Figure 4.1: Schematic diagram of one-dimensional model of thermocline ventilation

interpretation follows from the assumption that flow out of the surface mixed layer enters the thermocline adiabatically and passive tracer fields are advected and diffused predominantly along, rather than across isopycnals. In plan view, the model is construed to be aligned along a streamline of the large-scale flow with the diffusive

influence of neighboring streamlines neglected. The one-dimensional model assumes that all the water in the thermocline derived directly from the surface mixed layer; therefore the tracer inventories of the water parcels in the model are assumed to have been entirely renewed at the surface prior to subduction. As such, a one-dimensional description of thermocline ventilation cannot include or simulate the influence of water which re-circulates within the subtropical gyre without direct ventilation; a two-dimensional model will be developed in the next chapter to examine indirect ventilation of re-circulated waters. Effects of diapycnal mixing are neglected throughout this analysis. Previous studies [*Rooth and Östlund*, 1972; *Jenkins*, 1980; *Fine, Reid and Östlund*, 1981; *Sarmiento, Rooth and Roether*, 1982; *Fine, Peterson and Östlund*, 1987] have concluded that the penetration of tritium into the thermocline is predominantly an isopycnal process. Additional calculations presented in Appendix C of this thesis support the conclusion that diapycnal effects are second order in the temporal development of the transient tracer fields in the thermocline.

Appendix B employs scale analysis to examine the temporal evolution of the terms of the advective-diffusive balance of tritium,  $^3\text{He}$ , and tritium- $^3\text{He}$  age. The scale analysis serves as a platform for two special case studies: the case when the surface tritium boundary condition is steady and the case when this boundary condition changes rapidly. The qualitative effects of mixing determined from the basic scale analysis are then incorporated into a simplified analytic model of the evolution of tritium- $^3\text{He}$  age based on a linear hyperbolic partial differential equation (§B.2). The simple analytic model illustrates that the specific solutions of the temporal changes in the tracer age field determined by the numerical integrations of this chapter can be captured in a more general, yet tractable, analytic model.

## 4.2 A Numerical Model

### 4.2.1 Model Description

To study the temporal evolution of the advective-diffusive balance of the tritium- $^3\text{He}$  age field with realistic forcing conditions, the tracer balance equations must be integrated numerically. In practice, rather than integrate the nonlinear partial differential equation for the tritium- $^3\text{He}$  age balance (equation 4.1.1), the coupled tracer fields of  $^3\text{H}$  and  $^3\text{He}$  are integrated separately and their ratio is used to calculate age.

The balance equations for tritium (eq. B.1.1) and  $^3\text{He}$  (eq. B.1.2) are integrated using an implicit, centered space numerical scheme which is unconditionally stable for all time steps. The spatial and temporal distribution of the tritium- $^3\text{He}$  age diagnostic is computed from the individual fields of  $^3\text{He}$  and tritium. The advective-diffusive equation for tritium- $^3\text{He}$  age (equation 4.1.1) need not be integrated but, instead, is used as a basis to examine the spatial and temporal changes in the tritium- $^3\text{He}$  age field diagnosed from the  $^3\text{He}$  and tritium integrations.

The domain is taken to be  $x \in [0, L]$ ; the velocity,  $u$ , is assumed to be positive and constant throughout the domain. Boundary conditions are set at  $x = 0$  and a condition for zero tracer gradient is imposed at  $x = L$ . In general, the length of the domain,  $L$ , is large enough to prevent sensitivity of the solutions to the downstream boundary condition.  $^3\text{He}$  concentrations are set to zero at  $x = 0$  to simulate the out-gassing of excess helium from the surface mixed layer to the atmosphere. The time-dependent surface tritium boundary condition is taken from *Doney and Jenkins* [1988] and shown in figure 4.2. The initial conditions are set assuming a steady-state balance with a pre-bomb, cosmogenic surface water tritium concentration of 0.5 TU. The grid resolution is 30 km and the time step taken to be 0.1 yr. The magnitude of

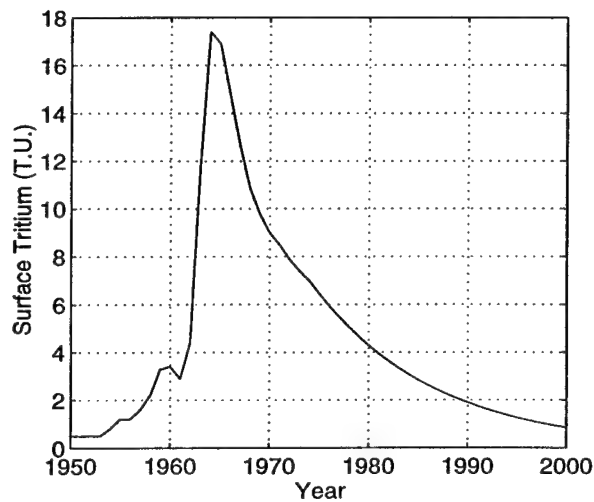


Figure 4.2: Time history of surface concentration of  $^3\text{H}$  for subtropical North Atlantic (based on *Doney and Jenkins* [1988] and *Dreisigacker and Roether* [1978])

the numerical diffusion for the implicit integration scheme is [*Roache*, 1982]

$$\kappa_n = \frac{u^2 \Delta t}{2}. \quad (4.2.2)$$

For a characteristic velocity scale used,  $0.5 \text{ cm s}^{-1}$ , the numerical diffusion is  $40 \text{ m}^2 \text{ s}^{-1}$ .

#### 4.2.2 General Character of Model Results

The structure of the numerical model solutions depends on the magnitude of radio-tracer Péclet number. Figures 4.3 and 4.4 illustrate space-time diagrams of the tracer fields for two different values of Péclet number. The spatial axis in each figure is transformed to an advective time scale by dividing by the characteristic velocity scale:  $T_{adv} = \frac{X}{V}$ . This normalization reduces the dependence only to the Péclet number and not the individual values of  $\kappa$  and  $V$ .

Figure 4.3 represents the numerical one-dimensional model results for ventilation dominated by advection. Large tritium values occur near the surface ( $x = 0$ ) in the early 1960's. The peak tritium values penetrate the model domain at the advective

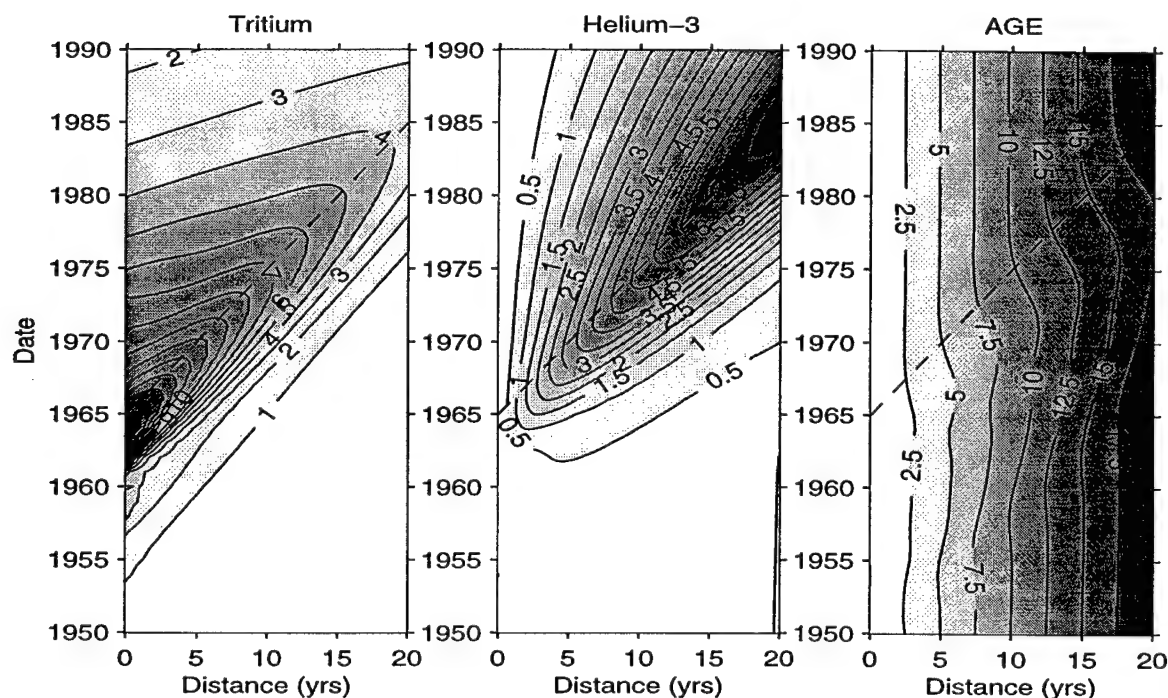


Figure 4.3: Time-Space diagrams of a) tritium, b)  $^3\text{He}$  and c) tritium- $^3\text{He}$  age evolution in one-dimensional model for radiotracer Péclet number = 56. The dashed line illustrates the characteristic for pure advection emanating from the  $X = 0$  in 1965, the time of the maximum surface tritium concentration. Contour units are TU for  $^3\text{H}$  and  $^3\text{He}$  values TU and years for age. The spatial axis in each figure is transformed to an advective time scale by dividing by the characteristic velocity scale:  $T_{adv} = \frac{X}{V}$ .

speed with values decreasing due to radioactive decay.  $^3\text{He}$  values are initially small but grow in response to the decay of tritium. The maximum  $^3\text{He}$  values form a narrow ridge aligned with the advective entry of tritium in the space-time domain.

The tritium- $^3\text{He}$  age field in figure 4.3 shows monotonically increasing values away from the surface. A distortion of the age field to younger values is evident and appears associated, but slightly in advance of the penetration of the  $^3\text{H}$  maximum. The slight distortion of the age field occurs when “young” water with high tritium content mixes with “older” water with low, pre-bomb concentrations of  $^3\text{He}$  and tritium. As illustrated in the simple mixing model of §1.3.3, when diffusion mixes water with differing net tracer concentrations, the resultant age is biased towards the age of the



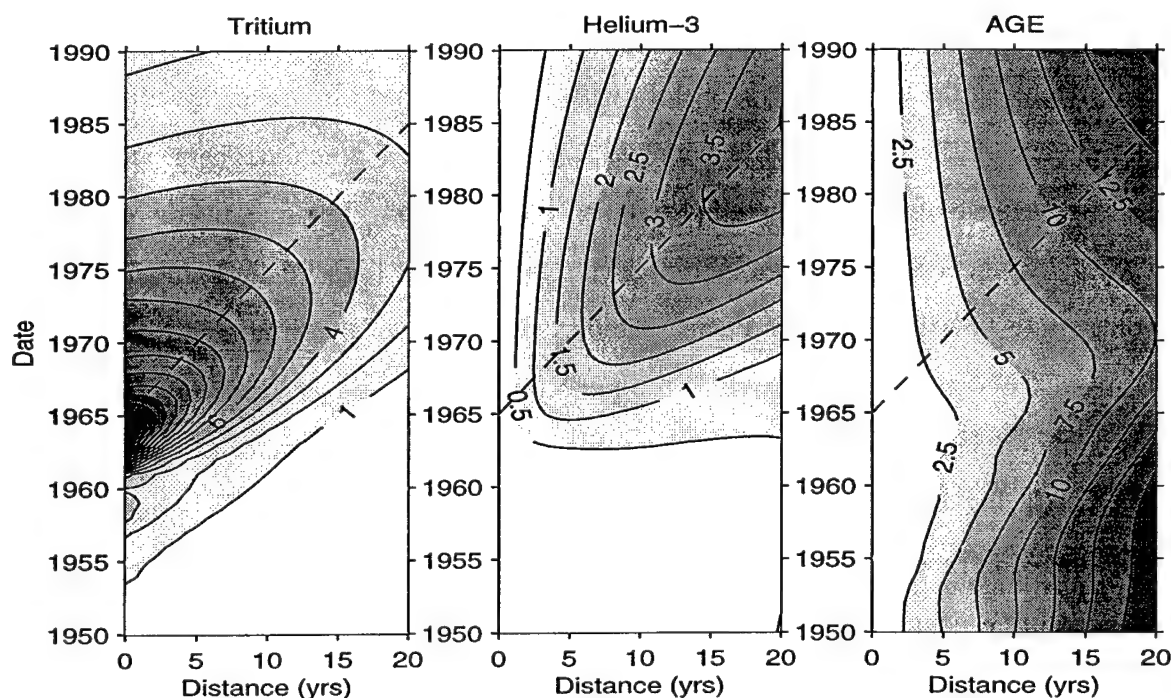


Figure 4.4: Same as figure 4.3 except radiotracer Péclet number = 5

water with the greater tracer burden. In the case illustrated in figure 4.3, the youngest waters have the highest tracer concentration in response to the injection of the bomb-produced tritium. Therefore, mixing effects bias the water in the deeper portions of the thermocline towards the young values at the surface. The maximum distortion of the tritium- $^3\text{He}$  age field leads the signal of the advective penetration of tritium because it is in this region where there is the greatest contrast in tracer concentrations between the “young” and “old” water.

A case with larger diffusive effects (lower Péclet number) is shown in figure 4.4. The general character of the solutions is the same as figure 4.3: penetration of high surface  $^3\text{H}$  values, *in situ* production of  $^3\text{He}$  and a tracer age field biased young. The details, however, are quite different. The increase in mixing causes tritium to enter the model domain more quickly after the peak input: large tritium concentrations are evident far in advance of the signal of advective penetration. Maximum  $^3\text{He}$  values are reduced and the ridge of high values is broader owing to the increased mixing

effects on both the  $^3\text{He}$  field and its tritium source. The tracer age field again shows distortion due to the mixing of waters with large contrasts in tracer inventories but the effects of the bias towards younger apparent age is much stronger and longer lasting because of the greater relative strength of diffusion. The magnitude of the bias towards younger apparent age increases compared to the high Péclet number case. In contrast to flows with higher Péclet number, the timing of maximum age anomaly in figure 4.4 occurs earlier relative to the penetration of the advective front. Again the maximum departure from the “true” advective age occurs in advance of the advective front carrying the bomb tritium because this is the region with the largest spatial gradients in tracer concentration. Additionally, while the age field in figure 4.3 has returned to a near steady-state balance by 1990, the age field at this date in figure 4.4 is still continuing to adjust in response to the bomb-tritium induced anomalies.

Prior investigation of the applicability of tritium- $^3\text{He}$  age [Roether, 1989b] concluded that measured tracer ages are accurate estimates of the true advective age if the value of the tracer age is less than the elapsed time since the injection of the bomb transient. Put another way, once the advective front carrying the injected bomb tritium has passed through a point in the thermocline, the tracer age field should reach a steady balance with the advective velocity. Comparison of figures 4.3 and 4.4 show that this is a reasonable conclusion for the highly advective case but with moderate amounts of diffusion, this simple rule-of-thumb breaks down. When the Péclet number is small, the tracer age field continues to adjust long after the information of the bomb-tritium input has advected by.

The failure of the tritium- $^3\text{He}$  age to behave as an ideal advective age can be understood in part from the balance of terms in the full advective-diffusive balance of the age equation (eq. 4.1.1) diagnosed from the one-dimensional numerical model (figure 4.5). The terms are evaluated at a position determined by the advective time scale, in this case 11 years, and therefore depend only on the radiotracer Péclet number. fig-

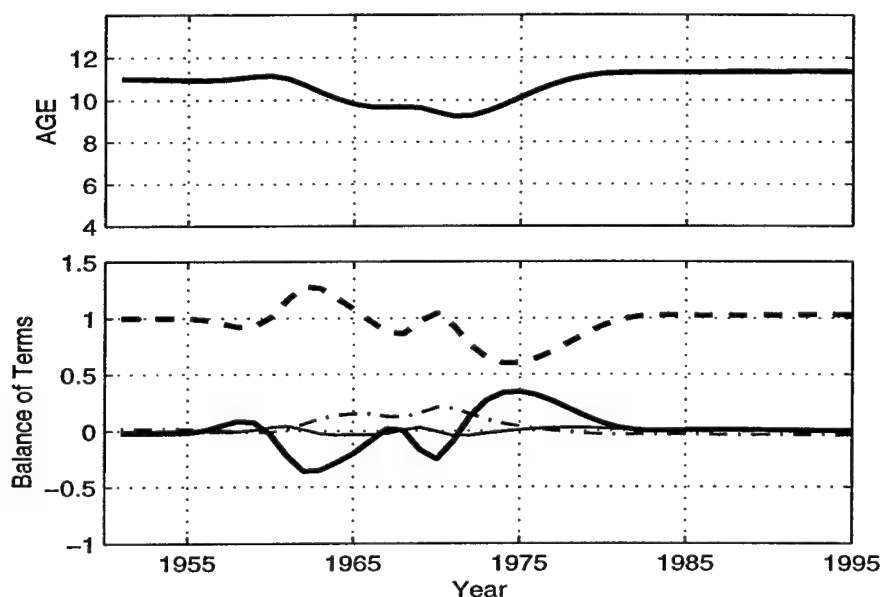


Figure 4.5: Temporal evolution of tracer age and balance of terms for Péclet number 56 at point where advective time is 11 years. Upper panel shows time series of tracer age. Lower panel shows relative magnitude of terms in the advective-diffusive balance equation for age: tendency (heavy solid), advective (heavy dashed), pseudo-advective (light dash dot), and Laplacian (light solid)

Figure 4.5 illustrates the case for a Péclet number of 56. The tracer age, shown in the upper panel, reaches a minimum value of 9.22 yr in 1971. The individual terms, lower panel, sum to 1 (the “aging term”) at all times. As expected for a high Péclet number system, the advective term dominates the overall balance and the simple balance of equation 4.1 provides a reasonably accurate approximation of the balance of terms for the tritium- $^3\text{He}$  age diagnostic over much of the temporal domain. The tendency term reaches a maximum value in 1974, consistent with the advective time lag and peak tritium input in the early 1960’s. The maximum impact of the pseudo-advective term is about 0.2 though its effects, as well as all non-advective terms, are negligible over the time-period of the hydrographic samples (post 1978).

The balance of terms for a more diffusive case, Péclet number 5, is displayed in figure 4.6. Comparison to the fields in figure 4.5 is dramatic. The minimum age is now 5 years and occurs in 1967. The pseudo-advective term reaches  $O(1)$  in the

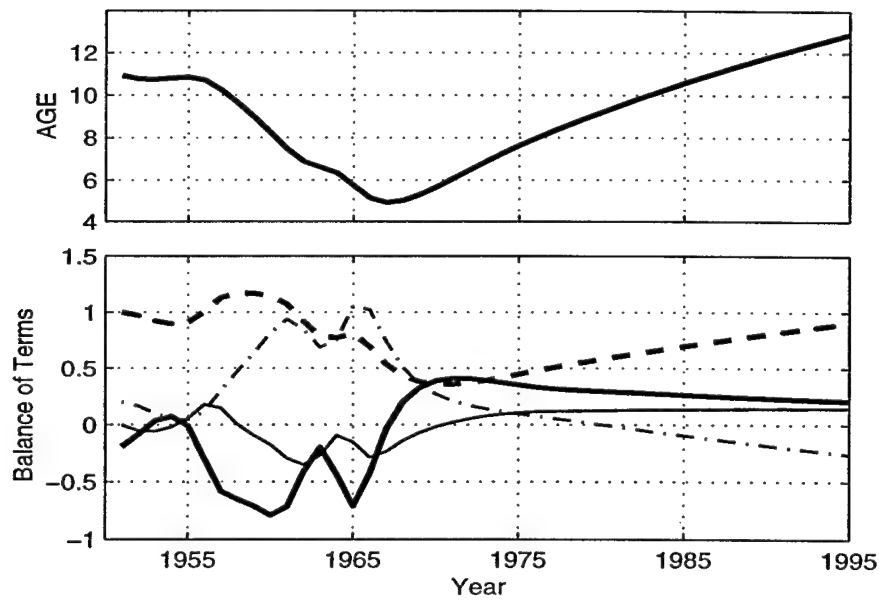


Figure 4.6: Same as figure 4.5 except radiotracer Péclet number = 5

early 60's driving large changes in the gradient of the age field (apparent in the large changes in the advective component). The tendency term reaches a maximum in the early 70's and slowly decreases thereafter. The upper panel in figure 4.6 shows that even at low Péclet number, the age diagnosed from the  $^3\text{H}$  and  $^3\text{He}$  in the period of the 1980's is a reasonably good estimate of the true advective age. Comparison of the tracer age value in the year 1986 in figures 4.5 and 4.5 reveals that a measure of the tritium- $^3\text{He}$  age at this point in time is relatively insensitive to the Péclet number of the flow. In contrast, the time rate of change of tritium- $^3\text{He}$  age in the 1980's does show a strong sensitivity to the Péclet number of the flow.

### 4.3 Comparison of Observed Age Tendencies and Numerical Model Simulations

Comparison of the model predictions with observations requires specification of the variables with which to make the comparison. Previous similar investigations have

used tritium inventory [*Sarmiento*, 1983; *Wunsch*, 1988a; *Mémery and Wunsch*, 1990], the tritium- $^3\text{He}$  relation [*Jenkins*, 1988a; *Musgrave*, 1990], or spatial gradients/structure of the age field [*Jenkins*, 1987; *Musgrave*, 1990; *Jia and Richards*, 1996; *Jenkins*, 1997]. The new observations presented in chapter 2 of this work are of the temporal evolution of the age field. The previous sections of this chapter have illustrated how the age tendency in a one-dimensional model depends on three quantities:

- The radiotracer Péclet number,
- The apparent (e.g. tracer) age of the water parcel,
- The date of observation relative to the bomb-tritium input.

In this section I will compare the observed age tendencies to numerical model simulations with varying Péclet number. The age-regression models in section 2.2.2 provide estimates of both the age tendency and mean age on isopycnal surfaces over the time period 1979 to 1993. The regression model yields estimates of age tendency as a function of age at the mid-point of this time series, 1986, which can be directly compared with the numerical model predictions of this relation for the same date. For purposes of comparison, age tendency in the model is calculated over a time period of 10 years to correspond to the time interval of the observations. Calculations of time-derivatives of model output based on differing intervals shows that the results presented below are not sensitive to this assumption.

The observed age tendencies are summarized in figure 4.7 which includes the results of both the regression model in spatial coordinates (§2.2.2) and the model based on the change of the age field with respect to oxygen (§ 3.3). As discussed previously, the two independent models give consistent estimates of the relation between age tendency and tracer age. The mean age for a given isopycnal is lower in the oxygen-

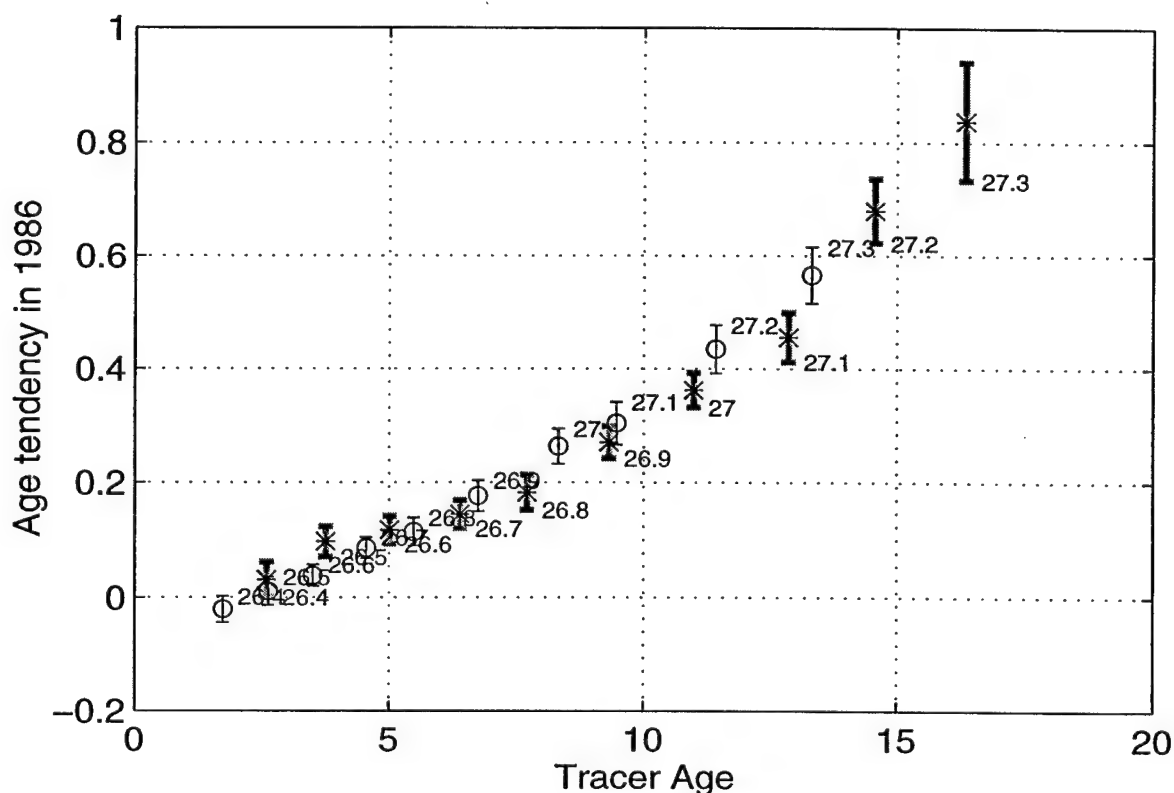


Figure 4.7: Age tendency vs. mean tracer age in 1986 determined from observations. Values are shown for isopycnals spanning the thermocline from  $\sigma_\theta = 26.4$  to 27.3. Results of temporally dependent geographic regression model are indicated with an '\*' and thick gray error bars. Results from age evolution against the oxygen field are indicated by 'o' and thin black error bars. Error bars represent 95% confidence intervals.

based models due to the exclusion of older waters with large AOU. The diagnosed age tendency is similarly reduced, however, so the results fall on the same trend of increasing tendency with age.

In the one-dimensional numerical model, the relation of age tendency and tracer age depends solely on the Péclet number and the elapsed time relative to the bomb-tritium input. Figure 4.8 shows the predicted relation of age tendency and age in the year 1986 for a variety of Péclet numbers. For a fixed Péclet number, the magnitude of the age tendency increases with tracer age. For a fixed tracer age, the magnitude of the tendency increases with reduction in Péclet number. figure 4.8 spans the parameter

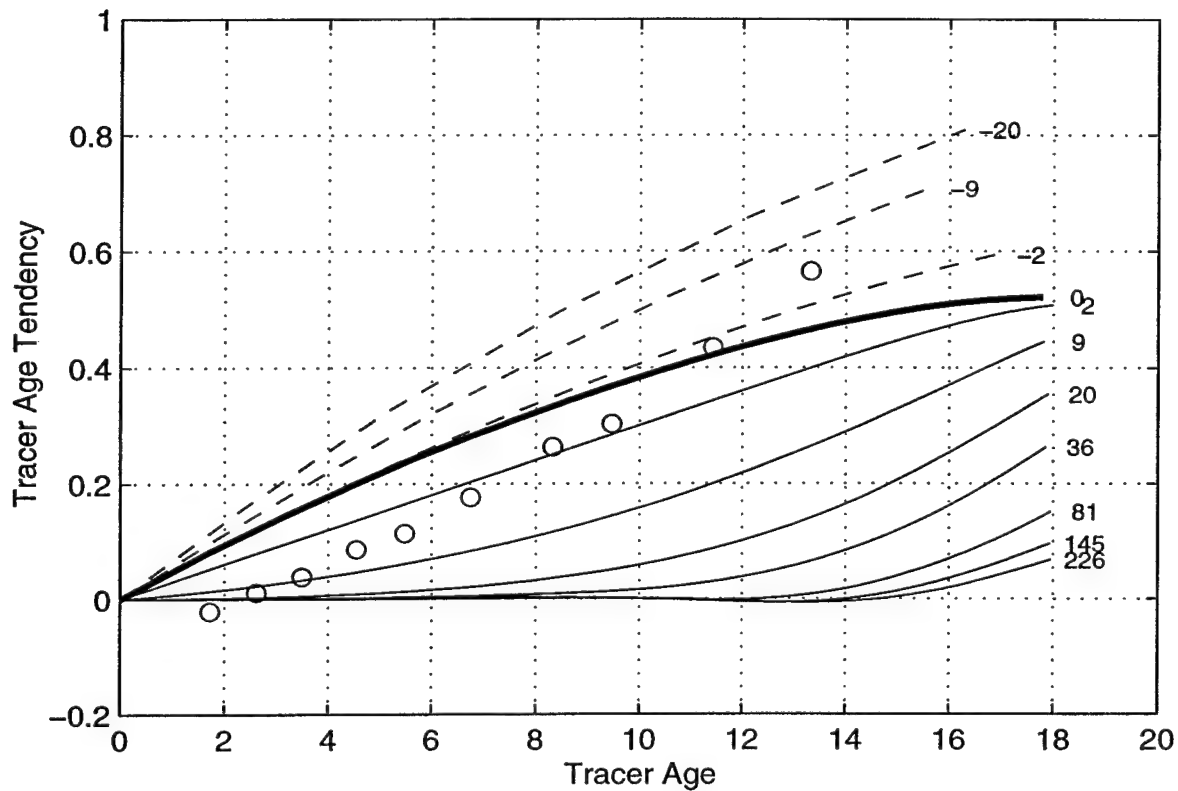


Figure 4.8: Age tendency vs. tracer age in 1986 determined from one-dimensional model. Each line represents the results of a model with fixed radiotracer Péclet number, indicated along right. The heavy line marks the pure diffusive model ( $Pe = 0$ ) and dashed lines represent models with negative subduction velocities. For purposes of comparison, the observed relation derived from the regression against AOU (figure 4.7) is shown as open circles.

range from highly advective models to a pure diffusion model ( $Pe = 0$ ). The case of pure advection ( $Pe = \infty$ ) would be represented by zero age tendency at all values of tracer age. In order to cover the parameter range of the observations (figure 4.7) some examples with negative subduction velocity (e.g. velocity directed out of the thermocline into the surface mixed layer) are also included and indicated as negative Péclet numbers.

The observed and modeled age tendencies can be combined to obtain an estimate of the Péclet number on each of the isopycnals in the eastern North Atlantic thermocline. For each isopycnal, the observed mean age and age tendency is matched

to a range of Péclet numbers for which the one-dimensional model yields a consistent relation. The results of this calculation for the age-oxygen regression model are shown in table 4.1. Comparable analysis for the age tendency-age relation determined

Isopycnal	Minimum Pe	Best Pe	Maximum Pe
26.4	19.6	$\infty$	$\infty$
26.5	6.9	13.2	$\infty$
26.6	6.0	8.3	12.4
26.7	4.1	5.2	7.0
26.8	3.6	4.8	6.6
26.9	2.2	3.4	4.6
27.0	0.9	1.9	3.0
27.1	0.6	1.7	3.0
27.2	-3.7	-0.8	0.7
27.3	-8.2	-5.1	-2.6

Table 4.1: Radiotracer Péclet numbers estimated from data and one-dimensional ventilation model. Range of values is determined from 95% confidence limits of diagnosed age tendency. Values indistinguishable from pure advection are indicated by Péclet number =  $\infty$ .

from the geographic regression model yield consistent results below  $\sigma_\theta = 26.6$ . In the upper thermocline, where the two methods for determining the age tendency diverge (figure 3.13), the geographic age regression model implies slightly lower estimates of Péclet numbers.

Radiotracer Péclet numbers are highest on the shallowest isopycnals indicating the dominance of advective ventilation for renewing properties along these surfaces. Values decrease with increasing density until estimates of Péclet number become indistinguishable from zero at  $\sigma_\theta = 27.2$ , suggesting that the observed age tendency is consistent with pure diffusive ventilation along this surface. Diffusivity dominated ventilation is congruous with expectations on this density surface since the position of its winter outcrop is near the zero-wind stress curl line of the North Atlantic [*Isemer and Hasse, 1987*]. The negative Péclet numbers required for  $\sigma_\theta = 27.3$  arise from the



apparent need for negative subduction velocities in the one-dimensional model in order to simulate the observations. This result is expected, within the credibility of such a simple model, for an isopycnal which outcrops in the subpolar gyre and therefore feels Ekman suction rather than pumping at the surface.

The radiotracer Péclet number, the parameter which controls the structure of the model solution, is, however, a somewhat artificial parameter for interpreting oceanic ventilation because the length scale has been concealed through the use of the radiotracer decay time scale (equation B.1.5); the implicit length scale of the radiotracer Péclet number is the product of the characteristic velocity and the time scale of tritium decay, 17.96 yr. Since the upper levels of the thermocline are ventilated more quickly than this characteristic time scale, the radiotracer Péclet number overestimates the actual Péclet number appropriate for ventilation.

The arbitrariness of the radio-decay time scale can be removed by employing the measured ventilation age to estimate a Péclet number consistent with the ventilation time and space scales of the tracer field:

$$Pe_{ventilation} = \frac{V^2}{\kappa\lambda} \lambda\tau. \quad (4.3.3)$$

Using the observed mean tracer age as a time scale and observed geostrophic velocity for the advective scales results in implied length scales ranging from 900 km at  $\sigma_\theta = 26.5$  to 1300 km on  $\sigma_\theta = 27.1$  (figure 4.10). Estimates of the ventilation Péclet number are shown in table 4.2. The differing implicit time scales must be kept in mind when directly comparing of the estimates of ventilation Péclet number for different isopycnals: at shorter time scales the relative impact of diffusive effects always increases. The general trend of decreasing Péclet number with greater density remains but now there is a marked decrease in the magnitude of the Péclet number estimates on the lighter density surfaces. The ventilation time scales on the shallower isopycnals are small compared to the radiotracer time scale of 17.96 yr resulting in large reduction in the estimated Péclet number. For the deeper surfaces, the ventilation time scale

Isopycnal	Minimum Pe	Best Pe	Maximum Pe
26.4	1.9	$\infty$	$\infty$
26.5	1.0	1.9	$\infty$
26.6	1.2	1.6	2.4
26.7	1.0	1.3	1.8
26.8	1.1	1.5	2.0
26.9	0.8	1.3	1.7
27.0	0.4	0.9	1.4
27.1	0.3	0.9	1.6
27.2	-2.4	-0.5	0.4
27.3	-6.1	-3.8	-2.0

Table 4.2: Ventilation Péclet numbers estimated from radiotracer Péclet number and observed ventilation time. Range of values is determined from 95% confidence limits of diagnosed age tendency. Values indistinguishable from pure advection are indicated by Péclet number =  $\infty$ .

approaches the radiotracer time scale so there is little difference between the radiotracer and ventilation Péclet numbers. In the lower thermocline ( $\sigma_\theta = 27.0$ ) advection and diffusion appear to have comparable time-scales for the ventilation of properties in the eastern Atlantic.

Estimates of the Péclet number on isopycnal surfaces can be combined with independent knowledge of the velocity scale to estimate the lateral diffusivity parameter:  $\kappa = \frac{V^2}{\lambda Pe}$ . Diffusivity estimates based on the the Péclet number estimates and the large-scale meridional geostrophic velocity are shown in figure 4.9. The same results could be obtained using the tritium- $^3\text{He}$  age to estimate the velocity scale due to the agreement of tracer-age and geostrophic advective scales in figure 3.3. The estimate of lateral diffusivity is  $O(1800 \text{ m}^2\text{s}^{-1})$  at  $\sigma_\theta = 26.5$  and shows a generally increasing magnitude with depth. The upper bound of the diffusivity estimate grows large on dense isopycnals as the estimate of the Péclet number approaches zero. These estimates of lateral diffusivity will be compared with other published values in §4.6.

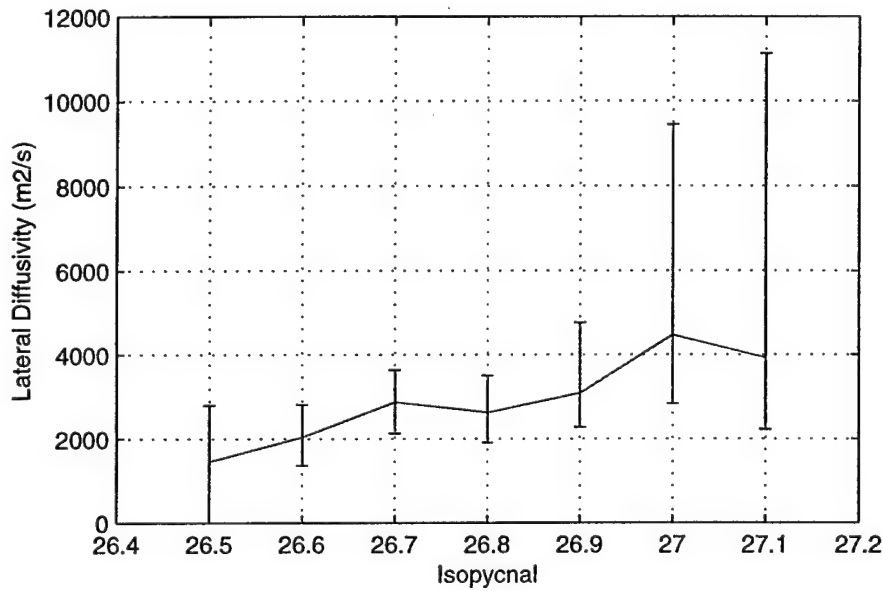


Figure 4.9: Lateral diffusivity,  $\kappa_H$ , implied by diagnosed Péclet number and geostrophic velocity scale. The geostrophic velocity scale is calculated from the zonal density gradient between 40 and 20°W at 26°N as shown in figure 3.3. Error bars represent the 95% confidence intervals derived from the Péclet number estimation.

Estimates of diffusivity must be accompanied by a length scale appropriate for their interpretation. The specification of the velocity scale, required to estimate the lateral diffusivity, implicitly sets the intrinsic length scale of the analysis. The length scale derived from the geostrophic velocity scale and the tracer age ventilation time is shown in figure 4.10. Length scales are of the order 1000 km, consistent with the magnitude of the distance between the center of the observation area and the winter outcrop latitude. Length scales increase with depth reflecting the northward march of the winter outcrop position for heavier isopycnals. The decrease in length scale at  $\sigma_\theta = 27.2$  likely arises from the young bias of tracer ages underestimating the true time scale on this surface. The lateral diffusivity estimates of figure 4.9 should be interpreted as valid only for these length scales. Comparison of the size of the length scale in figure 4.10 to the characteristic length of the mesoscale eddy field ( $\approx 150$  km [Krauss *et al.*, 1990; Joyce and Jenkins, 1993; Le Traon, Rouquet and Boissier, 1990]) supports the assumption of the Fickian parameterization of mixing.

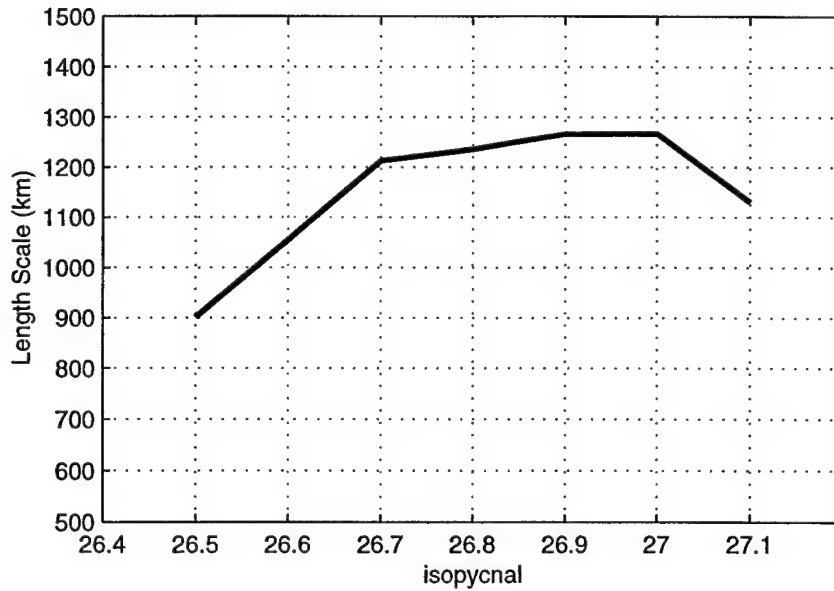


Figure 4.10: Implicit length scale for lateral diffusivity estimate. Length scale is calculated from the product of the tracer ventilation age and the characteristic meridional geostrophic velocity.

### 4.3.1 Contrast with Local Balance Estimates of Diffusivity

The information used to diagnosis diffusivity in the calculation presented above is distinctly different from previous estimates of mixing parameters based on  $^3\text{He}$  and  $^3\text{H}$  data. *Jenkins* [1997] constructed a diagnostic model based on estimates of the instantaneous balance of the advective-diffusive equations for tritium- $^3\text{He}$  age, salinity and oxygen in the eastern North Atlantic thermocline. This type of calculation solves for the relative magnitude of terms based on the observed spatial gradients of the tracer fields. Similar previous analyses [*Roether and Fuchs*, 1988] neglected the tendency term while *Jenkins* [1997] includes an estimate of the temporal changes in age based on the same data set used in this analysis.

The local-balance of the tritium- $^3\text{He}$  age equation (eq. 4.1.1), however, provides a poor estimate of lateral mixing rates because at the time of the observations (the early 1990's in this case) the magnitude of the mixing terms are small

(generally less than 10% of the total budget). Therefore, given the observational uncertainties, the instantaneous advective-diffusive balance of tracer age can be satisfied without explicit inclusion of the mixing terms. This is illustrated quantitatively in figure 4.11 which shows the magnitude of the tendency and advection terms diagnosed

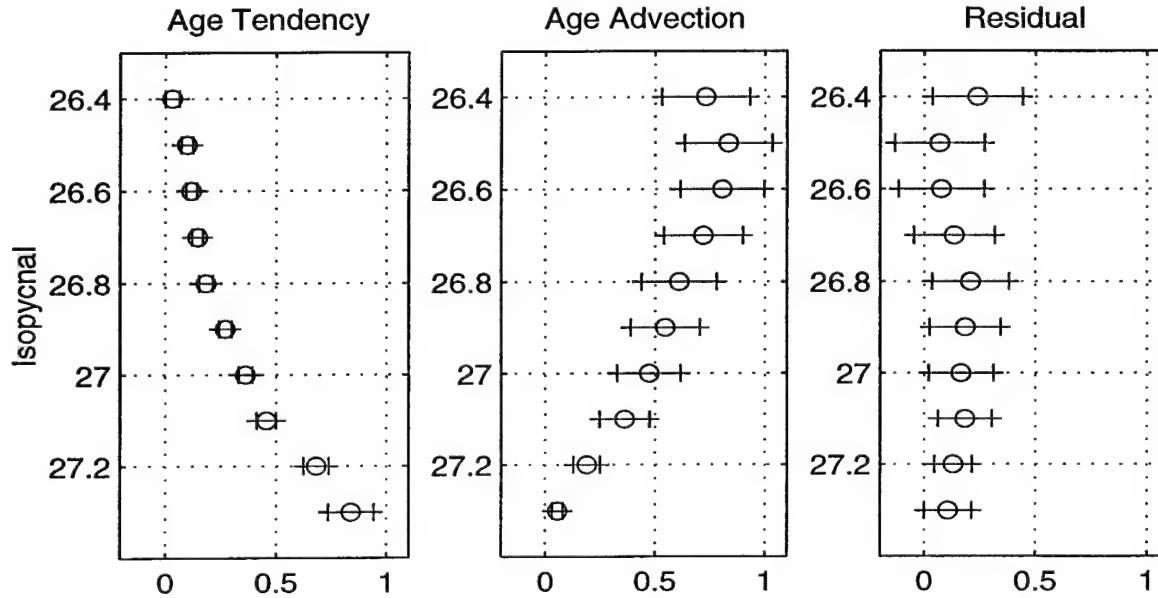


Figure 4.11: Primary balance of terms in the tritium-<sup>3</sup>He age equation evaluated at 1986. Left-hand panel shows diagnosed age tendency. Middle panel shows  $\vec{u} \cdot \nabla \tau$  evaluated from the observed age gradients and the large scale geostrophic velocity field referenced to 1300 dbar. The standard error of the spatial age gradients is determined from the regression model. An ad hoc 15% standard error is assigned to the velocity estimates to account for scale-dependent gradient uncertainties and the assumption of a geostrophic zero-velocity-surface. The right-hand panel shows the residual of the tritium-<sup>3</sup>He age balance when the effects of the mixing terms are neglected. Error bars in all panels represent the 95% confidence limits.

from observations in the eastern Atlantic. The tendency and spatial gradients of the tritium-<sup>3</sup>He age field are determined from the regression model in section 2.2.2. Geostrophic velocity estimates are calculated from the *Lozier, Owens and Curry* [1995] hydrographic atlas using spatial gradients over 10 degrees of latitude and longitude. A standard error of 15% is assigned to the velocity estimates to account for uncertainties of reference level velocities and the scale-dependence of the spatial gradient estimates.

The right-most panel of 4.11 illustrates the residual of the diagnostic calculation:

$$Residual = 1 - \frac{\partial \tau}{\partial t} - \vec{u} \cdot \nabla \tau. \quad (4.3.4)$$

For much of the density range spanning the thermocline, the residual of equation 4.3.4 is not distinct from zero. Attempts to employ this residual as a diagnostic of the mixing parameter,

$$\kappa = - \frac{1 - \frac{\partial \tau}{\partial t} - \vec{u} \cdot \nabla \tau}{\nabla^2 \tau + \left( \frac{\nabla[{}^3H]}{[{}^3H]} + \frac{\nabla[{}^3H+{}^3He]}{[{}^3H+{}^3He]} \right) \cdot \nabla \tau}, \quad (4.3.5)$$

can not provide well determined estimates of the lateral mixing coefficient: the direct effects of mixing are generally too small at the time of the observations to have a resolvable impact above the noise of the more dominant terms. In the local budget of tritium-<sup>3</sup>He age, the observed advective divergence of age is balanced predominantly by the tendency and aging terms, not by mixing. This behavior of the tracer age balance can be contrasted with the behavior of a steady-state tracer. For example, the diagnostic calculation of *Jenkins* [1997] includes constraints based on <sup>3</sup>H and <sup>3</sup>He observations but the information to determine the mixing parameters comes from the steady state salinity balance:

$$\kappa \nabla^2 S = \vec{u} \cdot \nabla S.$$

Unlike the tritium-<sup>3</sup>He age balance, any observed advective divergence of salinity must be balanced to first order by a diffusive convergence.

The estimate of diffusivity presented here (figure 4.9) does not depend on a spatial diagnostic analysis of the local balance of the tritium-<sup>3</sup>He age equation at the time of observation. The non-steadiness of the age field clearly demonstrates the importance of mixing effects in the overall balance of the tracer age field. This analysis shows, however, that mixing is more robustly determined from the magnitude of the temporal tendency of the age field rather than the direct spatial analysis of the mixing terms themselves. The change of the age field with time is the remnant effect of the earlier substantial action of the nonlinear mixing term. The sudden introduction of the

large amounts of tritium into the ocean drives the nonlinear mixing term to first-order importance in the overall balance. The effect of the nonlinear mixing is to “destroy” tritium- $^3\text{He}$  age, creating a young bias to the observed age field. The rate of recovery of the age field from this distortion provides a diagnostic of the Péclet number of the flow ventilating the thermocline. The diagnosed Péclet number, combined with independent estimates of the velocity scale of the flow, furnishes an estimate of the strength of lateral mixing.

## 4.4 Tritium Concentrations and Inventory

So far, the analysis and discussion of this chapter has focused on the tritium- $^3\text{He}$  age fields and their observed temporal development. This section will concentrate on the other information component of the  $^3\text{He}$ -tritium system, the transient tracer inventory. Previous analysis of ventilation of the thermocline utilized the observed tritium inventory to estimate the exchange rate between subsurface waters and the surface mixed layer [*Sarmiento*, 1983; *Wunsch*, 1988a]. In this section, two differing analyses of tritium inventory are examined. The first examines the relation between tritium concentration and tracer age on isopycnal surfaces. The second, more akin to the previous inventory studies, does not incorporate tracer age measurements and instead, analyzes the tritium inventory over some finite geographic domain.

### 4.4.1 The Tritium Concentration – Tracer Age Relation

Figure 4.12 illustrates the observed decay-normalized tritium concentrations<sup>a</sup> in 1986 in the eastern and western subtropical North Atlantic. Tritium concentrations are plotted as a function of the observed mean tracer age for isopycnal surfaces spanning

---

<sup>a</sup>see §2.5 for a discussion of this choice of measure for tracer inventory

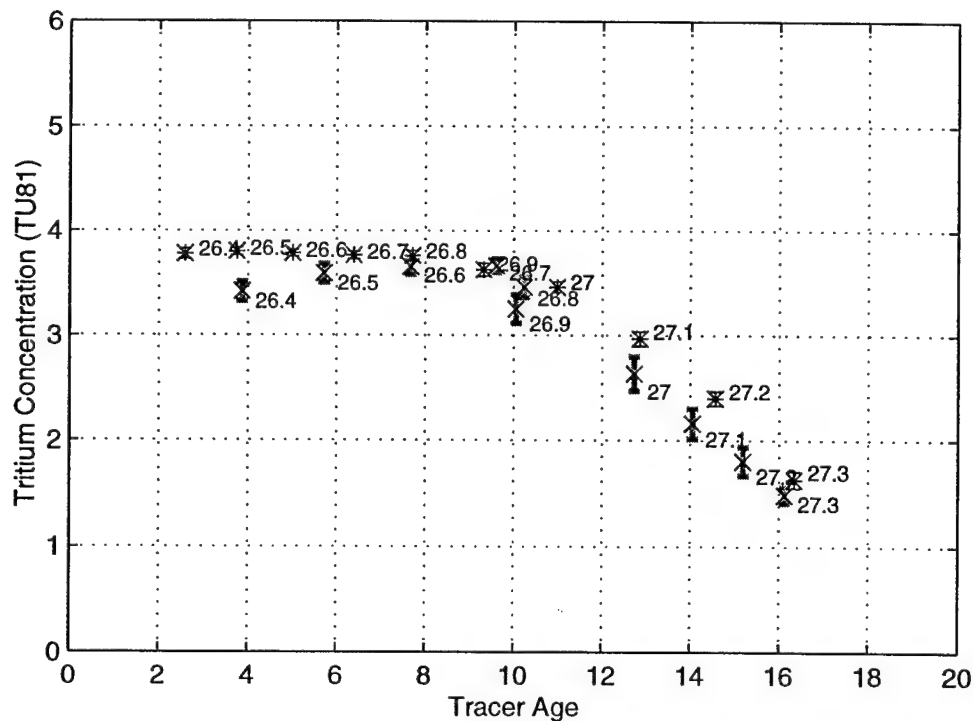


Figure 4.12: Tritium concentration (TU81) vs. mean tracer age in 1986 determined from observations. Values are shown for isopycnals spanning the thermocline from  $\sigma_\theta = 26.4$  to 27.3. Results of temporally dependent geographic regression model are indicated with an '\*' and thin black error bars. Results from time series observations at Bermuda are indicated by 'x' and thick gray error bars. Error bars represent 95% confidence intervals.

the thermocline. The highest tritium concentrations are observed on the lightest density surfaces with the youngest ventilation ages.

As found for the age tendency, the tritium concentration in a one dimensional advective-diffusive model is a function of:

- The radiotracer Péclet number,
- The apparent (e.g. tracer) age of the water parcel,
- The date of observation relative to the bomb-tritium input.



Figure 4.13 displays the relation between tritium and age in the year 1986 for simulations over a range of Péclet numbers. The curves for all the Péclet numbers converge

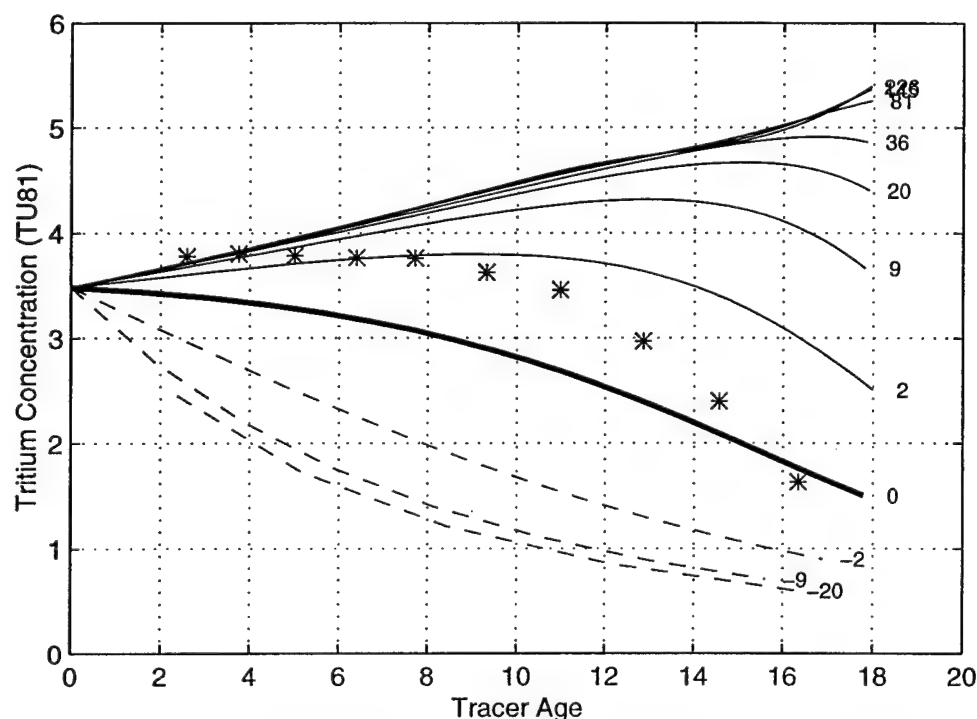


Figure 4.13: Tritium concentration (TU81) vs. tracer age in 1986 determined from one-dimensional model. Each line represents the results of a model with fixed radio-tracer Péclet number, indicated along right. The heavy line marks the pure diffusive model ( $Pe = 0$ ) and dashed lines represent models with negative subduction velocities. For purposes of comparison, the observed relation determined from the geographic regression (figure 4.12) is shown as asterisks.

at  $\tau = 0$  where the tritium concentration is the imposed boundary value for the year 1986. For high Péclet number, advectively dominated flows, tritium concentration increases with tracer age. In the limit of high advection, the tracer age is an accurate estimate of the true advective age and therefore, the increase of tritium concentration with elapsed age is a record of the prior history of the surface tritium concentration. For example, at high Péclet number, the tritium concentration at  $\tau = 12$  is simply the surface tritium concentration (in decay normalized units) 12 years prior to 1986.

For lower Péclet numbers, the simulated tritium concentration at large tracer ages decreases. When the flow is more diffusive, two effects work in concert to lower the position of the curves in figure 4.13. First, diffusion tends to wash out and reduce the peak associated with the penetration of the bomb-tritium spike (e.g. compare the tritium panels in figure 4.4 and 4.3). Second, the tracer age tends to underestimate the true advective age.

Comparison of the observed tritium concentrations to the one-dimensional model (figure 4.13) suggests the Péclet number decreases on the denser isopycnals. The numerical estimates of the Péclet number determined from the tritium concentration in figure 4.13 are in close agreement with those determined from observed relation of age tendency and tracer age (Table 4.1). The use of tritium concentration in this section has more similarities to the present analysis of tracer age tendency than to the previous use of observed tritium inventories in models of ventilation. Analyses, such as that illustrated in figure 4.13, are measures of the instantaneous relation between tritium concentration and the tracer age which implicitly incorporate the information of the  $^3\text{He}$  to  $^3\text{H}$  ratio. Since the ratio  $\frac{^3\text{He}}{^3\text{H}}$  is sensitive to mixing, the observed relation of coupled transient tracer properties is a measure of the Péclet number of the flow. Previous calculations based on transient tracer inventory, such as Sarmiento's box model, utilize the observed tritium concentration within a finite geographic region rather than as a function of tracer age. An example of this type of calculation is presented in the next section.

#### 4.4.2 Tritium Inventory Calculations

The calculations of the previous section involve the tritium concentration as a function of the tracer age. Obviously, one cannot perform this type of calculation if one is seeking to explain the transient tracer concentration data without using (or measuring)

the “age” component of the tracer information (in this case the  $\frac{{}^3\text{He}}{{}^3\text{H}}$  ratio). Without the tracer age information, the transient tracer data must be examined as a function of geographic position and time. Integrating over a spatial volume forms a measurement of inventory and typically yields a quantity with lower uncertainty. The ventilation box model of *Sarmiento* [1983] (discussed in §1.3.2) seeks to simulate the observed tritium inventory of the subtropical thermocline as a function of surface tritium concentration and the modeled exchange rate with subsurface isopycnal layers.

The ventilation exchange rate,  $\tau_{vent}$ , in Sarmiento’s model is conceptualized to be the sum of advective and diffusive fluxes:

$$\tau_{vent} = \frac{A}{V} \left( U + \frac{\kappa}{L} \right) \quad (4.4.6)$$

where  $U$  is the advective speed,  $\kappa$  is a diffusivity,  $V$  is the volume of an isopycnal layer and  $A$ ,  $L$  are the area and length of the surface outcrop of the isopycnal layer. In this notation, both diffusion and advection act to transport tritium from the surface into the thermocline and their individual contributions cannot be determined.

The one-dimensional numerical model can be used to examine a crude simulation of this calculation. The model is run for a parameter range of velocity and diffusivity appropriate for the eastern Atlantic thermocline. Tritium inventory is calculated by averaging the tritium concentration over a finite distance of the model domain. For the calculations presented here the average is taken over the first 3000 km, chosen as the length scale of the eastern portion of the gyre. Figure 4.14 displays a contour plot of the simulated tritium inventory in 1972 as a function of velocity and diffusivity in the numerical model. This date corresponds to the GEOSECS survey which Sarmiento used to estimate the thermocline tritium inventory. For much of the parameter space illustrated in figure 4.14 the tritium inventory in the model thermocline increases with increases in both advection and diffusion, in agreement with the conceptual notation of equation 4.4.6. This is most clearly seen at low velocities where the isopleths of tritium inventory slant down to the right. At higher velocities, however, the effects

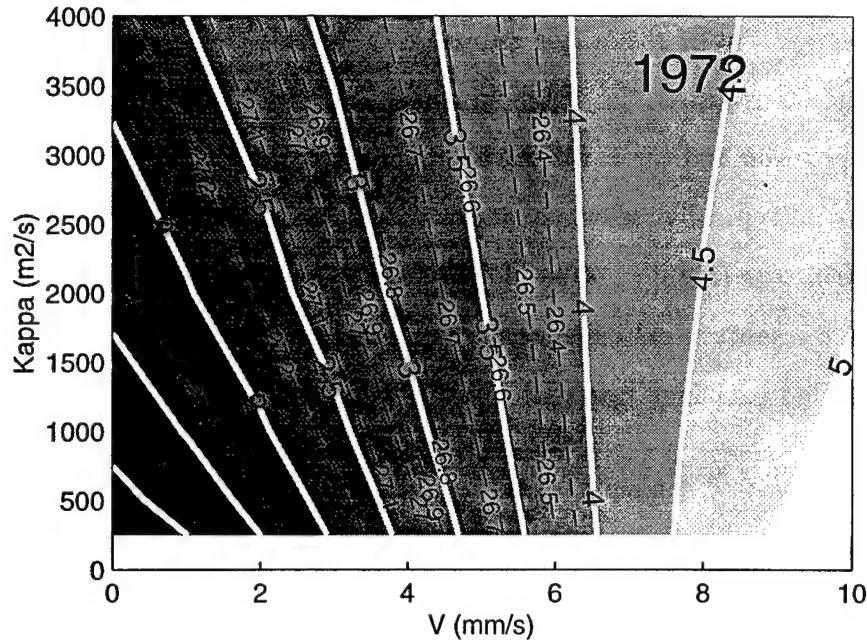


Figure 4.14: Average tritium concentration in first 3000 km of model domain in 1972 as function of advective and diffusive strengths. Average decay-normalized tritium concentrations (TU81) are contoured with contour intervals displayed as heavy white lines. The observed mean tritium values for each isopycnal layer in 1972 (as reported in *Sarmiento* [1983]) are displayed as dashed lines labeled with the density of the isopycnal. The curves of constant tritium inventory define the combination of parameters ( $V$  and  $\kappa$ ) needed to reproduce the observations in this simple simulation.

of diffusivity are reduced and eventually reverse for velocities above about 7 mm/s. At the higher velocities, increases in diffusivity act to lower the total inventory of tracer in the domain. The observed mean tritium concentration on each isopycnal in 1972 is also shown on figure 4.14. The curves of constant tritium inventory define the combination of parameters ( $V$  and  $\kappa$ ) needed to reproduce the observations in this simple simulation. Increases in diffusivity have the largest effect on the densest isopycnals. For example, at  $\sigma_\theta = 27.2$ , the observed inventory in 1972 can be simulated by a one-dimensional model with negligible advection and diffusivity of  $4000 \text{ m}^2 \text{ s}^{-1}$  or a model with negligible diffusion and an advective velocity of about 3.5 mm/s. For isopycnals in the upper thermocline ( $\sigma_\theta = 26.4$ ) the simulated inventory is relatively insensitive to the magnitude of lateral diffusivity.

The differing effects of diffusivity at low and high velocity scales is simply explained by examining the advective time-scale of the domain. For a velocity of 1 cm/s, the time scale to advectively flush the 3000 km domain of the integration region is 9.5 yrs. If the advective time-scale of the domain is long compared to the elapsed time since the peak bomb input, both advection and diffusion contribute to increasing the tracer concentration. In contrast, when the advective time of the model starts to approach the elapsed time since the peak bomb input, increases in lateral diffusion reduce the tritium inventory rather than increase it.

The importance of the advective time-scale is even more pronounced at later times. Figure 4.15 displays the tritium inventory in the model domain in 1986, the mid-point of the observations used in this study. This point in time is over 2 decades after the peak input of tritium and even weak velocities are capable of flushing the 3000 km domain over this time. As such, the parameter region for which increases in diffusivity lead to increased tritium inventories is limited to only the smallest velocities ( $V \leq 2.5$  mm/s). Maximum tritium inventories are found for a velocity scale of about 7 mm/s and minimal diffusion. Velocities greater than 7 mm/s result in lower inventories by completely flushing the peak bomb-tritium values from the domain of the model. Also displayed on figure 4.15 are the mean isopycnic tritium values determined from the geographic regression in the eastern Atlantic. Although these values are point estimates rather than integral estimates of the gyre inventory, they provide a crude reference of typical tritium concentrations in 1986. The generally lower velocities required to match the  $^3\text{H}$  concentrations on each isopycnal in 1986 compared to that for the same isopycnals in 1972 suggests a failure of the one-dimensional model to accurately represent the processes affecting the long-term evolution of the tritium inventory.

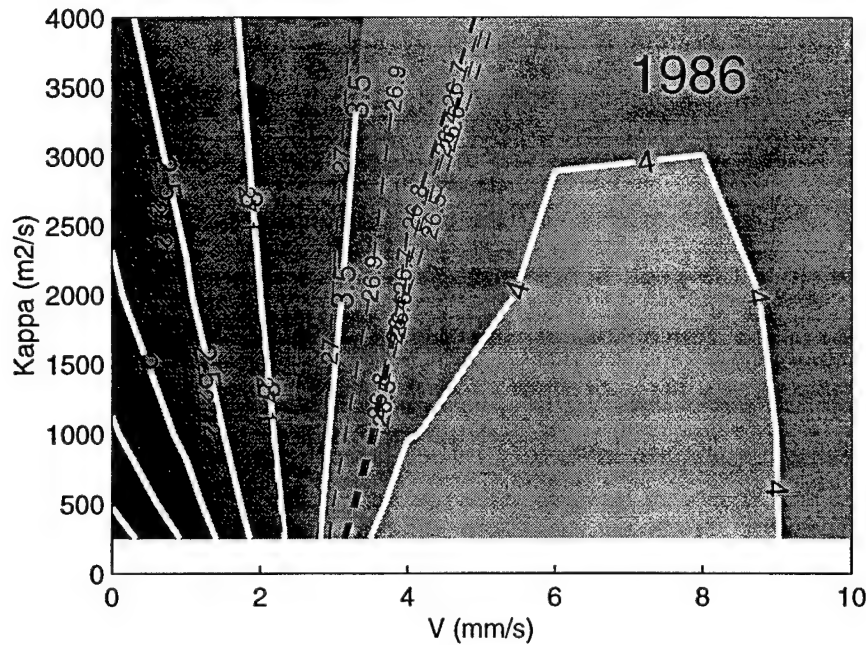


Figure 4.15: Average tritium concentration in first 3000 km of model domain in 1986 as function of advective and diffusive strengths. Decay-normalized tritium concentrations (TU81) are contoured with contour intervals displayed as heavy white lines. The observed mean tritium values for each isopycnal determined from the geographic regression model in the eastern Atlantic (§2.5) are displayed as dashed lines labeled with the density of the isopycnal. The curves of constant tritium inventory define the combination of parameters ( $V$  and  $\kappa$ ) needed to reproduce the observations in this simple simulation.

### Summary of Tritium Inventory Analysis

The simple models of tritium inventory presented in this section compare two differing analyses of tritium concentration observations in the thermocline. In the first case, tritium as a function of tracer age shows sensitivity to the radiotracer Péclet number in a manner similar to the temporal tendency of age. As with the age tendency analysis, the tritium-vs.-age relation implicitly contains information about the ratio  $\frac{{}^3\text{He}}{H}$  and observations show large deviations from that expected for an advectively dominated flow. The second form of analysis is analogous to the tritium inventory calculations of *Sarmiento* [1983]. These analyses do not incorporate the “age” component of the system and treat the tracer problem as a radioactive dye spreading into an initially

uncontaminated ocean. Analysis in this section supports the notion that the exchange rate determined by this calculation is the sum of advective and diffusive effects but only if the advective time-scale of the domain is long compared to the elapsed time since the tritium injection. When the elapsed time approaches the flushing time-scale of the domain, the inventory added by lateral diffusion is minimal and diffusive effects can reverse sign and lead to decreases in the inventory of the domain.

## 4.5 Sensitivity to Surface Boundary Condition

### 4.5.1 History of Surface Tritium Concentration

Previous analyses of transient tritium observations have demonstrated the high sensitivity of the observed subsurface tracer distributions to the poorly known surface boundary condition for tritium [*Wunsch*, 1988a; *Mémery and Wunsch*, 1990]. The peak rate of tritium input occurred before the first large-scale surveys to measure tritium concentrations in seawater. Even after measurement programs commenced, the sparse geographical and temporal coverage of tritium observations in the historical database limits the accuracy of any reconstruction of the history of tritium concentration in surface waters. An estimate of the surface input rates of tritium to the North Atlantic is shown in figure 1.1 and an estimate of the resultant mixed-layer tritium concentrations illustrated in figure 4.2. It is convenient when examining the time-history of tritium concentrations to convert the measurements to a decay-normalized tritium value, thereby removing the known temporally varying portion of the signal. Figure 4.16 shows a reconstruction of the decay-normalized surface tritium concentration of the North Atlantic based on analysis by *Doney and Jenkins* [1988] and *Dreisigacker and Roether* [1978]. Also shown on figure 4.16 are some of the tritium measurements upon which this reconstruction is based. As discussed before, there

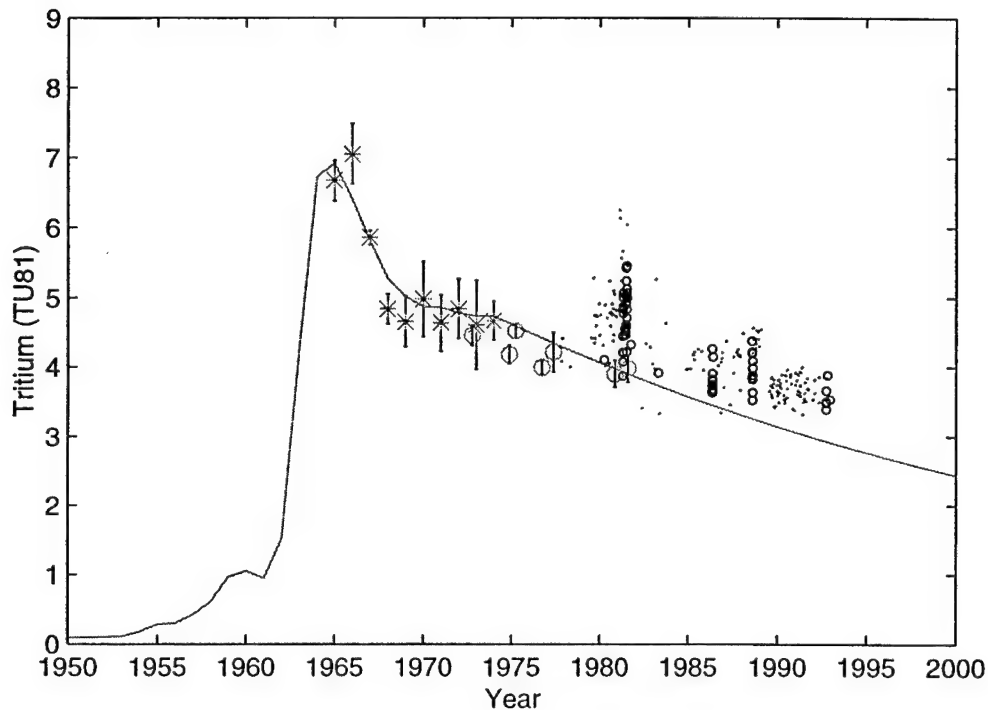


Figure 4.16: Surface tritium concentration from *Doney and Jenkins* [1988] and *Dreisigacker and Roether* [1978] in decay-normalized units (solid line). Data from various sources is also shown for comparison. Asterisks with errorbars are taken from mean values reported in *Dreisigacker and Roether* [1978] for region III (  $40^{\circ}$ –  $60^{\circ}$ N, east of  $35^{\circ}$ W). Errorbars represent 95% confidence interval calculated from number of data points reported assuming a standard error of 1 TU. Open circles with error bars are average values reported in [*Doney and Jenkins*, 1988] with 95% confidence interval calculated from their reported standard error. Small open circles are surface tritium values extracted from the data archives of the WHOI HIL for the region  $30^{\circ}$ –  $60^{\circ}$ N, east of  $55^{\circ}$ W. Small dots are computed from the data set used in this thesis (figure 2.1). Surface concentrations are calculated from tritium- $^3\text{He}$  age measurements less than 2 yr and between  $\sigma_{\theta} = 26.5$  and  $27.1$ . The observed net tritium and  $^3\text{He}$  are combined with the tracer age to estimate the surface tritium concentration at the time of subduction.



are no direct tritium measurements prior to the peak input in 1964. The earlier portion of the time-history is reconstructed from estimates of  $^{90}\text{Sr}$ , another byproduct of atmospheric nuclear bomb tests. The data show some scatter in the period after the peak input but the general level of decay-normalized tritium appears well determined. The estimate of the surface concentration of *Doney and Jenkins* [1988] appears systematically low after 1981, the last year of data used in their reconstruction. The estimate of surface tritium concentration by *Doney and Jenkins* [1988] is for the entire subtropical gyre while the data displayed for the period 1980-1994 is limited to only the densest isopycnal surfaces ( $26.5 \leq \sigma_\theta \leq 27.1$ ). The magnitude of the peak  $^3\text{H}$  values in 1964 is only determined by a few data points [*Dreisigacker and Roether*, 1978] and should be regarded with caution.

In addition to the temporal trend in surface tritium values, spatial variations are also well documented [*Doney and Jenkins*, 1988]. The input of tritium to the oceans was mostly confined to mid- and high-latitudes of the northern hemisphere; concentrations in southern hemisphere waters are comparatively low. The northward cross-equatorial transport of southern-hemisphere waters, and especially the northward surface Ekman transport, establishes a meridional gradient in the tritium concentrations in the surface mixed layer. The meridional gradient in surface tritium concentration partly explains the discrepancy in the surface tritium estimate of [*Doney and Jenkins*, 1988] and the data reported in figure 4.16. Rather than include a complete analysis and discussion of the precise spatial and temporal accuracy of the surface boundary condition shown in figure 4.16, I will instead illustrate the sensitivity of the diagnostics developed in this chapter to reasonable changes in the history of the surface tritium boundary condition.

## 4.5.2 An Idealized Boundary Condition

The temporal evolution of the tritium- $^3\text{He}$  age field depends on the relative changes in the surface tritium concentrations, in other words the shape of the input function. If the entire input function were scaled by a constant factor, the temporal development of tritium- $^3\text{He}$  age would remain the same since tracer age is a function only of the ratio of  $^3\text{He}$  and tritium. In contrast, measurements of the tritium inventory would scale directly with changes in the surface boundary condition. Therefore, sensitivity of the temporal tendency of tritium- $^3\text{He}$  age depends on the relative uncertainties in the shape of the surface tritium concentration in figure 4.16.

An idealized form of the surface tritium concentration is constructed in order to test the sensitivity of the diagnostics of the temporal tendency of the age field to the uncertainty in the shape of the surface tritium history. Figure 4.17 shows an approximation of the the decay-normalized surface tritium concentration constructed from linear line segments. This idealized boundary condition captures the large-scale shape of the estimated surface tritium concentrations. The break-points of the line segments forming the idealized boundary condition are listed in table 4.3. Using this idealization of the tritium boundary condition, one can alter the relative shape of the tritium boundary condition by independently varying the tritium concentration of each of the line segments. An uncertainty is assigned to each of the line segment break-points in the idealized boundary conditions. The magnitude of the uncertainty at break points 4 and 5 is chosen to yield the 18% uncertainty of the cumulative tritium inventory in 1981 as reported in *Doney, Jenkins and Östlund* [1993]. The tritium values at the other break points have less impact on the cumulative tritium inventory and the associated uncertainties have been chosen based on the assigned values in 1964 and 1970.

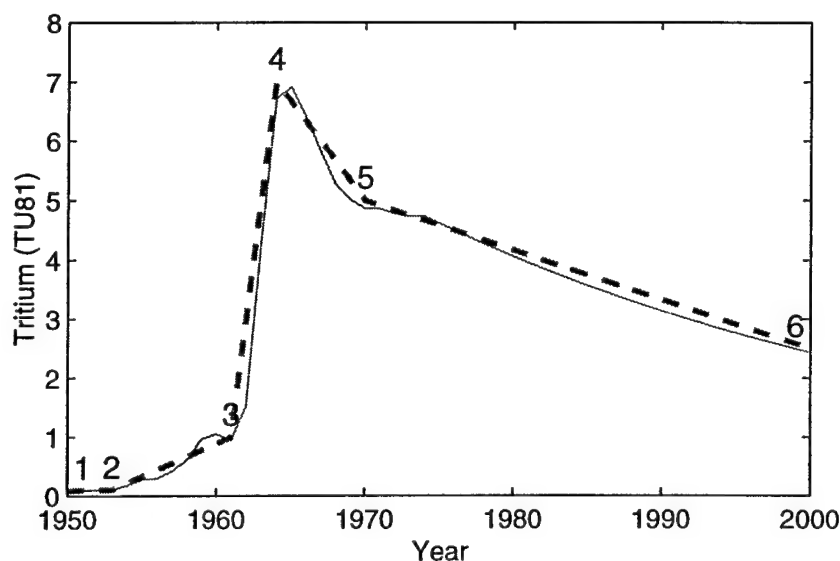


Figure 4.17: Idealized history of the surface tritium concentration. Solid line shows the [Doney and Jenkins, 1988] estimate of surface tritium concentration (in decay-normalized units) for North Atlantic. Dotted line is an approximation of the history composed of linear segments defined by end-points listed in table 4.3. The numbers on the figure correspond to the location of the indexes in table 4.3.

Figure 4.18 illustrates the impact of the assigned uncertainties on the ideal boundary condition. The envelope of the boundary condition uncertainties is shown for changes in tritium concentration at the break points in 1964, 1970 and 2000. Comparison with the direct observations suggests that the assigned uncertainties in the idealized boundary condition are likely an overestimate of the true uncertainty of the estimate of the surface tritium concentration.

#### 4.5.3 Sensitivity of Model Diagnostics to Boundary Condition Uncertainty

Changes in the shape of the idealized tritium boundary condition are used to explore the sensitivity of the diagnostics employed in this chapter to the uncertainty in the true boundary condition. A suite of boundary conditions is formed by systematically altering the tritium concentration of the linear segments composing the idealized

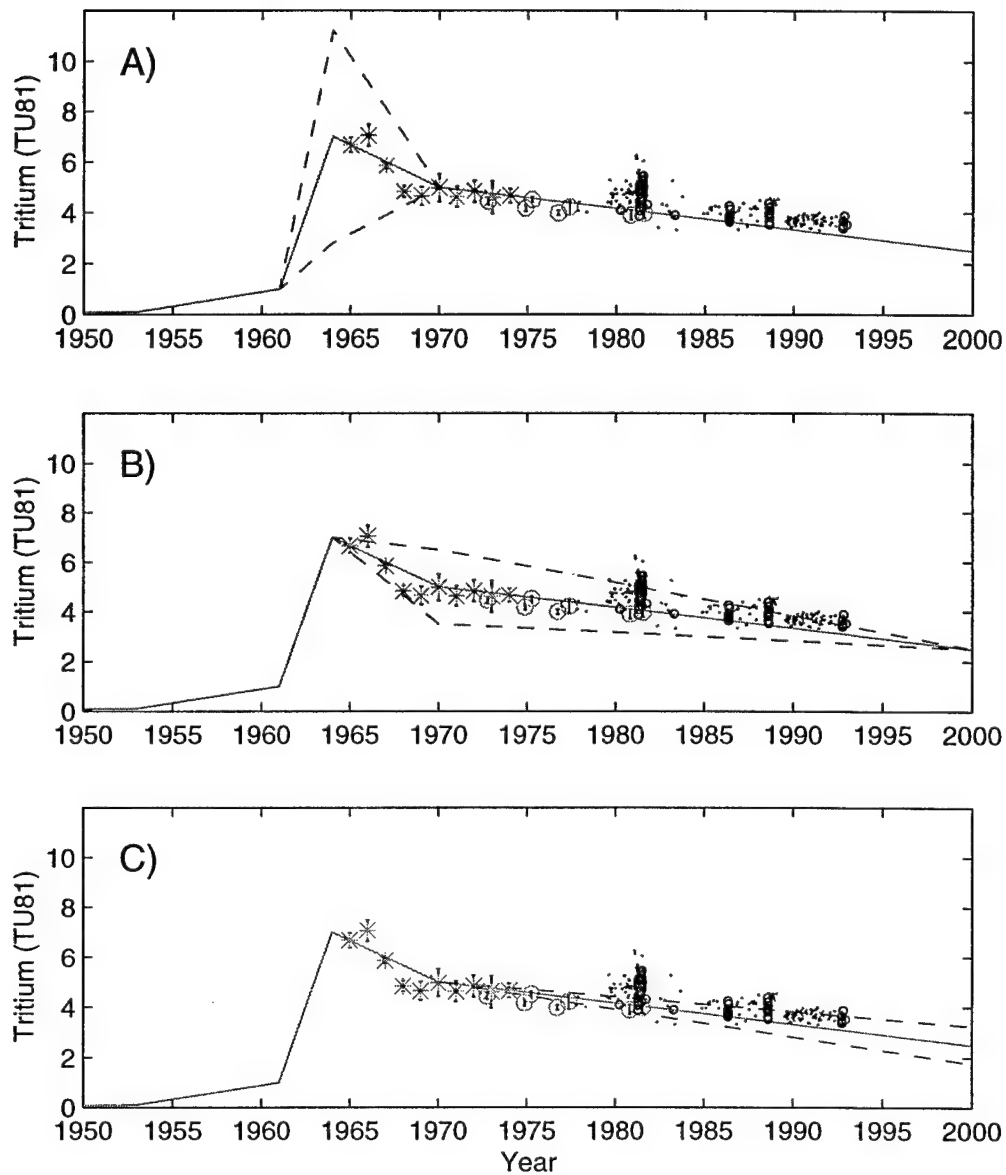


Figure 4.18: Idealized tritium boundary condition (decay normalized) and examples of assigned uncertainty. Solid line is idealized boundary condition and data points are as described in figure 4.16. The shape of the surface tritium boundary condition is altered by varying the magnitude of the tritium concentration at A) 1964 ( $\pm 60\%$ ), B) 1970 ( $\pm 30\%$ ) and C) 2000 ( $\pm 30\%$ ).

Break Point	Year	Tritium (Tu81)	uncertainty	$\Delta$ cumulative inventory in 1981
1	1950	0.089	60%	0.1%
2	1953	0.105	60%	0.3%
3	1961	1	60%	3.1%
4	1964	7	60%	18.0%
5	1970	5	30%	17.6%
6	2000	2.5	30%	1.6%

Table 4.3: Idealized history of surface tritium concentration composed of linear segments. The break-points of the segments and the associated year are shown in the first two columns. The third column lists the tritium concentration in decay-normalized units. The uncertainty of the tritium concentration at each break-point is listed in column four. The final column tabulates the impact of the uncertainty on the cumulative tritium inventory in 1981.

boundary condition. The magnitude of the decay-normalized tritium concentration at each of the break-points in table 4.3 is varied by the listed uncertainty. Numerical simulations of the tracer evolution are performed for the differing boundary conditions and the resulting fields diagnosed for variations in tracer age tendency and tritium concentrations.

### Temporal Tendency of Tracer Age

The analysis of this chapter has illustrated the large amplitude of the temporal response of the tracer age system to the sudden addition of bomb-produced tritium to the ocean in the early 1960's. This section explores the sensitivity of the diagnosed temporal change to alterations in the time-history of the tritium input. Figure 4.19 illustrates the changes in the temporal tendency of tracer age as a function of three effects:

- Alteration of the idealized tritium boundary condition by varying the tritium concentration at the listed break-points

- Changes in radiotracer Péclet number
- Changes in the value of tracer age where the temporal tendency is evaluated. The differing age values are taken from the observed tracer age on increasingly denser isopycnals so this serves as a proxy for variations across the density surfaces of the main thermocline.

Each panel in figure 4.19 shows a different tracer age and isopycnal surface. In terms of the relation between age tendency and tracer age previously studied in figure 4.8, each panel in figure 4.19 represents a vertical slice through the graph in figure 4.8 at a constant tracer age value. Within each panel the temporal tendency is calculated for variations in the boundary condition at each of the break-points of the idealized boundary condition. The calculation is repeated for three differing Péclet numbers represented by differing plot symbols. Error bars illustrate the variation of the calculation of age tendency to the listed uncertainty in the tracer boundary condition. Also shown for scale is the uncertainty of the tracer age tendency determined from the observations. As previously seen in figure 4.8, the magnitude of the age tendency increases with both Péclet number and tracer age.

The results in figure 4.19 illustrate several key points. First, the maximum uncertainty in the tracer age tendency due to uncertainties in the tritium boundary condition are comparable in magnitude to the accuracy of the age tendency determined from the observational data set. Second, the differences in age tendency due to variations in Péclet number are larger than magnitude of the uncertainty due to the poorly known boundary condition. Third, the relative uncertainty of the boundary condition prior to the peak input has a comparatively small effect on the diagnosis of tracer age tendency.

Although variations in the shape of the surface tritium history lead to some change in the magnitude of the temporal tendency of the age field, the general observa-

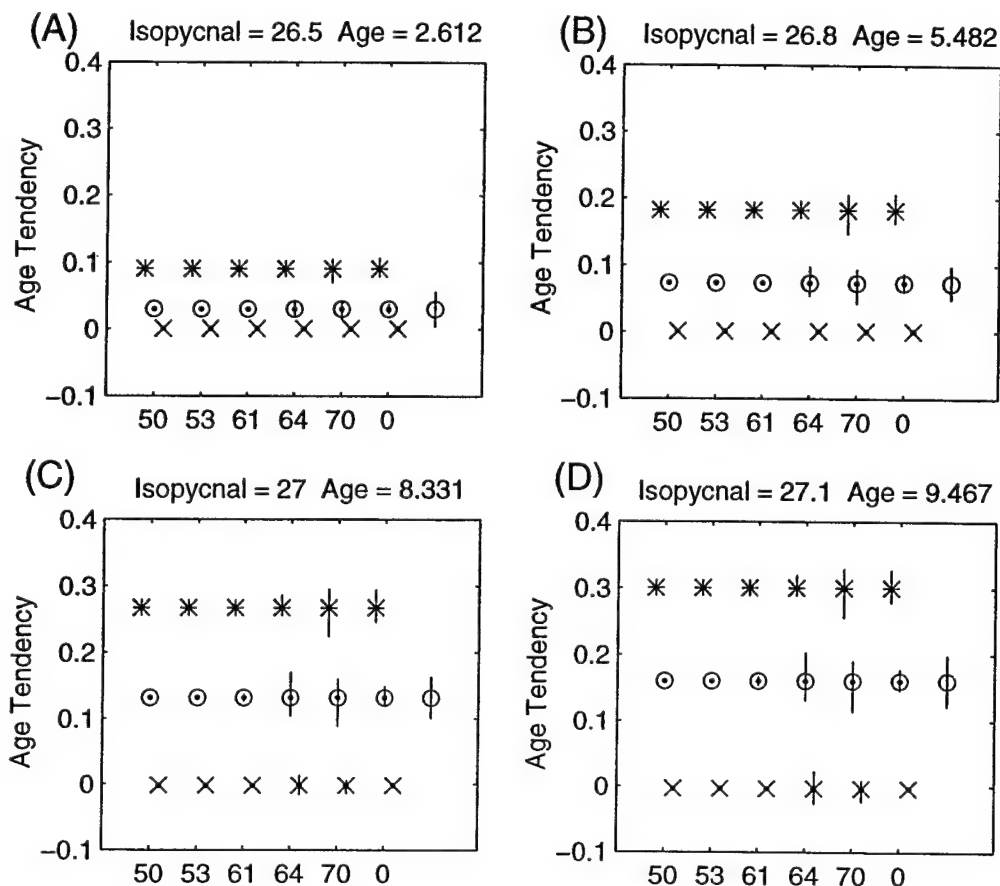


Figure 4.19: Sensitivity of temporal tendency of tracer age in 1986 to uncertainty in surface tritium history. The variation of tracer age is chosen to represent the mean observed age in the isopycnal surfaces  $\sigma_\theta =$  A) 26.5, B) 26.8, C) 27.0 and D) 27.1. Each panel shows the sensitivity of the temporal trend in age to variations in the ideal boundary condition at each break point in table 4.3. At some points, particularly early in the history, there is negligible variation in the age tendency in 1986 to the changes in the idealized boundary condition and thus the errorbars are essentially zero length. Temporal tendency for differing radiotracer Péclet numbers is indicated by differing plotting symbols: \*:56, o:7.1, x:1.3. The abscissa indicates the year of the break in the idealized boundary condition listed in table 4.3. For comparison, the uncertainty in the observation on each isopycnal is shown as the open circle and error bar at the right end of each panel.

tion of the temporal trends in the tracer age field are robust to the large uncertainty in the details of the tritium history. The changes in the age field are largely the response of the  $^3\text{He}$ -tritium system to the sudden step-like, addition of the bomb-tritium. Specifics of the finer structure of the tritium input appear to be secondary in the creation of the temporal response of the tritium- $^3\text{He}$  age field.

### **Tritium Concentration**

The minimal effect of the uncertainty of the boundary condition on tracer age tendency can be compared with the significant impact of the boundary condition uncertainty on observed tritium concentrations. Previous studies [*Wunsch*, 1988a; *Mèmerly and Wunsch*, 1990] have discounted the utility of transient tracer observations based on the large sensitivity of quantitative analysis to the details of the poorly known history of the boundary conditions.

Figure 4.20 illustrates the sensitivity of the tritium concentration to the uncertainties of the idealized boundary condition. As in figure 4.19, the tritium concentration is calculated as a function of the variation of the tritium boundary condition, tracer age, and Péclet number. In contrast to the age tendency, the magnitude of the tritium concentration shows large sensitivity to the detailed specification of the surface tritium history. The maximum variation of the diagnosed  $^3\text{H}$  concentration to the uncertainties in the idealized boundary condition are larger than the variations due to Péclet number. Therefore, in agreement with previous studies, the estimate of the tritium inventory for differing Péclet numbers is not clearly resolved within the uncertainty of the specification of the boundary condition.



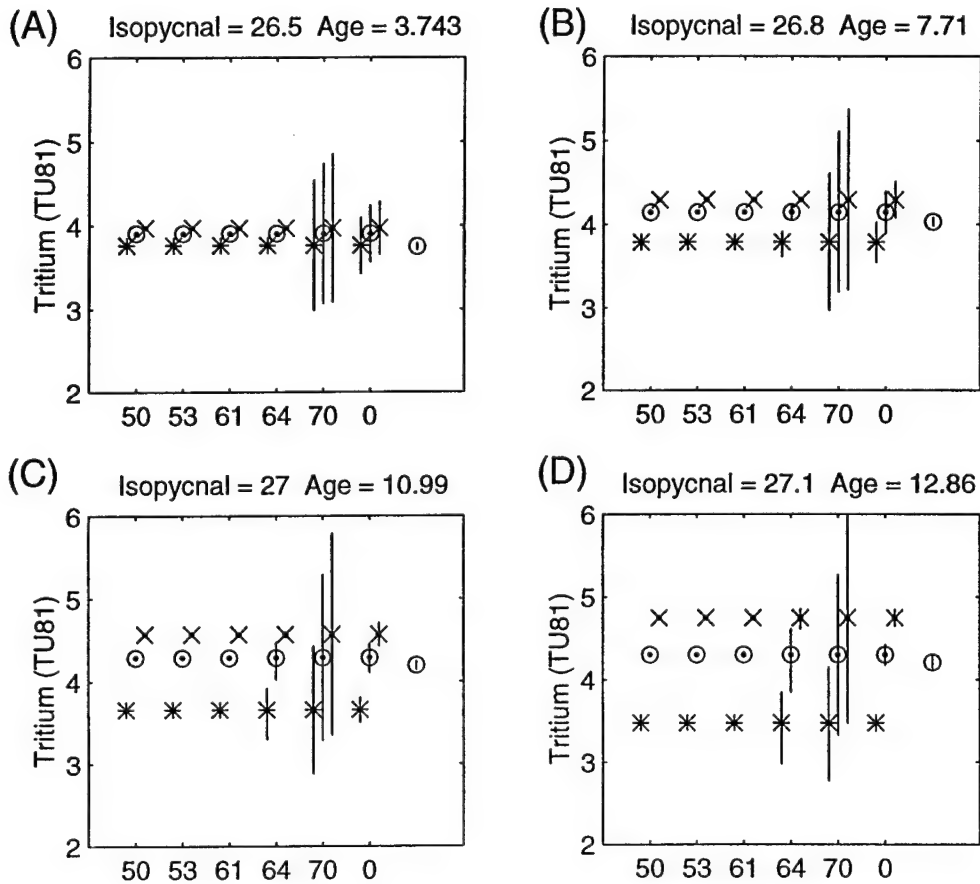


Figure 4.20: Sensitivity of tritium concentration in 1986 to uncertainty in surface tritium history. The variation of tracer age is chosen to represent the mean observed age in the isopycnal surfaces  $\sigma_\theta =$  A) 26.5, B) 26.8, C) 27.0 and D) 27.1. Each panel shows the sensitivity of the tritium concentration to variations in the ideal boundary condition at each break point in table 4.3. At some points, particularly early in the history, there is negligible variation in the tritium concentration in 1986 to the changes in the idealized boundary condition and thus the errorbars are essentially zero length. The  $^3\text{H}$  concentration for differing radiotracer Péclet numbers is indicated by differing plotting symbols: \*:56, o:7.1, x:1.3. The abscissa indicates the year of the break in the idealized boundary condition listed in table 4.3. For comparison, the uncertainty in the observation on each isopycnal is shown as the open circle and error bar at the right end of each panel.

## Summary of Boundary Condition Sensitivity

The results of this section show that the key diagnostic of this thesis, the temporal tendency of the age field, is not strongly sensitive to uncertainties in the history of the surface tritium concentration. The temporal evolution of the tracer age is largely responding to the large input of tritium to the surface ocean in the early 1960's. Details of the early, poorly measured portions of the surface history are of only secondary importance in the evolution of the tritium- $^3\text{He}$  age fields within the thermocline. In contrast, measures of tritium concentration, or inventory, scale directly with the uncertainties in the tritium boundary condition. Consistent with previous studies, the results of the sensitivity study in this section illustrate the difficulties associated with quantitative analysis of the observed tritium fields given the imperfect knowledge of the surface boundary concentrations.

## 4.6 Summary

This chapter has used simple one-dimensional models to examine the character of the temporal response of the  $^3\text{H}$ - $^3\text{He}$  tracer system to the large bomb-tritium depositions in the decade centered around 1965. Even in the absence of changes in the physical circulation, oceanic mixing can lead to changes in the large scale structure of the tracer age field by acting as a temporary sink of age. The degree to which the age field is distorted scales with the inverse of the radiotracer Péclet number. Unfortunately, the historical database of tritium and  $^3\text{He}$  measurements does not extend far enough back in time to document the predicted decrease of tracer age values in the 1960's. The observational record from 1979 to 1993 does, however, record the subsequent increase of the tracer age as the system relaxes back towards a steady-state balance. Under the assumption that the large scale flow field is not changing, the observed rate of increase

of tritium- $^3\text{He}$  age values in the thermocline is an indirect measure of the magnitude of the prior distortion in the tracer age field.

Comparison of the observed tracer age tendencies with numerical model predictions leads to estimates of the radiotracer Péclet number for isopycnal surfaces spanning the thermocline. The radiotracer Péclet number can be converted to a ventilation Péclet number using the observed ventilation time scale for each surface. Scale analysis reveals that the ventilation Péclet number quantifies the relative importance of advection and diffusion on length scales of order 1000 km. Ventilation Péclet numbers are highest near the surface where advective effects of ventilation are strongest. In the lower thermocline, the estimate of the Péclet number diminishes indicating the increasing importance of diffusive ventilation for the renewal of properties at these depths. Combining the diagnosed Péclet numbers with the measured meridional velocity (estimates based on either geostrophy or tracer age gradients give comparable results) yields estimates of the lateral diffusivity parameter,  $\kappa_H$ .

The sensitivity of the present analysis to the uncertainty of the tritium surface concentration history has been examined. The diagnosis of the Péclet number of the flow based on the observed temporal tendency of the tritium- $^3\text{He}$  age field is robust to the uncertainties in the  $^3\text{H}$  boundary condition. The evolution of the age field responds chiefly to the net addition of bomb-produced tritium to the surface ocean; details of the exact history of the surface tritium concentrations have only a secondary impact. In contrast to the findings for the evolution of tracer age, calculations of the tritium inventory (both those presented here as well as previous studies) show much greater sensitivity to the precise specification of the history of the tritium boundary condition.

The lateral diffusivity for the upper thermocline estimated from the analysis of the temporal evolution of tritium- $^3\text{He}$  age (figure 4.9) is roughly consistent with other estimates for this region (table 4.4). The apparent increase in strength of lateral mixing with depth, however, is unexpected and not in agreement with the overall

depth-dependent trend of the estimates in table 4.4. The results here also differ from those found by *Böning and Cox* [1988] who estimated diffusivity from the dispersion of simulated Lagrangian floats in an eddy-resolving numerical model of the subtropical thermocline and found a general decrease in the magnitude of  $\kappa_H$  with depth.

It is possible that the large estimates of  $\kappa_H$  in the lower thermocline reflect the spatial variability of this quantity, specifically the increased values of lateral mixing strength to the north. Since the estimates of  $\kappa_H$  follow from the interpretation of the observations in the context of the one-dimensional numerical model, the values represent a (likely weighted) average of diffusivity between the latitude of the winter outcrop and the center point of the observations (26°N, 30°W; figure 2.1). Additional experiments were conducted with the one-dimensional numerical model to test the effects of spatially varying lateral diffusivities. The results suggest that the strength of mixing in the region closest to the outcrop has the most influence for setting the temporal evolution of tracer age in the model. *Stammer and Böning* [1996] show values of eddy kinetic energy increasing by a factor of 2-4 between 25°N and 40°N along 30°W (figure 1.12). The deeper isopycnals in figure 4.9 outcrop progressively further north so the apparent increase of lateral diffusivity with depth is consistent with the interpretation that this quantity represents a spatial average biased towards the local strength of lateral diffusivity at the latitude of the winter outcrop.

Alternatively, the diagnosed increase of lateral mixing strength with depth could signal a failure of the one-dimensional interpretation to account for all the physical factors influencing the evolution of the tritium-<sup>3</sup>He age fields in the thermocline. The one-dimensional model assumes that all the water within the thermocline originates directly from the surface mixed layer. This postulate is consistent with the assumptions applied to the ventilated regions of the dynamical models of *Luyten, Pedlosky and Stommel* [1983] which set the interior potential vorticity field by the advection of the values imposed at the surface outcrop. In contrast to the models of

a directly ventilated thermocline, *Rhines and Young* [1982a] have constructed models of the wind-driven subtropical circulation where the majority of interior streamlines emanate from the western boundary region rather than the surface mixed layer. Water encompassed within these streamlines is not directly ventilated at the surface and tracer properties can only penetrate into the enclosed region via diffusive processes. The failure of the one-dimensional models to incorporate the effects of recirculated, unventilated waters could lead to erroneous conclusions regarding the strength of lateral mixing. This possibility will be further explored in the following chapter by examining the evolution of tracer age in simple two-dimensional model of thermocline ventilation.

Source	Region	Depth	$\kappa_H$ ( $m^2s^{-1}$ )
A) Advective-Diffusive Models			
<i>Olbers, Wenzel and Willibrand</i> [1985]	-	0-800 m	100-1000
<i>Thiele et al.</i> [1986]	> 29°N	$\sigma_\theta = 26.5-26.8$	1700-4900
	< 29°N	$\sigma_\theta = 26.5-26.8$	1000-2900
<i>Hogg</i> [1987]	22-45°N	700-1300 m	100-1000
<i>Bauer and Siedler</i> [1988]	15-30°N	$\sigma_\theta = 26.4-26.8$	600-1600
<i>Jenkins</i> [1997]	18-33°N	$\sigma_\theta = 26.4-27.1$	500-1200
<i>Joyce et al.</i> [1997]	19-34°N	$\sigma_\theta = 26.5$	800-1400
B) Mixing Length Models			
<i>Armi and Stommel</i> [1983]	22-31°N	600-1000 dbar	500
<i>Jenkins</i> [1987]	22-31°N	$\sigma_\theta = 26.2-27.15$	500
C) Float Dispersion			
<i>Krauss and Böning</i> [1987]	30-33°N	surface	2100
	39-43°N	surface	3300
<i>Spall, Richardson and Price</i> [1993]	28-38°N	1100 m	840
	20-28°N	1100 m	350
<i>Ollitrault</i> [1995]	30-45°N	700 m	1000-2000
<i>Sundermeyer and Price</i> [1997]	19-30°N	$\sigma_\theta \approx 26.5$	300-1100

Table 4.4: Previous estimates of lateral diffusivity in the eastern North Atlantic. If the original source calculated anisotropic diffusivities, only the meridional component is reported here. The estimates are divided into three groups depending on the methodology of the estimate: A) advective-diffusive model of tracer observations, B) mixing-length arguments based on characteristic eddy length and velocity scales, and C) observed dispersion of Lagrangian floats. For comparison, the results of the estimates derived here using the one-dimensional ventilation model are shown in figure 4.9 on page 141

## Chapter 5

# Tritium- $^3\text{He}$ Age Evolution in a Two-Dimensional Model of Thermocline Ventilation

### 5.1 Motivation for Extending Model to Two Dimensions

In the previous chapter I developed an interpretation of the observed temporal changes in the tritium- $^3\text{He}$  age field based on one-dimensional models of oceanic ventilation. The simplified model domain reflects the assumption that water properties in the thermocline derive directly from the isopycnal outcrops into the surface mixed layer. As such, the domain of the one-dimensional model is taken to be oriented along the axis of a mean streamline of the flow which originates at the surface; the influence of neighboring streamlines is neglected. The use of the one-dimensional models of tracer evolution are consistent with the analytic models of *Luyten, Pedlosky and Stommel*

[1983] that are founded on the assumption that direct ventilation sets the interior property fields by transporting surface boundary conditions along the axis of the flow.

Numerous observational studies of the eastern North Atlantic have interpreted the ventilation of the lower thermocline originating as southward flow out of the surface mixed layer. *McCartney* [1982] presents a picture of the mode water recirculation in the North Atlantic where isopycnal surfaces as deep as  $\sigma_\theta = 27.2$  are ventilated by southward advection derived from the surface winter mixed layer (figure 5.1). The

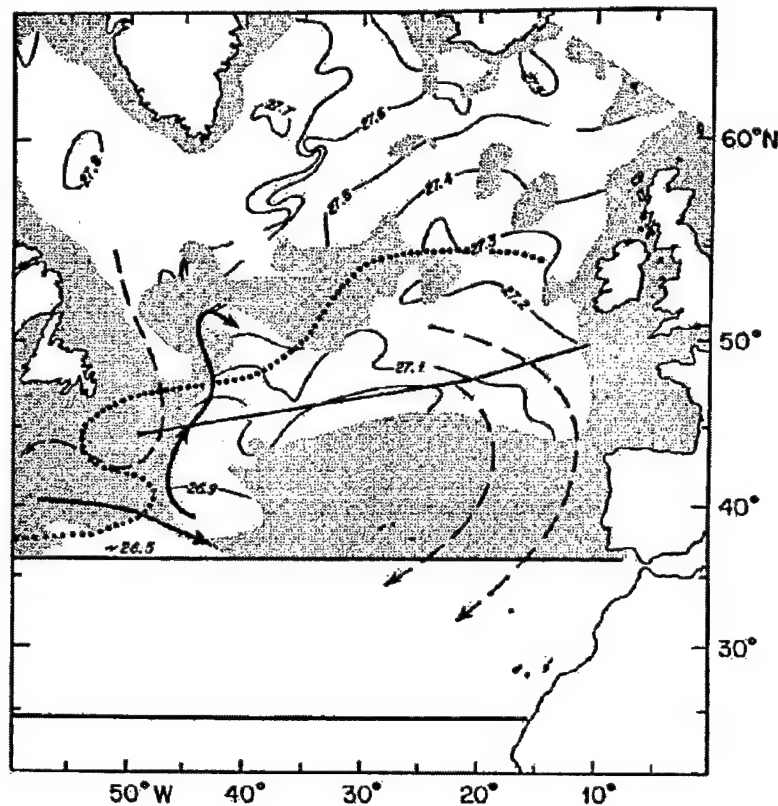


Figure 5.1: Diagram of the potential density of late winter deep convective mixed layers north of 35°N reproduced from *McCartney* [1982]. Shaded regions indicate winter mixed layers with depths less than 200 m. Dashed lines in eastern Atlantic indicate path of direct advective ventilation of subtropical mode waters between  $\sigma_\theta = 27.0$  and 27.2.

depth-integrated transport analysis of *Saunders* [1982] also deduced southward flow above 850m in the eastern Atlantic between 32° and 41.5°N. *Pollard and Pu* [1985],



using historical hydrography to describe the circulation and water mass structure northeast of the Azores, interpret direct advective ventilation of the thermocline at least as deep as  $\sigma_\theta = 27.1$ .

The essential role of the northeast Atlantic in the ventilation of the lower thermocline is also apparent in the signature of passive tracer fields. Prior analyses have tended to interpret the penetration of passive tracers along isopycnals as a manifestation of advective ventilation. Analysis of the observed tritium distribution soon after the peak bomb inputs [Sarmiento, Rooth and Roether, 1982] concluded that the region northeast of the Azores was the primary location for the introduction of tritium into the subtropical thermocline in the density range  $\sigma_\theta = 26.8$  to  $27.1$ .<sup>a</sup> Andri , Jean-Baptiste and Merlivat [1988] estimate a meridional advective ventilation rate of order 1 cm/s on  $\sigma_\theta = 27.1$ . Their calculation is based on the observed tritium gradient at this level and neglects all diffusive effects. The same conclusion is evident in the steady-state oxygen distribution. The structure of apparent oxygen utilization on isopycnal surfaces has its lowest values in the northeast Atlantic and suggests southwestward spreading of recently ventilated waters (figure 5.2). Indeed, Pollard and Pu [1985] use the observed isopycnal oxygen gradients on  $\sigma_\theta = 27.1$ , combined with independent estimates of the rate of oxygen consumption, to estimate the magnitude of the advective flow ventilating the lower thermocline.

Spall [1990] examined the regional circulation of the Canary Basin as simulated in an eddy-resolving primitive equation model of the North Atlantic. Southward transport of the Portugal Current was found to be  $8 \times 10^6 \text{ m}^3 \text{ s}^{-1}$  with some evidence of interannual variability apparent in the mean computed from a two year average. The model streamfunction fields also contain a representation of the Azores Current with

---

<sup>a</sup>Sarmiento, Rooth and Roether [1982] also suggest the possibility of small amounts of tritium entry into the subtropical gyre by lateral diffusion across the Gulf Stream in the northwest region of the gyre.

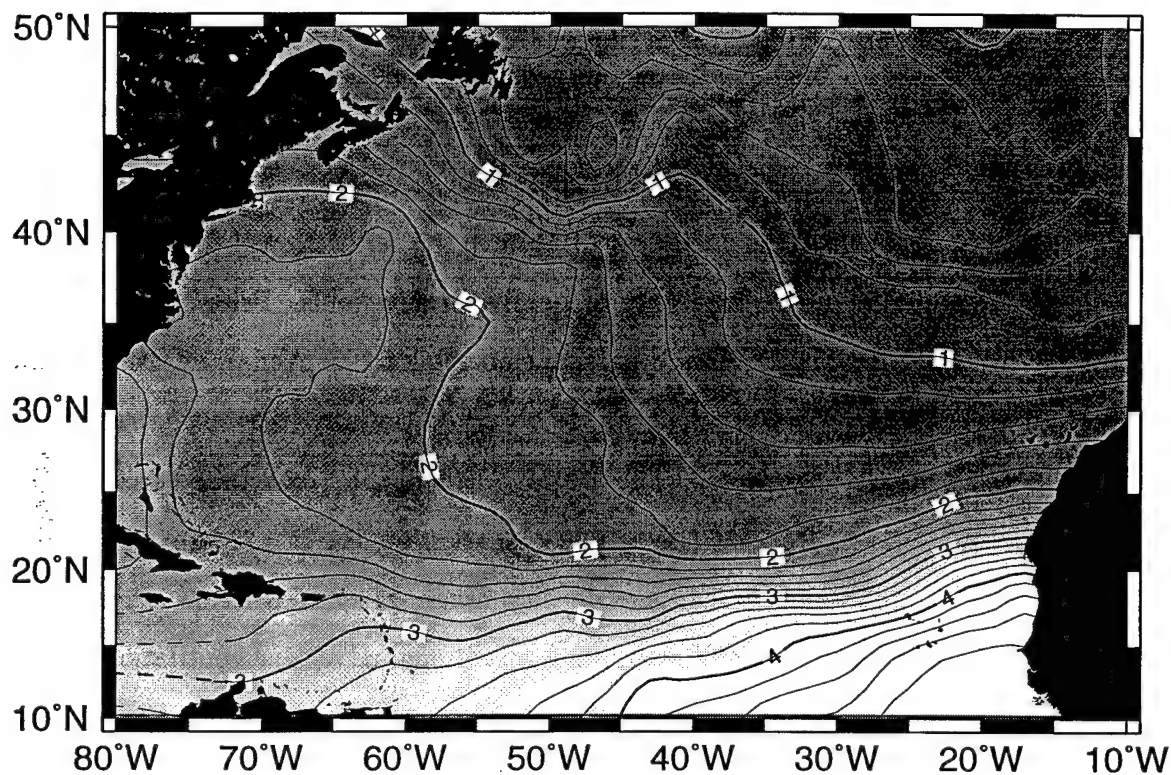


Figure 5.2: Distribution of Apparent Oxygen Utilization on  $\sigma_\theta = 27.0$ . Grided field is produced from data in the supplemented hydrographic atlas of *Lozier, Owens and Curry* [1995] (Appendix A) mapped onto isopycnal surfaces using the Hydrobase software package [Curry, 1996].

a tight recirculation south of the eastward flowing jet. Simulation of tracer age in the model shows significant ventilation due to both the Portugal and Azores Currents.

The mean meridional circulation in the eastern North Atlantic is relatively weak and the observational basis for the direct advective ventilation of the lower thermocline is open to question. Recently, *Pollard et al.* [1996] presented a re-analysis of the ventilation and circulation of the eastern north Atlantic based on extensive Sea-Soar surveys. Utilizing arguments based primarily on  $\theta/S$  relations, they conclude that there is no evidence for any direct ventilation of central water southward across  $40^\circ\text{N}$  in the region east of  $20^\circ\text{W}$ . Similar conclusions can be drawn from geostrophic streamfunctions estimated on the large-scale density structure. Figure 5.3 shows the

pressure-anomaly streamfunction [Zhang and Hogg, 1992; Montgomery, 1937] along the isopycnal  $\sigma_\theta = 27.0$ . There is no evidence in the structure of the mean circulation

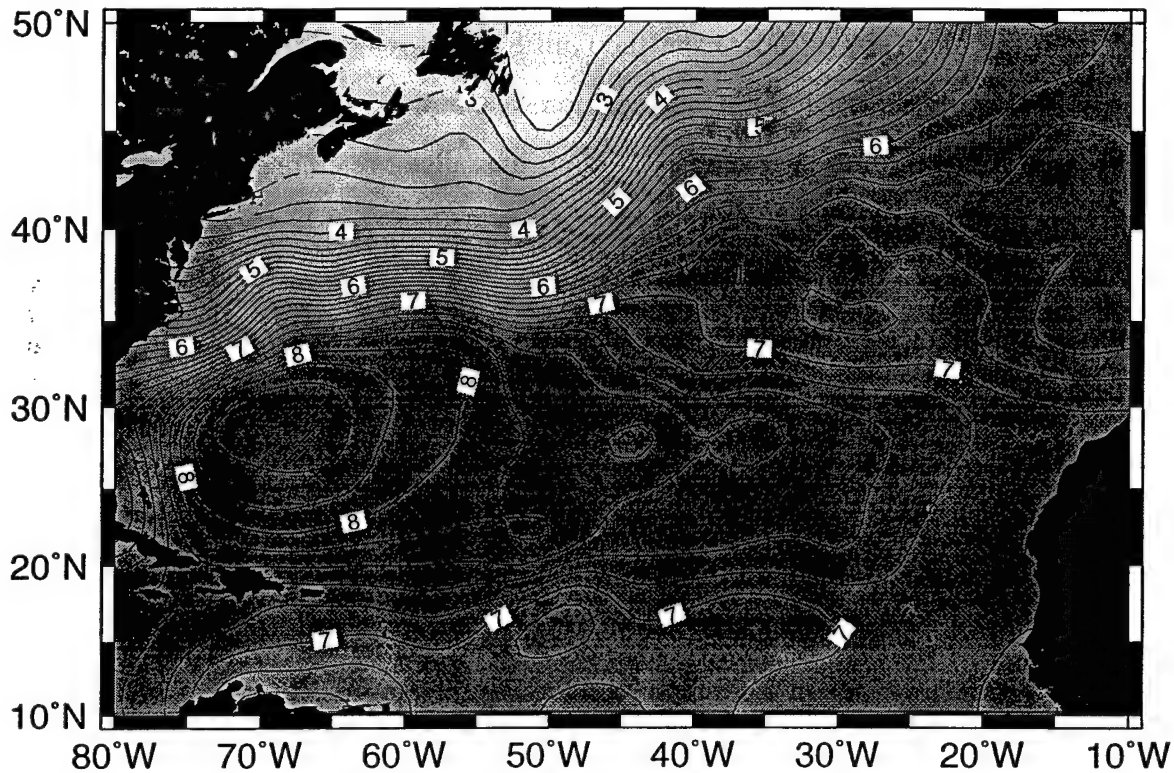


Figure 5.3: Pressure anomaly Montgomery streamfunction on  $\sigma_\theta = 27.0$  referenced to the isopycnal  $\sigma_1 = 32.3$  ( $\approx 1350$  dbar). The streamfunction is computed using the methods outlined in Zhang and Hogg [1992]. Grided fields of specific volume anomaly and pressure are produced from data in the supplemented hydrographic atlas of Lozier, Owens and Curry [1995] (Appendix A) mapped onto isopycnal surfaces using the Hydrobase software package [Curry, 1996].

for streamlines originating in the winter mixed layers north of  $40^\circ\text{N}$ , flowing southward and connecting into the anti-cyclonic subtropical circulation. On the contrary, the streamlines flushing the eastern subtropical gyre originate from the Gulf Stream extension and flow eastward via the Azores Current. Analysis of the origin of the fluid in Azores Current [Klein and Siedler, 1989] further confirm the geographic separation between the circulation of the anti-cyclonic gyre and the isopycnal outcrop locations poleward of  $40^\circ\text{N}$  (see figure 1.9).

The computation of Montgomery streamfunction (figure 5.3) is based on a thermal wind approximation which necessarily assumes a level of no motion along the reference isopycnal (in this case,  $\sigma_1 = 32.3$ ). The conclusion that the eastern Atlantic is fed, in the mean, by outflow from the Gulf Stream extension via the Azores Current is not overly sensitive to this assumption. A simple calculation shows that direct ventilation from the surface would require an unrealistic reference velocity. Suppose the streamlines in figure 5.3 are taken to represent flow on a layer with thickness of 100 m. In this case, the volume transport of flow per unit streamfunction is  $1.25 \text{ Sv}^b$ . In order for direct ventilation of the  $\sigma_\theta = 27.0$  surface to exist, a barotropic reference velocity in the region east of the Azores would need to flux approximately one additional Sv of water southward. This only requires a small change in the actual velocity scale but since the change is barotropic, one additional Sv of flow in a 100 m thick layer requires an additional 40 Sv of flow in the entire water column ( $1 \text{ Sv} \times \frac{4000 \text{ m}}{100 \text{ m}}$ ). There is no evidence for such a strong net flow in the region between the Azores and Portugal. Thus a change in the reference velocity sufficient to set up a mean flow from the surface outcrop north of the Azores Current to the lower layers of the ventilated thermocline is deemed unrealistic.

The apparent dominance of recirculated flow, as opposed to renewed direct ventilation, in the lower thermocline negates the assumptions of a one-dimensional, isopycnally-oriented concept of subduction. The possibility of confluence of recently ventilated water with flow originating from the western boundary requires a model of greater complexity. This chapter will examine the temporal evolution of tritium- $^3\text{He}$  age in such a two-dimensional model. As before, this model is oriented along an isopycnal surface, but now the domain is taken to incorporate the closed-gyre circulation of water in the subtropics.

---

<sup>b</sup>1 Sv =  $1 \times 10^6 \text{ m}^3 \text{ s}^{-1}$

## 5.2 Results of Previous Numerical Studies

The use of simple two-dimensional gyre models of the wind-driven subtropical circulation to study the ventilation of transient tracers is well-established [Musgrave, 1990; Thiele and Sarmiento, 1990; Jia and Richards, 1996; Doney, Jenkins and Bullister, 1997; Jenkins, 1997]. Such models incorporate the essential features of closed-gyre flow on isopycnal surfaces (poleward surface outcrops, intensified western boundary current, cross-streamline mixing) while retaining enough simplicity to be both computationally efficient and conceptually manageable. Other potentially important oceanic processes (e.g. diapycnal diffusion, time-dependent flows, seasonal deepening/shoaling of the surface mixed layer) are ignored.

A schematic of a two-dimensional model circulation and its representation of the full three-dimensional flow of the wind-driven circulation is shown in figure 5.4. The

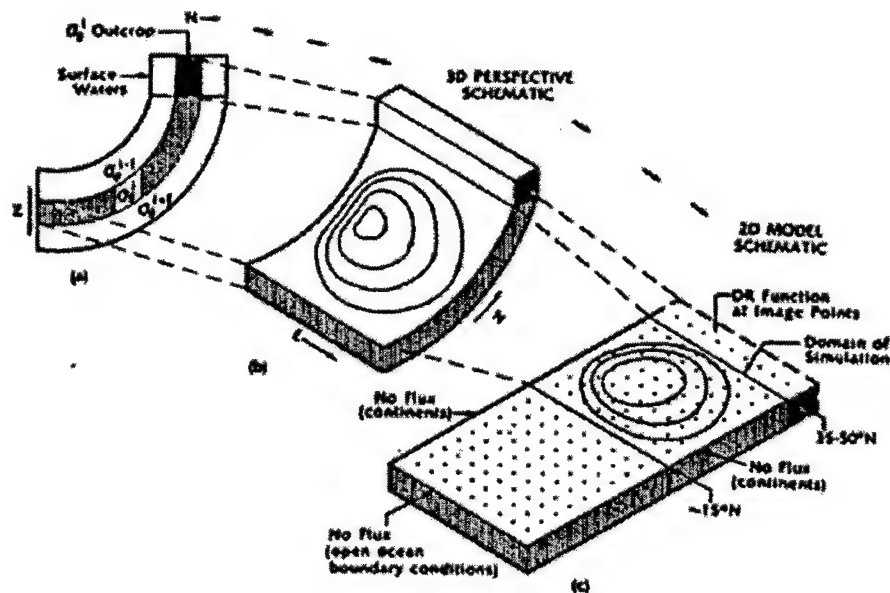


Figure 5.4: Schematic of two-dimensional gyre model reproduced from Musgrave [1990]: a) side view of layered isopycnals in thermocline, b) three-dimensional perspective of flow along isopycnal and c) geometry of two-dimensional numerical model.

flow field of the model is oriented along the topology of an isopycnal surface within the

ocean. A strip along the northern domain of the model represents the region where the isopycnal outcrops into the deep winter mixed layer, exposing water to direct atmospheric contact. The model developed by *Musgrave* [1990] includes a stagnant southern region to simulate the diffusive loss of tracer across the tropical/subtropical boundary. In contrast, *Jenkins* [1997] introduces an additional cyclonic gyre to simulate tropical circulation in the southern portion of the model while *Thiele and Sarmiento* [1990] limit the model region to the domain of the anti-cyclonic gyre.

The above numerical experiments are all similar in design: the advective and diffusive strengths of the flow field are systematically varied while a selected diagnostic of the resulting tracer field is compared with oceanic measurements. *Thiele and Sarmiento* [1990] compared both CFC-based ages and tritium- $^3\text{He}$  age with an ideal age (e.g. a tracer age unaffected by nonlinear mixing terms) at a fixed date (1977) to examine the accuracy of observationally derived ages under a variety of advective-diffusive regimes. *Musgrave* [1990] explored both the spatial structure of the tracer fields at fixed dates (1972 and 1981) as well as the  $^3\text{H}$  -  $^3\text{He}$  property relation. *Doney, Jenkins and Bullister* [1997] employed a two-dimensional model to simulate the property-property relationships of the tritium,  $^3\text{He}$  and CFC systems along a meridional section occupied in 1988. *Jia and Richards* [1996] examined the sensitivity of predicted tritium and age fields in 1972 and 1981 to the gyre model Péclet number. In addition to testing the sensitivity of the results to the magnitude of the Péclet number, some studies have also experimented with altering the relative position of the surface outcrop with respect to the geometry of the gyre [*Thiele and Sarmiento*, 1990; *Musgrave*, 1990].

*Musgrave* [1990] performed the most comprehensive exploration of the dependence of the tracer fields on the relative strengths of advection and diffusion in a gyre model. A key finding of this work was that in many cases, the results of the gyre model are analogous to those obtained employing the simpler one-dimensional model. If the

mixing rate is reasonably large, relative to the advective strength, the entire eastern portion of the gyre subject to the direct ventilation behaves as a “wide-throated” one-dimensional model (see figure 5.5). Lacking any strong horizontal shear in the interior

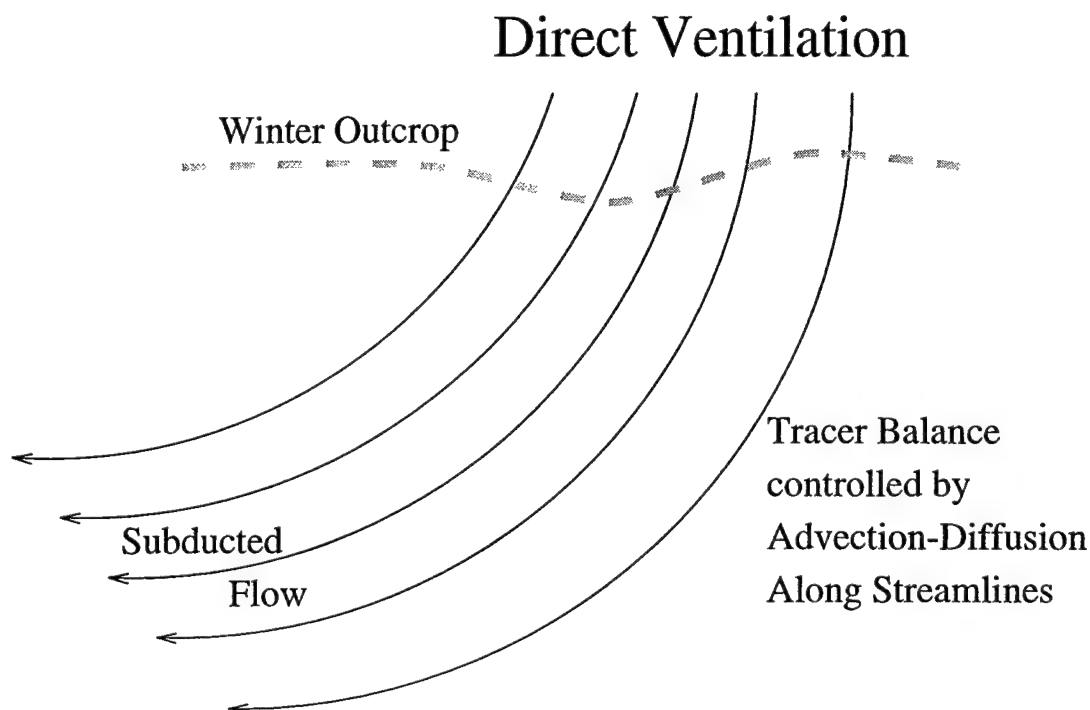


Figure 5.5: Schematic diagram of flow in directly ventilated region. Previous work [Musgrave, 1990] determined that, with moderate lateral diffusion, the structure of tracer fields along the axis of ventilation are analogous to results of the one-dimensional model.

of the gyre, there can be only small differences in the temporal development of neighboring streamlines after they leave the surface mixed layer. Lateral diffusion acts to reduce any cross-stream differences so that the entire directly ventilated region is well approximated by a single one-dimensional model oriented along the axis of the flow. In the case of very weak lateral mixing, Musgrave also found that the one-dimensional model provides a good analog. If lateral diffusion is weak the tracer development along each streamline of the directly ventilated flow is governed predominantly by advection. If a region of the gyre lacking direct ventilation also exists (e.g. a recirculation “pool” [Rhines and Young, 1982b]), tracer can only enter this region by cross-stream

diffusion (figure 5.6). Under very weak diffusion, the evolution of tracer in the “pool”

## Diffusive Ventilation

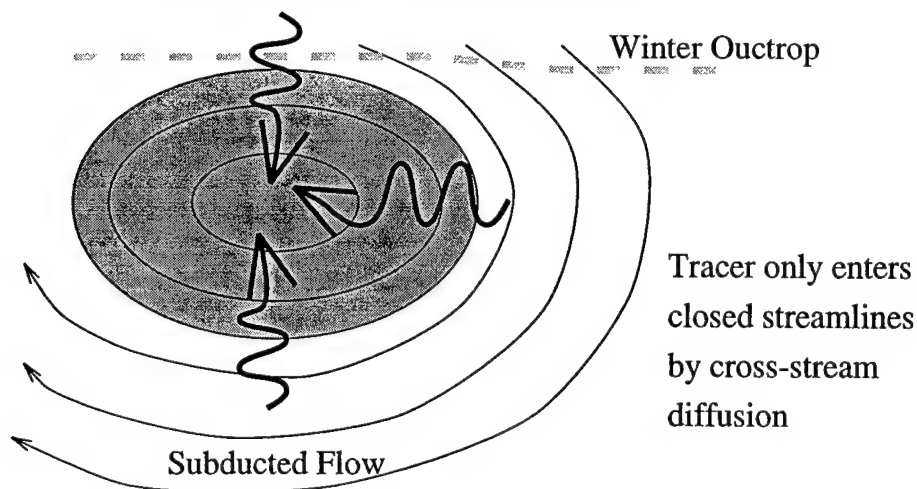


Figure 5.6: Schematic diagram of flow in diffusively ventilated region. Region of closed streamlines can only be ventilated by cross-stream diffusion. In limit of weak diffusion, tracer structure is homogenized along closed streamlines and behavior of closed region is analogous to a purely diffusive one-dimensional model [Musgrave, 1990; Rhines and Young, 1982b]. If diffusive and advective time scales are comparable, tracers penetrate the pool on the same time scale that fluid completes a circuit resulting in more complex structure of tracer fields.

region is well approximated by a purely diffusive one-dimensional model. Since the diffusive time scale is long compared to the time of advection, fluid quickly completes a circuit around the closed streamlines compared to the time-scale of the cross-stream diffusive flux. Therefore there is virtually no along-streamline structure of the tracer fields within the unventilated pool.

A scenario of particular interest here arises when the time-scales of diffusion and advection are comparable. Tracer can still only enter a region of closed streamlines by cross-stream diffusion, but now significant tracer gradients can also develop along streamlines since the time of diffusive ventilation is comparable to the time required to advect a parcel around a complete circuit of the pool. Such a scenario is plausible for the circulation implied by the Montgomery streamfunctions in figure 5.3. It appears from dynamic calculations based on the mean hydrography (also see §1.3.4) that the



lower ventilated thermocline ( $\Theta \approx 10^\circ\text{C}$ ) has little or no direct advective ventilation. Instead, water properties set at the ocean surface likely enter the ocean via lateral diffusion across a band of weak, unorganized flow north of the Azores Current ( $\approx 35^\circ\text{N}$ ). Once tracers penetrate southward to the latitude of the Azores Current, they can be picked up and carried by the anticyclonic advective circulation of the subtropical gyre. Comparison of figure 5.3 and 5.2 reveals significant structure of the oxygen field along the Montgomery streamlines of the subtropical gyre.

The scenario where the surface outcrop position is north of the latitude of western boundary outflow has not yet been examined in the previous gyre-scale simulations of transient tracers. Prior studies have generally employed a symmetric wind-driven gyre [Stommel, 1948] to prescribe the flow field and set the outcrop latitude between the mid-point and northern edge of the gyre. This results in direct advective ventilation for a large fraction of the total gyre transport. In addition to a simple Stommel-gyre, Jia and Richards [1996] experimented with a “nonlinear” gyre (based on a QG streamfunction from Rogers and Richards [1988]) which concentrated the western boundary current outflow into a narrow jet along the northern edge of the model domain. The outcrop position, however, was set south of this inflow so that the majority (70%) of the gyre was directly ventilated and the effects of the modified streamfunction are minor.

The remainder of this chapter will introduce and examine a two-dimensional gyre model with features that provide for testing the sensitivity of the tracer age tendency to the fraction of the gyre exposed to direct ventilation from the surface ocean. In contrast to previous studies, the model geometry will allow for the position of the surface outcrop to be placed north of the main body of the anticyclonic gyre. Geographically separating the gyre circulation from the outcrop region restricts the communication of surface properties to a diffusive transfer. In such a scenario it is

found that the observed temporal tendency of the tracer age can be reproduced with conventional estimates of lateral diffusivity.

## 5.3 A Two-dimensional Numerical Model

### 5.3.1 Description of Model

The numerical model is designed to advect and diffuse passive tracers in a prescribed flow field. The flow field in the current study is a modified version of the Stommel-gyre model employed in previous studies [*Musgrave, 1990; Thiele and Sarmiento, 1990; Jia and Richards, 1996; Doney, Jenkins and Bullister, 1997; Jenkins, 1997*]. Two gyres occupy the model domain; the northern gyre is meant to represent the anticyclonic subtropical circulation while the southern cyclonic gyre is added to provide a “flushed” diffusive sink for tracers along the southern boundary of the subtropical gyre [*Doney, Jenkins and Bullister, 1997*].

The advective flow field is specified by a streamfunction that, for the simple Stommel-gyre, takes the form:

$$\Psi(x, y) = -A \sin\left(\frac{2\pi y}{L_y}\right) \left(c_1 \exp^{\frac{\lambda_1 x}{L_x}} + c_2 \exp^{\frac{\lambda_2 x}{L_x}} + 1\right), \quad (5.3.1)$$

where

$$\begin{aligned} \lambda_1 &= \frac{-1 + (1 + 4\pi^2 \epsilon^2)^{1/2}}{2\epsilon}, \\ \lambda_2 &= \frac{-1 - (1 + 4\pi^2 \epsilon^2)^{1/2}}{2\epsilon}, \\ c_1 &= \frac{1 - \exp^{\lambda_2}}{\exp^{\lambda_2} - \exp^{\lambda_1}}, \\ c_2 &= -(1 + c_1). \end{aligned}$$

The constant  $A$  sets the total transport of the gyre; the sharpness of the western boundary intensification is controlled by  $\epsilon$ . The anticyclonic subtropical gyre occu-

pies the northern half of the meridional domain from  $y = \frac{1}{2}L_y$  to  $L_y$ . Velocities are determined using the standard definition of streamfunction:

$$\begin{aligned} u &= -\frac{\partial \Psi}{\partial y}, \\ v &= \frac{\partial \Psi}{\partial x}. \end{aligned}$$

The structure of the streamfunction of the basic Stommel-gyre is modified in this study to simultaneously provide for the ability to shift the outcrop latitude to a position north of the main transport of the gyre as well as to include a representation of the eastward flowing Gulf Stream Extension/Azores Current. This is accomplished by multiplying the streamfunction specification in equation 5.3.1 by an additional meridional structure function,  $\Phi(y)$ , applicable for the poleward half of the subtropical gyre ( $y \geq \frac{3}{4}L$ ):

$$\Phi(y) = 1 - \frac{1}{2} \left( \tanh \left( \frac{\gamma}{L_y}(y - y_{Az}) \right) - \tanh \left( \frac{\gamma}{L_y}(\frac{3}{4}L_y - y_{Az}) \right) \right) \quad (5.3.2)$$

The structure function of equation 5.3.2 concentrates the outflow of the western boundary transport into a narrow eastward jet centered at the nominal position of the Azores Current:  $y = y_{Az}$ . The parameter  $\gamma$  controls the sharpness of the front. For small  $\gamma$ , the value of equation 5.3.2 is near unity for all  $y$  and the standard Stommel-gyre is obtained. As  $\gamma$  increases, the outflow of the western boundary current becomes concentrated in a jet, located at  $y = y_{Az}$ , with characteristic width  $\frac{L_y}{\gamma}$ . The right-hand-most term in equation 5.3.2 allows a match with the standard solution at  $y = \frac{3}{4}L_y$ . Figure 5.7 illustrates an example of the streamfunction for the modified Stommel-gyre. For all the model simulations presented here, the position of the eastward jet,  $y = y_{Az}$ , is set to  $0.875L_y$ .

The modified Stommel-gyre allows simulation of the fundamental features of the observed mean circulation shown in figure 5.3: isopycnal outcrop position north

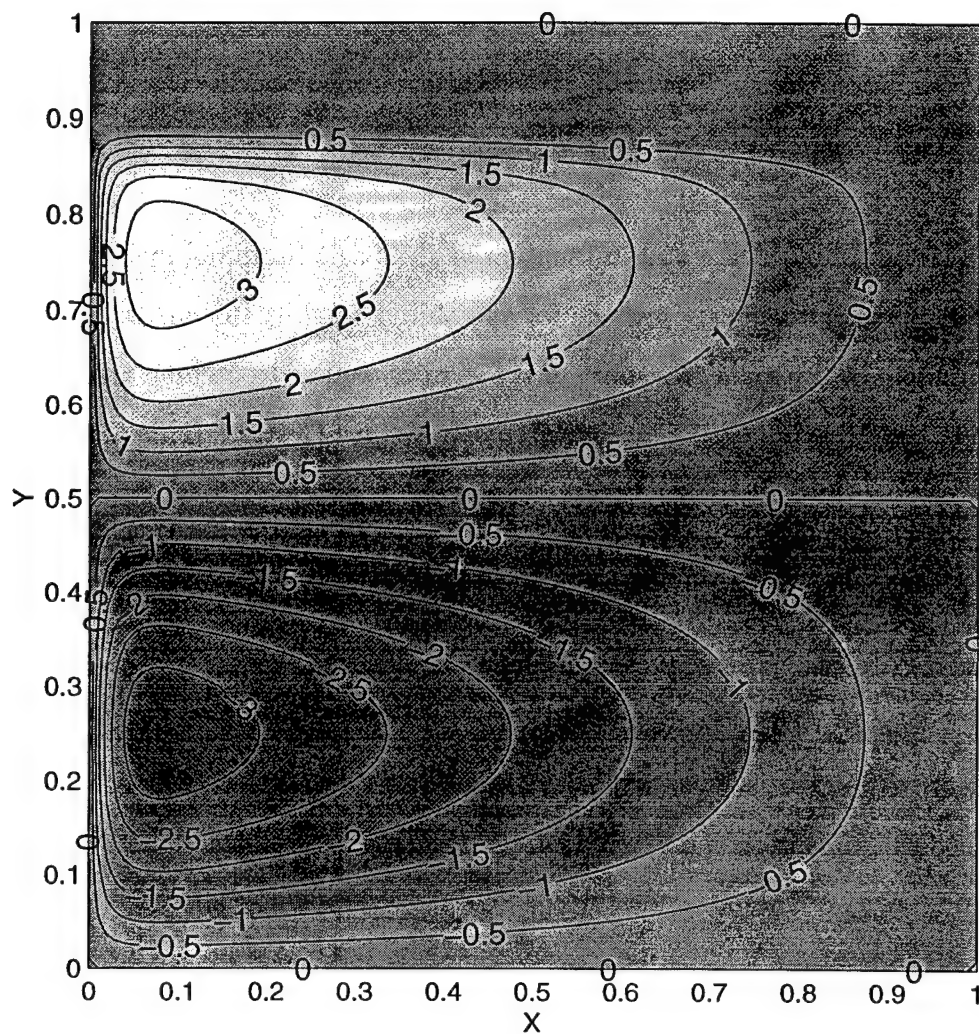


Figure 5.7: Streamfunction of double-gyre two-dimensional model. The anticyclonic subtropical gyre is depicted in the upper half of the domain. The streamfunction of the Stommel-gyre is modified to incorporate a representation of the narrow eastward flow in the Gulf Stream Extension/Azores Current. Model parameter specification in this figure are  $\epsilon = 0.02$ ,  $\gamma = 40$ ,  $y_{Az} = 0.875L_y$ .

of a zonal jet which supplies the fluid to the interior subtropical circulation. This drastically reduces the direct ventilation of the thermocline and, instead, ventilates the gyre via diffusive fluxes across the quiescent region north of the jet. Figure 5.8 illustrates the reduction of direct ventilation as the sharpness factor,  $\gamma$ , of the eastward jet increases. The figure shows the fraction of the total transport that is ventilated as

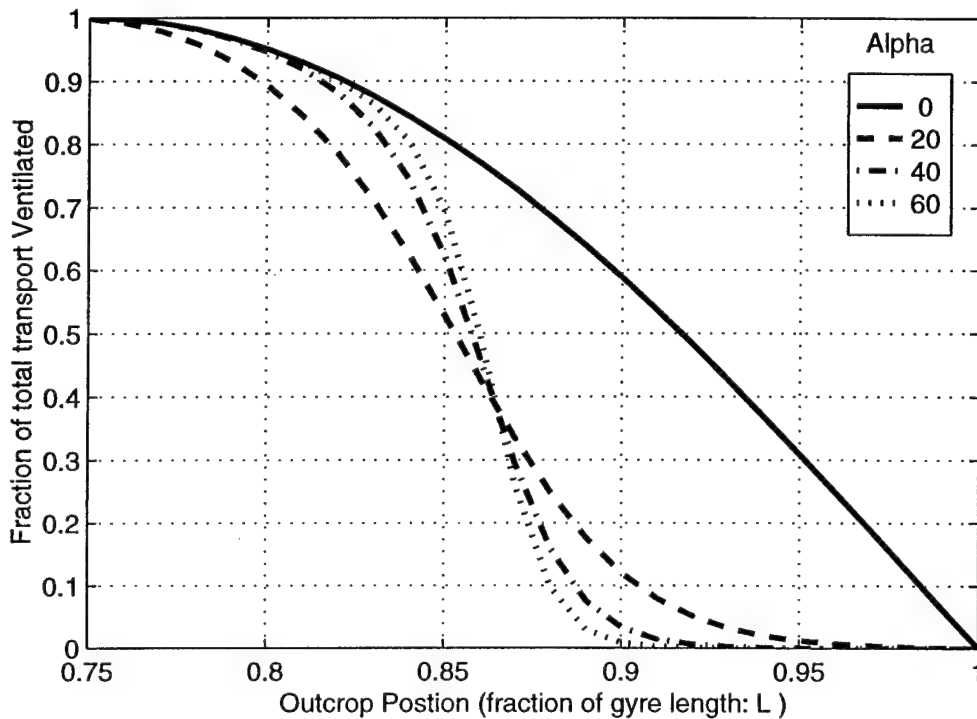


Figure 5.8: Fraction of gyre directly ventilated as function of outcrop position and sharpness of eastward jet. The different line-types represent various magnitudes of  $\gamma$ ; sharpness of the eastward flowing jet increases with  $\gamma$ . The curves plot the normalized fraction of the total gyre transport which is exposed to direct surface forcing in the region north of the outcrop latitude. Outcrop position is expressed as a fraction of  $L_y$ , the total meridional extent of the two-gyre system illustrated in figure 5.7.

a function of both outcrop position and sharpness of the eastward jet. The solid line illustrates the standard Stommel-gyre. For this standard circulation, the fraction of the gyre exposed to direct ventilation is quite significant even if the surface outcrop position is far north. For example, when only the northern-most 10% of the subtropical gyre is allowed to outcrop ( $y_{outcrop} = 0.95L_y$ ), 31% of the flow is directly ventilated. In

contrast, for the case of the modified gyre, the fraction of the total transport traversing the northern quarter of the gyre is greatly reduced. For comparison, if the outcrop position is the same as the previous example and  $\gamma = 10$ , the direct ventilation is 7%. In the case of a sharp front,  $\gamma = 40$ , the fraction of the gyre directly ventilated is less than 0.2%. If the outcrop position is placed south of the latitude of the eastward jet (e.g.  $y_{outcrop} = 0.8L$ ) nearly the entire gyre is directly ventilated regardless of the sharpness of the front.

The velocity determined from the streamfunction specification is employed in the two-dimensional advective-diffusive equation for  $^3\text{He}$  and tritium. For the results presented here, the lateral diffusivity parameter is varied in different simulations but always specified as a constant throughout the model domain. The model domain is a square 100x100 grid covering a domain 6000x6000 km. Tracer concentrations are integrated forward in time with a first upwind differencing scheme [Roache, 1982]. The magnitude of the streamfunction ( $A$  in eq. 5.3.1) is determined from the specified characteristic velocity scale of the gyre where the characteristic velocity scale is taken to be the average meridional velocity of the interior flow at the latitude of maximum transport.

The surface boundary condition is applied at all grid points north of the specified outcrop latitude. Boundary conditions for  $^3\text{H}$  are taken from the time history of North Atlantic surface waters [Dreisigacker and Roether, 1978; Doney and Jenkins, 1988]. Surface  $^3\text{He}$  concentrations are restored towards zero with a time-scale of 0.1 years. The time-scale of the  $^3\text{He}$  boundary condition is determined from gas exchange dynamics and is short compared to the residence time of waters in the outcrop region. The position of the outcrop latitude is varied to expose between 2% and 30% of the northern portion of the gyre to atmospheric forcing.

The model described above is characterized by 5 parameters:

- $V$ : characteristic meridional velocity of interior flow
- $\kappa_H$ : lateral diffusivity
- $\epsilon$ : sharpness of western boundary current
- $\gamma$ : sharpness of Gulf Stream Extension/Azores Current
- $y_{outcrop}$ : meridional position of surface outcrop

Sensitivity of the tracer fields to all of these parameters will be explored except for the western boundary parameter  $\epsilon$ . *Musgrave* [1990] investigated the sensitivity of simulated tracer fields to  $\epsilon$  and found only weak dependence. Additionally, since the emphasis of this work is on the interpretation of tracer signals in the eastern extent of the gyre, there should be little dependence on the parameterization of the western boundary current.

### 5.3.2 General Character of Simulated Tracer Fields

Unlike the semi-infinite one-dimensional model, the results of the two-dimensional model cannot be characterized simply as a function of the radiotracer Péclet number. Numerical simulations are performed for the full four-dimensional parameter range defined in table 5.1. The values of the characteristic velocities are chosen based on

Parameter	range	units
$V$	3 4 5 6 8 10 14	$mm\ s^{-1}$
$\kappa_H$	500 1000 1500 2000 3000 4000	$m^2 s^{-1}$
$\gamma$	1 20 40 60	-
$y_{outcrop}$	0.86 - 0.98; steps of 0.02	-

Table 5.1: Parametric range explored with two-dimensional model

the magnitude of observed geostrophic velocity for the selected range of isopycnals.

Diffusivity values range from relatively low values often used in numerical simulations (e.g.  $500 \text{ m}^2 \text{ s}^{-1}$ ) to the large values required to reach agreement between the data and the one-dimensional model ( $4000 \text{ m}^2 \text{ s}^{-1}$ ). Position of the outcrop is varied to include locations south of the eastward jet which provides for strong direct ventilation, as well as locations well poleward of the jet, limiting the introduction of tracers into the gyre to diffusive flux. The new parameter introduced in this study, controlling the sharpness of the jet representing the Azores Current, is varied from 1 (very broad current approaching the limit of Stommel-gyre) to 60 (narrow current with characteristic width comparable to width of simulated western boundary current).

Definition of a single Péclet number for each simulation is problematic since the magnitude of the velocity field varies spatially. For purposes of comparison, however, one can choose to define the Péclet number based on the characteristic velocity of the gyre; the velocity scale,  $V$ , is defined as the mean meridional velocity at the latitude of maximum interior transport (table 5.1). The length scale,  $L$ , is taken to be  $1/4$  of the size of the model domain (1500 km). The factor of  $1/4$  is chosen as an approximation of latitudinal distance between the midpoint of the anticyclonic gyre and the outcrop latitude.

Examples of the simulated tracer fields are shown in figures 5.9 and 5.10. Each figure illustrates the tritium,  $^3\text{He}$ , and tracer age field for a single combination of the parameters in table 5.1. The tracer fields are shown at two points in time, 1981 and 1991, marked by good observational coverage in the eastern North Atlantic thermocline. The parameters controlling the character of the Azores Current and the position of the surface outcrop are identical in the two figures; only the velocity and lateral diffusivity are altered. The position of the winter outcrop is placed north of the core of the eastward flow so the fraction of the gyre exposed to direct ventilation is less than 1%. Figure 5.9 illustrates a moderately advective scenario ( $\text{Pe} = 15$ ), while figure 5.10 is slightly more diffusive ( $\text{Pe} = 3$ ). Neither of these cases is at the extremes



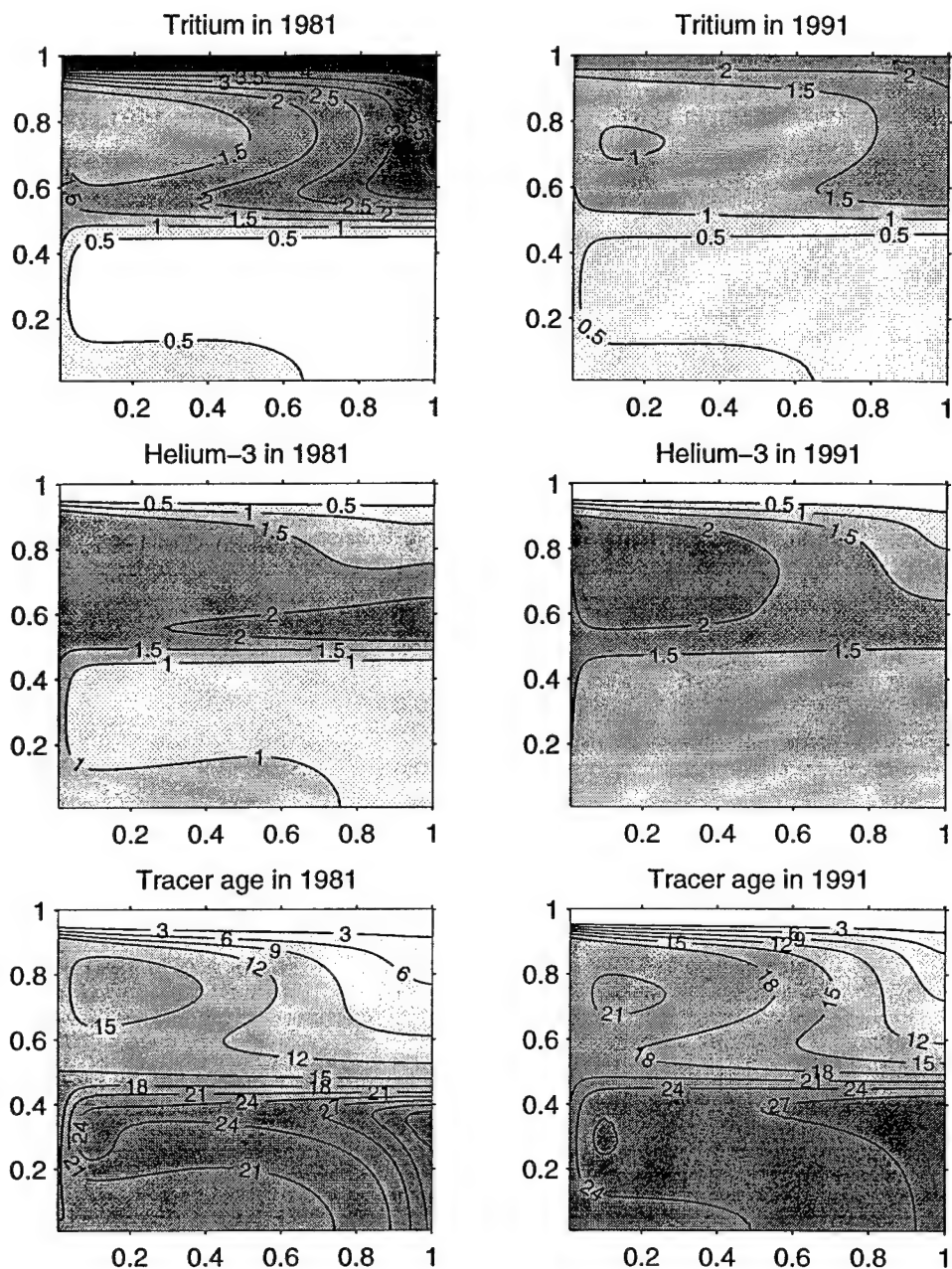


Figure 5.9: Simulated tracer fields for Péclet number = 15 and surface outcrop position north of Azores Current. Each panel presents a contour plot of tracer concentration as a function of  $X$  and  $Y$ . The left-hand column shows the modeled fields of tritium,  $^3\text{He}$  and tracer age in 1981. The right-hand column illustrates the same fields in 1991. The full model domain is presented: the region representing the subtropical North Atlantic is from  $Y = 0.5$  to 1. Parameters used for this simulation:  $V = 1.0$  cm/s,  $\kappa_H = 1000$   $\text{m}^2\text{s}^{-1}$ ,  $\gamma = 40$  and,  $y_{\text{outcrop}} = .94L_y$ . Fraction of gyre transport exposed to direct surface ventilation is less than 1%.

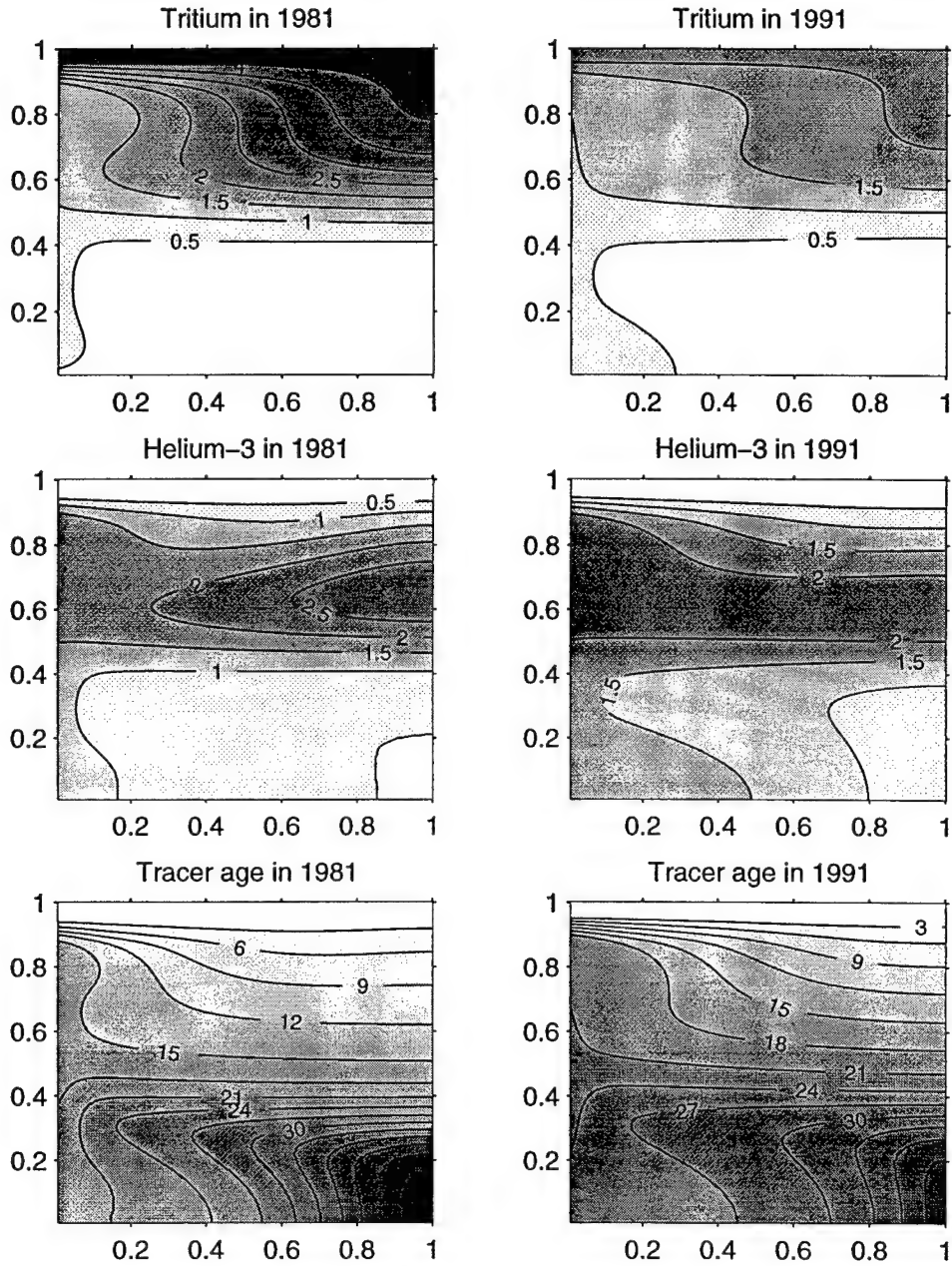


Figure 5.10: Simulated tracer fields for Péclet number =3 and surface outcrop position north of Azores Current. See caption for figure 5.9. Parameters used for this simulation:  $V = 0.4 \text{ cm/s}$ ,  $\kappa_H = 2000 \text{ m}^2\text{s}^{-1}$ ,  $\gamma = 40$  and,  $y_{outcrop} = .94L_y$ .

of the parameter range used; rather, they are selected to illustrate the sensitivity of the tracer fields to moderate changes in the advective-diffusive character of the flow.

The closed streamlines of the "pool" region in the western portion of the basin are clearly evident in the tracer fields of the advectively dominated simulation (figure 5.9). Despite the lack of direct ventilation, tritium enters the gyre in the east by lateral diffusion producing a spatial structure suggestive of advective ventilation. Tritium must diffuse from the position of the outcrop to the latitude of the eastward flowing Azores Current. Once in the core of the flow, however, the tracer is entrained and transported around the gyre predominantly by advection. Therefore, even though the eastern portion of the anti-cyclonic gyre is within the domain of closed streamlines, the comparable time scales of advection and diffusion results in significant along-streamline structure of the tracer fields, seen here as a tongue of high tritium. In 1981, the tongue of high tritium values penetrates across the southern limb of the anti-cyclonic gyre to the western boundary. Comparison of tritium distribution in 1981 and 1991 shows a reduction in inventory over time, due to radioactive decay, and a general trend towards homogenization. Tritium enters the "pool" region only by diffusion across streamlines and isolated low concentrations are still evident in 1991. Some  $^3\text{H}$  is seen entering the southern gyre by diffusion across the inter-gyre boundary. Tritium advects southward along the western boundary of the southern gyre and subsequently spreads into the interior along the southern boundary.

The  $^3\text{He}$  field in figure 5.9 displays a maximum value in the eastern portion of the gyre in 1981 due to the radioactive decay of subducted tritium. Helium values north of the outcrop are set to zero by the boundary condition. By 1991, the maximum has shifted towards the western portion of the domain: radiodecay of the surface tritium concentrations results in a reduced tritium source for the eastern portion of the basin. Advection has transported the  $^3\text{He}$  maximum towards the west where it accumulates in the closed "pool".

The tritium- $^3\text{He}$  age fields illustrated in figure 5.9 show youngest values in the northeast corner of the anti-cyclonic gyre. The clockwise gyre circulation is evident in the tongue of low age water advected along the southern limb of the gyre. Again, the “pool” region is clearly seen in the closed contours of high tracer age in the western portion of the gyre. Comparison of the age field in 1981 and 1991 reveals a similar pattern but a shift towards older ages at a fixed point. The southern cyclonic gyre contains large age gradients resulting from tracer which has diffused across the inter-gyre boundary and subsequent advected cyclonically around the gyre. The tritium and  $^3\text{He}$  fields in the southern gyre tend to homogenize over time and the age field shows much less structure in 1991.

Comparison of the previous case with the more diffusive scenario (figure 5.10) illustrates many of the features previously described by *Musgrave* [1990]. Specifically, much of the gyre is strongly influenced by surface boundary conditions through lateral diffusion and the distinct nature of the “pool” region has disappeared. The anti-cyclonic advection is still visible in the clockwise twisting of the tritium isopleths. The age field, however, shows a predominantly meridional structure for the eastern half of the basin. The age field again shows a shift in time with the tendency towards older ages at a fixed point.

### 5.3.3 Comparison with Tracer Observations on $\sigma_\theta = 27.0$

This section will compare diagnostics of the two-dimensional simulations with the observations of the transient tracer fields on the isopycnal surface  $\sigma_\theta = 27.0$ . This isopycnal is chosen for analysis because of the robust signal of observed tracer age tendency at this level (figure 2.18) and the unexpectedly large estimates of lateral diffusivity required to simulate the observations in the one-dimensional model incorporating only direct ventilation (figure 4.9). Though the winter outcrop of this

isopycnal is south of the position of the zero wind-stress curl, previous studies do not present a clear picture for either the case of direct or indirect ventilation for this layer of the thermocline (§5.1).

### Sharpness of Azores Current

In comparison to previous gyre models, the model used here concentrates the eastward outflow of the western boundary current into a sharp zonal jet meant to mimic the effect of the Gulf Stream Extension and Azores Current. Does this modification of the model effect the ventilation of tracer and, specifically, the temporal tendency of the tracer age field in the eastern region of the gyre? Figure 5.11 shows the effect of the sharpness of this concentrated eastward flow on the tritium concentration and age tendency in the eastern gyre in 1986 at the position where the tracer age equals 8.3 yr. In the limit that  $\gamma$ , the sharpness of the Azores current, goes to zero, the streamfunction field approaches the Stommel-gyre. The observational estimate (based on regression models in §3.3) with the associated uncertainty is displayed as a solid gray bar in each panel. As expected, decreasing the fraction of direct ventilation, by increasing the sharpness of the Azores Current reduces the tritium inventory within the thermocline. Concurrent with the slight decrease in tritium inventory is an increase in the apparent tracer age tendency. Figure 5.11 illustrates that modifying the flow field to include the presence of an eastward jet alters the ventilation of tracers, however, the tracer fields do not seem overly sensitive to the actual value of the parameter controlling the sharpness of the jet. Additionally, for large values of  $\gamma$ , which lack significant direct ventilation, diffusive ventilation appears to be an efficient mechanism for introducing surface signals into the eastern thermocline as tritium inventories are still quite large.

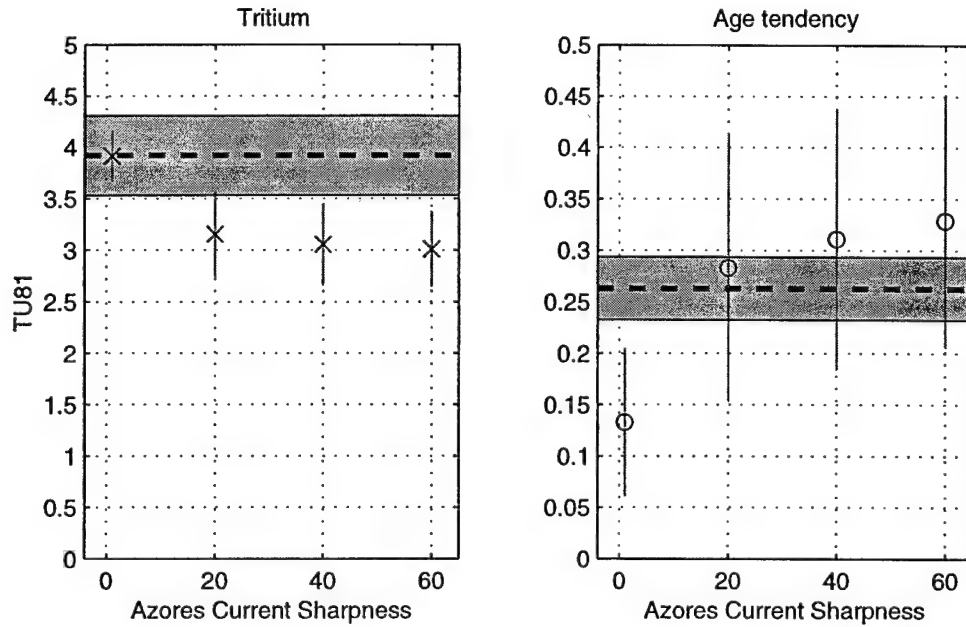


Figure 5.11: Sensitivity of tracer fields to sharpness of Azores Current. Left-hand panel displays tritium inventory (in tritium units decay corrected to 1981 [TU81]) and the right-hand panel displays the temporal tendency of the age field. The sharpness of the Azores Current,  $\gamma$ , is varied while other model parameters are held fixed:  $V = 0.6$  cm/s,  $\kappa_H = 1500$   $m^2 s^{-1}$ ,  $y_{outcrop} = 0.96L_y$ . Model simulations are evaluated at model year 1986 at  $X = 0.85L_x$  with an uncertainty estimated based on the variation of the model fields between  $X = 0.75L_x$  and  $0.95L_x$ . Simulations are evaluated at the meridional position where the model age equals the observed mean tracer age, 8.3 yr on  $\sigma_\theta = 27.0$ . Observational estimates and associated uncertainties (95% c.i.) based on age-oxygen regression (§3.3) are shown as a dashed line bracketed by a gray bar. A 5% standard error is added to the observational estimate of tritium inventory to account for uncertainty in the surface tritium boundary condition.

### Position of the Winter Outcrop

The key new feature introduced in this two-dimensional model is the ability to place the position of the surface outcrop north of the main body of the anti-cyclonic circulation. Confining the ventilation to a diffusive process results in a pronounced effect on the temporal tendency of the tracer age field. Figure 5.12 compares the simulated age tendency with the observed estimate of this quantity. The temporal regression model of tracer age against AOU (§3.3) on  $\sigma_\theta = 27.0$  yielded an age tendency of  $0.26 \pm .03$

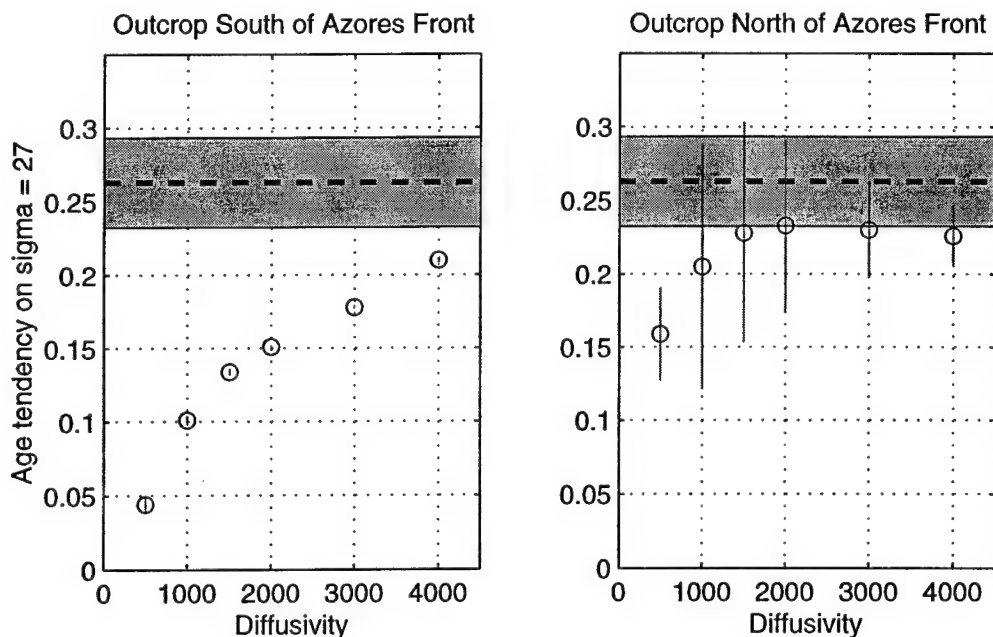


Figure 5.12: Sensitivity of tracer fields to direct versus diffusive ventilation. Left-hand panel shows tracer age tendency when position of surface outcrop is south of the core of eastward flow,  $y_{outcrop} = 0.86L_y$ , leading to direct ventilation of the eastern region. The right-hand panel shows the case where the outcrop is positioned north of the jet,  $y_{outcrop} = 0.98L_y$ , allowing for only diffusive ventilation. The position of the eastward jet is at  $y = 0.875L_y$ . Model results are presented as a function of lateral diffusivity. Other model parameters are held fixed:  $V = 0.6$  cm/s,  $\gamma = 40$ . See caption of figure 5.11 for a description of how model fields are evaluated.

at a mean age of 8.3 yr.<sup>c</sup> For purposes of comparison, the model simulations are analyzed by locating the latitudinal position in the eastern basin,  $X = 0.85L_x$ , where the simulated tracer age equals 8.3 yr in 1986. The model age tendency is then computed using a time interval of 10 years to match the approximate time extent of the observations. An error is assigned to the model diagnostic by repeating the calculation over the longitudinal range from  $X = 0.75L_x$  to  $0.95L_x$ . This uncertainty is meant to represent navigational uncertainty in comparing the observations with model simulations. The method of comparison avoids navigational uncertainty in the

<sup>c</sup>The temporal regression model using spatial coordinates (§2.2.2) estimates the temporal tendency on  $\sigma_\theta = 27.0$  to be  $0.36 \pm 0.03$  at a mean age of 11.0 years. Equivalent results are obtained in the present analysis if the model is compared to these estimates.

latitudinal direction by using the mean tracer age value to identify the position for the intercomparison.

Figure 5.12 illustrates the sensitivity of the simulated age tendency as a function of diffusivity for two cases: surface outcrop positions north and south of the Azores Front. The characteristic velocity and sharpness of the front are held fixed. The left-hand panel shows the case if the position of the winter outcrop is south of the main inflow into the region ( $y_{outcrop} = 0.86L_y$ ). In this case the majority of the gyre is directly ventilated and the sensitivity of the age tendency to diffusivity are similar to the results of the one-dimensional model. When diffusivity is low (large Péclet number) there is only a small temporal tendency to the age field. As the diffusivity is increased the temporal tendency of the age field becomes large. These results are similar to those of *Musgrave* [1990]: in the directly ventilated region of a two-dimensional gyre, the tracer distribution is well described by a one-dimensional model oriented along the path of the large-scale flow. Using the one dimensional model of chapter 4, high lateral diffusivities ( $> 4000 \text{ m}^2\text{s}^{-1}$ ) are required to recreate the observed temporal tendency of tracer age in the lower thermocline.

The right-hand panel of figure 5.12 shows the situation if the position of the outcrop is placed north of the front ( $y_{outcrop} = .98L_y$ ), virtually eliminating all direct ventilation of the gyre. In this case, the sensitivity of the age tendency to diffusivity is greatly reduced: the model produces a large temporal tendency for the entire range of lateral diffusivity. The uncertainty of the simulation is large for low values of diffusivity indicating a significant degree of cross-stream structure in the eastern portion of the gyre. In comparison, the minimal error bars in the left-hand panel illustrates the absence of cross-stream structure in the flow in the domain of direct ventilation. Large age tendencies occur for even low diffusivities because the entry of tracer into the gyre is controlled by lateral diffusive transport across the region between the position of the surface outcrop and the position of the eastward flowing Azores Current. Flux of



tracer across this region can be approximated by a purely diffusive one-dimensional model (figure 4.8 includes an illustration of the dependence of temporal tendency as a function of age for a solely diffusive ventilation). Once tracer reaches the position of the Azores Current, it will become entrained into the advective gyre circulation and further effects of mixing will be small if  $\kappa_H$  is small. However, the age tendency set by the initial diffusive transport will be preserved and advected with the flow.

Figure 5.13 illustrates the sensitivity of the tracer age field to the latitudinal distance between the eastward jet and the surface outcrop. The figure displays the

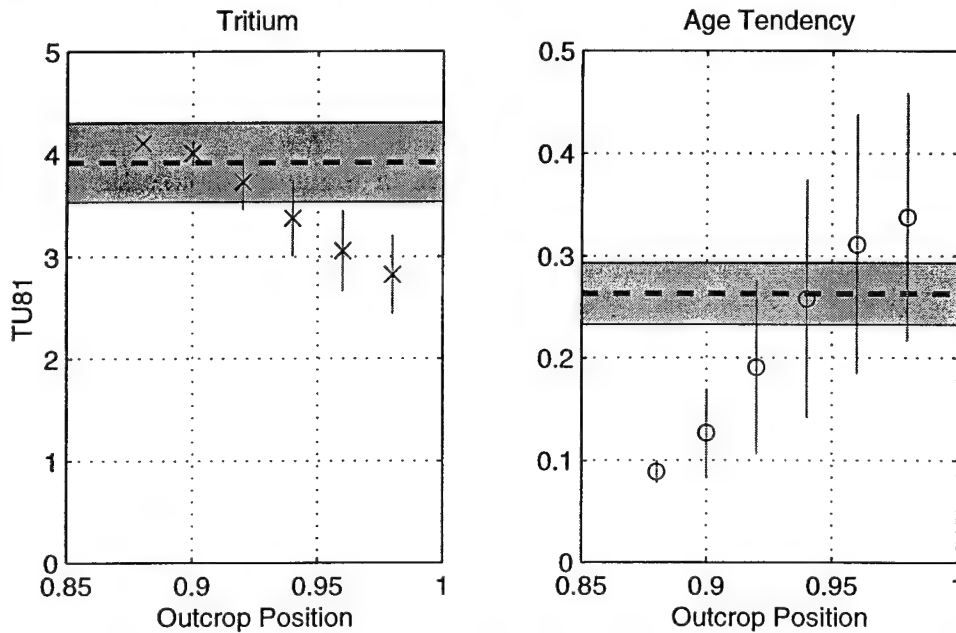


Figure 5.13: Sensitivity of tracer fields to position of surface outcrop. Left-hand panel displays tritium inventory (in tritium units decay corrected to 1981 [TU81]) and the right-hand panel displays the temporal tendency of the age field. The position of the surface outcrop,  $y_{outcrop}$  is varied while other model parameters are held fixed:  $V = 0.6$  cm/s,  $\kappa_H = 1500$   $m^2s^{-1}$ ,  $\gamma = 40$ . See caption of figure 5.11 for a description of how model fields are evaluated.

response of both the tritium inventory and the age tendency as the position of the surface outcrop is marched northward, away from the eastward jet. Not surprisingly, increasing the width of this diffusive buffer zone decreases the amount of tritium entering the anti-cyclonic gyre while steadily increasing the magnitude of the age

tendency. Furthermore, as the diffusive barrier widens, the degree of cross-stream structure of the tracer field increases, as evidenced by the large range of variance in the model results.

### Temporal tendency of age as function of the diffusive time-scale

The previous analysis has shown that the time evolution of tracer age in a gyre ventilated by a diffusive flux along its northern edge can be comparable to that observed in the eastern North Atlantic, regardless of the Péclet number characterizing the gyre circulation itself. The lateral diffusion of  $^3\text{He}$  and  $^3\text{H}$  across the band of quiescent flow sets the age tendency along the northern edge of the gyre circulation. As the tracers, subsequently advect around the gyre, diffusion in the gyre may further increase the apparent temporal tendency, but even in the case of pure advection within the gyre, the age tendency set along the northern edge of the gyre is “locked in” and swept along with the circulation. What determines the magnitude of the age tendency of the water flowing eastward in the Azores Current? Investigation of the simple analytic model (§B.2) as well as the numerical one-dimensional diffusive model (figure 4.8) show that the magnitude of the age tendency increases with tracer age. This suggests that the tracer age tendency “felt” by the fluid in the Azores Current should be a function of the time scale for tracers to diffuse across the stagnant barrier between the edge of the gyre and the outcrop position. The diffusive time scale is given by:

$$T_D = \frac{L_d^2}{\kappa}, \quad (5.3.3)$$

where  $L_d$  is characteristic diffusive length scale. The positive dependence of age tendency on distance to outcrop (figure 5.13) supports the hypothesis that the age tendency increases with the diffusive time scale. Figure 5.14 displays the tritium inventory and the tracer age tendency as a function of the diffusive time scale of the stagnant barrier region. Plotting the diagnostics as a function of the diffusive time scale collapses the

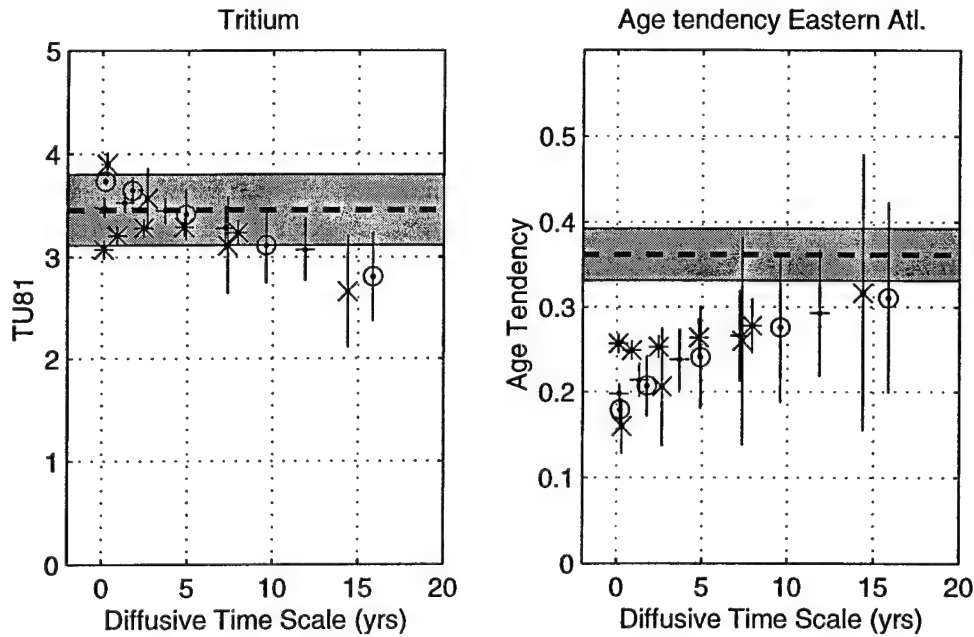


Figure 5.14: Sensitivity of tracer fields to diffusive time scale of quiescent region north of the Azores Current. Left-hand panel displays tritium inventory (in tritium units decay corrected to 1981 [TU81]) and the right-hand panel displays the temporal tendency of the age field. Both lateral diffusivity,  $\kappa_H$ , and position of the outcrop,  $y_{outcrop}$ , are varied and results are plotted as function of diffusive time scale:  $\frac{L^2}{\kappa}$  where  $L$  is the distance between the surface outcrop and the northern edge of the simulated Azores current. Model simulations with different parametric combinations are shown as symbols with error-bars. Observations are shown as dashed line with gray bar representing uncertainty. Values of lateral diffusivity ( $m^2s^{-1}$ ) and associated plotting symbols are: 1000 (small x), 1500 (o), 2000 (+), 3000 (\*) and 4000 (large x). Other model parameters are held fixed:  $V = 0.6$  cm/s,  $\gamma = 40$ . See caption of figure 5.11 for a description of how model fields are evaluated.

results for a wide variety of lateral diffusivities and outcrop positions. As expected, age tendency increases with the diffusive time scale while the tritium inventory decreases. This scaling still results in some scatter amongst the output of the numerous model simulations because it does not account for any subsequent effects of mixing within the closed streamlines of the gyre circulation. The greatest deviations from the general trend occur for the simulations with the largest lateral mixing rates.

Comparison of the model simulations presented in figure 5.14 with the observations on  $\sigma_\theta = 27.0$  suggest that the observations of Chapter 2 could be explained by a

gyre-model in which the communication with the surface mixed layer is not via a path of direct ventilation but rather is mediated by a region of quiescent flow characterized by a diffusive time-scale of 5-10 years (figure 5.15). Within the structure of this model,

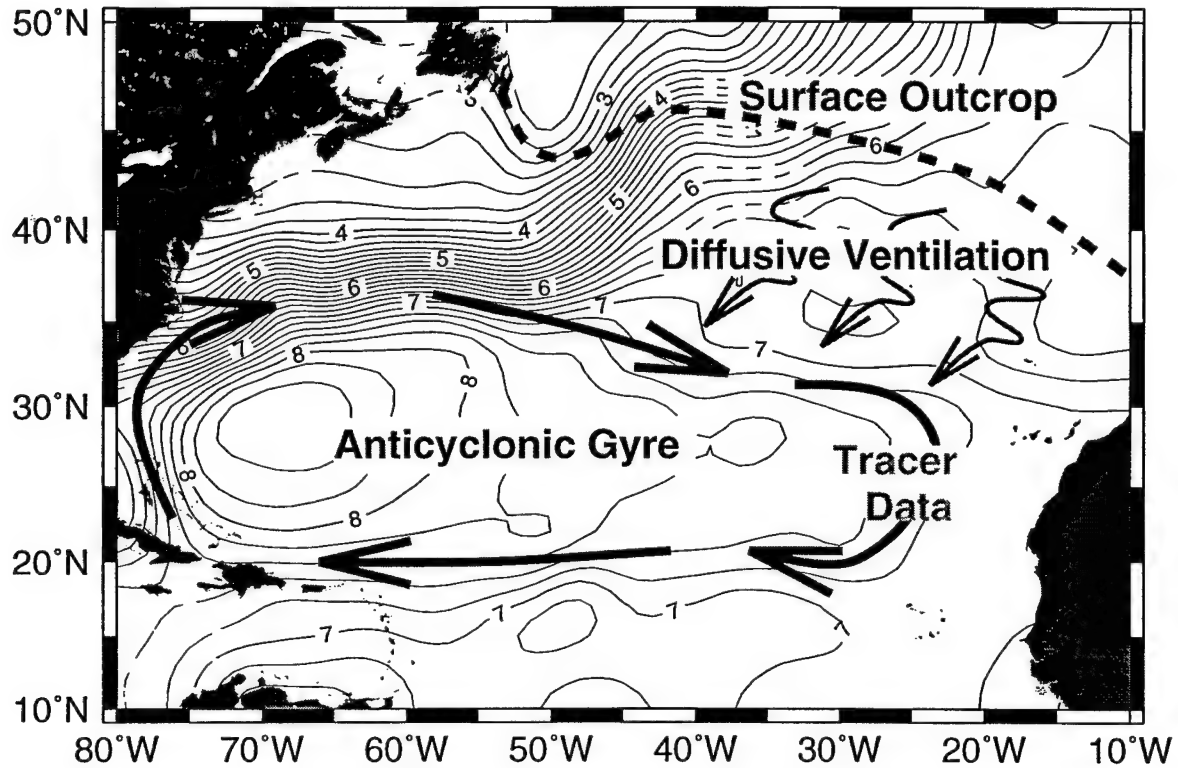


Figure 5.15: Schematic of implied ventilation on  $\sigma_\theta = 27.0$ . Contours show the isopleths of the pressure anomaly Montgomery streamfunction referenced to  $\sigma_1 = 32.3$ .

the estimate of the diffusive time-scale is largely independent of the advective-diffusive character of the gyre circulation itself. The diffusive time-scale is approximately the same as the mean tracer age obtained from the data analysis, consistent with the idea that advection within the gyre is relatively rapid compared to diffusive transport across the quiescent region. If the characteristic length scale of this buffer region is  $O(800\text{km})$  (estimated from figure 5.3), then the associated lateral diffusivity is order  $2000\text{--}4000\text{ m}^2\text{s}^{-1}$ . Lateral diffusivity estimates of this magnitude agree with those of obtained from drifting buoys [Krauss and Böning, 1987] for this region (see table 4.4).

The method outlined above provides only a rough approximation of the numeric value of lateral diffusivity; the range of appropriate diffusive time-scales is large and the conversion to  $\kappa_H$  depends on the square of the length scale,  $L_d$ . Despite this uncertainty, the simulations demonstrate that tracer fields modeled in a simple two-dimensional gyre diffusively coupled to the surface mixed layer yields features consistent with the observations. In contrast, a model assuming direct ventilation requires exceedingly large values of the lateral mixing coefficient to simultaneously reproduce all these features. In a two-dimensional circulation model, the observations do not constrain the size of lateral mixing but rather are sensitive to the time-scale of the diffusive coupling between the gyre and surface ocean. The diffusively coupled ventilation not only provides for the observed tongue-like penetration of tracers (tritium, oxygen) into the lower ventilated thermocline (e.g. figure 5.9), but additionally recreates the observed temporal evolution of age. The results from scale analysis of the tritium- $^3\text{He}$  age balance show that the temporal evolution of the tracer age field is a sensitive diagnostic of mixing processes because mixing destroys the closed-system assumption built into the idealized concept of tracer age dating.

## 5.4 Application of Two-dimensional Model to Other Isopycnals

The methodology employed to compare observations on  $\sigma_\theta = 27.0$  to the simulated tracer fields in the modified gyre model can be repeated for other isopycnal surfaces within the thermocline. Figure 5.16 reproduces the analysis of tritium inventory and age tendency as a function of the diffusive time scale for the isopycnal surfaces  $\sigma_\theta = 26.5, 26.7, 26.9$  and  $27.1$ .

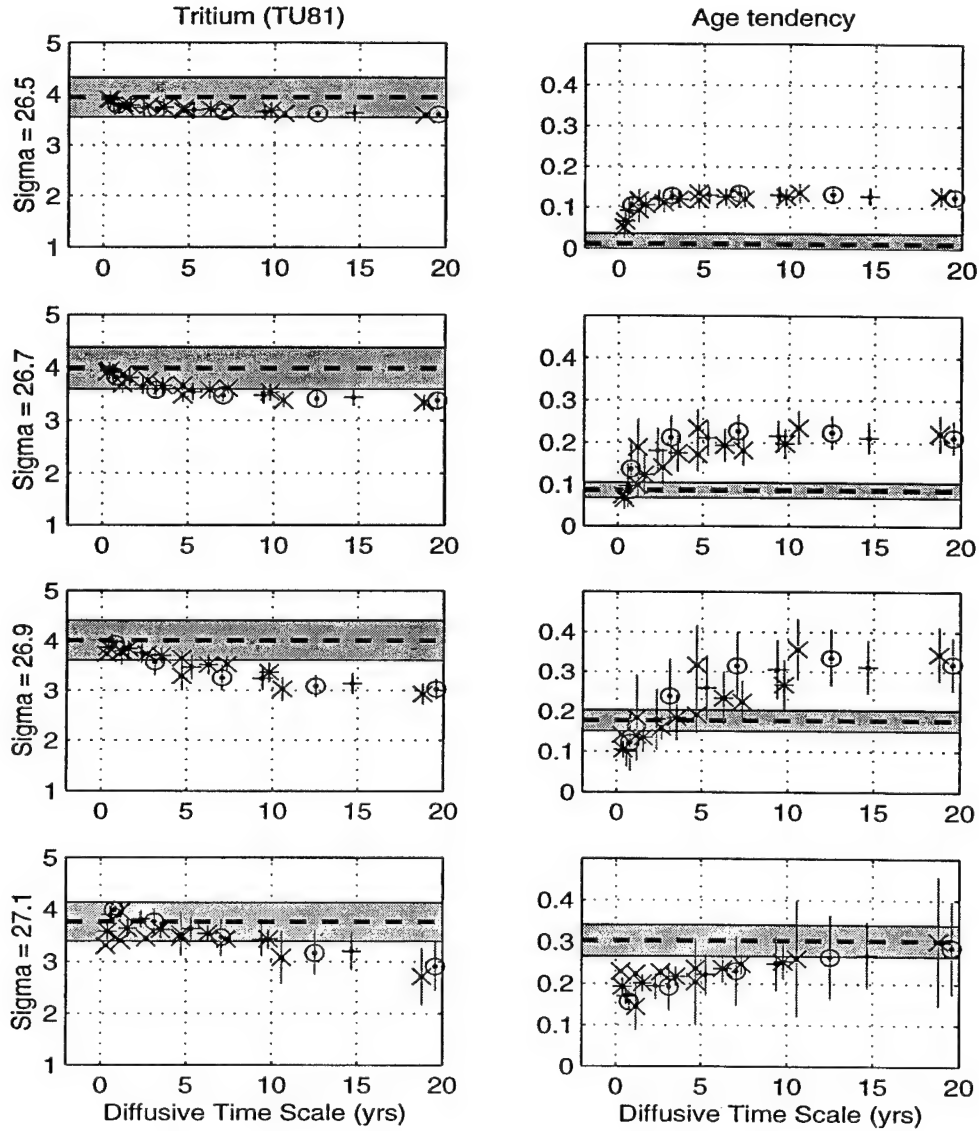


Figure 5.16: Tritium inventory and tracer age tendency evaluated in model year 1986 as a function of diffusive time-scale of quiescent region between surface outcrop and simulated Azores Current. Isopycnals spanning the thermocline are illustrated: from top down:  $\sigma_\theta = 26.5$ ,  $26.7$ ,  $26.9$  and  $27.1$ . Model simulations with different parametric combinations are shown as symbols with error-bars. Observations are shown as dashed line with gray bar representing uncertainty. Mean tracer ages at which the model is evaluated on each surface are 2.6 yr ( $\sigma_\theta = 26.5$ ), 4.5 yr ( $\sigma_\theta = 26.7$ ), 6.7 yr ( $\sigma_\theta = 26.9$ ) and 9.5 yr ( $\sigma_\theta = 27.1$ ). Values of lateral diffusivity ( $m^2s^{-1}$ ) and associated plotting symbols are: 1000 (small x), 1500 (o), 2000 (+), 3000 (\*) and 4000 (large x). See caption of figure 5.14 for further details.

Figure 5.16 indicates that tritium inventory provides only a weak constraint on the strength of the mixing of ventilation: on all the isopycnals illustrated, the model is able to reproduce observed tracer inventories for a wide range of diffusive time scales. In the shallow thermocline ( $\sigma_\theta = 26.5$ ) the tritium inventory is reproduced regardless of the time-scale of diffusive ventilation. In the lower thermocline, diffusive time scales longer than about 10 years fail to sufficiently ventilate the thermocline. If the characteristic time of the diffusive coupling is less than 10 years, however, the models show that a gyre model coupled to the surface outcrop solely by lateral diffusion can reasonably reproduce the tritium inventories. The current findings that tritium inventory is relatively insensitive to the process of diffusive ventilation are similar to those based on simple box models of the thermocline. *Sarmiento* [1983] used tritium inventories to estimate the mean ventilation time of isopycnals within the North Atlantic thermocline and found that box-models based only on tritium inventory provided estimates of the ventilation time-scales but could not be used to distinguish between diffusive and advective ventilation.

Unlike the tritium inventory, the observed tracer age tendency does show sensitivity to the processes of diffusive ventilation (figure 5.16). On  $\sigma_\theta = 26.5$ , the negligible observed age tendency can only be reproduced in a model with a diffusive-time scale near zero, e.g. direct ventilation. If ventilation on this surface is simulated as a closed gyre diffusively coupled to the surface, as in figure 5.15, age tendencies larger than observed are predicted for even short (1 year) diffusive time scales. The conclusion that  $\sigma_\theta = 26.5$  is directly ventilated is in agreement with the results of the one-dimensional model (Chapter 4) which, based on the assumption of direct advective ventilation, found consistency with the observations without requiring excessively large rates of lateral mixing. The isopycnal  $\sigma_\theta = 26.5$  is the core of the subtropical model water and earlier studies [*Siedler, Kuhl and Zenk*, 1987; *Joyce and Jenkins*,

1993] have concluded that direct advective subduction occurs along this isopycnal in the eastern North Atlantic.

The age tendency on isopycnals deeper than  $\sigma_\theta = 26.5$ , demonstrates the increasing importance of diffusive transfer with depth. On  $\sigma_\theta = 26.5$ , comparison of model and observations suggests that diffusive coupling with a time-scale of about a year can reproduce the observed age tendency of 0.1. For deeper isopycnals there is a trend of progressively longer diffusive time-scales and a clear failure of models with direct ventilation (diffusive time-scale equal zero) to reproduce the observed temporal features of the tracer age field. Longer diffusive ventilation time-scales are expected for denser isopycnals since these surfaces outcrop further north, increasing the distance between the surface outcrop and the Azores Current, depicted here as the northern edge of the anti-cyclonic gyre.

## 5.5 Summary

This chapter examined the simulation of tritium- $^3\text{He}$  age, especially the temporal evolution of age, in a simplified two-dimensional gyre of the subtropical circulation. For ventilation of the eastern region of the gyre, the primary feature introduced by adding another dimension, is the possibility of indirect, diffusive ventilation. Regions of closed streamlines, not directly exposed to surface forcing, can only gain tracer inventory by a cross-stream, lateral diffusive flux. Earlier simulations of transient tracers in numerical models have constructed flow fields characterized by a predominance of direct advection and typically only allowed for regions of closed streamlines in the western portion of the basin. Analysis of the hydrography of the eastern North Atlantic, however, implies that the lower thermocline is not exposed to direct advective ventilation and is, rather, best characterized by a closed, recirculation pool.



The current study has employed two-dimensional gyre model designed specifically to examine the sensitivity of the transient tracer fields to either advective or diffusive coupling to the surface mixed layer. Rather than the broad western boundary outflow of the Stommel-gyre circulation, the northern portion of the gyre-model introduced here has a narrow eastward flowing jet meant to simulate the transport of the Gulf Stream extension and Azores Current. The position of the surface outcrop of the isopycnal layer can then be placed either south of this jet, simulating direct ventilation, or north of it, allowing for only diffusive transfer between the gyre circulation and the ocean mixed layer.

Analysis of the two-dimensional model for a wide range of flow parameters shows that the observed tracer characteristics can be reproduced in gyre models in which the lower thermocline communicates with the surface ocean by diffusion rather than direct advection. The transport of tracers within the gyre may still be carried by advection but the entry of properties from the surface ocean must be mediated by a diffusive flux across a region characterized by weak mean flow. The diffusive transfer of tracers across the band of quiescent flow produces tracer age tendencies comparable to those observed in the eastern Atlantic. Unlike models characterized by direct ventilation, the temporal tendency of the tracer age field can be significant even if the coefficient of the lateral mixing rate,  $\kappa_H$ , is relatively small. In the case of the two-dimensional gyre, the age tendencies are largely a function of the diffusive time-scale of the conduit coupling the subtropical gyre-circulation to the surface mixed layer. The diffusive ventilation of the lower thermocline, consistent with diffusivities estimated by other means, appears to be characterized by a time-scale of 5-10 years. Application of the diffusively coupled gyre-model to the upper portion of the thermocline reveal an inconsistency with the observations supporting prior conclusions that this region of the ocean is characterized by direct advective ventilation.



# Chapter 6

## Discussion

### 6.1 Summary of Thesis Research

This thesis has examined the ventilation of the North Atlantic thermocline by analyzing the fields of bomb-produced tritium and its daughter product,  $^3\text{He}$ . Atmospheric testing of hydrogen bombs in the 1950's and early 1960's resulted in large quantities of tritium being deposited into the surface ocean. Subduction from the surface mixed layer has transported the high surface values of tritium into the ocean interior. Tritium decays radioactively, with a half-life of 12.43 yr, to form an isotope of helium,  $^3\text{He}$ . Water exposed to the atmosphere in the surface mixed-layer quickly equilibrates its  $^3\text{He}$  burden via air-sea gas exchange; excess  $^3\text{He}$  is interpreted as the product of tritium decay following subduction.

Observations of tritium and  $^3\text{He}$  in subsurface waters can be combined with the known time-scale of radioactive decay to estimate the elapsed time since the water was in the surface mixed layer, commonly referred to as the "age" of the water parcel (equation 1.3.1). Tritium- $^3\text{He}$  age provides an unbiased estimate of the true

ventilation age only if the effects of mixing are negligible: tracer age estimates based on the measured ratio of two properties necessarily assume that the concentrations of the constituent chemicals have evolved as if the water parcel was isolated from both the atmosphere and all other fluid within the ocean [Jenkins and Clarke, 1976]. Mixing breaks this assumption by altering the observed  $^3\text{He}$  and tritium concentrations through diffusive exchange with surrounding waters.

The advective-diffusive balance of tritium- $^3\text{He}$  age includes a term which incorporates these complex effects of mixing (equation 4.1.1)[Jenkins, 1987]. This term, referred to here as the nonlinear term, can act as either an apparent source or sink of age. Scale analysis (§B.1) illustrates that nonlinear mixing effects behave as a pseudo-velocity. For steady boundary conditions of tritium, the magnitude of the pseudo-velocity is expected to be relatively small. Rapid changes of the tritium boundary condition, however, are likely to cause the nonlinear terms to increase to first order in the total balance. Changes in the relative balance of terms may, in turn, lead to a temporal change in the spatial structure of the age field.

The sensitivity of tracer age estimates to mixing reflects the ambiguity of fluid "age" in a diffusive environment. If a flow is highly advective, the contents of a subducted water parcel are effectively preserved intact and the age of the water within a specific sample of ocean water is well defined. In a more diffusive regime, however, a water parcel will be composed of water with a myriad of tracer histories: a discrete water sample may contain a small fraction of relatively young water, mixed with a bit of very old water as well as water of intermediate age. What is meant by the "age" of such a water parcel? The standard definition of "age" (e.g. the elapsed time since a parcel was resident in the surface mixed layer) is only precisely defined for a homogeneous water parcel, not a parcel composed of water with a variety of independent histories. The most useful interpretation of "age" when water has been mixed might be the volume weighted average age over all the water within the sample.

As pointed out in previous analyses of transient tracer observations [*Jenkins and Clarke, 1976; Jenkins, 1987; Pickart, Hogg and Smethie, 1989; Thiele and Sarmiento, 1990; Wallace et al., 1992*], transient tracer derived age does not always provide an unbiased estimate of the true mean age of a water parcel since the youngest waters often have a higher concentration of tracer. When young water with high tracer concentration mixes with older water which subducted at time of lower surface tracer concentration, the resulting average is biased low (compared to the volume-weighted average) because of the greater tracer inventory, and hence greater weight, of the younger sample. The strength of the bias is expected to be the largest soon after the peak tritium input when the disparity in tritium inventory between the young and old waters is greatest. The magnitude of this bias may be expected to decrease with time as tracer concentration builds up in the older waters.

An indication that diffusive effects may be an important in the North Atlantic thermocline comes from deviations in the behavior of the observed tracer age field from that expected for an ideal advective age. Whereas previous analyses have examined the spatial structure of the tracer age field [*Jenkins, 1988a; Jenkins, 1987; Joyce and Jenkins, 1993; Jenkins, 1997; Andri , Jean-Baptiste and Merlivat, 1988; Roether and Fuchs, 1988*], this thesis has specifically focused on the temporal behavior the age field. Chapter 2 presents 15 years of tritium-<sup>3</sup>He age observations in the eastern North Atlantic thermocline. Multivariate regression analysis demonstrates a significant change in the age field on isopycnal surfaces throughout the thermocline. The magnitude of the changes are slight in the mid- to upper-thermocline but become quite significant in the lower levels of the wind-driven circulation (figure 2.16). Tracer age in the lower thermocline increases by up to 6 years (an increase of 50%) over the course of the observations. Comparison of trends observed in the eastern North Atlantic with a time-series at Bermuda demonstrate that the changes in the age field

observed in the eastern portion of the gyre typify a pattern which extends throughout the subtropical thermocline.

Chapter 3 tests the hypothesis that the tritium- $^3\text{He}$  age field behaves as an ideal advective age. Under this hypothesis, the observed changes in the tracer age distribution reflect a change in the rate of the underlying physical circulation. Historical hydrography [Lozier, Owens and Curry, 1995] from the region is used to examine the time history of the density field. No discernible changes in the large-scale structure of the density field are found; there is no evidence of change in the geostrophic flow. However, the uncertainties in the estimation of the density field owing to mesoscale variability are not negligible compared to the changes in flow required by the observed changes in the tracer age gradient. Thus the hypothesis of a slowly changing circulation cannot be conclusively rejected on this basis. Comparing the ventilation of tritium- $^3\text{He}$  age with oxygen, however, is more conclusive. The distribution of dissolved oxygen shows no statistically significant changes over the time of the  $^3\text{H}$  and  $^3\text{He}$  observations supporting the inference of a ventilation rate which is essentially steady with time. Therefore, the bulk of the observed changes in the tritium- $^3\text{He}$  age field cannot be explained by a secular trend in the ventilation rate. A direct comparison of the relation between oxygen and tritium- $^3\text{He}$  age reveals a change over time; regression analyses of the trend in the property-property relation yields estimates of the change in tracer age, assuming that the oxygen field is steady. The quantitative agreement of the age tendency estimated from regressions against oxygen and against geographic position (figure 3.13) refutes the hypothesis that tritium- $^3\text{He}$  age is behaving as an ideal advective age in a temporally varying flow field.

Having established that the tritium- $^3\text{He}$  age in the eastern Atlantic thermocline is not behaving as an ideal advective age, Chapter 4 introduces simple models of ventilation which include the varying tritium boundary condition and horizontal diffusion. Scale analysis shows the tracer age field is expected to change in response to large

shifts in the surface boundary condition of tritium. For a steady flow field, the magnitude of the temporal response of the tracer age field to the sudden input of bomb tritium depends on the Péclet number of the flow; the time-dependence of the age field increases for more diffusive flows. A one-dimensional model of thermocline ventilation is constructed based on the assumption that all the fluid in the thermocline is derived from advection out of the surface mixed layer. The simulated fields of tracer age and age tendency depend on the radiotracer Péclet number of the flow. Comparison of numerical simulations with the observations leads to estimates of the Péclet number for isopycnal surfaces within the thermocline. Péclet number estimates, using a length scale of 1000 km, vary from 2 in the upper thermocline ( $\sigma_\theta = 26.5$ ) to about 1 in the lower thermocline ( $\sigma_\theta = 27.0$ ). Given the characteristic velocity determined from geostrophy, estimates of lateral diffusivity can be derived (figure 4.9). In the upper thermocline, estimates of the magnitude of lateral diffusivity are consistent with values determined from other methods:  $\kappa_H \approx 1800 \text{ m}^2 \text{ s}^{-1}$ . In the lower portion of the thermocline, however, the estimates of lateral diffusivity based on the temporal evolution of the tritium- $^3\text{He}$  age field exceed other estimates by a factor of 2 - 4:  $\kappa_H \approx 4000 \text{ m}^2 \text{ s}^{-1}$ . Estimates of lateral diffusivity which increase with depth are not consistent with expectations based on the vertical structure of eddy-kinetic energy and, thus, the one-dimensional models of ventilation of the lower thermocline must be rejected. Comparison of this analysis with previous calculations based on measurements of the instantaneous spatial distribution of tracer fields shows the greater sensitivity of a temporal analysis for estimating the magnitude of mixing. The direct effects of mixing in the instantaneous advective-diffusive balance or tritium- $^3\text{He}$  age in the 1980's are small and easily obscured by the uncertainty in measurements of the dominant terms.

The one-dimensional numerical model has been used to examine the sensitivity of the present analysis to the uncertainty of the tritium surface concentration history.

Analysis in §4.5 shows that the diagnosis of the Péclet number of the flow based on the observed temporal tendency of the tritium- $^3\text{He}$  age field is robust to the uncertainties in the  $^3\text{H}$  boundary condition. The decadal-scale evolution of the tritium- $^3\text{He}$  age field observed in the north Atlantic thermocline records the oceanic response to the large addition of bomb-produced tritium to the surface ocean. The net increase in surface mixed layer tritium concentrations is well determined from data; the precise details of the history of the surface tritium concentrations have only a secondary impact on the evolution of tracer age. In contrast to the findings for the evolution of tracer age, calculations of the tritium inventory (both those presented here as well as previous studies) show much greater sensitivity to the precise specification of the history of the tritium boundary condition. Changes in tritium concentrations within the thermocline scale directly with the uncertainty in the boundary condition history.

Prior studies [Rooth and Östlund, 1972; Jenkins, 1980; Fine, Reid and Östlund, 1981; Sarmiento, Rooth and Roether, 1982; Fine, Peterson and Östlund, 1987] have concluded that the penetration of tritium into the thermocline is predominantly an isopycnal process. Additional calculations presented in Appendix C of this thesis support the conclusion that diapycnal effects are second order in the temporal development of the transient tracer fields in the thermocline.

A potential shortcoming of the one-dimensional model is the necessary assumption that all the fluid in the thermocline results from subduction directly from the surface mixed layer. Observational evidence suggests that a majority of the fluid in the lower thermocline recirculates within the subtropical gyre without any direct exposure to surface forcing. In contrast, the upper thermocline ( $\sigma_\theta \leq 26.4$ ) is locally ventilated in eastern gyre. Computation of the pressure-anomaly Montgomery streamfunction [Montgomery, 1937; Zhang and Hogg, 1992] along with independent observational interpretations [Pollard *et al.*, 1996; Klein and Siedler, 1989; Stramma, 1984] suggest that the eastern thermocline is fed by waters flowing eastward from the Gulf Stream



extension, rather than by southward flow from the surface winter mixed layer (§5.1). In such a scenario, transient tracers can only enter the non-locally ventilated layers of the gyre circulation via cross-stream diffusive transport. Chapter 5 explores simulations of ventilation and tracer age in a two-dimensional gyre model that can treat this process. The numerical model employed here is a derivative of one used in previous studies [Musgrave, 1990; Thiele and Sarmiento, 1990; Doney, Jenkins and Bullister, 1997; Jenkins, 1997; Jia and Richards, 1996]. The model configuration is altered to allow a geographical separation between the surface outcrop of an isopycnal and the closed streamlines of the subtropical gyre circulation.

Analysis of a wide parameter range of the two-dimensional model reveals the sensitivity of tritium- $^3\text{He}$  age to the physical process which ventilate the thermocline. If properties within the thermocline are renewed by advective subduction out of the surface mixed layer, the behavior of the eastern region of the gyre model is analogous to the results obtained from the one-dimensional analysis: excessively large lateral diffusivity is required to create the observed tendencies in tracer age. On the other hand, at depths where the isopycnal circulation is carried in a closed recirculation “pool” extending across the entire basin, age within the gyre senses the surface boundary conditions only via lateral diffusion. In that case, the tendency of the tracer age field proves not to be a diagnostic of the magnitude of local lateral mixing, but rather of the diffusive time-scale characterizing the coupling to the surface ocean. Comparison of model simulations with observations suggests that the lower thermocline of the eastern North Atlantic ( $\sigma_\theta \geq 26.9$ ) is not ventilated by direct flow from the surface but rather is diffusively coupled to the surface mixed layer with a time-scale of 5-10 years. Simulations with diffusive coupling alone cannot match the observations in the upper thermocline ( $\sigma_\theta \leq 26.5$ ), however, supporting the conclusions that this level is ventilated predominantly by advective flow directly from the surface ocean.

## 6.2 Comparison of Results with Other Direct Observations of Thermocline Ventilation

### 6.2.1 Advective Ventilation of the Lower Thermocline

Numerous previous studies of lower thermocline ventilation have interpreted the presence of spatial gradients of passive tracers along isopycnals as evidence of advective flow from the surface outcrop: *Pollard and Pu* [1985] examined the oxygen gradients, *Andri , Jean-Baptiste and Merlivat* [1988] studied tritium and *Roether and Fuchs* [1988] looked at tritium- $^3\text{He}$  age. The assumption that advection establishes the property distributions seems to derive from subjective assessment of the spatial structure of the property fields: the tracer distributions show water with properties of recent ventilation spreading away from the region of the surface outcrop (e.g. see the oxygen distribution in figure 5.2). In all the above analyses, lateral diffusive effects were neglected and horizontal velocities were diagnosed directly from the spatial gradients of the tracer fields. Typical estimates of meridional advection are order  $1 \text{ cm s}^{-1}$  at  $\sigma_\theta \approx 27.0$ .

In contrast to the above analyses, the temporal evolution of tritium- $^3\text{He}$  age in the lower thermocline is inconsistent with advective flow from the surface outcrop unless the magnitude of lateral diffusivity at these depths is higher than conventional estimates by a factor of 2 to 4. Rather, the picture presented here is of a buffer region, where diffusive effects are dominant, separating the flow of the subtropical gyre from the surface mixed layer (figure 5.15). Such a scenario still provides for the penetration of surface properties into the lower thermocline, however the spatial gradients of these properties, especially in the region of the outcrop, cannot be interpreted simply as a signature of the advective flow field alone. Figure 6.1 displays results of the numerical gyre model when the outcrop position is placed north of the body of the

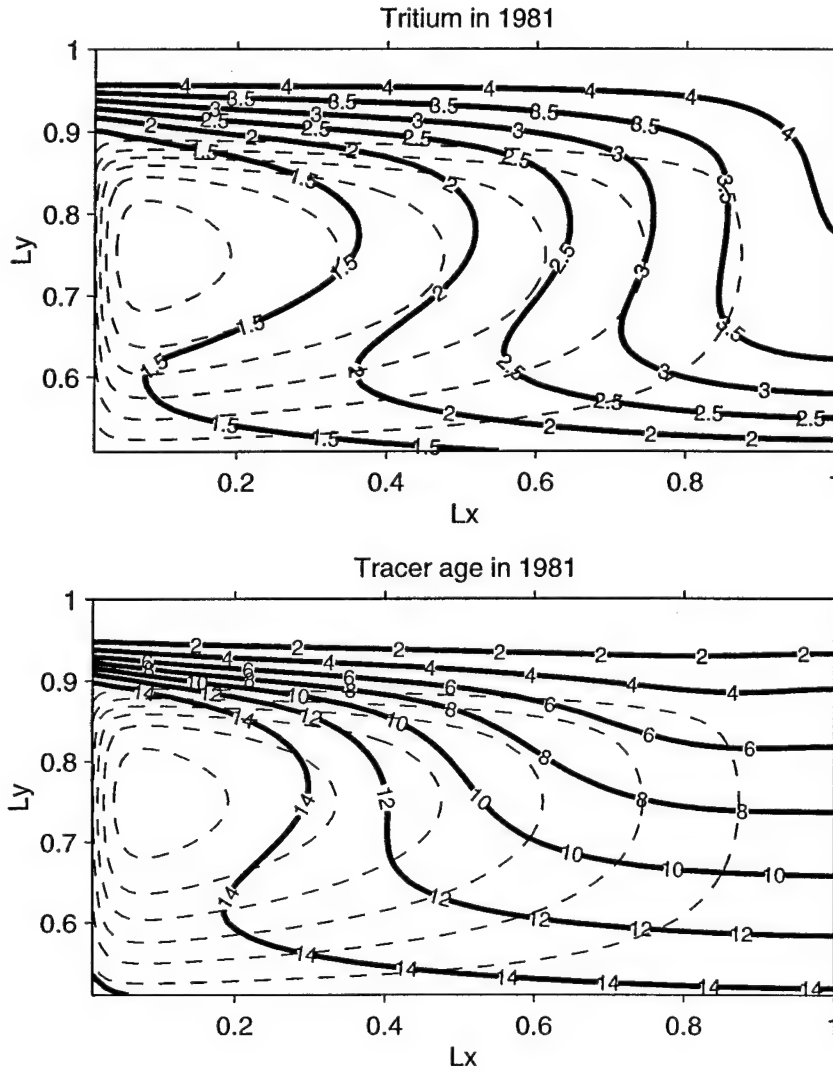


Figure 6.1: Simulated tracer fields of gyre model superposed on streamlines of flow. Tritium (TU) and tracer age (years) are contoured with heavy solid line. Streamline of subtropical gyre are shown as dashed line. The area between  $0.9-0.96L_y$  is essentially stagnant; tracer crosses this region by diffusive transport only. Only the northern half of the model domain is presented. Parameters used for this simulation:  $V = 0.6 \text{ cm/s}$ ,  $\kappa_H = 1500 \text{ m}^2\text{s}^{-1}$ ,  $\gamma = 40$  and,  $y_{outcrop} = 0.96L_y$ . The tritium boundary condition is applied to all points north of the outcrop at  $0.96L_y$ .

subtropical circulation. The tracer gradients in the eastern portion of the basin reveal the spreading of properties from the surface outcrop across the buffer region and into the ocean interior. An interpretation based solely on the distribution of tracers would likely lead to erroneous conclusions of direct southward advection from the surface outcrop. In the vicinity of the surface outcrop, however, the isopleths of tracer age are not perpendicular to the streamlines of the flow field as would be expected for an advectively dominated distribution. Diagnosis of an advective flow from observed tracer age distributions may thus lead to significant misinterpretation, even in regions which appear strongly ventilated.

### 6.2.2 Renewal of Thermocline Waters

The view of thermocline ventilation derived from the temporal evolution of tritium- $^3\text{He}$  age is similar in several respects to that deduced by *Speer and Tziperman* [1992] and *Speer, Isemer and Biastoch* [1995] based on the combination of air/sea buoyancy exchange and tritium inventories. *Speer and Tziperman* [1992] employed estimates of the air/sea transfer of heat and freshwater to estimate the flux convergence/divergence of mass in the surface North Atlantic as a function of density class (figure 6.2). They found that buoyancy exchange with the atmosphere results in net surface convergence of water in the density ranges classically defined as subtropical and subpolar mode waters [*McCartney*, 1982; *McCartney and Talley*, 1982]. In contrast, the density classes associated with the lower subtropical thermocline (e.g.  $\sigma_\theta \approx 27.0$ ) have only a very small net mass source at the surface, implying minimal advective subduction in this density class. This analysis, however, does not rule out the possibility that water of this density could be exposed to the atmosphere, without an associated net cooling, as it circulates along the northern limb of the subtropical gyre.

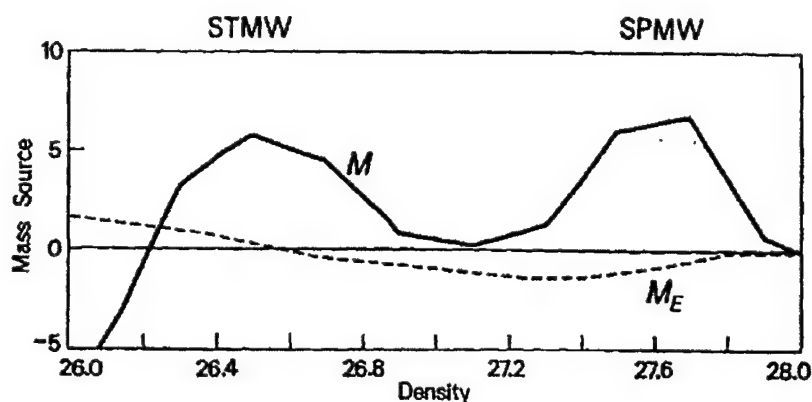


Figure 6.2: Mass source ( $\times 10^6 \text{ m}^3 \text{ s}^{-1}$ ) determined from integral air/sea buoyancy flux as function of density class for North Atlantic (reproduced from *Speer and Tziperman* [1992]). Solid line represents convergence of water in surface mixed layer due to atmospheric buoyancy exchange. Dashed line shows magnitude of Ekman pumping. Fluxes are calculated for density bins of width  $0.1 \sigma_\theta$ .

*Speer and Tziperman* [1992] contrast the view of ventilation implied by mass convergence with the estimates of thermocline renewal based on observed tritium inventories (figure 6.3) [*Sarmiento*, 1983]. *Sarmiento* employed a simple layered model of the thermocline to estimate the exchange time of isopycnal thermocline layers with the surface ocean based on the tritium inventories observed in 1972 [*Sarmiento, Rooth and Roether*, 1982]. Tritium invasion into the lower thermocline was clearly evident in 1972 implying the need for strong ventilation of the deeper isopycnals despite the apparent lack of strong Ekman pumping in the region of their surface outcrop.

Comparison of the figures 6.2 and 6.3 show a consistency between the replacement of waters in the upper thermocline ( $\sigma_\theta = 26.5$ ) and the magnitude of the mass source of water of this density class in the surface mixed layer. The analysis of this thesis also finds that the observed temporal evolution of tritium- $^3\text{He}$  age at this level is most consistent with direct advective subduction from the surface mixed layer with canonical lateral mixing values ( $\approx 1500 \text{ m}^2 \text{ s}^{-1}$ ). In contrast, tritium inventories in the lower thermocline ( $\sigma_\theta = 27.0$ ) also require substantial renewal of water from the surface, however there is no evidence in the analysis of *Speer and Tziperman* [1992]

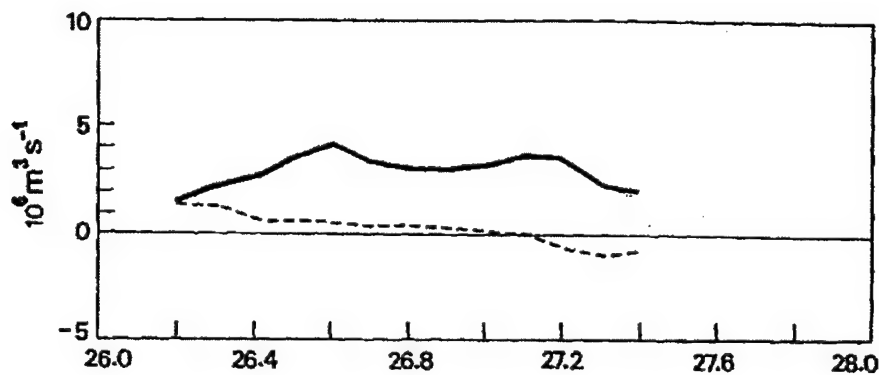


Figure 6.3: Ventilation rate of isopycnals estimated from observed tritium inventory of North Atlantic subtropical thermocline [Sarmiento, 1983] (adaption reproduced from *Speer and Tziperman* [1992]). Solid line shows exchange rate estimated from box model of tritium inventory in thermocline. Dashed line is estimate of Ekman pumping. Fluxes are calculated for density bins of width  $0.1 \sigma_\theta$ .

for a convergence of water in the surface mixed layer to feed the subducting flow. Analysis presented in Chapter 5 illustrates that the renewal of tracer age in the lower thermocline is most consistent with a view of predominantly diffusive exchange with the distant surface mixed layer rather than advective subduction. The predominance of diffusive ventilation of the lower thermocline is consistent with the lack of fluid convergence of this density class in the surface mixed layer. The current work extends the findings of *Speer and Tziperman* [1992] since their method cannot discern between an isopycnal surface which is either diffusively ventilated or directly exposed to the atmosphere without an accompanying convergence of mass. Results presented here rule out the possibility that the majority of recirculating flow in the lower subtropical thermocline is ever directly exposed to the atmosphere within the anticyclonic subtropical gyre. The gyre-model simulations in Chapter 5 show that the observed trends in tritium- $^3\text{He}$  age can only be reconciled with conventional estimates of lateral diffusivity if the connection between the gyre circulation and the surface ocean is limited to diffusive transport across a band of weak mean flow.

## 6.3 Comparison with Models of Thermocline Ventilation

### 6.3.1 Thermocline Theory

Our present understanding of the fundamental dynamics and structure of baroclinic mid-latitude circulation is founded on two complementary analytic theories, both of which are based on the assumption that potential vorticity is conserved along geostrophic streamlines. *Luyten, Pedlosky and Stommel* [1983], hereafter LPS, introduced a layered model of the thermocline in which isopycnals outcrop at the surface ocean. Potential vorticity of a streamline is set when the flow, subducting beneath a lighter layer, leaves contact with the atmosphere. In contrast, the models of *Rhines and Young* [1982a], hereafter RY, consist of stacked layers with only the lightest density class in contact with atmospheric forcing. Lower layers are set in motion when their potential vorticity structure is distorted by flow in the overlying layers: momentum transferred by weak dissipation excites flow along the closed geostrophic contours of the lower layers. The two original theories of LPS and RY provide contrasting views of the fundamental dynamics of subtropical circulation. They were subsequently united [*Pedlosky and Young*, 1983; *Liu et al.*, 1993] and extended to include buoyancy flux [*Luyten and Stommel*, 1986], time dependence [*Dewar*, 1989; *Liu*, 1993], and mixed layers of variable depth [*Huang*, 1989; *Pedlosky and Robbins*, 1991; *Williams*, 1991].

An important extension of the LPS model was accomplished by *Huang* [1989] which achieved solutions for more realistic forcing boundary conditions of the North Atlantic: wind-stress curl, background stratification, and observed winter mixed-layer depth. Examples of flow solutions on isopycnals are illustrated in figure 6.4. The northwest boundary of the subtropical gyre is defined in this analysis by the location of the zero wind-stress curl line. As is evident in the solutions displayed in figure 6.4,

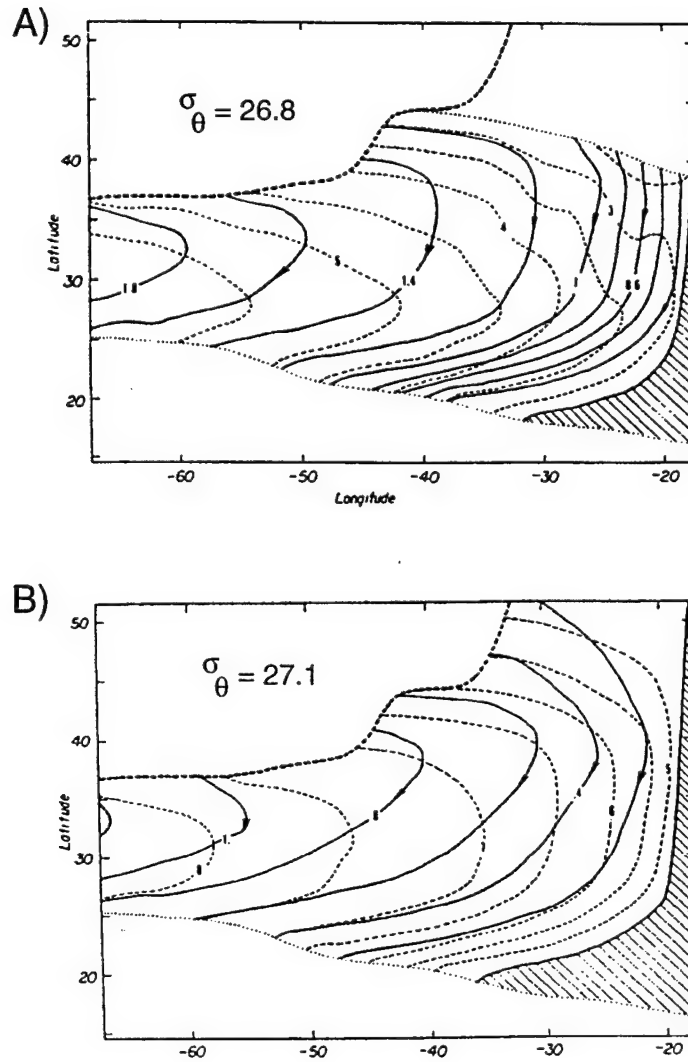


Figure 6.4: Flow patterns on A)  $\sigma_\theta = 26.8$  and B)  $\sigma_\theta = 27.1$  from idealized thermocline model of North Atlantic [Huang, 1989]. Streamlines are represented as solid lines with numbers indicating geostrophic volume fluxes ( $\times 10^6 m^3 s^{-1}$  per  $0.1-\sigma_\theta$  units). Depth (in 100's of meters) of the isopycnal surface is shown as thin dashed line. Heavy dashed line marks the location of the inter-gyre boundary defined by the zero of the wind-stress curl. Dotted lines marked isopycnal outcrops to the north and southern boundary of the model to the south. The shadow zone is designated by the hashed region.



a significant portion of the flow in the lower layers of the thermocline originates from this inter-gyre domain rather than directly from the surface outcrop. The actual origin of this water in the model formulation is not clearly specified but the co-location of the inter-gyre boundary and the Gulf Stream extension suggests that the bulk of this water derives from outflow of the Gulf Stream. Huang refers to the region fed by waters from the inter-gyre boundary as “ventilated” and suggests that “owing to strong eddy activity within the Gulf Stream the outflow water carries strong signals characteristic of the subpolar gyre.” Analysis of hydrography and tritium- $^3\text{He}$  age in Chapter 5 supports the gross features of the isopycnal circulation patterns shown in figure 6.4, however, the interpretation of ventilation is different. In the advective model of Huang, properties on the lower isopycnal layers (e.g.  $\sigma_\theta = 27.1$ ) can only be renewed if the water entering the domain from the inter-gyre boundary is considered to be recently “ventilated”. In the present analysis, however, rather than viewing the water originating from the inter-gyre boundary as “ventilated”, the temporal development of tritium- $^3\text{He}$  age suggests that these isopycnals are predominantly characterized by recirculation with the renewal of surface properties arising by cross-stream diffusion. The entry of surface boundary conditions is likely to occur by a combination of isopycnal outcrops in the northeast corner of the basin as well as cross-stream transfer in the region of the Gulf Stream extension.

The simple advective models of thermocline ventilation based on the original work of *Luyten, Pedlosky and Stommel* [1983] assume that the potential vorticity structure of the fluid is controlled entirely by the advective flow field: effects of diffusion are taken to be negligible. The findings of this thesis, that the effects of lateral mixing are an important process in the ventilation of transient tracers in the thermocline, contradict the *a priori* assumptions of these models. The conclusion that mixing is an important process in the evolution of the observed tracer fields should not be construed as a statement that mixing is the dominant process. While mixing effects are

important, they are still generally smaller than advective effects as seen in the estimates of Péclet number greater than unity (table 4.2), especially in the lighter layers of the thermocline.

Nonetheless, the purely advective models of thermocline ventilation reasonably reproduce the main features of the observed mean density structure of the subtropical gyres of the Atlantic [*Luyten, Pedlosky and Stommel, 1983*], North Pacific [*Talley, 1985*], and South Pacific Oceans [*De Szoeke, 1987*]. This suggests that although mixing influences the potential vorticity of fluid parcels subsequent to subduction, the lateral gradients of potential vorticity are sufficiently weak that the effects of mixing are not first order. One might expect this to be especially the case in the North Atlantic where the lines of winter outcrop tilt towards the southeast. Under these conditions, the spatial gradients of PV in the ventilated region will be small since all of the water leaving the surface mixed layer in a specified density class will have similar initial values of potential vorticity.

Compared to the simple analytic model, the present work results in a distinctly different picture of the flow in the lower portions of the main thermocline (e.g. below  $\sigma_\theta = 26.7$ ) and the interrelation between the mean circulation and ventilation. Whereas models such as LPS and *Huang* [1989] predict ventilation of the lower thermocline by mean advective flow from the surface mixed layer, the results of the tritium- $^3\text{He}$  age analysis combined with analysis of the mean hydrography suggest that these layers are predominantly ventilated by diffusive exchange with the surface ocean (figure 5.15). This discrepancy may result not only from the neglect of lateral mixing in the analytic solutions but also from the differences between the observed mean circulation and the Sverdrup approximation of interior flow implicit in the analytic solutions. The presence of the strong zonal flow of the Azores Current (figure 5.3) results in an observed mean circulation of the eastern North Atlantic which is not predicted from linear vorticity dynamics and the observed surface wind forcing (figure 1.6). Analytic

models of the subtropical gyre lack the Azores Current and the associated isolation of the lower thermocline from direct ventilation.

The suppression of direct ventilation of the lower thermocline by the zonal "short-circuit" of the Azores Current appears to be a feature unique to the North Atlantic basin. Maps of potential vorticity [Keffer, 1985] reveal a different spatial structure in the North Atlantic thermocline compared to other basins of the global ocean. Specifically, the layer defined by  $\sigma_\theta = 26.5$  to  $27.0$  shows a largely homogeneous field in the interior of the North Atlantic, a finding consistent with the closed recirculation gyre extending across the width of the entire basin. In contrast, other subtropical basins (North and South Pacific, South Indian and South Atlantic) reveal tongue-like isopleths of PV originating at the northern edge of the gyre and wrapping anti-cyclonically around the gyre. Keffer's analysis on a deeper density layer ( $\sigma_\theta = 26.0$  to  $27.3$ ) suggests a similar picture: low vorticity mode waters penetrate and fill all the subtropical basins except the North Atlantic where the southward penetration of the low PV is arrested at the latitude of the Azores Current. The PV of the water of this density class in the interior of the North Atlantic appears to be a mixture of the convectively formed low-PV mode water and higher-PV water originating from the western boundary current. In other ocean basins, the low-PV mode water appears to spread easily into the majority of the subtropical domain. The cause of the differing thermocline ventilation scenario in the North Atlantic remains an open question. Perhaps the superposition of the overturning thermohaline circulation perturbs the basic mean flow of the subtropical gyre and especially the relation between the formation of mode waters and the wind-driven circulation.

## Numerical Experiments

The fundamental ideas proposed in these simple analytic thermocline models have been tested in a series of numerical experiments. In the first comparative experiments, *Cox and Bryan* [1984] found broad similarity in the results of a numerical simulation and the analytic theory; specifically they were able to identify the three predicted regions of the LPS solution: the ventilated region, the pool, and the shadow zone. *Cox* [1985] next examined a higher resolution numerical model which permitted mesoscale eddies. While the presence of eddies had little effect on the pattern of mean flow, the distribution of passive tracers and potential vorticity was significantly altered. The lateral mixing due to eddy motions blurs the distinction between the directly ventilated region and the closed “pool”: the ventilation age of fluid in the pool was significantly reduced. Whereas homogenization in the analytic models of RY results from weak diffusion over long time-scales, the numerical model shows evidence of tracer homogenization on much shorter time-scales. The results of the analysis presented in this thesis agree with the conclusions of the eddy-resolving numerical model: diffusive time scales are comparable to advective time scales for the ventilation of the eastern subtropical thermocline. The assumption of weak dissipation is not supported by the observed evolution of the tritium- $^3\text{He}$  age.

Isopycnic eddy stirring in the thermocline was further detailed in *Böning and Cox* [1988] which explored the Lagrangian behavior of particles in the same eddy-resolving numerical model. Based on the statistics of the simulated particle dispersion, they calculate the effective diffusivity and Péclet number of the model flows. Their reported values of diffusivity ( $\kappa_{xx} = 8000$ ,  $\kappa_{yy} = 3000 \text{ m}^2\text{s}^{-1}$ ) are comparable to those found in the one-dimensional simulations in Chapter 4 but large compared to most other estimates. Their estimate of the Péclet number of the thermocline varied from 4 to 2, with values decreasing with depth. The general numerical agreement between the diagnosed mixing strength of the eddy-resolving model and those estimated here

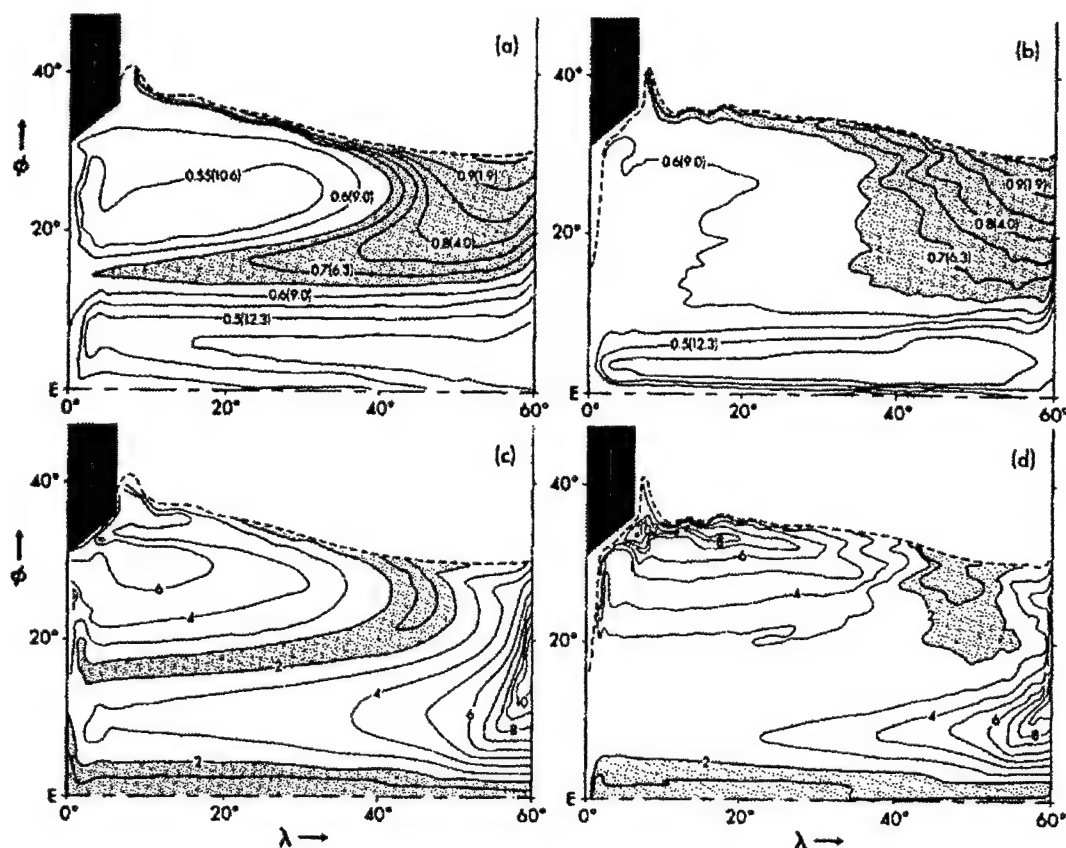


Figure 6.5: Potential vorticity and tracer age evaluated on  $\sigma_\theta = 26.0$  in a numerical model of the ventilated thermocline (reproduced from *Cox* [1985]). Tracer age (ventilation time in years in parenthesis) for (a) coarse model resolution, (b) eddy-permitting model. Potential vorticity ( $10^{-9} \text{ cm}^{-1} \text{ s}^{-1}$ ) for (c) coarse model resolution, (d) eddy-permitting model.

from the tritium- $^3\text{He}$  age suggest that the eddy-resolving simulations of *Cox* [1985] accurately portray the eddy diffusion effects on the real oceanic distributions of passive tracers.

While the above numerical model experiments focus on the description of the ventilation of the upper thermocline ( $\sigma_\theta = 26.0$ ), recent analysis of a primitive equation model of the North Atlantic [*Williams, Spall and Marshall*, 1995] include maps of tracer ventilation in the lower thermocline. As in the original experiments of *Cox*, *Williams, Spall and Marshall* [1995] perform dual experiments with an eddy-resolving and

coarse resolution numerical model. In the coarse resolution study, the lower thermocline ( $\sigma_\theta = 27.0$ ) is ventilated solely by a thin plume along the eastern boundary. When eddies are permitted, ventilation of the lower thermocline is dramatically enhanced and tracer penetration is evident across the entire longitudinal extent of the gyre. Though not discussed in their paper, the later scenario is clearly more consistent with the observed tritium distributions of the lower thermocline. As such, the numerical simulations of *Williams, Spall and Marshall* [1995] are consistent with the conclusions of Chapter 5 that ventilation of the lower thermocline is predominantly mediated by a lateral diffusive transport across the northern boundary of the gyre.

### 6.3.2 Simulations of Transient Tracers in General Circulation Models

Recent attempts to simulate observed transient tracer distributions in general circulation models of the North Atlantic have highlighted the importance lateral mixing by mesoscale eddies. *Jia and Richards* [1996], hereafter JR, attempted to simulate the  $^3\text{H}$  and  $^3\text{He}$  age distributions in an isopycnic model of the North Atlantic [*New et al.*, 1995]. The Atlantic Isopycnic Model (AIM) is an implementation of the MICOM model [*Bleck et al.*, 1992] consisting of 20 vertical layers and a  $1^\circ$  horizontal grid resolution. Mesoscale eddies are not resolved and there is no prescribed diapycnic diffusion. The lateral diffusivity of the AIM model is set to  $1000 \text{ m}^2 \text{ s}^{-1}$ .

Two diagnostics are used to compare transient tracer observations with the output of the numeric model: tritium distributions in 1972 [*Sarmiento, Rooth and Roether*, 1982] and tritium- $^3\text{He}$  age in 1981 [*Jenkins*, 1988a]. An initial simulation using the off-line model flow field results in unrealistic tracer distributions in the lower subtropical thermocline: compared to observed fields, the simulated tritium- $^3\text{He}$  age shows weaker gradients and the tritium inventory displays unobserved subsurface

maxima. In an attempt to understand the shortcomings of the isopycnic model, JR conducted a series of experiments using a two-dimensional gyre model similar to those discussed in Chapter 5. Their key finding is that the Péclet number of the AIM isopycnic model is much too large to accurately simulate the observed transient tracer fields. Based on their analysis of the two-dimensional gyre model, they estimate the maximum value of the Péclet number consistent with the observed transient tracer fields is 3.3 ( $L = 1000$  km).<sup>a</sup> In contrast, calculations of the Péclet number of the AIM model thermocline (table 6.1) vary from 40 in the upper thermocline to 10 in the lower.

Layer	Potential Density	Model Péclet	% ventilation
8	26.55	40	70
10	26.85	20	65
12	27.15	10	40

Table 6.1: Péclet number estimates at different levels of of Atlantic isopycnic numerical model from *Jia and Richards* [1996]. Péclet number is estimated from ratio of advective and diffusive time scale assuming a characteristic length of 1000 km. Right-hand most column shows the fraction of the isopycnal layer renewed by direct contact with surface ocean.

JR conclude that in order for the AIM model to accurately reproduce the observed  $^3\text{H}$  and  $^3\text{He}$  fields, the diffusivity must be increased to order  $10,000 \text{ m}^2\text{s}^{-1}$ . In part, JR note that the large magnitudes of diffusivity may partially be an artifact of overly swift advective rates in the model, however, this alone cannot account for the entire discrepancy. Their conclusions are analogous to the results of Chapter 4: large magnitudes of lateral mixing (small Péclet numbers) are required to simulate the observed temporal development of tritium- $^3\text{He}$  age. Indeed, comparison of the estimated ventilation Péclet number in Chapter 4 (table 4.2) shows agreement with

<sup>a</sup> *Jia and Richards* [1996] report the values of Péclet number based on a length-scale equal to the size of the model domain: 6000 km. All of their values reported in this work are scaled using a length-scale of 1000 km to allow direct comparison with the estimates of this study.

the maximum permissible values estimated by JR, 3.3. The one-dimensional model analogy is appropriate when the bulk of the fluid in the thermocline originates from water in the surface mixed layer. This is the case in the AIM model: the eastern subtropical thermocline is well ventilated by direct advective flow from the surface (table 6.1).

The results presented in Chapter 5 of this thesis offer an alternative explanation for the failure of the AIM model to simulate the transient tracer distributions in the lower thermocline. Numerical simulations have shown that the low Péclet number required to reproduce the transient tracer fields results from the assumption that the lower thermocline is ventilated by direct advection from the surface. If the lower thermocline is coupled to the surface ocean via a band of diffusively mediated transports, the observed tracer fields can be reconciled with numerical models characterized by more conventional magnitudes of lateral diffusivity (e.g. order  $10^3 \text{ m}^2\text{s}^{-1}$ ). Since tracer age distributions are sensitive to the relative effects of advection and diffusion, accurate simulation of the mean advective flow is a prerequisite for determination of the magnitude of lateral mixing. Sensitivity of transient tracer fields to advective-diffusive effects will be further discussed in §6.4.

### 6.3.3 Comments on Fickian Parameterization of Mixing

The numerical simulations used in both Chapters 4 and 5 have assumed a Fickian diffusion parameterization for the isopycnic mixing of tracers. Fickian diffusion equates the flux divergence of a property,  $S$ , due to the correlation of the time-dependent eddy field to a function based on the local mean field:

$$-\nabla \cdot \overline{u'S'} = \kappa \nabla^2 \overline{S} \quad (6.3.1)$$

While an assumption of homogeneous, isotropic lateral diffusivity is typical for coarse-resolution models of the ocean, numerical experiments which do permit mesoscale



eddy variability have revealed clear deficiencies of this local Fickian parameterization in many situations. Additionally, observations of float dispersal in the ocean reveal evidence for an inhomogeneous, anisotropic field of effective diffusivity [Spall, Richardson and Price, 1993; Böning, 1988]. A review of prior work examining the simulation of lateral mixing in coarse resolution oceanic models will not be undertaken here. Rather, I will discuss a few numerical experiments specifically examining the impact of eddy-resolution on the simulation of transient tracer ventilation.

As discussed in the previous section, the comparison of tracer ventilation between a coarse resolution and eddy-resolving model of the North Atlantic [Williams, Spall and Marshall, 1995] revealed enhanced ventilation of the lower thermocline when the action of mesoscale-eddies was resolved. It is unclear from their analysis if the increased ventilation of the lower thermocline in the presence of eddies is due to: A) a stronger effective diffusivity or B) a lateral eddy-flux which is not well characterized by a homogeneous Fickian parameterization of mixing. A similar assessment can be made based on simulation of bomb  $^{14}\text{C}$  in the North Atlantic [Follows and Marshall, 1996]. Comparison of coarse resolution ocean model with an eddy-permitting version shows a substantial improvement in the ventilation of bomb  $^{14}\text{C}$  in the lower thermocline when eddies are present in the model. The enhanced ventilation is likely due to the combination of a larger, mean diffusivity as well as spatial variations in the effective diffusivity in the region of the Gulf Stream [Follows, *personal communication*].

Figueroa [1994] carefully examined the transport of passive tracers by mesoscale eddies in a comparison of idealized models of a double gyre circulation. This study focused on the inter-gyre transport of properties across the meandering frontal region separating the two gyre domains. To the extent that this is analogous to transport of tracers across the meandering Azores Current, the results of this study have direct bearing on the interpretation of coarse-resolution simulations performed in this thesis. Figueroa found significant differences in the magnitude of cross-gyre exchange

of tracer when the effects of eddies were explicitly resolved by the grid-scale of the ocean model. The presence of mesoscale eddies increased the effective diffusive exchange across the front with the majority of the enhancement due to eddy correlations between the velocity and tracer anomaly fields. His study concludes that coarse resolution models with homogeneous diffusivity will fail to simulate accurately the inter-gyre transport of tracers.

This thesis has examined the ventilation of isopycnal surfaces which outcrop south of the boundary separating the subpolar and subtropical gyre. Although this ventilation is not strictly "inter-gyre", the mean hydrography of the region indicates that the Azores Front/Current separates the lower thermocline from the region of surface outcrop; the net meridional flow across this front is small. One-dimensional models of thermocline ventilation (Chapter 4) were rejected because the lateral diffusivity determined from the observed transient tracer evolution appeared unacceptably large. The simulations of *Figueroa* [1994] suggest the possibility that the seemingly large diffusivity requirements of the one-dimensional models could stem from mesoscale, cross-frontal fluxes not included in the homogeneous Fickian parameterization of the models used here.

## 6.4 Remarks on Information Content of Tracer Age Observations

This thesis has demonstrated that the temporal development of the diagnostic tritium- $^3\text{He}$  age shows large sensitivity to the relative effects of mixing and advection for the ventilation of the thermocline. It is likely that similar conclusions could have been reached using an approach that focused on character of the the tracer fields of the individual components  $^3\text{He}$  and tritium. The sensitivity of the tritium- $^3\text{He}$  age field

demonstrates, however, that the observed dependence on mixing is a property of the information that is contained in the combination of the two individual tracer fields. Analysis based solely on one transient tracer component, such as measures of tritium inventory (§4.4), do not show a similar robustness to the mechanisms of the physical processes ventilating the ocean. Tritium- $^3\text{He}$  age is a convenient diagnostic which captures the combination of information recorded in the radioactive mutation of  $^3\text{H}$  into  $^3\text{He}$ .

The analysis of this thesis combined with the discussion in §6.3.2 demonstrates that estimates of eddy diffusive effects based on the observations of the coupled tracers  $^3\text{He}$  and tritium are sensitive to the geometry and magnitude of the mean advective field. Somewhat surprisingly, in the case of tritium- $^3\text{He}$  age, a model which overestimates the magnitude of advective communication from the surface outcrop, also requires a overly large magnitude of lateral diffusivity (e.g. the one-dimensional models of Chapter 4 and analysis of JR). It might be expected that overestimating one of these transports (advection) would lead to an underestimate of the other (diffusion). This would be true for estimates of ventilation based on tracer inventory since it is the sum of the two processes (mixing and advection) which transports tracer from the surface ocean into the shielded layers of the thermocline (§ 4.4.2). Indeed, ventilation estimates based on tritium inventory [*Sarmiento*, 1983; *Wunsch*, 1988a] resolve the **net** exchange between the thermocline and the surface ocean but cannot resolve the individual contributions of advection and diffusion.

For the temporal development of coupled transient tracers, however, mixing and advection create distinct consequences on the relation between the  $^3\text{H}$  and  $^3\text{He}$  distributions: the two tracer fields remain tightly coupled only in strongly advective flows. Scale analysis in this thesis demonstrates the evolution of a diagnostic based on the coupled relation between two transient tracers (e.g. a tracer age) is sensitive to the Péclet number which measures the **relative** contributions of mixing and advection

rather than their sum. Therefore, if a model is biased by overly strong advective effects, as in the one-dimensional models in Chapter 4 and the GCM simulations of JR, the effects of mixing will need to be correspondingly strengthened to maintain the proper proportion of the two effects.

The distinct types of information content in the ventilation of transient tracers can be summarized as follows:

- **Transient tracer inventory** contains information about the *sum* of advective and diffusive transport. Both advection and mixing carry a transient tracer from the surface ocean into the interior. Diagnostics based solely on observed inventories of transient tracers cannot distinguish between effects of mixing and advection.
- **Transient tracer age** (or any quantity defined by the ratio of two coupled transient tracers) contains information about the relative strengths of advection and diffusion: deviations in behavior of observed fields from that expected assuming solely advection (tight coupling) are a diagnostic of relative impact of mixing.

The manifestation of diffusion on the coupling between  $^3\text{H}$  and  $^3\text{He}$  is evident in the earlier work of *Jenkins* [1988a], *Musgrave* [1990], and *Doney, Jenkins and Bullister* [1997]. All these studies found that relation between  $^3\text{He}$  and tritium served as a useful diagnostic of the bulk Péclet number of the ocean (e.g. see figure 6.6). The observed property-property relation differs from the relation expected for a highly advective system. The research presented in this thesis extends the previous property-property analysis. Inclusion of measurements across many years contributes information of the temporal change of the tracer fields. Temporal changes are evident in  $^3\text{H}$  -  $^3\text{He}$  plots constructed for the subtropical North Atlantic (figure 6.7), however determining a diagnostic to measures this shift is problematic: the property-property relation is a

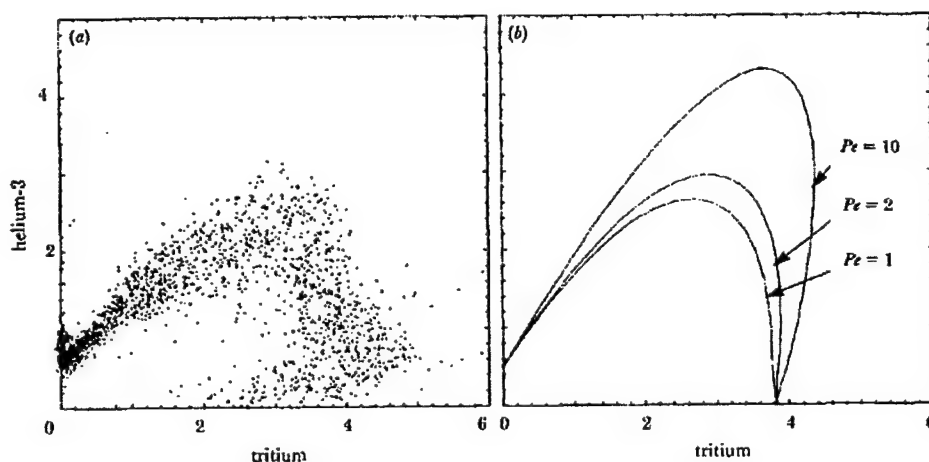


Figure 6.6: Tritium- $^3\text{He}$  relation in North Atlantic reproduced from *Jenkins* [1988a]: a) data at all depths from TTO and TAS programs. b) calculation from one-dimensional model for various radiotracer Péclet numbers.

complex curve and much of the change in the relation is due to the reduced inventories of tritium caused by decreasing value of the tritium surface boundary condition.

The diagnostic employed in this study is the relation between the tracer age field and the temporal tendency of the tracer age field (e.g. 4.8). Like the tritium- $^3\text{He}$  relation, the relation between  $\tau$  and  $\frac{\partial \tau}{\partial t}$  measures the coupling between  $^3\text{H}$  and  $^3\text{He}$  fields and thereby records information about the effects of diffusion. The diagnostics used in this study, however, offer two important advantages over previous work based on the tritium- $^3\text{He}$  relation. Firstly, calculation of tritium- $^3\text{He}$  age depends only on the ratio of  $^3\text{He}$  and tritium and thereby minimizes the effects of changes in total tracer inventory caused by the reductions in surface concentrations of tritium over time. Secondly, calculation of the temporal tendency of the tracer age field directly incorporates information about the temporally-evolving relation between  $^3\text{He}$  and tritium. Evidence of diffusive effects become apparent in the discrepancy between observed tracer age and that expected for an ideal advective age. Although the difference between these two measures of age may be difficult to detect in a single snapshot of the *spatial* tracer distribution, simple models of oceanic ventilation demonstrate that mixing effects should be clearly evident in the *temporal* evolution of the tracer age

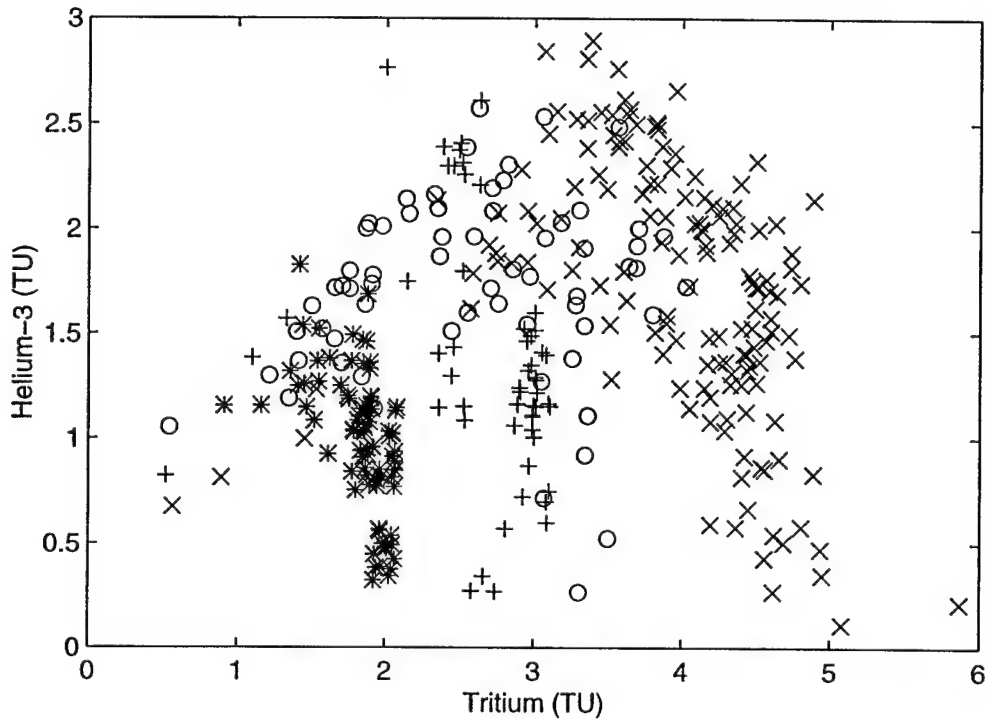


Figure 6.7: Temporal evolution of  $^3\text{He}$ -tritium relation in subtropical thermocline. Data on the isopycnal surface  $\sigma_\theta = 26.8$  is shown for four time periods: x:1978-82, o:1982-86, +:1986-90, and \*:1990-94.

field. Therefore, a diagnostic which records the temporal change in the tritium- $^3\text{He}$  relation provides a means for estimating the bulk effects of mixing.

## 6.5 Directions of Future Work

This thesis has presented the first analysis of the temporal evolution of transient tracer age in the subtropical thermocline. The fundamental conclusion is that the discrepancy between the observed evolution of the tritium- $^3\text{He}$  age field and that expected for a purely advective age provides a measure of the relative balance of advection and diffusion in the ventilation of the upper ocean. The analysis introduced here could be extended in several directions.

This work has compared diagnostics of the observed transient tracer distributions with the output of simple numerical simulations. The parameters of the numerical models were systematically varied to examine the sensitivity of the diagnostics to a range of physical circulation regimes. A more exact determination of the range of lateral diffusivities consistent with the observed transient tracers could be obtained by casting the analysis as an inverse problem. As discussed in §1.4.2, a formal linear terminal constraint problem can only incorporate the individual tracer components,  $^3\text{He}$  and tritium, rather than the tracer age. Such a problem involves parameter estimation in a non-linear model since features of the flow field (diffusivity, velocity) are included as unknown parameters of the problem. Formulation of so-called "eclectic" models require numerous subjective and scientific decisions during their construction and analysis. The analyses presented in this thesis serves as the preliminary basis for the more formal problem. The present use of tritium- $^3\text{He}$  age and comparison with the dissolved oxygen field has provided a clear demonstration that the coupled temporal evolution of  $^3\text{H}$  and  $^3\text{He}$  cannot be explained by temporal trends in the rate of ventilation. Furthermore, sensitivity of the tracer observations to the details of the upstream model configuration (Chapters 4 and 5) highlight additional issues involved in formulating the inverse problem: overestimates of the direct advective ventilation of the thermocline will lead to overly large requirements of lateral diffusivity.

Previous numerical simulations of transient tracers have found the spatial distribution of tracers depends on model resolution. Models with sufficient resolution to permit mesoscale eddy motions appear to more rapidly ventilate the lower thermocline. It is currently unclear to what extent this enhancement is due to either A) a systematic underestimate of the magnitude of lateral mixing in coarse-resolution models or B) mesoscale dynamics which are not well simulated by homogeneous Fickian diffusion. Further examination of transient tracers, and especially the temporal evolution of tracer age fields, in eddy-permitting numerical simulations would be helpful

for understanding the communication between the thermocline and the surface mixed layer.

Finally, this work has emphasized the importance of observations of the relative concentrations of tracers whose expected time-histories are coupled. The discrepancy between the observed tracer ratios and that expected in a purely advective system provides a measure of mixing effects. This thesis has focused solely on the tracer pair of  $^3\text{He}$  and tritium. The analysis developed here could be extended to other transient tracer systems such as CFCs or  $^{14}\text{C}$ . The advective-diffusive balance equation for CFC-age contains a nonlinear mixing term which is expected to behave quite differently from that for tritium- $^3\text{He}$  age [Doney, Jenkins and Bullister, 1997]. Scale analysis in Chapter 4 demonstrates that the time-scale over which a tracer-defined age field is distorted depends on the time-scale of the surface forcing condition as well as the intrinsic time-scale of the tracer system (e.g. the radiodecay time-scale). Tracer ages based on multiple component systems have the potential to record the manifestation of oceanic processes over a wide range of time-scales.



# Appendix A

## Climatological Hydrographic Atlas

The distribution of  $^3\text{He}$  and  $^3\text{H}$  measurements presented in this thesis is sparse in both space and time. Interpretation of the large-scale setting of the transient tracer data has been supplemented with a hydrographic atlas of temperature, salinity and oxygen measurements. The atlas data is used for preparing maps of property distributions along isopycnal surfaces and for calculation of geostrophic velocity.

The hydrographic atlas consists of data from two sources. The first source is the compiled North Atlantic climatology [*Lozier, Owens and Curry, 1995*] based on data archived at the National Oceanic Data Center. As part of the analysis of the Subduction Experiment, this original climatology was supplemented with data from recent cruises in the eastern North Atlantic. Cruise information of data added to the *Lozier, Owens and Curry* [1995] is summarized in table A.1. In addition to data from the specific cruises listed, 1374 additional CTD casts from this region were extracted from archived data at Woods Hole Oceanographic Institution and Scripps Institution of Oceanography.

Ship	Cruise	Dates	No. stations
<i>F/S Meteor</i>	04	10/28 - 11/29/1986	48
<i>F/S Meteor</i>	06	11/03 - 11/27/1987	38
<i>F/S Meteor</i>	09	01/03 - 02/03/1989	81
<i>F/S Meteor</i>	11	10/25 - 11/01/1989	6
<i>F/S Meteor</i>	14	09/23 - 10/04/1990	13
<i>F/S Meteor</i>	44	01/13 - 01/15/1977	2
<i>F/S Meteor</i>	46	12/05 - 12/09/1977	3
<i>F/S Meteor</i>	53	04/02/1980	1
<i>F/S Meteor</i>	56	10/16 - 10/17/1980	2
<i>F/S Meteor</i>	60	03/20 - 04/10/1982	27
<i>F/S Meteor</i>	64	04/17 - 05/05/1983	23
<i>F/S Meteor</i>	69	10/21 - 11/21/1984	52
<i>F/S Poseidon</i>	124	11/07 - 12/03/1985	43
<i>F/S Poseidon</i>	182	05/24 - 05/28/1991	36
<i>F/S Poseidon</i>	189	01/21 - 02/06/1992	16
<i>F/S Poseidon</i>	200	07/12 - 07/14/1993	4
<i>F/S Polarstern</i>	8	10/01 - 10/11/1985	11
<i>F/S F. Heincke</i>	2092	01/12 - 01/29/1992	25
<i>F/S Alexander von Humboldt</i>	692	09/10 - 09/24/1992	57
<i>R.R.S. Charles Darwin</i>	58	05/04 - 05/14/1991	17
<i>R.R.S. Charles Darwin</i>	59	05/28 - 05/29/1991	8
<i>R.R.S. Charles Darwin</i>	68	05/08 - 06/08/1992	44
<i>R.R.S. Charles Darwin</i>	73	09/30 - 10/26/1992	58
<i>R.R.S. Charles Darwin</i>	78	04/23 - 05/20/1993	241
<i>R/V Oceanus</i>	240/2	05/18 - 06/02/1991	66
<i>R/V Oceanus</i>	250/4	03/26 - 04/22/1992	155
<i>R/V Oceanus</i>	254/2	09/24 - 10/18/1992	51
<i>R/V Oceanus</i>	254/3	10/29 - 11/16/1992	133
<i>R/V Oceanus</i>	254/4	11/29 - 12/14/1992	6
<i>R/V Oceanus</i>	258/3	05/15 - 06/14/1993	75
<i>R/V Seward Johnson</i>	9404	10/18 - 10/27/1994	33
<i>C.S.S. Hudson</i>	93053	04/08 - 05/14/1993	165
<i>C.S.S. Hudson</i>	92014	05/28 - 06/03/1992	11
<i>Hesperides</i>	06/3	07/21 - 08/16/1992	59
<i>SRS Dmitrii Mendeleev</i>	46/2	10/06 - 11/09/1991	55
<i>SRS Professor Shtokman</i>	P4-31/1	10/11 - 10/23/1993	35
<i>SRS Akademik Vernandski</i>	43/1	07/10 - 08/02/1991	77

Table A.1: Summary of CTD data added to climatological hydrographic atlas

## Appendix B

# Scale Analysis and an Analytic Model of Tracer Age Equation

### B.1 Scale Analysis

Previous empirical studies of the dominant balance of the tritium- $^3\text{He}$  age advective-diffusive balance have been based on measurements collected after 1980. In this section I will use a non-dimensionalized form of the age equation along with the known history of the tritium surface boundary condition to estimate how the dominant balance has evolved since the time of bomb-tritium injection (early 1960's) to the present. The advective-diffusive balance equations for  $^3\text{H}$  and  $^3\text{He}$ ,

$$\frac{\partial[^3\text{H}]}{\partial t} + u \frac{\partial[^3\text{H}]}{\partial x} - \frac{\partial}{\partial x} \left( \kappa \frac{\partial[^3\text{H}]}{\partial x} \right) = -\lambda[^3\text{H}] \quad (\text{B.1.1})$$

$$\frac{\partial[^3\text{He}]}{\partial t} + u \frac{\partial[^3\text{He}]}{\partial x} - \frac{\partial}{\partial x} \left( \kappa \frac{\partial[^3\text{He}]}{\partial x} \right) = +\lambda[^3\text{H}] \quad (\text{B.1.2})$$

can be cast in non-dimensional form by defining new variables with unit magnitudes determined by the characteristic scales of the problem. In this analysis, only the one-dimensional form of the equations is presented but the results are readily generalized

to two- or three-dimensions. Choosing a characteristic velocity scale,  $V$ , and a characteristic time scale set by the radioactive decay time of tritium,  $\lambda^{-1}$ , one gets the following new variables:

$$\begin{aligned} u^* &= \frac{u}{V}, \\ t^* &= \lambda t, \\ x^* &= \frac{\lambda}{V} x. \end{aligned}$$

The advective-diffusive equations for  $^3\text{H}$  and  $^3\text{He}$  then become

$$\frac{\partial [^3\text{H}]}{\partial t^*} + u^* \frac{\partial [^3\text{H}]}{\partial x^*} - \frac{\partial}{\partial x} \left( \frac{1}{Pe} \frac{\partial [^3\text{H}]}{\partial x} \right) = -[^3\text{H}] \quad (\text{B.1.3})$$

$$\frac{\partial [^3\text{He}]}{\partial t^*} + u^* \frac{\partial [^3\text{He}]}{\partial x^*} - \frac{\partial}{\partial x} \left( \frac{1}{Pe} \frac{\partial [^3\text{He}]}{\partial x} \right) = [^3\text{H}] \quad (\text{B.1.4})$$

where the radiotracer Péclet number is defined, following *Jenkins* [1988a], as

$$Pe = \frac{V^2}{\kappa \lambda}. \quad (\text{B.1.5})$$

The radiotracer Péclet number differs from the more traditionally defined Péclet number,  $\frac{UL}{\kappa}$ , owing to the use of the time scale of the tracer decay to eliminate the characteristic length scale.

The non-dimensional form of the tritium- $^3\text{He}$  age becomes:

$$\tau^* = \log_e \left( \frac{[^3\text{H}] + [^3\text{He}]}{[^3\text{H}]} \right) \quad (\text{B.1.6})$$

where the decay time scale,  $\lambda$ , has now vanished because non-dimensional time has been scaled by this quantity. A non-dimensional form of the advective-diffusive balance equation for tritium- $^3\text{He}$  age can now be derived following the argument outlined in Appendix A of *Jenkins* [1987]:

$$\tau_i^* + u^* \tau_x^* - \left( \frac{1}{Pe} \tau_x^* \right)_x - \frac{1}{Pe} \left( \frac{[^3\text{H}] + [^3\text{He}]}{[^3\text{H}]} \right)_x \tau_x^* = 1 \quad (\text{B.1.7})$$

where the subscripts now represent partial derivatives against the non-dimensional variables. For purposes of generality of the derivation, the Péclet number is allowed

to vary spatially in order to accommodate possible spatial changes in diffusivity. The rightmost term of the l.h.s represents a nonlinear mixing term dependent on the gradients of the fields of  $^3\text{H}$  and  $^3\text{He}$ . This term is proportional to  $\tau_x^*$  and thus acts as a pseudo-velocity.

Combining the "velocity-like" terms in equation B.1.7 yields

$$\tau_t^* + \left[ u^* - \left( \frac{1}{Pe} \right)_x - \frac{1}{Pe} \left( \frac{[^3\text{H} + ^3\text{He}]_x}{[^3\text{H} + ^3\text{He}]} + \frac{[^3\text{H}]_x}{[^3\text{H}]} \right) \right] \tau_x^* - \frac{1}{Pe} \tau_{xx}^* = 1. \quad (\text{B.1.8})$$

For the analysis below, it is convenient to define two quantities based on the terms of the above equation. The first term is the effective velocity of the physical circulation. This is the resultant velocity field which acts on all tracers (linear or non-linear), defined as the sum of the advective velocity and the spatial gradients in the field of diffusivity:

$$u_0 = u^* - \left( \frac{1}{Pe} \right)_x. \quad (\text{B.1.9})$$

Based on the analysis in Chapter 3, I will assume that the physical circulation,  $u_0$  is steady with time. Temporal changes in the circulation, if known, are easily added to the time-dependent analytic model developed below. The second notational convenience is to express the term containing all the gradient information of  $^3\text{H}$  and  $^3\text{He}$  as a simple parameter:

$$\alpha(x, t) = \frac{[^3\text{H} + ^3\text{He}]_x}{[^3\text{H} + ^3\text{He}]} + \frac{[^3\text{H}]_x}{[^3\text{H}]}. \quad (\text{B.1.10})$$

Equation B.1.10 shows that  $\alpha(x, t)$  incorporates the effects of the spatial inhomogeneity of the transient tracer concentrations in the ocean. As illustrated in the simple examples of § 1.3.3, the effects of mixing in the presence of large spatial differences in tracer concentration can lead to significant bias in the estimate of age determined from transient tracer ratios. The parameter  $\alpha$  is taken to be time-dependent since the spatial gradients of tritium and  $^3\text{He}$  are expected to evolve with time in response to the relatively rapid increase in surface tritium values resulting from the hydrogen bomb detonations.

Two special cases of the dominant balance of equation B.1.8 will be discussed below: the case for steady state tritium boundary conditions and the case for rapidly increasing tritium boundary conditions. These cases serve as two extremes in the history of the tritium- $^3\text{He}$  age field in the subtropical thermocline to the entry of the large amounts of tritium resulting from the atmospheric bomb tests. The first case, steady-state boundary conditions for tritium, is an approximation of the transient tracer fields in subtropical thermocline for the periods both before the bomb-tritium input and for times long after the peak tritium perturbation. The second case, rapidly changing tritium boundary condition, is an idealization of the response of the tritium- $^3\text{He}$  age field to the sudden increase in tritium concentrations in the 1960's. For times soon after the peak input, the large increase in tritium concentrations will only impact the youngest, most rapidly ventilated waters. Older waters will have lower tracer concentration resulting in large spatial gradients of tracer concentration and thus, large positive values for the simplified parameter  $\alpha(x, t)$ .

One further simplification will be made regarding equation B.1.8: the Laplacian term,  $\tau_{xx}^*$ , will be neglected. Observations of the oceanic tritium- $^3\text{He}$  age field reveal small curvature in the age field within the thermocline (Analysis in §2.2.2 and *Jenkins* [1987], *Jenkins* [1997]). A small curvature is not surprising given the strong inhomogeneous term, 1, which leads to uniform increases of age with time and creates a largely planar distribution of age in the ventilated regions of the ocean.

### B.1.1 Case I: Steady State

First, consider one-dimensional flow on a semi-infinite domain for  $x > 0$ . Assume that  $u_0 > 0$  and that the boundary conditions for tritium- $^3\text{He}$  age and  $^3\text{He}$  at  $x = 0$  are fixed. This case is analogous to the simple mixing example illustrated in figure 1.4. To evaluate the terms in equation B.1.8 requires estimates of the normalized gradients

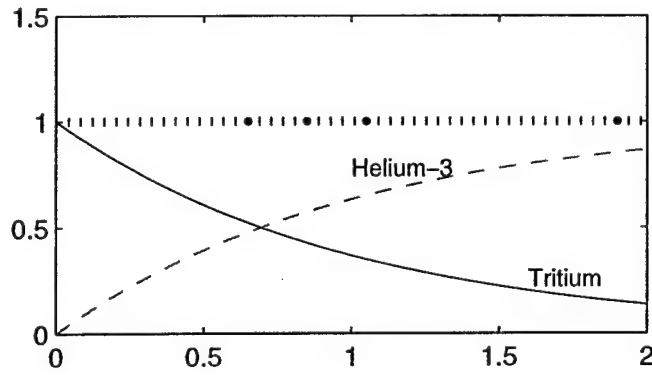


Figure B.1:  $^3\text{H}$  and  $^3\text{He}$  distribution for one-dimensional model with steady surface  $^3\text{H}$  boundary concentration. The abscissa is non-dimensional distance within the domain. For non-dimensionalized fields, tritium (solid line) decays with e-folding time-scale of 1. The daughter product of tritium is  $^3\text{He}$  (dashed line). For steady tritium boundary condition at  $x = 0$ , the sum of the two tracers is constant (dotted line).

of the  $^3\text{H}$  and  $^3\text{He}$  fields. If the boundary conditions at  $x = 0$  for  $^3\text{H}$  is constant, radioactive decay leads to tritium concentrations which decrease with distance into the domain but the sum of  $^3\text{H}$  and  $^3\text{He}$  will remain constant throughout the domain (figure B.1). This example represents a time prior to the first bomb-detonation when the only tritium source was steady cosmogenic production in the atmosphere. Additionally, surface tritium values in the present ocean are only slowly changing so this case-study approximates the present dominant balance.

Since the sum of  $^3\text{H}$  and  $^3\text{He}$  is constant,

$$\frac{[{}^3\text{H} + {}^3\text{He}]_x}{[{}^3\text{H} + {}^3\text{He}]} = 0.$$

However, because of the non-dimensional length-scale was chosen to correspond to the time-scale of radioactive decay, the spatial gradient of the tritium field is order one:

$$\frac{[{}^3\text{H}]_x}{[{}^3\text{H}]} = e^{-1}.$$

Therefore the coefficient of the net nonlinear mixing effect can be approximated as

$$\alpha = e^{-1},$$

and the steady-state form of equation B.1.8 becomes

$$\left(u_0 - \frac{e^{-1}}{Pe}\right) \tau_x^* = 1. \quad (\text{B.1.11})$$

Equation B.1.11 shows that the spatial gradient of the age field is distorted from a pure advective balance by the addition of a term proportional to the inverse of the Péclet number. For very advective flows,  $Pe$  is large and the contribution of this additional term is small. For more diffusive flows the value of the Péclet number approaches unity and the contribution of the nonlinear mixing term increases and can lead to small, but non-negligible, (e.g. order 30%) decreases in the spatial gradients of age. In this case, the effects of mixing will only be apparent in the deviation of the steady-state age gradient from that expected for a pure advective balance. To see such deviations in observations would likely require highly accurate direct measures of the absolute circulation along with detailed and accurate information of changes in the rate of subduction.

### B.1.2 Case II: Rapidly Changing Tritium Boundary Condition

If the boundary condition for tritium at  $x = 0$  is not held constant but allowed to change with time, the advective-diffusive balance for tritium- $^3\text{He}$  age (eq. B.1.8) will be impacted by possible time dependence in the nonlinear mixing term,  $\alpha$ . Rapidly changing boundary conditions introduce large spatial gradients in the concentration of  $^3\text{H}$  and  $^3\text{He}$ . The large gradients of tracer concentration are parameterized as  $\alpha(x, t)$  in the current simplified model. Figure B.2 illustrates an example of the tracer distributions in response to rapidly increasing tritium concentrations at  $x = 0$ . The example of this section simulates the oceanic response to bomb-produced tritium and is analogous to the simple mixing example shown in figure 1.3. Tritium concentrations first increase in the portion of the domain closest to the surface boundary. Over time the high concentrations will spread further in to the interior and  $^3\text{He}$  concentrations



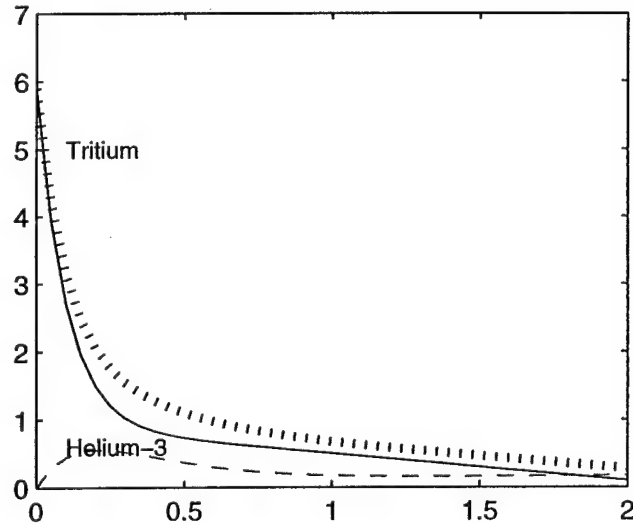


Figure B.2:  $^3\text{H}$  and  $^3\text{He}$  distribution for one-dimensional model with rapidly increasing  $^3\text{H}$  concentration. The abscissa is non-dimensional distance within the domain. Tritium (solid line),  $^3\text{He}$  (dashed line), sum (dotted line).

will build up in response to the radioactive decay. Initially, however, the high  $^3\text{H}$  concentrations will be confined to the youngest waters and the  $^3\text{He}$  concentrations will be relatively low (in comparison to tritium) throughout the domain.

The effect of the changing boundary condition on the advective-diffusive balance of age can be estimated by rearranging the balance equation for tritium (equation B.1.3) and neglecting the Laplacian mixing term:

$$\frac{[^3\text{H}]_x}{[^3\text{H}]} = -\frac{1}{u_0} \left( \frac{1}{[^3\text{H}]} + \frac{[^3\text{H}]_t}{[^3\text{H}]} \right). \quad (\text{B.1.12})$$

Keeping in mind that both  $u_0$  and  $[\text{}^3\text{H}]$  are  $\text{O}(1)$ , equation B.1.12 shows that the ratio  $\frac{[^3\text{H}]_x}{[^3\text{H}]}$  will become large compared to unity when the  $[\text{}^3\text{H}]$  field changes more rapidly than the characteristic time scale set by radioactive decay. Therefore, for a rapidly increasing tritium concentration at  $x = 0$  (e.g. the input of bomb-produced tritium), one would expect

$$\frac{[^3\text{H}]_x}{[^3\text{H}]} \ll -1.$$

An analogous argument holds true for the term  $\frac{[{}^3\text{H} + {}^3\text{He}]_x}{[{}^3\text{H} + {}^3\text{He}]}$ . The large gradient in tracer concentration deduced here is similar to the large finite-difference of tracer inventory in the initial water parcels in figure 1.3.

The dominant balance of the non-dimensional age equation (eq. B.1.8) for a rapidly increasing  ${}^3\text{H}$  boundary condition then becomes:

$$\tau_t^* + \left(u_0 + \frac{\alpha}{Pe}\right) \tau_x^* = 1 \quad (\text{B.1.13})$$

where the magnitude of  $\alpha$  is large compared to one. This example illustrates that for rapidly changing boundary conditions, the effects of mixing/diffusion, as represented here in last term on the l.h.s. of equation B.1.13, become more prominent in the overall balance equation for tracer age. Furthermore, because of the structure of the nonlinear mixing term in the age equation, the Péclet number enters as a coefficient of terms dependent on the gradients of the tracer fields, not the curvature. The effect, for increasing  ${}^3\text{H}$  concentrations is to increase the effective pseudo-velocity, thereby requiring weaker spatial gradients of age to maintain the overall balance in equation B.1.13. A weaker spatial gradient lowers the tracer age values throughout the domain. This bias towards weaker gradients of the age field necessitates a negative temporal tendency in the magnitude of the tracer age value at a fixed point in the domain.

The magnitude of change in tritium boundary conditions required for the nonlinear mixing term to become significant in the advective diffusive age equation is

$$\left(\frac{[{}^3\text{H} + {}^3\text{He}]_x}{[{}^3\text{H} + {}^3\text{He}]} + \frac{[{}^3\text{H}]_x}{[{}^3\text{H}]}\right) \approx 2 \frac{[{}^3\text{H}]_t}{[{}^3\text{H}]} \geq Pe \quad (\text{B.1.14})$$

where again, the time scale of the  ${}^3\text{H}$  tendency term is the scale of the radioactive decay. For the case of tritium input to the surface ocean, surface tritium values increased by a factor of 3-4 over the course of a few years in the early 1960's [Dreisigacker and Roether, 1978]. Given the characteristic time scale of tritium decay of 17.96 years,

this suggests that the value of  $\alpha$  in equation B.1.13, appropriate for the time period of peak bomb-tritium input is order 30. In other words, the large-scale spatial gradient of tritium is at least 30 times larger soon after the bomb-tritium input compared to the spatial gradients arising from radiodecay of tritium introduced by steady-state boundary conditions. Therefore for even fairly advective flows (e.g.  $Pe = O(30)$ ), one would expect some distortion of the tracer age field in response to the rapidly changing tritium boundary conditions in the 1960's.

After the peak oceanic tritium input in 1964-65, surface tritium values decreased at a rate roughly comparable to radioactive decay. Examination of equation B.1.12 suggests that, for times after the peak tritium input, the magnitude of  $\frac{[^3H]_x}{[^3H]}$  will diminish with time. Observations of the large-scale tritium distribution in the thermocline [Sarmiento, Rooth and Roether, 1982; Jenkins, 1987; Jenkins, 1997] are consistent with this, showing a reduction of spatial gradients and tendency towards homogenization over time. Therefore, if one wishes to apply the idealized equation B.1.13 to the ventilation of tritium- $^3\text{He}$  age in the oceanic thermocline, the coefficient representing the nonlinear effects,  $\alpha$ , should have a time-dependent magnitude with a step-function to large values at the time of peak bomb-tritium input and subsequent decay towards zero. The behavior of a simple analytic model incorporating these features will be explored in the next section.

Based on these case studies, one can qualitatively estimate the evolution of the non-linear mixing effects parameterized by  $\alpha(t)$ . The temporal changes in  $\alpha(t)$  represent the effects arising from the penetration of the high concentration tritium signal into the thermocline. Prior to the first detonation of nuclear devices, the tritium input to the ocean derived solely from cosmogenic sources and was in steady or quasi-steady state. Case Study I shows that the values of the non-linear mixing parameter,  $\alpha(t)$ , is small for steady-state forcing conditions. The expectation of large initial gradients of  $^3\text{H}$  in response to the tritium input from atmospheric bomb tests

corresponds to large values in  $\alpha(t)$ : large spatial gradients of tracer concentrations lead to distortions in the tracer age field when mixing effects are significant (Case Study II). As the bomb-tritium signal spreads into the ocean, the magnitude of the spatial gradients of tritium decrease. With the homogenization of the tracer fields, the effects of non-linear mixing decrease and, thus, the value of  $\alpha(t)$  relaxes towards smaller values.

## B.2 A Simple Analytic Model

The scale analysis of the previous section suggests that the dominant balance for the evolution of tritium- $^3\text{He}$  age in the one-dimensional model can be captured by the partial differential equation:

$$\tau_t + a(t)\tau_x = 1 \quad (\text{B.2.15})$$

where  $a(t)$  has a constant component due to the mean physical circulation,  $u_0$ , and a time-dependent component which represents the effects of the nonlinear mixing term,  $\alpha(t)$ :

$$a(t) = u_0 + \frac{1}{Pe}\alpha(t). \quad (\text{B.2.16})$$

If the physical circulation was also time dependent, its time varying component could be added as an additional term in this equation without changing structure of the solutions. The magnitude of the pseudo-advective term scales as the inverse of the Péclet number such that the overall amplitude grows with increases in the diffusion parameter  $\kappa$ . Equation B.2.15 is meant to capture only the most basic behavior of the evolution of tracer age in the ocean; in the case of the age evolution in the real ocean, the parameter  $\alpha(t)$  is not a prescribed variable but depends on the evolution of the  $^3\text{H}$  and  $^3\text{He}$  which are in turn dependent on the Péclet number of the flow (equations B.1.3 and B.1.4). Additionally, a more realistic model might incorporate  $\alpha(t)$  as a function of position as well as time. Analysis of the full temporal and spatial

structure of the nonlinear term (equation B.1.10) is complex. This analytic model simplifies the nonlinear term to a single, time-dependent parameter and examines the temporal response of the tracer age to temporal changes in the magnitude of  $\alpha$ . The full temporal and spatial effects of the nonlinear term will be included later in the numerical simulations, but for now, the pseudo-advective consequences of the nonlinear mixing terms will be proscribed.

Guided by the results of the previous section, I will assume that  $\alpha(t)$  has a structure similar to that shown in figure B.3: initially negligible magnitude which rapidly becomes large at the time of peak bomb input,  $t_0$ . The structure of  $\alpha(t)$

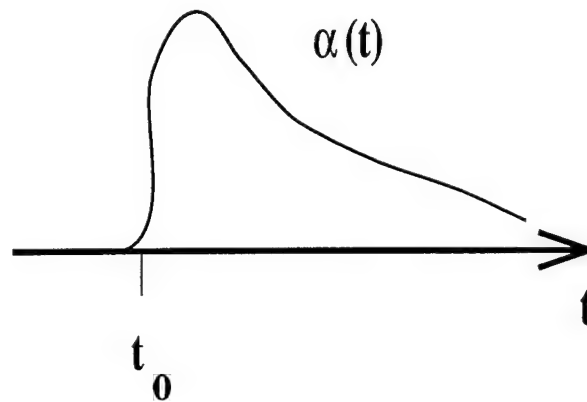


Figure B.3: Schematic of pseudo-advective forcing function,  $\alpha(t)$ . Value is initially small but increases rapidly at time of maximum bomb-tritium input,  $t_0$ . For time long after  $t_0$ ,  $\alpha(t)$  decreases asymptotically towards zero.

represents the mixing effects arising from the spatial inhomogeneity of the transient tracer concentrations and is chosen based on the results of the case studies of the previous section. The small initial value reflects the steady-state age distribution resulting from the pre-bomb, cosmogenic production of tritium (case study I). When the surface tritium boundary condition suddenly increases in the early 1960's, the spatial gradients of  $^3\text{H}$  suddenly become large and the pseudo-advective effects, which  $\alpha$  represents, are expected to also become large. As the internal tracer fields adjust

to the input of the bomb tritium, the spatial gradients of  $^3\text{H}$  and  $^3\text{He}$  become weaker and the value of  $\alpha(t)$  relaxes back toward small values.

Equation B.2.15 is a linear hyperbolic partial differential equation with non-constant coefficients which can be solved using the method of characteristics. Solutions on the semi-infinite domain,  $x \geq 0$ , require specification of both an initial condition,  $\tau_0(x, t = 0)$  and boundary condition,  $\tau(x = 0, t)$ . The general form of the solution of equation B.2.15 is

$$\tau(x, t) = t + \tau_0\left(x - \int_0^t a(t)dt; 0\right). \quad (\text{B.2.17})$$

The solutions in the  $x$ - $t$  plane fall into two regions (figure B.4) separated by a

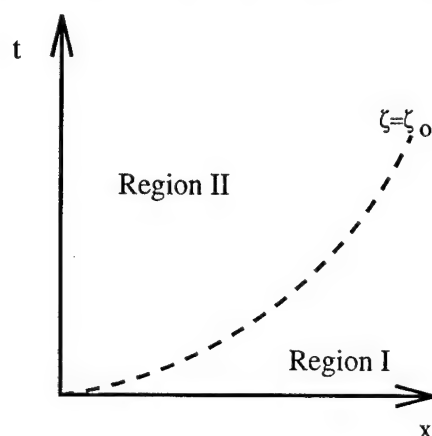


Figure B.4: Schematic of bounding characteristic separating two regions of solution of equation B.2.15. In Region I, the solution is determined by characteristics emanating from the initial condition at  $t = 0$ . In Region II, characteristics originating along the boundary condition,  $x = 0$ , determine the solution.

characteristic emanating from the origin. The bounding characteristic is given by:

$$\zeta_0 = x = \int_0^t a(t)dt.$$

In region I, the characteristics emanate from the initial condition along  $t=0$ . In the oceanic case, the initial condition, prior to atmospheric fusion bomb-tests, is determined by cosmogenically produced tritium. The pre-bomb surface ocean tritium

boundary condition was small compared to the anthropogenic inputs (0.2-0.4 TU [Begemann and Libby, 1957; Libby, 1961]) but large enough to establish an initial distribution of tritium-<sup>3</sup>He age in the thermocline. If the initial condition is specified so that the pre-bomb age field is in equilibrium with the steady-state velocity field,

$$\tau_0 = \frac{x}{u_0}, \quad (\text{B.2.18})$$

then the solution in Region I is given by

$$\tau(x, t) = t + \frac{1}{u_0} \left( x - \int_0^t a(t) dt \right). \quad (\text{B.2.19})$$

Substituting from equations B.2.16 and B.2.18 yields

$$\tau(x, t) = \tau_0 - \frac{1}{u_0 Pe} \int_0^t \alpha(t) dt. \quad (\text{B.2.20})$$

Provided  $\alpha(t)$  is always positive, the value of the solution  $\tau(x, t)$  in Region I will be always less than the initial condition  $\tau_0$ . Furthermore, the age tendency,  $\frac{\partial \tau}{\partial t}$ , is always negative so the tracer age at a fixed point decreases throughout region I. The rate of change of  $\tau$  scales with the Péclet number: the more diffusive the flow, the more rapidly the age field changes in response to a change in the tritium boundary condition.

In Region II, the solution is determined by characteristics which emanate from the boundary condition at  $x = 0$ . Setting the boundary condition appropriate for age,  $\tau(0, t) = 0$ , the solution given in equation B.2.17 takes the form

$$\tau(x, t) = \Delta t, \quad (\text{B.2.21})$$

where  $\Delta t$  satisfies the equation

$$x = \int_{t-\Delta t}^t a(t) dt = u_0 \Delta t + \frac{1}{Pe} \int_{t-\Delta t}^t \alpha(t) dt. \quad (\text{B.2.22})$$

If  $\alpha(t)$  is slowly varying this is well approximated by

$$x \approx u_0 \Delta t + \frac{\alpha(t - \Delta t/2) \Delta t}{Pe} \quad (\text{B.2.23})$$

and the age in region II can be approximated by

$$\tau(x, t) = \Delta t \approx \frac{x}{u_0 + \frac{\alpha(t-\Delta t/2)}{Pe}}. \quad (\text{B.2.24})$$

For positive  $\alpha$ , the bias of the observed age is always young. The difference between the observed age and  $\tau_0$  will be greatest at a time lag,  $\tau/2$ , after  $\frac{\alpha}{Pe}$  reaches its largest value. As  $\frac{\alpha}{Pe}$  decreases with time, the tracer age field will relax back towards the steady state value expressed in equation B.1.11.

The analysis of observations presented in chapter 2 entailed estimates of the temporal change of the observed age field. The rate of change of the tracer age field in Region II (equation B.2.24) can be approximated by

$$\frac{\partial \tau(x, t)}{\partial t} \approx - \frac{x}{\left(u_0 + \frac{\alpha(t-\tau/2)}{Pe}\right)^2} \frac{[\alpha(t) - \alpha(t - \tau)]}{Pe}.$$

Substituting from equation B.2.24 and approximating  $[\alpha(t) - \alpha(t - \tau)]$  as  $\tau \frac{\partial \alpha}{\partial t}|_{(t-\tau/2)}$  yields

$$\frac{\partial \tau}{\partial t} \approx - \frac{\tau^2 \frac{\partial \alpha}{\partial t}|_{(t-\tau/2)}}{Pe [u_0 + \alpha(t - \tau/2)/Pe]}. \quad (\text{B.2.25})$$

Equation B.2.25 shows that tendency of the age field takes the opposite sign to changes in the pseudo-advective term,  $\alpha$ : if  $\alpha(t)$  is decreasing with time, then the age field will be increasing. The magnitude of the age tendency scales quadratically with  $\tau(x, y)$  indicating that larger ages change increasingly more rapidly than younger ages. The presence of the Péclet number in the denominator causes the magnitude of the age tendency to increase for more diffusive flows. The lag,  $t - \tau/2$ , arises because the age field at  $(x, t)$  requires an elapsed time, comparable to the magnitude of the age, to adjust to changes in the pseudo-advective term. Water with older age values requires longer time periods to adjust.

The advantage of a relation such as equation B.2.25 for interpreting oceanic measurements of transient tracer fields is that it provides a general relationship



between two quantities, the age field and its tendency, which depend on the flow parameters, advection and mixing, but not on the spatial structure of the age field. This is in contrast to more traditional estimates of diffusive mixing which rely on accurate measurement of the curvature of tracer fields. In practice the pseudo-advective term,  $\alpha$ , is not a prescribed characteristic of the flow field but rather represents the response of the tracers  $^3\text{H}$  and  $^3\text{He}$  to changing boundary conditions. The precise form of  $\alpha(x, t)$  is a function of the spatial distribution of the  $^3\text{H}$  and  $^3\text{He}$  fields and thus, is dependent on mixing and advection as well as the initial and boundary conditions of the tracer field.

### B.2.1 An Example

To illustrate the ideas developed in this section based on the analysis of equation B.2.15 I will examine a simple example. This example is meant to simulate the tritium- $^3\text{He}$  age in the period subsequent to the peak of the bomb-tritium input. Suppose that the pseudo-advective term has the form:

$$\alpha(t) = \alpha_0 e^{-\frac{t}{\gamma}} \quad (\text{B.2.26})$$

where  $t = 0$  is taken to be the time of the large bomb-tritium input (1964-65). The structure of equation B.2.26 is chosen to simulate a decaying response to the initially strong effects of the input of bomb produced tritium. The partial differential equation governing the temporal development of age takes the form:

$$\tau_t + \left(u_0 + \frac{\alpha_0}{P_e} e^{-\frac{t}{\gamma}}\right) \tau_x = 1, \quad (\text{B.2.27})$$

and solutions are sought for positive  $x$  and  $t$  given the initial condition in equation B.2.18 and boundary condition  $\tau(0, t) = 0$ . For the oceanic case, where the input time scale of the tritium boundary condition is less than the radioactive time scale of decay, one would expect  $\gamma < 1$ .

The general solution of equation B.2.27 is shown in figure B.5 for two values of the pseudo-advective function,  $\alpha(t)$ . The figure is a contour plot of  $\tau(x, t)$  in the

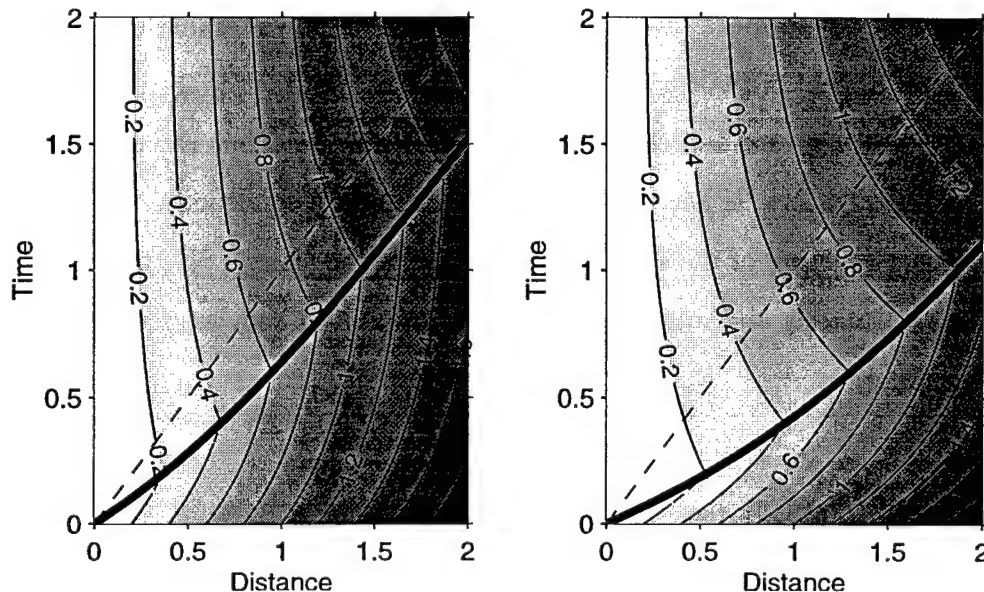


Figure B.5: Space-time diagram of solution of analytic age balance equation. Units are non-dimensionalized by tracer decay time scale and characteristic velocity. The dashed line indicates the advective speed. The two panels illustrate solutions with different strengths of the time-dependent pseudo-advective term. Left hand panel shows solution for  $\frac{\alpha_0}{P_e} = 1$  and right hand panel for  $\frac{\alpha_0}{P_e} = 2$ . The characteristic time scale of  $\alpha(t)$  is set to  $1/2$  for both cases.

x-t domain with non-dimensional time and space scales normalized by the decay time of tritium, 17.96 yr, and the characteristic velocity,  $V$ . The bounding characteristic separating the two regions of the solution is shown as a heavy dark line. The dashed line indicates the advective speed: the rate at which advection carries a disturbance at the surface into the interior solely by advection. For  $\alpha_0$  and  $u_0$  equal to constants, the right hand figure illustrates a doubling of the diffusivity compared to the left hand panel. Age values are zero at the boundary condition  $x = 0$  and increase with  $x$ . In region I, the lower right portion of the domain, age values decrease with time, however, the spatial gradient of age remains fixed. Equation B.2.19 shows that the solution in region I is simply a uniform translation of the initial condition and thus the spatial gradient of age in this region is always  $\frac{\partial \tau_0}{\partial x}$ . In region II, the upper left portion, age

values increase with time, asymptotically relaxing back to the initial condition. Since  $\frac{\partial \alpha}{\partial t} < 0$  for all time, the temporal tendency of the age field in region II is positive for all  $x$  and  $t$  (eq. B.2.25). Unlike region I, the spatial gradient of age in region II varies in response to the pseudo-advective forcing (eq. B.2.24). The gradient of tracer age are lowest along the bounding characteristic and increase towards higher values as strength of the pseudo-advective forcing decays and the field relaxes towards the steady state.

Comparison of the two panels in figure B.5 shows that the magnitude of the age distortion increases with a decrease in Péclet number (increased diffusivity). The time at which the age reaches a minimum is always prior to the advective time for communication with the surface and moves forward for the smaller Péclet number. This relation is more clearly seen in figure B.6 which shows the age at a fixed position

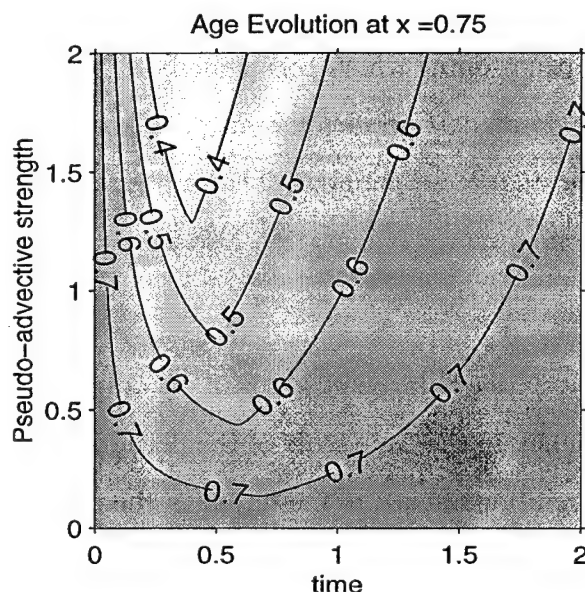


Figure B.6: Predicted age field at  $x = 0.75$  as a function of time and pseudo-advective forcing. The ordinate is non-dimensional time and the abscissa is the value of  $\frac{\alpha_0}{P_e}$ . The time scale,  $\gamma$ , of the pseudo-advective decay is  $1/2$ .

as a function of time and strength of the nonlinear term. For small values of  $\frac{\alpha_0}{P_e}$  there is only a slight deviation from the steady-state solution for age at this point. As the

magnitude of  $\frac{\alpha_0}{P_e}$  increases, the minimum value of  $\tau$  decreases and its occurrence moves to shorter times. Changes in the magnitude of the age tendency are also evident in figure B.6; as the strength of the distortion increases the rate of change of the age field,  $\frac{\partial \tau}{\partial t}$  over the time range  $t = [1,2]$  increases. In dimensional time units, if  $t = 0$  is set to 1965, the non-dimensional range  $t = [1,2]$  roughly corresponds to the time span of the observations discussed in chapter 2. The sensitivity of the simulated age tendency to the Péclet number suggests that observations of the evolution of the tritium- $^3\text{He}$  age field over this time period might serve as a diagnostic of the bulk diffusivity of the flow field over the Lagrangian history of the tracer.

Comparison of the temporal evolution of the tracer age fields in the one-dimensional numerical model (figures 4.3 and 4.4) shows qualitative agreement with the predictions of the analytic model shown in figure B.5. The plots can be compared directly by noting that the analytic model was presumed to start,  $t = 0$ , at the time of maximum bomb-tritium input which corresponds to about 1964 in the numerical model predictions. Both models predict the magnitude and duration of the age bias to increase with decreasing Péclet number. The impact of increased diffusive mixing on the timing of the maximum age distortion also shows agreement between the two models.

Examining the relative balance of terms in equation B.2.27 illustrates the sensitivity of the age tendency to the time scale of the pseudo-advective term. Figure B.7 shows the temporal evolution of each of the terms on the r.h.s of equation B.2.27. The terms illustrated are always required to sum to one. Since  $u_0$  is constant, changes in the size of the the advective term reflect changes in the magnitude of  $\frac{\partial \tau}{\partial x}$ . For small times, the solution is determined by characteristics emanating from the initial condition (Region II) and the gradient of the age is fixed. The pseudo-advective term is large, so the tendency term must become negative to maintain the balance. As the strength of the nonlinear mixing term decreases the tendency term increases in kind.

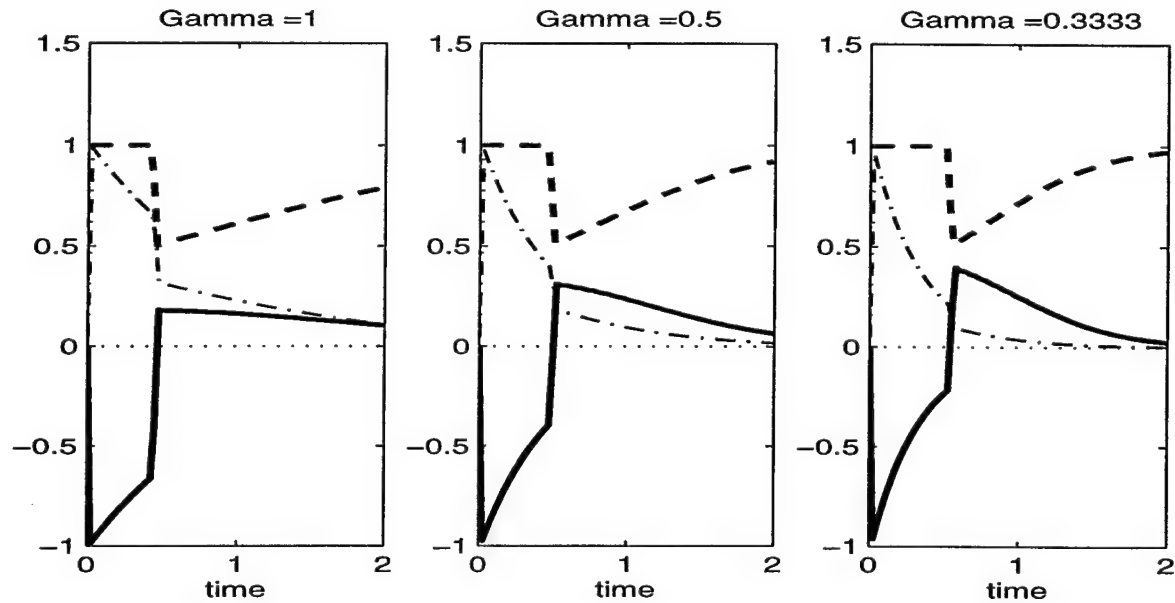


Figure B.7: Time evolution of balance of terms of equation B.2.27. Time is non-dimensionalized by radiotracer decay time. Each panel illustrates a different decay time scale of the pseudo-advective forcing varying from 1 to  $1/3$ . Individual terms are indicated by line type: tendency (heavy solid), advective (heavy dashed), pseudo-advective (dash dot).

When the solution reaches the characteristic bounding region II and I, a large shift occurs in the relative balance of terms. The gradient of the age field suddenly decreases as the solution moves into a regime which is determined by characteristics emanating from the boundary condition at  $x = 0$ . The sudden decrease in the contributions of the advective and pseudo-advective terms require the tendency term to increase to maintain the overall balance. The tendency of the age field becomes positive and the tracer age values begin to increase with time. Comparison of the panels in figure B.7 shows that even after the pseudo-advective term has largely damped out, the tendency of the age field can still be large as the solution relaxes back towards the steady-state value. Surprisingly, the magnitude of the tendency term is larger in the later part of the time series when the pseudo-advective term damps out quickly. The distortion of the age gradient is created by the initial perturbation of the pseudo-advective term. Even if this term decays quickly, the distorted age gradient remains and requires finite time to

re-adjust to the steady-state value. If the pseudo-advective term is damped out, the tendency term is the only remaining term that can maintain the overall balance. With larger age tendencies, the age field returns more rapidly to its equilibrium value, as evidenced in the comparison of the panels in figure B.7. Thus in the later portion of the temporal evolution, although the direct measurable effects of the pseudo-advective terms might be small (e.g. the pseudo-advective term is a negligible component of the overall balance), the cumulative effects of the nonlinear mixing of age have distorted the age field such that the contributions of the nonlinear mixing effects persists in the guise of the significant non-zero age tendency term.

The changing balance of terms seen in the numerical model (figure 4.6) is similar to the results of the analytic model shown in figure B.7 except now the Laplacian term, shown for the numerical results, is not incorporated into the analytic model. The analytic example assumed that the effects of the pseudo-advective term peaked at  $t = 0$  (1964) and afterward damped out towards zero, however, the results in figure 4.6 show that in the numerical model, although the value of this term does peak in the 60's, it subsequently decreases through zero to become significantly negative in the 1990's. The Laplacian becomes slightly positive and tends to cancel the effects of the pseudo-advective terms so the net direct effects of mixing in the later time period remain relatively small.

In summary, scale analysis of the non-dimensional age equation has shown that the temporal evolution of the age field can be approximated by the balance

$$\tau_t + a(t)\tau_x = 1$$

where the time-dependent coefficient is expected to be large after the initial introduction of bomb-tritium to the surface ocean and subsequently decrease with time. The structure of the analytic solutions of this equation have been examined and the general form of the solutions is displayed in figure B.5. The nonlinear mixing terms of the age balance equation create a positive pseudo-velocity term which leads to a bias of

the tracer age field towards younger values. As the internal tracer fields of the ocean adjust to the added tritium burden, the strength of the nonlinear mixing terms are expected to decrease and the age field will relax back towards its equilibrium value. Figure B.7 illustrates that even when the pseudo-advective term no longer appears in the dominant balance of terms, the ‘fossilized’ evidence of its earlier contribution may remain in the age tendency terms.

This section has illustrated the fundamental behavior that might be expected in the tritium- $^3\text{He}$  age field in response to a large  $^3\text{H}$  transient at the surface boundary. To explore more precisely the temporal dependence of the age field, I will use a numerical model which integrates the evolution of the individual  $^3\text{H}$  and  $^3\text{He}$  fields and thereby includes a full representation of all components of the nonlinear term represented by the parameter  $\alpha(t)$ .





## Appendix C

### Diapycnal Mixing Effects

Previous analysis of the penetration of transient tracers (predominantly bomb produced tritium) have concluded that observations are only consistent with models of the ocean in which isopycnal processes dominate diapycnal mixing [*Rooth and Östlund*, 1972; *Jenkins*, 1980; *Fine, Reid and Östlund*, 1981; *Sarmiento, Rooth and Roether*, 1982; *Fine, Peterson and Östlund*, 1987]. Small magnitudes of diapycnal mixing are also deduced from measurements of fine- and micro-structure variability [*Gregg*, 1987; *Toole, Polzin and Schmitt*, 1994; *Moum*, 1996]. Direct measurement of diapycnal mixing based on the temporal evolution of a purposefully released tracer in the subtropical thermocline yield the most conclusive estimate of the rate of diapycnal mixing:  $0.11 \pm 0.02 \text{ cm}^2 \text{ s}^{-1}$  [*Ledwell, Watson and Law*, 1993]. This Appendix examines the effects of weak diapycnal mixing on the evolution of transient tracer age in the eastern subtropical thermocline with an emphasis on two questions: How important is diapycnal mixing for the penetration of bomb tritium into the thermocline? Are the conclusions based on the simulations of the simulations in Chapters 4 and 5 significantly altered if diapycnal mixing effects are included?

## C.1 Scale Analysis of Diffusive Ventilation

A simple scale analysis can be used to estimate the possible influence of diapycnal diffusivity on the evolution of transient tracer fields in the ventilated thermocline. The diffusive time scale,  $T_d$ , for the penetration of transient signals by diffusive processes is given by

$$T_d = \frac{L^2}{\kappa}, \quad (\text{C.1.1})$$

where  $L$  is a characteristic length scale and  $\kappa$  is the diffusivity. Table C.1 compares the isopycnal and diapycnal time scales for a representative point in the main thermocline of the eastern North Atlantic. Comparison of the characteristic diffusive time scales

Coordinate	$L$	$\kappa$	Time-scale
Diapycnal	350 m	$0.1 \text{ cm}^2 \text{ s}^{-1}$	400 yr
Isopycnal	1000 km	$1000 \text{ m}^2 \text{ s}^{-1}$	32 yr

Table C.1: Comparison of diffusive time scales in the main thermocline of the eastern North Atlantic. The characteristic depth (350 m) and distance to surface isopycnal outcrop (1000 km) are representative of the isopycnal  $\sigma_\theta = 27.0$ .

shows that, in the absence of advective flows, the rate at which diapycnal diffusivity will renew properties in the lower thermocline is an order of magnitude slower than that due to isopycnal mixing.

The analysis of table C.1 compares two completely diffusive one-dimensional analyses of ventilation. The absence of advective effects in this simple analysis yields ventilation time scales long compared to those actually observed (order 10 yr for this surface based on the measured tritium- $^3\text{He}$  age). Additionally, it is possible that features of the three-dimensional advective flow, especially the vertical shear of the horizontal velocity, might heighten the effects of the diapycnal flux. For instance, lateral advection might quickly carry the transient tritium signal into the upper layers of the thermocline which may, in turn, lead to greater diapycnal fluxes into the lower,

more slowly ventilated levels. This possible interplay of the mean advective field with diapycnal mixing will be examined in a simple numerical simulation of ventilation in a stratified thermocline.

## C.2 A Numerical Model

### C.2.1 Model Description

A numerical model is constructed to examine the effects of diapycnal mixing. The model (figure C.1) is limited to two dimensions: one horizontal and one vertical (diapycnal). Each layer in the model is analogous to that in Chapter 4 except that now

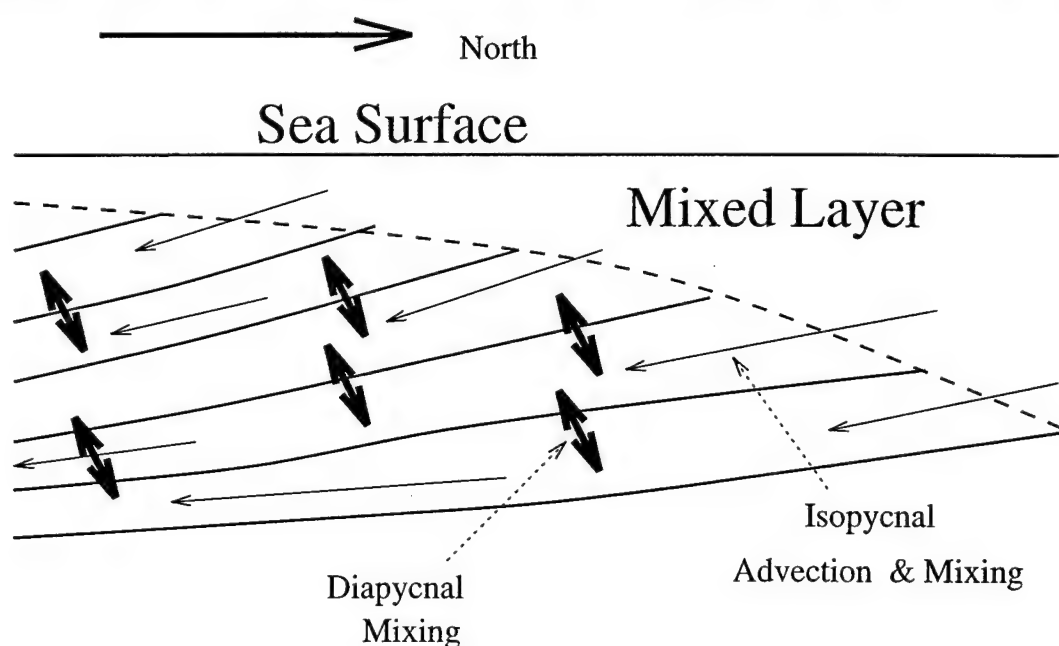


Figure C.1: Schematic diagram of diapycnal ventilation numerical model. The model is composed of multiple layers each representing a layer of constant potential density. Fluid flows out of the surface mixed layer and along each of the isopycnal layer. The diffusivity tensor has two components: one oriented along each layer (isopycnal) and one oriented orthogonal to the layer (diapycnal).

diffusive fluxes are added to allow diapycnal exchange with underlying and overlying

layers. The properties of the surface mixed are used as the upstream boundary condition for each layer: the history of surface tritium concentration is based on the work of *Doney and Jenkins* [1988] and  $^3\text{He}$  concentrations are set to zero.

The geometry of the model is determined from the mean hydrographic data base. Layers are defined for isopycnal surfaces from  $\sigma_\theta = 26.2$  through 27.3 at with layer separation of  $0.1 \sigma_\theta$ . The layer thickness (in meters) is determined from the mean hydrography along  $30^\circ\text{W}$ . The vertical domain of the model extends from the base of the winter mixed layer to approximately 750 m. The advective speed on each surface is taken to be the mean meridional geostrophic velocity at  $30^\circ\text{W}$ ,  $25^\circ\text{N}$  referenced to 1000 dbar. The advective speed is southward at all levels and order 1.5 cm/s in the lightest layers, decreasing to 0.3 cm/s in the densest. In order for the net transport in each layer to be conserved throughout the domain, the advective speed varies inversely with the layer thickness.

The lateral and diapycnal diffusivity of the model is proscribed. Diapycnal diffusivity is varied from zero to  $1 \text{ cm}^2 \text{ s}^{-1}$ . Isopycnal diffusivity is kept fixed at  $1000 \text{ m}^2 \text{ s}^{-1}$ . This value of isopycnal diffusivity is at the lower end of estimates of both the present work and previous studies (table 4.4). Larger values of isopycnal diffusivity, if used, would further decrease the relative of effects of diapycnal diffusive fluxes.

## C.2.2 Examples of Model Solutions

Numerical simulations are conducted for diapycnal mixing strengths,  $\kappa_v$ , of 0, 0.1, 0.2, 0.4, and  $1 \text{ cm}^2 \text{ s}^{-1}$ . The case where  $\kappa_v = 0$  reproduces the results of the one-dimensional ventilation model of Chapter 4 and serves as a reference for the comparison when the diapycnal diffusivity is set to non-zero values.

Representative examples of the tracer fields resulting from model simulations are shown in figures C.2 and C.3. Both figures show simulated tracer fields for the canonical value of diapycnal mixing:  $0.1 \text{ cm}^2 \text{ s}^{-1}$ . Figure C.2 displays a cross section of the simulated tracer fields for the year 1986. This figure can be compared to direct observations along a meridional section in the eastern North Atlantic (figure 2.5). The general character of the simulated fields is similar to the observations except the model does not show the presence of the strong fronts (Cape Verde and Azores) seen in the observations. Additionally, the magnitude of the subsurface  $^3\text{He}$  maxima is larger in the simulations than in the observations. The previous one-dimensional simulations (§ 4.2.2) have shown that this discrepancy (the value of the  $^3\text{He}$  maxima) arises from model simulations with overly strong advective flows (e.g. compare figures 4.3 and 4.4).

Figure C.3 is a space-time diagram illustrating the evolution of the tracer fields at a fixed point in the model domain roughly corresponding to a latitude of  $25^\circ\text{N}$ . The penetration of high concentration bomb-tritium forms of weak subsurface maximum of tritium in the model simulation. The resultant  $^3\text{He}$  distribution shows a strong maximum with the peak value shifting deeper into the thermocline over time. The space-time diagram of the tritium- $^3\text{He}$  age shows increasing age with depth and the now expected decrease in tracer age value associated with the penetration of bomb-tritium into the thermocline.

### C.2.3 Diapycnal Diffusive Effects on the Evolution of Tritium- $^3\text{He}$ age in the Lower Ventilated Thermocline

The impact of diapycnal mixing on the model diagnostics used in this thesis (temporal tendency of tritium- $^3\text{He}$  age and mean decay corrected tritium concentration) is examined by varying the magnitude of the diapycnal mixing rate over a series of

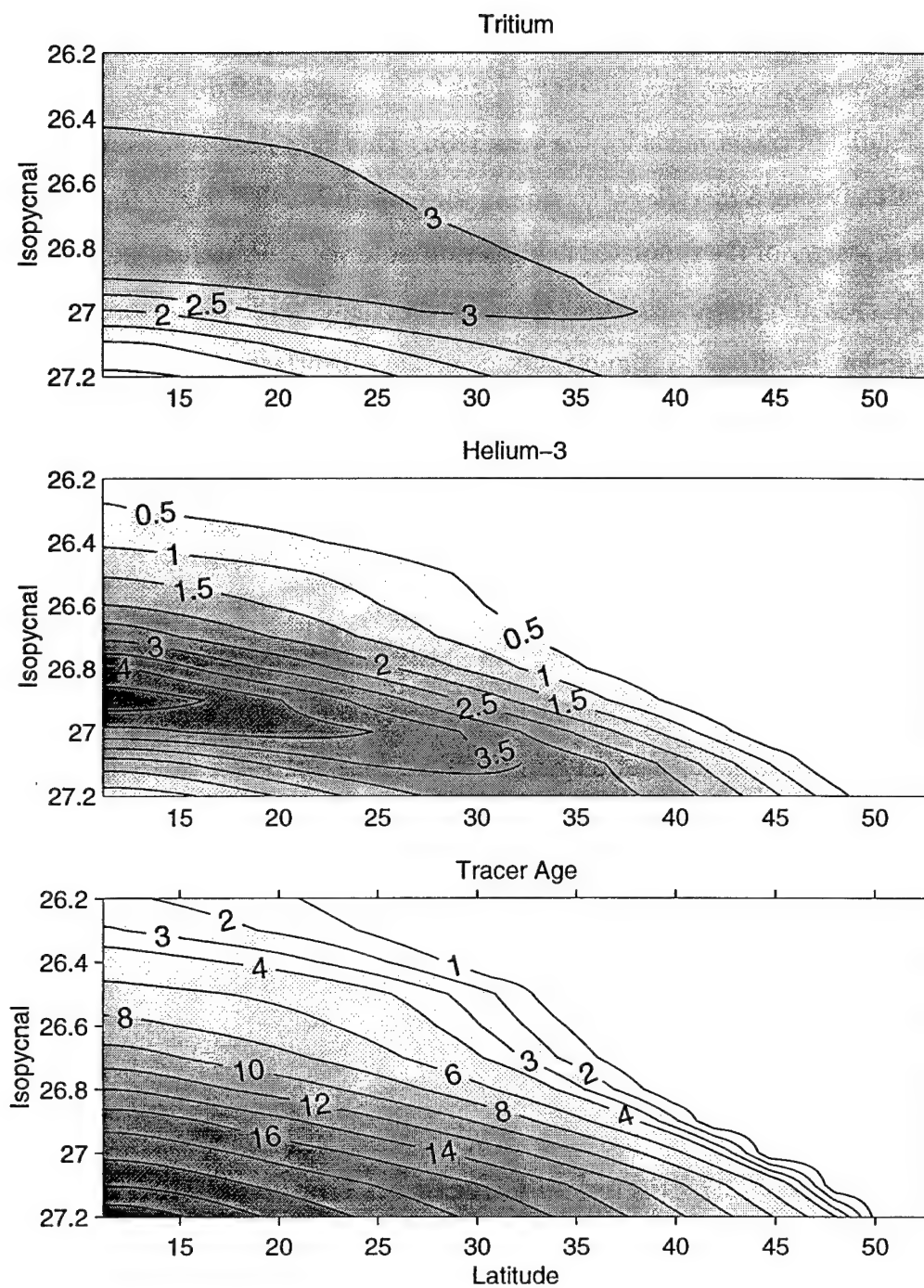


Figure C.2: [Simulated tracer fields in 1986: A) Tritium (TU) B)  $^3\text{He}$  (TU) and C) tritium- $^3\text{He}$  age (yr). Diapycnal diffusivity is  $0.1 \text{ cm}^2 \text{ s}^{-1}$  and other model characteristics are as described in text.

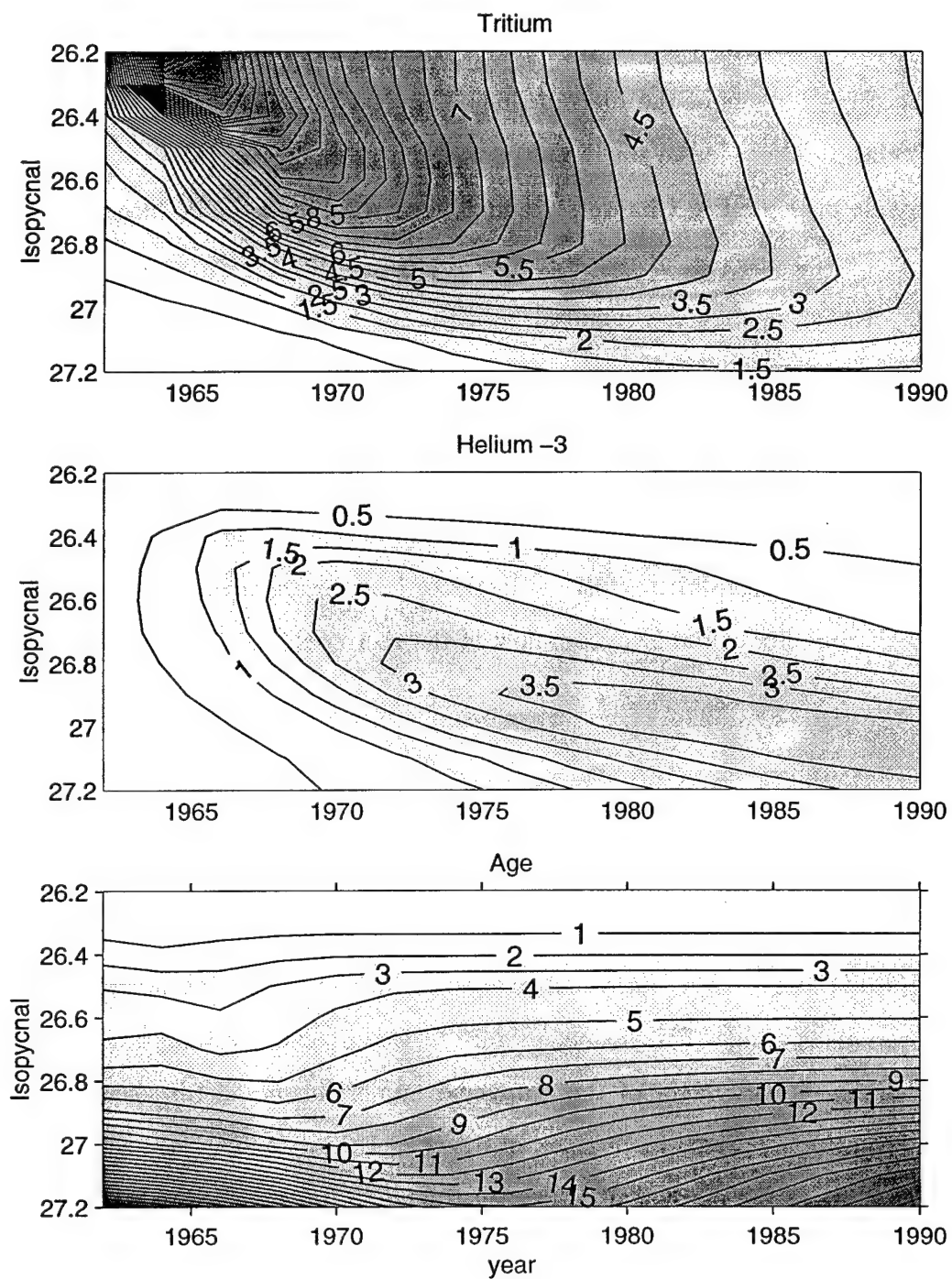


Figure C.3: Space time diagram of tracer fields in diapycnal model: A) Tritium (TU) B) <sup>3</sup>He (TU) and C) tritium-<sup>3</sup>He age (yr). Diapycnal diffusivity is  $0.1 \text{ cm}^2 \text{ s}^{-1}$  and other model. Model fields are analyzed at position in domain roughly corresponding to  $25^\circ\text{N}$ .

parallel model simulations. Inclusion of non-zero diapycnal mixing adds another diffusively mediated path whereby the surface tritium and  $^3\text{He}$  signals can communicate with the deeper layers of the thermocline. The analysis of this thesis has calculated bulk Péclet numbers based on the observed character of the transient tracer fields. The models presented in Chapters 4 and 5 have attributed the deduced mixing to a purely isopycnal process. If the neglected diapycnal mixing also provides a significant flux of tracers, then the required bulk mixing must be partitioned into both an isopycnal and diapycnal component. A strong diapycnal mixing flux rate will reduce the requirement of an overly strong isopycnal mixing rate. Therefore, when diapycnal mixing effects are included, the estimated rate of isopycnal mixing will be lower than that required when lateral isopycnal diffusion is the sole mixing process. As such, the neglect of diapycnal mixing effects is likely to lead to an underestimate of the true bulk Péclet number of the isopycnal flow of the thermocline.

The size of the bias of the estimates of isopycnal Péclet numbers and mixing rates in the simulations which neglect diapycnal processes (Chapters 4 and 5), is directly related to the efficiency of diapycnal vs isopycnal mixing for the ventilation and communication of properties from the sea surface to the lower thermocline. Simple scale analysis (§ C.1) suggests that the effects of isopycnal processes are an order of magnitude larger than diapycnal analysis. Integration of the layered numerical model reveals a similar conclusion. Figure C.4 compares the temporal evolution of tritium- $^3\text{He}$  age on a layer of the diapycnal numerical model representing the isopycnal surface  $\sigma_\theta = 27.0$ . Each panel of figure C.4 shows a space-time diagram for a differing value of the diapycnal diffusivity. Increases in the rate of diapycnal mixing leads to slightly lower minimum values of tritium- $^3\text{He}$  age in (e.g. compare the age at  $20^\circ\text{N}$ , 1975 for each simulation). However, comparison of the zero diapycnal mixing case (figure C.4A) with the simulation using the nominal value of  $\kappa_v$  ( $0.1 \text{ cm}^2 \text{ s}^{-1}$ ,



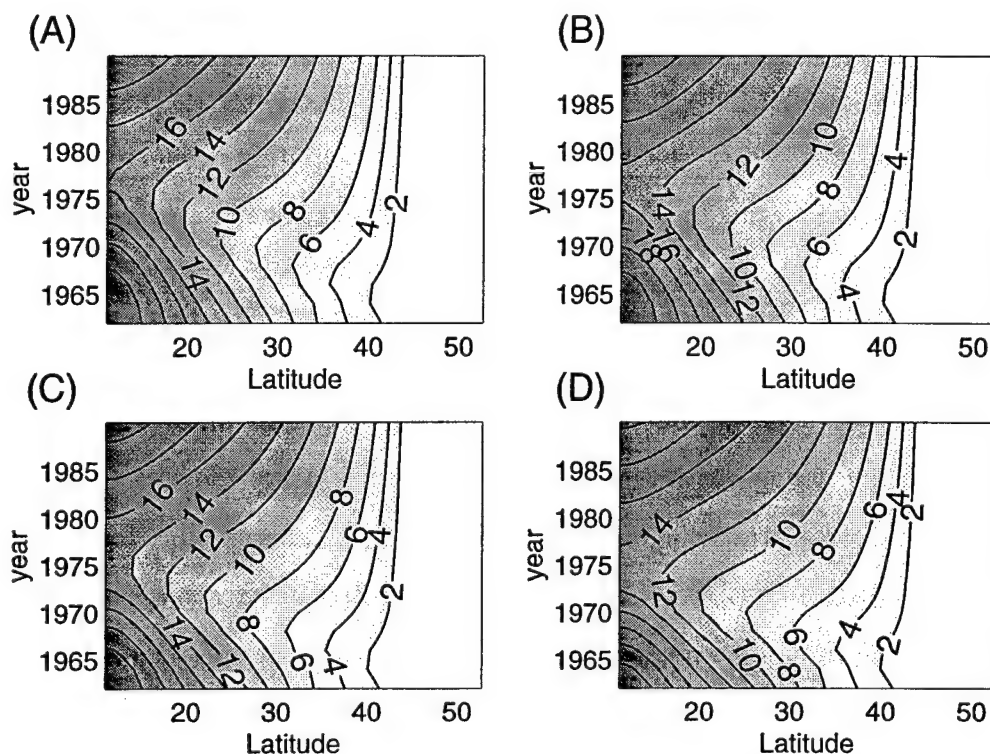


Figure C.4: Space time diagram of tracer age for different values of diapycnal diffusivity. Each panel shows the temporal evolution of tritium- $^3\text{He}$  age (yr) on the model level representing the surface  $\sigma_\theta = 27.0$ . Values of diapycnal diffusivity are varied: A) zero, B) 0.1, C) 0.4 and D) 1.0 (all  $\text{cm}^2 \text{s}^{-1}$ ). Note that the decrease in tracer age in the early 70's is robust to changes in the diapycnal mixing rate. The magnitude of the maximum age bias varies with the strength of diapycnal mixing rate, but the differences between zero mixing and nominal observed values ( $0.1 \text{ cm}^2 \text{s}^{-1}$ ) are negligible.

figure C.4B) shows only small quantitative differences in the evolution of the tracer age signal at this depth in the thermocline.

### C.3 Conclusions

This thesis has analyzed and interpreted the ventilation of transient tracers in the subtropical thermocline as being a predominantly isopycnal process. The simulations in Chapters 4 and 5 have led to the conclusion that isopycnal mixing plays an im-

portant role in the ventilation of the lower layers of the main thermocline. Diapycnal diffusion offers another path of transient tracers into the lower thermocline which is mediated by mixing effects. Therefore, mistakenly attributing property fluxes resulting from diapycnal mixing to isopycnal processes may result in an overestimate of the importance of the later.

Scale analysis and a simple numerical simulation have shown that the penetration of transient tracers into the thermocline by diapycnal mixing is second order compared to the strong ventilation of these properties along isopycnals. Comparison of simulations of the tracer age evolution in the lower thermocline for a variety of diapycnal mixing rates (figure C.4) shows that the first-order response of the tracer age field is predominantly an effect of the isopycnal processes and the presence (or absence) of diapycnal fluxes causes only slight modification of the tracer fields. Quantitative comparison of rate of the tritium- $^3\text{He}$  age tendency in the simulations with  $\kappa_v = 0$  and  $0.1 \text{ cm}^2 \text{ s}^{-1}$  suggests that the estimates of isopycnal Péclet number determined in Chapter 4 (table 4.1) may underestimate of the oceanic Péclet number by approximately 20%. Chapter 6, however, discusses the failings of models based on the assumption that all fluid in the thermocline derives from flow originating in the surface mixed layer. Two- (or three-) dimensional flow allows for recirculation of fluid within the subtropical gyre. The simulations of Chapter 6 emphasize the importance of mixing effects and indirect ventilation for the renewal of properties of the lower thermocline. This fundamental conclusion is not altered if the mixing is in fact both diapycnal and isopycnal.

# Bibliography

- Akima, H., A New Method of Interpolation Based on Local Procedures, *J. of the Association of Computing Machinery*, 17, 589-602, 1970.
- Andrié, C., P. Jean-Baptiste and L. Merlivat, Tritium and Helium 3 in the Northeastern Atlantic Ocean During the 1983 Topogulf Cruise, *J. Geophys. Res.*, 93, 12511-12524, 1988.
- Armi, L. and H. Stommel, Four views of a portion of the North Atlantic Subtropical Gyre, *J. Phys. Oceanogr.*, 13, 828-857, 1983.
- Bauer, E. and G. Siedler, The Relative Contributions of Advection and Isopycnal and Diapycnal Mixing Below the Subtropical Salinity Maximum, *Deep-Sea Res.*, 35, 811-837, 1988.
- Begemann, F. and W. F. Libby, Continental Water Balance, Ground Water Inventory and Storage Times, Surface Ocean Mixing Rates and World Wide Circulation Patterns From Cosmic Ray and Bomb Tritium, *Geochim. Cosmochim. Acta*, 12, 277-296, 1957.
- Bleck, R., C. Rooth, D. Hu and L. T. Smith, Salinity-Driven Thermocline Transients in a Wind- and Thermohaline-Forced Isopycnal Coordinate Model of the North Atlantic, *J. Phys. Oceanogr.*, 22, 1486-1505, 1992.
- Böning, C. W., Characteristics of Particle Dispersion in the North Atlantic: and Alternative Interpretation of SOFAR Float Results, *Deep-Sea Res.*, 35, 1379-1385, 1988.
- Böning, C. W. and M. D. Cox, Particle Dispersion and Mixing of Conservative Properties in an Eddy-Resolving Model, *J. Phys. Oceanogr.*, 18, 320-338, 1988.

- Böning, C. W., R. Doscher and H. -J. Isemer, Monthly Mean Wind Stress and Sverdrup Transports in the North Atlantic: a Comparison of the Hellerman-Rosenstein and Isemer-Hasse Climatologies, *J. Phys. Oceanogr.*, **21**, 221–235, 1991.
- Broecker, W. S., T. Takahashi, H. J. Simpson and T. H. Peng, Fate of Fossil Fuel Carbon Dioxide and the Global Carbon Budget, *Science*, **206**, 409–418., 1979.
- Bryan, F. O., C. W. Böning and W. R. Holland, On the Midlatitude Circulation in a High-Resolution Model of the North Atlantic, *J. Phys. Oceanogr.*, **25**, 289–305, 1995.
- Bullister, J. L. and R. E. Weiss, Anthropogenic Chlofouomethanes in the Greenland and Nortwegian Seas, *Science*, **221**, 265–268, 1983.
- Cox, M. D., An Eddy Resolving Numerical Model of the Ventilated Thermocline, *J. Phys. Oceanogr.*, **15**, 1312–1324, 1985.
- Cox, M. D. and K. Bryan, A Numerical Model of the Ventilated Thermocline, *J. Phys. Oceanogr.*, **14**, 674–687, 1984.
- Curry, R. G., HydroBase: A Database of Hydrographic Stations and Tools for Climatological Analysis, Woods Hole Oceanographic Institution, Technical Report WHOI-96-01, 1996.
- Dantzler, Jr., H. L., Potential Energy Maxima in the Tropical and Subtropical North Atlantic, paper presented at J. Phys. Oceanogr., 1977.
- De Szoeke, R. D., On the Wind-Driven Circulation of the South Pacific Ocean, *J. Phys. Oceanogr.*, **17**, 613–630, 1987.
- Dewar, W. K., A Nonlinear, Time-Dependent Thermocline Theory, *J. Marine Res.*, **47**, 1–31, 1989.
- Doney, S. C. and W. J. Jenkins, The Effect of Boundary Conditions on Tracer Estimates of Thermocline Ventilation Rates, *J. Marine Res.*, **46**, 947–965, 1988.
- Doney, S. C., W. J. Jenkins and J. L. Bullister, A Comparison of Ocean Tracer Dating Techniques on a Meridional Section in the Eastern North Atlantic, *Deep-Sea Res.*, **44**, 603–626, 1997.

- Doney, S. C., W. J. Jenkins and H. G. Östlund, A Tritium Budget for the North Atlantic, *J. Geophys. Res.*, **98**, 18069–18081, 1993.
- Dreisigacker, E. and W. Roether, Tritium and  $^{90}\text{Sr}$  in North Atlantic Surface Waters, *Earth & Planet. Sci. Lett.*, **38**, 301–312, 1978.
- Figueroa, H. A., Eddy Resolution Versus Eddy Diffusion in A Double Gyre GCM. Part II: Mixing of Passive Tracers, *J. Phys. Oceanogr.*, **24**, 387–402, 1994.
- Fine, R. A., R. Lukas, F. M. Bingham, M. J. Warner and R. H. Gammon, The Western Equatorial Pacific: a Water Mass Crossroads, *J. Geophys. Res.*, **99**, 25063–25080, 1994.
- Fine, R. A. and R. L. Molinari, A Continuous Deep Western Boundary Current Between Abaco (26.5°N) and Barbados (13°N), *Deep-Sea Res.*, **35**, 1441–1450, 1988.
- Fine, R. A., W. H. Peterson and H. G. Östlund, The Penetration of Tritium Into the Tropical Pacific, *J. Phys. Oceanogr.*, **17**, 553–564, 1987.
- Fine, R. A., J. L. Reid and H. G. Östlund, Circulation of Tritium in the Pacific Ocean, *J. Phys. Oceanogr.*, **11**, 3–14, 1981.
- Follows, M. J. and J. C. Marshall, On Models of Bomb  $^{14}\text{C}$  in the North Atlantic, *J. Geophys. Res.*, **101**, 22,577–22,582, 1996.
- Fuchs, G., Ventilation der Warmwasserschaäre des Nordostatlantiks Abgeleitet aus  $^3\text{Helium}$ - und Tritium-Verteilungen, Institut Für Umweltphysik, University of Heidelberg, Doctoral Dissertation, 1987.
- Gregg, M. C., Diapycnal Mixing in the Thermocline: a Review, *J. Geophys. Res.*, **92**, 5249–5286, 1987.
- Hellerman, S. and M. Rosenstein, Normal Monthly Wind Stress Over the World Ocean with Error Estimates, *J. Phys. Oceanogr.*, **13**, 1093–1104, 1983.
- Hogg, N., A Least-Squares Fit of the Advective Diffusive Equations to the Levitus Atlas Data., *J. Marine Res.*, **45**, 347–375, 1987.
- Huang, R. X., On the Three-Dimensional Structure of the Wind-Driven Circulation in the North Atlantic, *Dynamics of Atmospheres and Oceans*, **15**, 117–159, 1989.

- Iselin, C. O'D., The Influence of Vertical and Lateral Turbulence on the Characteristics of the Waters at Mid-Depths., *Trans. Amer. Geophys. Union*, 20, 414–417, 1939.
- Isemer, H. -J. and L. Hasse, *The Bunker Climate Atlas of the North Atlantic Ocean, Volume 2: Air-Sea Interactions*, Springer-Verlag, 1987.
- Jenkins, W. J., Tritium and  $^3\text{He}$  in the Sargasso Sea, *J. Marine Res.*, 38, 533–569, 1980.
- Jenkins, W. J., On the Climate of a Subtropical Ocean Gyre: Decade Time-Scale Variations in Water Mass Renewal in the Sargasso Sea, *J. Marine Res.*, 40(Supp.), 265–290, 1982a.
- Jenkins, W. J., Oxygen Utilization Rates in the North Atlantic Subtropical Gyre and Primary Production in Oligotrophic Systems, *Nature*, 300, 246–248, 1982b.
- Jenkins, W. J.,  $^3\text{H}$  and  $^3\text{He}$  in the Beta Triangle: Observations of Gyre Ventilation and Oxygen Utilization Rates., *J. Phys. Oceanogr.*, 17, 763–783, 1987.
- Jenkins, W. J., The Use of Anthropogenic Tritium and Helium-3 to Study Subtropical Gyre Ventilation and Circulation, *Phil. Trans. R. Soc. Lond. A.*, 325, 43–61, 1988a.
- Jenkins, W. J., Nitrate Flux Into the Euphotic Zone Near Bermuda, *Nature*, 331, 521–523, 1988b.
- Jenkins, W. J., Determination of Isopycnal Diffusivity in the Sargasso Sea, *J. Phys. Oceanogr.*, 21, 1058–1061, 1991.
- Jenkins, W. J., Studying Thermocline Ventilation and Circulation Using Tritium and  $^3\text{He}$ , in *Application of Trace Substance Measurements to Oceanographic Problems: Proceedings of the Ewing Symposium October, 1995*, edited by P. Schlosser, W. M. Smethie and W. S. Broecker, 1997.
- Jenkins, W. J. and W. B. Clarke, The Distribution of  $^3\text{He}$  in the western Atlantic Ocean, *Deep-Sea Res.*, 23, 481–494, 1976.
- Jenkins, W. J. and P. B. Rhines, Tritium in the Deep North Atlantic Ocean, *Nature*, 286, 877–880, 1980.

- Jia, Y. and K. J. Richards, Tritium Distributions in an Isopycnic Model of the North Atlantic, *J. Geophys. Res.*, 101, 11883–11901, 1996.
- Joyce, T. M. and W. J. Jenkins, Spatial Variability of Subducting Water in the North Atlantic: a Pilot Study, *J. Geophys. Res.*, 98(C6), 10111–10124, 1993.
- Joyce, T. M., J. R. Luyten, A. Kubryakov, F. B. Bahr and J. S. Pallant, Meso- and Large-scale Structure of Subducting Water in the Subtropical Gyre of the Eastern North Atlantic Ocean., *J. Phys. Oceanogr.*, 27, XXX–XXX, 1997.
- Joyce, T. M. and P. Robbins, The Long-Term Hydrographic Record at Bermuda, *J. of Climate*, 9, 3121–3131, 1996.
- Käse, R. H., J. F. Price, P. L. Richardson and W. Zenk, A Quasi-Synoptic Survey of the Thermocline Circulation and Water Mass Distribution Within the Canary Basin, *J. Geophys. Res.*, 91(C8), 9739–9748, 1986.
- Keeling, R. F. and S. R. Shertz, Seasonal and interannual variations in atmospheric oxygen and implications for the global carbon cycle, *Nature*, 358, 723–727, 1992.
- Keffer, T., The Ventilation of the World's Oceans: Maps of the Potential Vorticity Field, *J. Phys. Oceanogr.*, 15, 509–523, 1985.
- Klein, B. and G. Siedler, On the Origin of the Azores Current, *J. Geophys. Res.*, 94, 6159–6168, 1989.
- Koster, R. D., W. S. Broecker, J. Jouzel, R. J. Souzzo, G. L. Russell, D. Rind and J. W. C. White, The Global Geochemistry of Bomb-Produced Tritium: General Circulation Model Compared to Available Observations and Traditional Interpretations, *J. Geophys. Res.*, 94, 18,305–18,326, 1989.
- Krauss, W. and C. W. Böning, Lagrangian Properties of Eddy Fields in the North Atlantic As Deduced From Satellite-Tracked Buoys, *J. Marine Res.*, 45, 259–291, 1987.
- Krauss, W., R. Döscher, A. Lehmann and T. Viehoff, On Eddy Scales in the Eastern and Northern North Atlantic Ocean As a Function of Latitude, *J. Geophys. Res.*, 95, 18049–18056, 1990.

- Le Traon, P. Y., M. C. Rouquet and C. Boissier, Spatial Scales of Mesoscale Variability in the North Atlantic As Deduced From Geosat Data, *J. Geophys. Res.*, **95**, 20267–20285, 1990.
- Ledwell, J. R., A. J. Watson and C. S. Law, Evidence for Slow Mixing Across the Pycnocline From an Open-Ocean Tracer-Release Experiment, *Nature*, **364**, 701–703, 1993.
- Levitus, S., Climatological Atlas of the World Ocean, *NOAA Professional Papers*, **13**, 1–173, 1982.
- Libby, W. F., Tritium Geophysics, *J. Geophys. Res.*, **66**, 3767–3782, 1961.
- Liu, Z., Thermocline Forced by Varying Ekman Pumping. Part II: Annual and Decadal Ekman Pumping, *J. Phys. Oceanogr.*, **23**, 2523–2540, 1993.
- Liu, Z., J. Pedlosky, D. Marshall and T. Warncke, On the Feedback of the Rhines-Young Pool on the Ventilated Thermocline, *J. Phys. Oceanogr.*, **23**, 1592–1596, 1993.
- Lozier, M. S., W. B. Owens and R. G. Curry, The Climatology of the North Atlantic, *Prog. Oceanogr.*, **36**, 1–44, 1995.
- Luyten, J. and H. Stommel, Gyres Driven by Combined Wind and Bouyancy Flux, *J. Phys. Oceanogr.*, **16**, 1551–1560, 1986.
- Luyten, J. R., J. Pedlosky and H. Stommel, The Ventilated Thermocline, *J. Phys. Oceanogr.*, **13**, 292–309, 1983.
- Marshall, J. C., A. J. G. Nurser and R. G. Williams, Inferring the Subduction Rate and Period Over the North Atlantic, *J. Phys. Oceanogr.*, **1315**(7), 1315–1329, 1993.
- Mayer, D. A. and R. H. Weisberg, A Description of COADS Surface Meteorological Fields and the Implied Sverdrup Transports for the Atlantic Ocean From 30°S to 60°N, *J. Phys. Oceanogr.*, **23**, 2201–2221, 1993.
- McCartney, M. S., The Subtropical Recirculation of Mode Waters, *J. Marine Res.*, **40**, Supp., 427–464, 1982.
- McCartney, M. S. and L. D. Talley, The Subpolar Mode Water of the North Atlantic Ocean, *J. Phys. Oceanogr.*, **12**, 1169–1188, 1982.



- Mémery, L. and C. Wunsch, Constraining the North Atlantic Circulation with Tritium Data, *J. Geophys. Res.*, 94, 5239–5256, 1990.
- Montgomery, R. B., A Suggested Method for Representing Gradient Flow in Isentropic Surfaces, *Bulletin of the American Meteorological Society*, 18, 210–212, 1937.
- Montgomery, R. B., Circulation in the Upper Layers of the Southern North Atlantic Deduced with Use of Isentropic Analysis., Mass. Inst. Tech and Woods Hole Ocean. Inst., Papers in Physical Oceanography and Meteorology, 1938.
- Moum, J. N., Efficiency of Mixing in the Main Thermocline, *J. Geophys. Res.*, 101(12,057), 1996.
- Musgrave, D., Numerical studies of  $^3\text{H}$  and  $^3\text{He}$  in the thermocline, *J. Phys. Oceanogr.*, 20, 334–373, 1990.
- New, A. L., R. Bleck, Y. Jia, R. Marsh, M. Huddleston and S. Barnard, An Isopycnic Model Study of the North Atlantic, 1, Model Experiment, *J. Phys. Oceanogr.*, 25, 2667–2699, 1995.
- Olbers, D. J., M. Wenzel and J. Willibrand, The Inference of North Atlantic Circulation Patterns From Climatological Data, *Rev. Geophys.*, 23, 313–356, 1985.
- Ollitrault, M., The General Circulation of the Subtropical North Atlantic, Near 700m Depth, Revealed by the TOPOGULF SOFAR Floats, *International WOCE Newsletter*, 20, 15–18, 1995.
- Östlund, H. G. and C. G. H. Rooth, The North Atlantic Tritium and Radiocarbon Transients in 1972–1983., *J. Geophys. Res.*, 95, 20147–20165, 1990.
- Pallant, J. S., F. B. Bahr, T. M. Joyce, J. P. Dean and J. R. Luyten, in *Subduction in the Subtropical Gyre: Seasoar Cruises Data Report*, p. 213pp, Woods Hole Oceanographic Institution Tech Report WHOI-95-13, Woods Hole, MA, 1995.
- Pedlosky, J., Thermocline Theories, in *General Circulation of the Ocean*, edited by H. D. I. Abarbanel and W. R. Young, pp. 55–101, Springer-Verlag, New York, 1987.
- Pedlosky, J. and P. Robbins, The Role of the Finite Mixed-Layer Thickness in the Structure of the Ventilated Thermocline, *J. Phys. Oceanogr.*, 21, 1018–1031, 1991.

- Pedlosky, J. and W. R. Young, Ventilation, Potential-Vorticity Homogenization and the Structure of the Ocean Circulation, *J. Phys. Oceanogr.*, **13**, 2020–2037, 1983.
- Peng, T. -H. and W. S. Broecker, The Utility of Multiple Tracer Distributions in Calibrating Models for the Uptake of Anthropogenic CO<sub>2</sub> by the Ocean Thermocline, *J. Geophys. Res.*, **90**, 7023–7035, 1985.
- Pickart, R. S., N. G. Hogg and W. M. Smethie, Determining the Strength of the Deep Western Boundary Current Using the Chlorofluorine Ratio, *J. Phys. Oceanogr.*, **19**, 940–951, 1989.
- Pollard, R. T., M. J. Griffiths, S. A. Cunningham, J. F. Read, F. F. Perez and A. F. Rios, Vivaldi 1991 - a Study of the Formation, Circulation and Ventilation of Eastern North Atlantic Central Water., *Prog. in Ocean.*, **37**, 167–192, 1996.
- Pollard, R. T. and S. Pu, Structure and Circulation of the Upper Atlantic Ocean Northeast of the Azores, *Prog. in Ocean.*, **12**, 443–462, 1985.
- Quay, P. D., B. Tilbrook and C. S. Wong, Oceanic Uptake of Fossil Fuel CO<sub>2</sub>: Carbon-13 Evidence, *Science*, **256**, 74–79, 1992.
- Rhines, P. B. and W. R. Young, A Theory of the Wind-Driven Circulation. I. Mid-Ocean Gyres, *J. Marine Res.*, **40**(Supp.), 559–596, 1982a.
- Rhines, P. B. and W. R. Young, Homogenization of Potential Vorticity in Planetary Gyres, *JFM*, **122**, 347–367, 1982b.
- Roache, P. J., *Computational Fluid Dynamics*, Hermosa Publishing, Albuquerque, N.M., 1982.
- Roemmich, D. and C. Wunsch, Two Transatlantic Sections: Meridional Circulation and Heat Flux in the Subtropical North Atlantic Ocean, *Deep-Sea Res.*, **32**, 619–664, 1985a.
- Roemmich, D. and C. Wunsch, Is the North Atlantic in Sverdrup Balance?, *J. Phys. Oceanogr.*, **15**, 1876–1880, 1985b.
- Roether, W., An Account of Tritium in the Ocean, Report Prepared for the IAEA Under Special Service Agreement, 1989a.

- Roether, W., On Oceanic Boundary Conditions for Tritium, on Tritiogenic  $^3\text{He}$ , and on the Tritium- $^3\text{He}$  Age Concept., in *Oceanic Circulation Models: Combining Data and Dynamics*, edited by D. L. T. Anderson and J. Willibrand, pp. 377–407, Kluwer Academic Publishers, Boston, 1989b.
- Roether, W. and G. Fuchs, Water Mass Transport and Ventilation in the Northeast Atlantic Derived From Tracer Data, *Phil. Trans. R. Soc. Lond. A.*, **325**, 63–69, 1988.
- Rogers, C. F. and K. J. Richards, On the Vertical Structure Description of Quasi-Geostrophic Ocean Models, *Dyn. Atmos. Oceans*, **12**, 207–232, 1988.
- Rooth, C. G. H. and H. G. Östlund, Penetration of Tritium Into the Atlantic Thermocline, *Deep-Sea Res.*, **19**, 481–492, 1972.
- Sarmiento, J. L., A Tritium Box Model of the North Atlantic Thermocline, *J. Phys. Oceanogr.*, **13**, 1269–1274, 1983.
- Sarmiento, J. L., C. G. H. Rooth and W. Roether, The North Atlantic Tritium Distribution in 1972, *J. Geophys. Res.*, **87**, 8047–8056, 1982.
- Sarmiento, J. L. and E. T. Sundquist, Revised Budget for the Oceanic Uptake of Anthropogenic Carbon Dioxide, *Nature*, **356**, 589–593, 1992.
- Sarmiento, J. L., G. Thiele, R. M. Key and W. S. Moore, Oxygen and Nitrate New Production and Remineralization in the North Atlantic Subtropical Gyre, *J. Geophys. Res.*, **95**, 18303–18315, 1990.
- Saunders, P. M., Circulation in the Eastern North Atlantic, *J. Marine Res.*, **40**(Supp.), 641–657, 1982.
- Schmitz, Jr., W. J. and M. S. McCartney, On the North Atlantic Circulation, *Reviews of Geophysics*, **31**, 29–49, 1993.
- Siedler, G., A. Kuhl and W. Zenk, The Madeira Mode Water, *J. Phys. Oceanogr.*, **17**, 1561–1570, 1987.
- Spall, M. A., Circulation in the Canary Basin: a Model/Data Analysis, *J. Geophys. Res.*, **95**, 9611–9628, 1990.
- Spall, M. A., P. L. Richardson and J. Price, Advection and Eddy Mixing in the Mediterranean Salt Tongue, *J. Marine Res.*, **51**, 797–818, 1993.

- Speer, K. and E. Tziperman, Rates of Water Mass Formation in the North Atlantic, *J. Phys. Oceanogr.*, 22, 93–104, 1992.
- Speer, K. G., H. -J. Isemer and A. Biastoch, Water Mass Formation From Revised COADS Data, *J. Phys. Oceanogr.*, 25, 2444–2457, 1995.
- Stammer, D. and C. W. Böning, Generation and Distribution of Mesoscale Eddies in the North Atlantic Ocean, in *The Warmwatersphere of the North Atlantic*, edited by W. Krauss, pp. 159–193, Gebrüder Borntraeger, Berlin, 1996.
- Stommel, H., The Westward Intensification of Wind Driven Ocean Currents., *Transactions of the American Geophysical Union*, 29, 202–236, 1948.
- Stommel, H., Determination of Water Mass Properties Pumped Down From the Ekman Layer to the Geostrophic Flow Below, *Proceedings of the National Academy of Sciences, U.S.A.*, 76, 3051–3055, 1979.
- Stramma, L., Geostrophic Transport in the Warm Water Sphere of the Eastern Subtropical North Atlantic, *J. Marine Res.*, 42, 537–558, 1984.
- Stramma, L. and G. Siedler, Seasonal Changes in the North Atlantic Subtropical Gyre, *J. Geophys. Res.*, 93(C7), 8111–8118, 1988.
- Sundermeyer, M. and J. F. Price, Lateral Mixing and the North Atlantic Tracer Release Experiment: Observations and Numerical Simulations of Lagrangian Particles and Passive Tracer, XXX, *in preparation*, 1997.
- Sy, A., Investigation of Large-Scale Circulation Patterns in the Central North Atlantic: the North Atlantic Current, the Azores Current, and the Mediterranean Water Plume in the Area of the Mid-Atlantic Ridge, *Deep-Sea Res.*, 35, 383–413, 1988.
- Talley, L. D., Ventilation of the Subtropical North Pacific: the Shallow Salinity Minimum, *J. Phys. Oceanogr.*, 15, 633–649, 1985.
- Talley, L. D. and M. E. Raymer, Eighteen Degree Water Variability, *J. Marine Res.*, 40(Supp.), 757–775., 1982.
- Tans, P. P., I. Y. Fung and T. Takahashi, Observational Constraints on the Global Atmospheric CO<sub>2</sub> Budget, *Science*, 247, 1431–1438, 1990.

- Taylor, C. B. and W. Roether, A Uniform Scale for Reporting Low-Level Tritium Measurements in Water, *Int. J. Appl. Radiat. Isot.*, **33**, 377–382, 1982.
- Thiele, G., W. Roether, P. Schlosser, R. Kuntz, G. Siedler and L. Stramma, Baroclinic Flow and Transient Tracer Fields in the Canary-Cape Verde Basin, *J. Phys. Oceanogr.*, **16**, 814–826, 1986.
- Thiele, G. and J. L. Sarmiento, Tracer Dating and Ocean Ventilation, *J. Geophys. Res.*, **95**, 9377–9391, 1990.
- Toole, J. M., K. L. Polzin and R. W. Schmitt, Estimates of Diapycnal Mixing in the Abyssal Ocean, *Science*, **264**, 1120–1123, 1994.
- Tsuchiya, M., L. D. Talley and M. S. McCartney, An Eastern Atlantic Section From Iceland Southward Across the Equator, *Deep-Sea Res.*, **39**, 1885–1917, 1992.
- Wallace, D. W. R., P. Schlosser, M. Krysell and G. Bönsch, Halocarbon Ratio and Tritium/<sup>3</sup>He Dating of Water Masses in the Nansen Basin, Arctic Ocean, *Deep-Sea Res.*, **39**(Supp. 2), S435–S458, 1992.
- Weiss, R. E., J. L. Bullister, R. H. Gammon and M. J. Warren, Atmospheric Chlorofluoromethanes in the Deep Equatorial Atlantic, *Nature*, **314**, 608–610, 1985.
- Weiss, W. and W. Roether, The Rates of Tritium Input to the World Oceans, *Earth and Planet. Sci. Lett.*, **49**, 435–446, 1980.
- Williams, R. G., The Role of the Mixed Layer in Setting the Potential Vorticity of the Main Thermocline, *J. Phys. Oceanogr.*, **21**, 1803–1814, 1991.
- Williams, R. G., M. A. Spall and J. C. Marshall, Does Stommel's Mixed Layer "demon" Work?, *J. Phys. Oceanogr.*, **25**, 3089–3102, 1995.
- Woods, J. D., Physics of Thermocline Ventilation, in *Coupled Atmosphere-Ocean Models*, edited by J. C. J. Nihoul, pp. 543–590, Elsevier, Amsterdam, 1985.
- Worthington, L. V., The 18° Water in the Sargasso Sea, *Deep-Sea Res.*, **5**, 297–305, 1959.
- Wunsch, C., Using Transient Tracers: the Regularization Problem, *Tellus*, **39B**, 477–492, 1987.

- Wunsch, C., An Eclectic Atlantic Ocean Circulation Model. II. Transient Tracers and the Ventilation of the Eastern Basin Thermocline, *Phil. Trans. R. Soc. Lond. A*, 325, 201–236, 1988a.
- Wunsch, C., Transient Tracers As a Problem in Control Theory, *J. Geophys. Res.*, 93, 8099–8110, 1988b.
- Wunsch, C., *The Ocean Circulation Inverse Problem*, Cambridge University Press, New York, 1996.
- Wunsch, C. and D. Stammer, The Global Frequency-Wavenumber Spectrum of Oceanic Variability Estimated From TOPEX/POSEIDON Altimetric Measurements, *J. Geophys. Res.*, 100, 24,895–24,910, 1995.
- Zhang, H.-M. and H. G. Hogg, Circulation and Water Mass Balance in the Brazil Basin, *J. Marine Res.*, 50, 385–420, 1992.

## DOCUMENT LIBRARY

*Distribution List for Technical Report Exchange - February 1996*

University of California, San Diego  
SIO Library 0175C  
9500 Gilman Drive  
La Jolla, CA 92093-0175

Hancock Library of Biology & Oceanography  
Alan Hancock Laboratory  
University of Southern California  
University Park  
Los Angeles, CA 90089-0371

Gifts & Exchanges  
Library  
Bedford Institute of Oceanography  
P.O. Box 1006  
Dartmouth, NS, B2Y 4A2, CANADA

NOAA/EDIS Miami Library Center  
4301 Rickenbacker Causeway  
Miami, FL 33149

Research Library  
U.S. Army Corps of Engineers  
Waterways Experiment Station  
3909 Halls Ferry Road  
Vicksburg, MS 39180-6199

Institute of Geophysics  
University of Hawaii  
Library Room 252  
2525 Correa Road  
Honolulu, HI 96822

Marine Resources Information Center  
Building E38-320  
MIT  
Cambridge, MA 02139

Library  
Lamont-Doherty Geological Observatory  
Columbia University  
Palisades, NY 10964

Library  
Serials Department  
Oregon State University  
Corvallis, OR 97331

Pell Marine Science Library  
University of Rhode Island  
Narragansett Bay Campus  
Narragansett, RI 02882

Working Collection  
Texas A&M University  
Dept. of Oceanography  
College Station, TX 77843

Fisheries-Oceanography Library  
151 Oceanography Teaching Bldg.  
University of Washington  
Seattle, WA 98195

Library  
R.S.M.A.S.  
University of Miami  
4600 Rickenbacker Causeway  
Miami, FL 33149

Maury Oceanographic Library  
Naval Oceanographic Office  
Building 1003 South  
1002 Balch Blvd.  
Stennis Space Center, MS, 39522-5001

Library  
Institute of Ocean Sciences  
P.O. Box 6000  
Sidney, B.C. V8L 4B2  
CANADA

National Oceanographic Library  
Southampton Oceanography Centre  
European Way  
Southampton SO14 3ZH  
UK

The Librarian  
CSIRO Marine Laboratories  
G.P.O. Box 1538  
Hobart, Tasmania  
AUSTRALIA 7001

Library  
Proudman Oceanographic Laboratory  
Bidston Observatory  
Birkenhead  
Merseyside L43 7 RA  
UNITED KINGDOM

IFREMER  
Centre de Brest  
Service Documentation - Publications  
BP 70 29280 PLOUZANE  
FRANCE

REPORT DOCUMENTATION PAGE	1. REPORT NO. MIT/WHOI 97-27	2.	3. Recipient's Accession No.
4. Title and Subtitle  Temporal Evolution of Tritium- <sup>3</sup> He Age in the North Atlantic: Implications for Thermocline Ventilation			5. Report Date September 1997
			6.
7. Author(s) Paul E. Robbins			8. Performing Organization Rept. No.
9. Performing Organization Name and Address  MIT/WHOI Joint Program in Oceanography/Applied Ocean Science & Engineering			10. Project/Task/Work Unit No. MIT/WHOI 97-27
			11. Contract(C) or Grant(G) No. (C) N00014-95-1-0824 (G)
12. Sponsoring Organization Name and Address  Office of Naval Research			13. Type of Report & Period Covered Ph.D. Thesis
			14.
15. Supplementary Notes  This thesis should be cited as: Paul E. Robbins, 1997. Temporal Evolution of Tritium- <sup>3</sup> He Age in the North Atlantic: Implications for Thermocline Ventilation. Ph.D. Thesis. MIT/WHOI, 97-27.			
16. Abstract (Limit: 200 words)  This thesis studies the physical mechanisms which ventilate the subtropical thermocline of the eastern North Atlantic. The coupled transient tracers tritium and <sup>3</sup> He define a tracer age diagnostic which estimates the elapsed time since a water parcel was resident at the ocean surface. Analysis of the historical database of <sup>3</sup> He and tritium measurements reveals large, systematic changes in the observed tracer age. The first hypothesis examined is that the observed shift in tracer age results from a weakening of the physical ventilation. Examination of a time-series of the meridional geostrophic velocity and the large-scale oxygen distribution, both based on historical hydrography, reveal no evidence for such a change. Therefore, the temporal trend in observed tritium- <sup>3</sup> He age cannot be explained by an alteration of the physical ventilation of the thermocline. A second hypothesis is that the temporal change in the tritium- <sup>3</sup> He age field reflects a signal of the tritium invasion itself. Numerical simulations of the thermocline ventilation of <sup>3</sup> H and <sup>3</sup> He are performed to examine the steadiness of the tracer age field under different advective-diffusive regimes. The temporal behavior of the tracer age field is dependent on the relative importance of the advection and diffusion of the flow field. The observed temporal behavior of the tracer age field is evidence of a significant role for lateral mixing in the ventilation of the thermocline.			
17. Document Analysis    a. Descriptors  ventilation tritium thermocline  b. Identifiers/Open-Ended Terms      c. COSATI Field/Group			
18. Availability Statement  Approved for publication; distribution unlimited.		19. Security Class (This Report) UNCLASSIFIED	21. No. of Pages 286
		20. Security Class (This Page)	22. Price